NUSC Technical Report 4860

A Study of the Drag Characteristics and Polymer Diffusion in the Boundary Layer of an Axisymmetric Body

John E. Sirmalis

Weapons Department

12 March 1976

NAVAL UNDERWATER SYSTEMS CENTER

Newport Laboratory

PREFACE

This research was conducted under NUSC Project No. A-385-10, "Noise Research," Principal Investigator — J. E. Sirmalis (SB32), and Primary Subproject No. ZR-000-0101.

The Technical Reviewer for this report was R. H. Nadolink (SB323).

REVIEWED AND APPROVED: 12 March 1976

C. A. Spero, Jr.
Director, Systems Development

The author of this report is located at the Newport Laboratory, Naval Underwater Systems Center, Newport, Rhode Island 02840.

UNCLASSIFIED
SECURITY CLASSIFICATION OF THIS PAGE (When Data Entered)

REPORT DOCUMENTATION PAGE		READ INSTRUCTIONS BEFORE COMPLETING FORM
1 REPORT NUMBER C-TR-4860	2 GOVT ACCESSION NO.	3 RECIPIENT'S CATALOG NUMBER
4 TITLE (and Subtitle) A STUDY OF THE DRAG CHARACTERISTICS AND POLYMER DIFFUSION IN THE BOUNDARY LAYER OF AN AXISYMMETRIC BODY.		5 TYPE OF REPORT & PERIOD COVERED Technical 6 PERFORMING ORG. REPORT NUMBER
7 AUTHOR(s) John E. Sirmalis		8 CONTRACT OR GRANT NUMBER(s)
9 PERFORMING ORGANIZATION NAME AND ADDRESS Naval Underwater Systems Center Newport Laboratory Newport, Rhode Island 02840		10 PROGRAM ELEMENT, PROJECT, TASK AREA & WORK UNIT NUMBERS Project No. A-385-10 Subproject No. ZR000-0101
11 CONTROLLING OFFICE NAME AND ADDRESS		12 REPORT DATE 12 March 1976 13 NUMBER OF PAGES 276
14 MONITORING AGENCY NAME & ADDRESS (if different from Controlling Office)		15 SECURITY CLASS. (of this report) UNCLASSIFIED 15a DECLASSIFICATION/DOWNGRADING SCHEDULE

16 DISTRIBUTION STATEMENT (of this Report)

Approved for public release; distribution unlimited.

17 DISTRIBUTION STATEMENT (of the abstract entered in Block 20, if different from Report)

18 SUPPLEMENTARY NOTES

A thesis submitted to the University Of Rhode Island in partial fulfillment of the requirements for the degree of doctor of philosophy in mechanical engineering (1975).

19 KEY WORDS (Continue on reverse side if necessary and identify by block number)

polymer ejection
boundary layer
axisymmetric body
drag reduction

20 ABSTRACT (Continue on reverse side if necessary and identify by block number)

Drag reduction by ejection of high molecular weight polymers on free-running bodies of revolution has been demonstrated repeatedly. The quantities of polymer required have made the gains achieved marginal from a volume utilization tradeoff. The ejection process is hypothesized to be the controlling factor. Limited data obtained in pipe flow and flat plate flow experiments on ejection into developing boundary layers indicate a drastic reduction in polymer requirements for equivalent percent drag reductions.

DD FORM 1 JAN 73 1473 EDITION OF 1 NOV 65 IS OBSOLETE
S/N 0102-014-6601

UNCLASSIFIED
SECURITY CLASSIFICATION OF THIS PAGE (When Data Entered)

Extension to axisymmetric flow could result in significant achievable gains in volume utilization.

This study examines these polymer ejection processes through measurement of wall and boundary layer concentration profiles and through a photographic study of the boundary layer. Tests performed with fresh water ejection and solutions of the drag reducing polymer, Polyox WSR-301, lead to the hypothesis that optimal ejection for minimum polymer usage requires ejection into a laminar boundary layer prior to turbulent flow transition.

Analytical routines are developed which predict boundary layer parameters and polymer wall concentrations for this postulated optimal ejection process or the suboptimal case. Limited verification of the model is made.

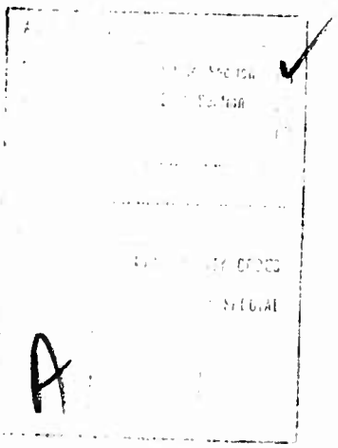

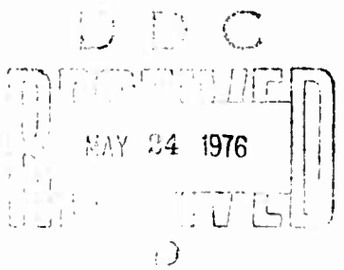

SUMMARY

Drag reduction by ejection of high molecular weight polymers on free-running bodies of revolution has been demonstrated repeatedly. The quantities of polymer required have made the gains achieved marginal from a volume utilization tradeoff. The ejection process is hypothesized to be the controlling factor. Limited data obtained in pipe flow and flat plate flow experiments on ejection into developing boundary layers indicate a drastic reduction in polymer requirements for equivalent percent drag reductions. Extension to axisymmetric flow could result in significant achievable gains in volume utilization.

The object of the research described herein was to examine the processes described above through measurement of wall and boundary layer concentration profiles and through a photographic study of the boundary layer. Tests were performed with fresh water ejection and solutions of the drag reducing polymer, Polyox WSR-301. Predictive analytical routines were developed and experimentally verified.

The experimental apparatus used in this experiment was a drop tank with several velocity measurement stations and photographic equipment. Several specially designed axisymmetric bodies were constructed. Three of these ejected dye by aspiration at the minimum pressure point near the nose. The fourth had a capability to eject through a nose-screen type orifice at a constant rate

and withdraw wall or boundary layer samples at four stations along the body. All bodies had a maximum diameter of three inches and applied a half-body forebody. The three dye ejecting bodies incorporated different tail configurations: 6^{o} cone tail, L/D = 8.33; 12^{o} cone tail, L/D = 6.7; and spherical tail, L/D = 5.54. The polymer ejection body was similar in configuration to the 6^{o} tail body.

Tests were performed in a Reynolds number range of one to five million. The first series of tests were performed in fresh water and in a polymer "ocean" of various concentrations; 1.25, 2.5, 5, 10, 20, 50, and 60 WPPM. Skin friction reduction obtained on all bodies approached 70 percent at polymer concentrations of 20 WPPM, agreeing well with data from other experimenters. Total drag reductions of 33 percent for the 6^{o} body, 16 percent for the 12^{o} body, and 10 percent for the spherical tail body were obtained, the effect of higher percentage form drag being evident.

Photographic studies of dyed boundary layers in these tests and in ejection tests with 50 WPPM, 500 WPPM, and 1000 WPPM displayed several interesting characteristics. Addition of small quantities of polymer, 2.5 WPPM, eliminated the fine-scale turbulent structure leaving only coarse turbulence. Higher concentrations resulted in suppression of the coarse turbulence and extreme thinning of the boundary layer. In the ejection tests, concentrations of 500 WPPM and 1000 WPPM displayed no turbulent structure or

mixing. A dye streaking phenomenon with spacing equivalent to that characteristic of laminar sublayer streaks was displayed. The number of streaks was also approximately equal to the number of ejection holes, approximately 700, supporting the fact that mixing had essentially ceased.

Concentration profiles were measured in the ejection tests using a fluorometric method. Tracer-contaminated water, 5 WPPM, 10 WPPM, 20 WPPM, 50 WPPM, 500 WPPM, and 1000 WPPM solutions, were ejected. Four measurement stations, the last at an x/L of .48, were sampled. The water data displayed expected concentration profiles, agreeing well with those of other investigators. At all polymer concentrations tested, unexpected results were achieved. Wall concentrations remained at levels predicted by molecular diffusion. As evidenced from the photographs, no diffusion was occurring. An initial mixing zone neglected by most investigators was the controlling zone in these tests. Only for the 5 WPPM case did a higher diffusion rate begin part way along the body. The data for this axisymmetric case were compared with data from the single flat plate experiment evidencing the same phenomenon. A dimensionless distance developed in the flat plate experiment used to predict the extent of this initial zone was modified and compared favorably with this experiment. It is hypothesized from these tests that optimal ejection for minimum polymer usage requires ejection into a laminar boundary layer prior to transition to turbulent flow.

Analytical routines are developed which predict boundary layer parameters and polymer wall concentrations for this postulated optimal ejection process or the suboptimal case. Limited verification of the model is made.

TABLE OF CONTENTS

LIST OF ILLUSTRATIONS

LIST OF TABLES

LIST OF SYMBOLS

A = body area	ft^2
A_e = ejection area	ft^2
A_f = body frontal area	ft^2
A_s = body surface area	ft^2
a = acceleration	ft/sec
b = Batchelor's Constant	dimensionless
B = Buoyant force on body	lbs
c = concentration	WPPM
c_i = ejected concentration	WPPM
c_f = local skin friction coefficient	dimensionless
C_F = skin friction coefficient	dimensionless
c_w = wall concentration	WPPM
C_D = total drag coefficient	dimensionless
C_p = pressure coefficient	dimensionless
D = body diameter	ft
D_c = Eddy diffusivity	$\frac{lb\ sec^2}{ft^2}$
D_{POLY} = total drag with polymer	lbs
D_W = total drag in water	lbs
F = force	lbs
g = gravitational acceleration	ft/sec^2
k = gas constant	dimensionless
K = mixing length constant	dimensionless
K_2 = defined by equation (114)	dimensionless

K_3	= defined by equation (119)	dimensionless
K_5	= defined by equation (117)	dimensionless
ℓ	= length dimension	ft
L	= body length	ft
M	= mass	$\frac{lb_f\ sec^2}{lb_w\ ft^2}$
p	= pressure	lb/ft^2
p_c	= pressure at edge of boundary layer	lb/ft^2
q_z	= flux of diffused matter	$\frac{lb\ sec}{ft^3}$
Q	= volume flow rate	ft^3/sec
Q_i	= ejection rate	ft^3/sec
r	= radial distance from body centerline	ft
r_h	= distance from origin for body coordinate generation	ft
r_o	= radius of body	ft
r^+	= $\frac{r\ v^*}{\nu}$	dimensionless
r_o^+	= $\frac{r_o\ v^*}{\nu}$	dimensionless
R_e	= Reynold's number	dimensionless
R_L	= $\frac{U_o L}{\nu}$	dimensionless
SD_{POLY}	= shear drag with polymer	lbs
SD_w	= shear drag with water	lbs
SFR	= total skin friction reduction	%
t	= time	second
T	= temperature	^oR

T_f	= temperature of injected fluid	^oR
TDR	= total drag reduction	%
$u(z)$	= local boundary layer velocity	ft/sec
u^+	= u/v^*	dimensionless
$u(\bar{Y})$	= velocity at $\bar{Y}$	ft/sec
U	= U_o freestream or body velocity	ft/sec
U_e	= velocity at edge of boundary layer	ft/sec
v	= velocity	ft/sec
v_i	= ejection velocity	ft/sec
v^*	= characteristic or friction velocity	ft/sec
v_o^*	= critical shear velocity = τ_w/ρ	ft/sec
V	= U_e/U_o	dimensionless
V_s	= storage volume	ft^3
W	= body weight in air	lbs
x	= linear dimension	ft
x_s	= surface length	ft
x^*	= x/L	dimensionless
y	= distance normal to body	ft
y^+	= $\frac{y\ v^*}{\nu}$	dimensionless
$\bar{y}$	= mean vertical position of particles	ft
$\bar{Y}$	= mean vertical position of single particle	ft
Y	= RAO variable defined by equation (15)	ft
Y^+	= $\frac{Y\ v^*}{\nu}$	dimensionless
α	= defined by equation (29)	dimensionless
β	= defined by equation (10)	dimensionless

γ = defined by equation (43)	dimensionless
ϵ = Eddy viscosity	$\frac{\text{lb sec}}{\text{ft}^2}$
ΔB = defined by equation (42)	dimensionless
δ = boundary layer thickness	ft
δ_J = diffusion boundary layer thickness	ft
ϕ = angle for definition of half body	degrees
θ = angle from normal to bad	degrees
II = defined by equation (11)	dimensionless
ψ = stream function	seconds
$\lambda = (\frac{2}{c_f})^{\frac{1}{2}}$	dimensionless
w = gas flow rate	lb/sec
ρ = density	slugs/ft^2
μ = viscosity	lb sec/ft^2
τ_w = wall shear stress	lb/sec^2
ν = kinematic viscosity	ft^2/sec

ACKNOWLEDGMENTS

The author acknowledges the generous assistance of his colleagues at the Naval Underwater Systems Center (Dr. J. F. Brady, R. H. Nadolink, J. W. Hooker, and A. R. Lagasse), and the helpful guidance of Dr. Rodger Dowdell (University of Rhode Island).

I. INTRODUCTION

A. General Considerations

High speed flow of both gases and liquids past a fixed boundary generates a turbulent boundary layer which exerts both a fluctuating normal stress (flow noise) and fluctuating shear stress (whose average is drag) on the body. The reduction of resistance to the turbulent shear flows of liquids through the addition of small quantities of high molecular weight polymers into the boundary layer of the flow has been demonstrated repeatedly. This phenomenon of drag reduction has far-reaching importance in the reduction of power required for pumping of fluids or transport of bodies through liquids.

Until recently, the phenomenon of drag reduction was confined essentially to characterizing the manner in which the boundary layer velocity profiles were affected, thus allowing predictions of boundary layer thickness and shear drag. Additionally, the early work primarily dealt with well-developed pipe flows where the observation of drag reduction was first made. An added complication results from the fact that data obtained with commonly used instrumentation have been found to be affected by the polymers resulting in erroneous readings. As a result, the mechanism of shear stress reduction remains undefined although emperical techniques predicting the benefits of application of the phenomenon have been developed.

Interest in the problem has expanded with recent investigators examining the effect of polymers on external flows, as over flat plates. Similar results as in the pipe flows have been achieved. The magnitude of the turbulent fluctuations have been found to decrease with a thickening of the laminar sublayer and a lowering of the shear stress.

Shear stress reduction for external flows over bodies can be achieved by proper ejection of polymer solutions. A limit to the amount of drag reduction achievable with polymer use has been demonstrated and increases in shear stress has been obtained when excess polymer is used.

It is evident that a better understanding of the mechanisms of drag reduction in developing flows with polymer ejection is required if an advantage is to be taken of the phenomenon. For most cases, of interest in external flows, a carried polymer supply would be used for ejection into the boundary layer. Limits on diffusion result in a far too high concentration initially - with, possibly, shear drag increases - and then, further downstream on the body, too little polymer resulting in insignificant gains in drag reduction. One might envision, to circumvent the problem, multiple ejection ports to optimize the polymer wall concentration and maximize the drag reduction.

Many investigators have addressed portions of the problem outlined above as discussed in the following chapter. The

effect of long chain polymers on suppressing boundary layer turbulence has been investigated for pipe flows and external flows; methods of characterizing the boundary layer velocity profiles with polymers present have been developed and methods for prediction of flow separation have been postulated.

The object of the research described herein was to develop predictive methods for design of polymer ejection system for bodies of revolution and to perform experiments to verify the predictive methods. Additionally, a study of the effects of polymers on boundary layer separation was made. Several "half body" configurations were used in the testing, differing in their conical to hemispherical tail configurations. The bodies were dropped in a twenty-foot long cylindrical tank and allowed to achieve a steady state velocity. On three of the bodies, dye was ejected in the boundary layer and photographic records of the growth and separation of the boundary layer at several velocities were made. For these tests, the ambient fluid was water and a water polymer mix (polymer ocean) of several concentrations. Another series of tests were made with a body having a significantly different internal configuration. This body has the capability to store and eject concentrated polymer solution from its nose and withdraw boundary layer samples at four stations along its length. The boundary layer samples in turn were either wall samples or samples at three heights within the boundary layer. The stored

polymer was contaminated with a fluorescent dye which was later used in analyzing the concentrations from these boundary layer samples. Thus, it was possible to measure the change in wall concentration and concentration profile in the boundary layer, measure steady state body velocity and compare simultaneously with computed results. This research, therefore, concentrates on the prediction and verification of the drag reduction mechanism on bodies of interest for underwater application to gain insight which will help in the design of vehicle ejection systems.

B. Selection of Experimental Apparatus

The intended research could be carried out in water tunnels, towing tanks, ring channels, in buoyant vehicle experiments, or in drop tank tests.

For the desired research, the drop tank has a number of attractive features. Conceptually, it is a relatively simple experimental tool. The ambient turbulence level is very low, flow visualization is easily achieved and velocity measurements readily made. Tests over a reasonable range of Reynolds numbers are achieved by weighting the body being dropped.

One of the chief drawbacks of the drop tank facility as compared to a water tunnel, ring channel or towing tank is the inability to easily measure velocity profiles since the body being measured is moving. Since flow visualization gives an approximate boundary layer thickness, this limitation was not considered to be an important drawback.

Fortunately, the author's employer, Naval Underwater Systems Center, had available a drop tank with suitable dimensions for this research. The potential for meaningful research and the availability of the capital equipment led to the decision to proceed with axisymmetric boundary layer research described herein.

C. Results

Tests were performed in a Reynolds number range of one to five million. The first series of tests were performed in fresh water and in a polymer "ocean" of various concentrations; 1.25, 2.5, 5, 10, 20, 50, and 60 WPPM. Skin friction reduction obtained on all bodies approached 70 percent at polymer concentrations of 20 WPPM agreeing well with data from other experimenters. Total drag reductions of 33 percent for the 6^{o} body, 16 percent for the 12^{o} body, and 10 percent for the spherical tail body were obtained, with the effect of higher percentage form drag being evident.

Photographic studies of dyed boundary layers in these tests and in ejection tests with 50 WPPM, 500 WPPM, and 1000 WPPM displayed several interesting characteristics. Addition of small quantities of polymer, 2.5 WPPM, eliminated the fine-scale turbulent structure leaving only coarse turbulence. Higher concentrations resulted in suppression of the coarse turbulence and extreme thinning of the boundary layer. In the ejection tests, concentrations of 500 WPPM and 1000 WPPM displayed no turbulent structure or mixing. A dye streaking phenomenon with spacing equivalent to that characteristic of laminar sublayer streaks was displayed. The number of streaks

was also approximately equal to the number of ejection holes, approximately 700, supporting the fact that mixing had essentially ceased.

Concentration profiles were measured in the ejection tests using a fluorometric method. Tracer-contaminated water, 5 WPPM, 10 WPPM, 20 WPPM, 50 WPPM, 500 WPPM, and 1000 WPPM solutions, were ejected. Four measurement stations, the last at an x/L of .48, were sampled. The water data displayed expected concentration profiles, agreeing well with those of other investigators. At all polymer concentrations tested, unexpected results were achieved. Wall concentrations remained at levels predicted by molecular diffusion. As evidenced from the photographs, no diffusion was occurring. An initial mixing zone neglected by most investigators was the controlling zone in these tests. The data for this axisymmetric case were compared with data from the single flat plate experiment evidencing the same phenomenon. A dimensionless distance developed in the flat plate experiment used to predict the extent of this initial zone was modified and compared favorably with this experiment. It is hypothesized from these tests that optimal ejection for minimum polymer usage requires ejection into a laminar boundary layer prior to transition to turbulent flow.

Analytical routines are developed which predict boundary layer parameters and polymer wall concentrations for this postulated optimal ejection process or the suboptimal case. Limited verification of the model is made.

II. LITERATURE REVIEW

The reduction of resistance to the turbulent shear flows of liquids through addition of small quantities of polymer into the boundary layer flowing over a body has received considerable attention. The first reportings occurring independently by Mysel (1949), Toms (1949), and Oldroyd (1949). Although extensive theoretical and experimental work has been carried out with steady pipe flows where the resistance is due to turbulent skin friction alone, relatively few studies have been conducted on the effect of additives on the flow about axisymmetric bodies where the development of the boundary layer, the position of the separation point, and the unsteady wake significantly contributes to the total resistance. Polymer injection in developing boundary layers has only recently come under study. Polymer ejection type data for external flows with pressure gradients are virtually non-existent. Hoyt (1972) presents an encellent summary of the research efforts and results available in the field of drag reduction.

Literature pertaining to the current study will be reviewed under four separate headings:

1. Bluff body experiments with polymer solutions,
2. Turbulent boundary layer theory,
3. Homogeneous polymer flow, and
4. Polymer ejection studies.

Bluff Body Experiments With Polymer Solution

The earliest known experiment with bluff bodies in drag reducing polymers was carried out by Crawford and Pruitt (1963). Additional experiments with different sizes and shapes of bodies (mostly spheres cones and cylinders) in various types and concentration of polymers were conducted by others. Work performed by Lang and Patrick (1966) is representative of much of the effort. They found, as did many of the other investigators, that the drag on a sphere was considerably reduced probably due to the rearward movement of the point of boundary layer separation. These experiments were performed in a drop tank where the fluid ahead of the ball was stationary. A drag reduction of 69% was attained for a 2-inch diameter steel sphere dropped in a 1000 WPPM solution of Polyox at a water Reynolds number of 1.4×10^5. It was also shown that the polymer produced little or no drag reduction on stable bluff-based bodies whose point of boundary layer separation is fixed. The additives produced an apparent decrease in turbulent mixing in the mean wake and had a tendency to display a stringiness in the wake at high polymer concentration.

Contradictory results were achieved by Stow and Elliot, 1970, who demonstrated no significant drag reduction on a tethered ball suspended in a fully developed turbulent pipe flow. This is not surprising, if the flow about the sphere exhibits a turbulent type rearward movement of the separation point.

The performance of additives in reducing drag on an immersed body is complicated by a number of factors. Certainly, with well streamlined bodies, drag reduction is effected through reduced skin friction

just as with internal flow. With blunter bodies, however, the drag consists primarily of form drag and is dominated by the wake size and point of flow separation, skin friction frequently being negligible in comparison. On typical free-running underwater bodies of revolution, the form drag can represent 25% of the total drag. The two investigations previously reported demonstrate the importance of the "free stream" condition on the movement of the separation point with polymers. The effect of polymers on boundary layer separation for bodies of revolution warrants further study to define if reduction in the form drag as well as the skin friction drag can be affected by application of polymers.

Turbulent Boundary Layer Theory

Since the concept of transition from laminar to turbulent flow was demonstrated by Osborne Reynolds, in his classic original transition experiment in pipe flow, many attempts have been made to predict the conditions at which laminar to turbulent flow transition will take place. Many attempts have also been made to predict velocity profiles and wall shear. So many, in fact, that in 1968 the Stanford conference was called in which a total of 29 methods for performing turbulent boundary layer analysis were graded. These proceedings have been edited by Kline (1968). Such general analysis can be divided into two types: (1) integral methods averaged across the boundary layer, and (2) finite difference, or differential methods which attempt to solve the full partial differential equations of the boundary layer. A text by F. M. White (1974) neatly summarizes and discusses many of the competing analysis methods.

By considering the relative importance of viscous and turbulent shear, the velocity distribution in a turbulent boundary layer follows a three-layer concept. The layers are:

Inner Layer: Viscous shear dominates

Outer Layer: Turbulent shear dominates

Overlap Layer: Both types of shear important

The mean velocity distribution in a two-dimensional turbulent boundary layer, u(y), depends upon four local parameters -- τ_w, the local wall shear stress; ρ, the fluid density; μ, the fluid viscosity; and δ, the boundary layer thickness. Prandtl (1933) deduced for the inner law that the mean velocity did not depend on δ resulting in a functional expression for the inner law of

$$u = f(\tau_w, \rho, \mu, y). \tag{1}$$

Karman (1930) deduced that the wall acts as a source of retardation reducing the local velocity, u, below the freestream velocity U_e, in a manner independent of viscosity, μ. The outer or velocity defect relationship is then

$$U_e - u = f(\tau_w, \rho, y, \delta). \tag{2}$$

Coles (1954) performed a dimensional analysis on these relationships resulting in

$$\text{Inner Law} \qquad \frac{u}{v^*} = f\left(\frac{yv^*}{\nu}\right) \tag{3}$$

$$\text{Outer Law} \qquad \frac{U_e - u}{v^*} = g(y/\delta) \tag{4}$$

where v^* is a characteristic velocity called the wall shear velocity defined as

$$v^* = \left(\frac{\tau_w}{\rho}\right)^{\frac{1}{2}}. \tag{5}$$

By equating equations (3) and (4) in the overlap region, one may obtain the commonly known relation for the "law of the wall" based on inner variables

$$\frac{u}{v^*} = \frac{1}{K} \ln \frac{yv^*}{\nu} + B \tag{6}$$

where K and B are constants determined by the data of Nikuradse (1930), to be .4 and 5.5, respectively. Coles (1954) displays the correlation of the dimensionless velocity profile, u/v* with the dimensionless distance for the wall $\frac{uv^*}{\nu}$ up to a wake of about 300. With the exception of separating flows, all the data nicely collapse into regions defined by the inner and logarithmic laws having dimensions

Inner Law $$\frac{u}{v^*} = \frac{yv^*}{\nu} \qquad 0 < \frac{yv^*}{\nu} < 10 \tag{7}$$

Logarithmic Law $$\frac{u}{v^*} = 2.5 \ln \frac{yv^*}{\nu} + 5.5 \qquad 35 < \frac{yv^*}{\nu} < 300. \tag{8}$$

For regions beyond $\frac{yv^*}{\nu} = 300$, the outer region or wake region, Coles (1956) postulates a function defined as

$$\frac{II}{K} W(\frac{y}{\delta})$$

be added to the equation (6) resulting in

$$u^+ = \frac{1}{K} \ln y^+ + B + \frac{II}{K} W(\frac{y}{\delta}) \tag{9}$$

where II is related to Clauser's (1954, 1955) equilibrium parameter

$$\beta = \frac{\delta^*}{\tau_w} \frac{dp_e}{dx}. \tag{10}$$

A reasonable fit to data is given by the relationship

$$II \approx 0.8 \, (\beta + 0.5)^{0.75}. \tag{11}$$

Coles (1956) proposed the following curve fit to the wake function W:

$$W\left(\frac{y}{\delta}\right) = 2 \sin^2 \left(\frac{\pi}{2} \frac{y}{\delta}\right) \tag{12}$$

Thus, for two-dimensional flow, empirical relations for the velocity profile in the boundary layer are available. These relations will also hold for thin axisymmetric boundary layers where $\delta << r_o$.

Rao (1967) observed that in the viscous sublayer of a thick axisymmetric turbulent boundary layer the momentum equation reduces to

$$\frac{\partial}{\partial r} (r\tau) = 0 = \frac{\partial}{\partial r} \left(\mu r \frac{\partial u}{\partial r}\right) \tag{13}$$

Integrating with $u = 0$ at $r = r_o$, an inner law for the sublayer results

$$u^+ = r_o^+ \ln \frac{r}{r_o} \tag{14}$$

where $r = r_o + y$.

When $\frac{y}{r_o} << 1$, the familiar $u^+ = y^+$ relationship returns since the $\ln(1 + \frac{y}{r_o})$ approaches y/r_o.

Rao also postulated that by defining

$$Y^+ = r_o^+ \ln \frac{r}{r_o} \tag{15}$$

and inserting Y^+ into the familiar law of the wall (6) in place of y^+, a correlation with the two-dimensional case would result. The final relations are

$$u^+ = Y^+ \qquad Y^+ < 5.0 \tag{16}$$

and

$$u^+ = \frac{1}{K} \ln Y^+ + B \qquad Y^+ > 30. \tag{17}$$

Figure 1, reproduced from Rao's paper, displays this correlation with data obtained by Richmond (1957) and Yu (1958). As the body curvature effects become greater, the agreement improves since the wake tends to disappear. For axisymmetric cases where y/r_o may not be considerably less than 1, equation (15) must be corrected to account for the outer wake region. White, et al (1972), accounts for the wake region using an inner variable approach. The basic idea of the method is that in inner variables, the velocity profile is approximately a logarithmic function of Y^+ plus a wake which depends on Y^+ and a single dimensionless parameter $\xi(x)$. For example,

$$u^+ = \frac{1}{K} \ln y^+ + B + f[y^+, \xi(x)] \tag{18}$$

for the two-dimensional case. The derivation of the functional relation for the axisymmetric case is carried through here, since the resulting velocity relationship is not in a form readily recognizable. Recalling Prandtl's mixing length theory:

$$\tau = \varepsilon \frac{\partial u}{\partial y}. \tag{19}$$

Consistent with equation (17) for the axisymmetric case, ε, the eddy viscosity, equals

$$\varepsilon = \rho \ell^2 \left|\frac{\partial u}{\partial Y}\right| \tag{20}$$

where l is the mixing length.

$$\text{Now} \qquad \frac{\partial u}{\partial Y} = \frac{r}{r_o} \frac{\partial u}{\partial y} \tag{21}$$

substituting in (20)

$$\varepsilon = \rho \ell^2 \frac{r}{r_o} \left|\frac{\partial u}{\partial y}\right|. \tag{22}$$

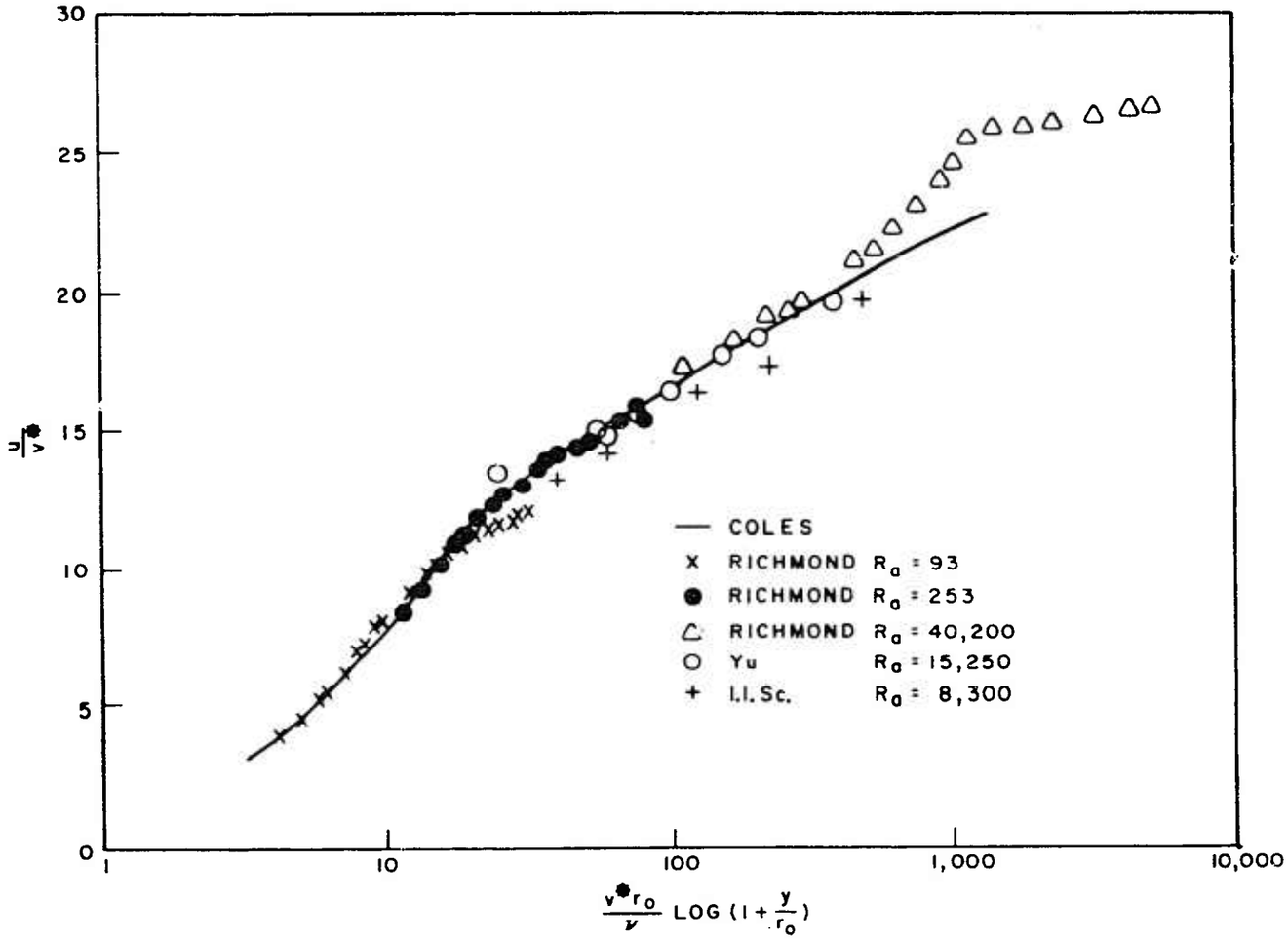

Figure 1. Law of the wall in an axisymmetric turbulent boundary layer (from Rao (1971))

Fairly near the wall in the overlap layer

$$\ell = KY \tag{23}$$

resulting in an eddy viscosity which is

$$\epsilon = \rho K^2 Y^2 \frac{r}{r_o} \left|\frac{\partial u}{\partial y}\right|. \tag{24}$$

Finally, upon substitution in (19):

$$\tau = \rho K^2 Y^2 \frac{r}{r_o} \left(\frac{\partial u}{\partial y}\right)^2. \tag{25}$$

Equation (25) may be used to derive an axisymmetric law of the wall, using a Couette flow approximation for the near wall momentum:

$$\left(\frac{\partial}{\partial r}\right)(r\tau) - r \left(\frac{dp_e}{dx}\right) = 0. \tag{26}$$

Integrating with

$$r = r_o, \quad r\tau = r_o \tau_w,$$

$$r = r, \quad r\tau = r\tau,$$

$$r\tau = r_o \tau_w + \frac{1}{2} \left(\frac{dp_e}{dx}\right)(r^2 - r_o^2). \tag{27}$$

Substituting (25) into (27) gives

$$r_o \tau_w + \frac{1}{2} \left(\frac{dp_e}{dx}\right)(r^2 - r_o^2) = \rho K^2 Y^2 \frac{r}{r_o} \left(\frac{\partial u}{\partial y}\right)^2 \tag{28}$$

The pressure gradient parameter α is defined as

$$\alpha = \left(\frac{\nu_w}{\tau_w v^*}\right) \frac{dp_e}{dx}. \tag{29}$$

Solving (29) for $\frac{dp_e}{dx}$ and substituting in equation (28) and rearranging results in

$$\tau_w \left[1 + \frac{1}{2} r_o \frac{v^*}{\nu_w} \alpha \left(\frac{r^2}{r_o^2} - 1\right)\right] = \rho K^2 Y^2 \frac{r^2}{r_o^2} \left(\frac{\partial u}{\partial y}\right)^2 . \tag{30}$$

Equation (30) may be placed in law of the wall variables by applying equations (5), (15), and (16) and equalities from Figure 2.

Equation (30) becomes

$$\frac{du^+}{dY^+} = \frac{1}{KY^+} \left[1 + \frac{\alpha}{2} r_o^+ \left(e^{2Y^+/r_o^+} - 1\right)\right]^{\frac{1}{2}} . \tag{31}$$

This equation reduces in the limit of large radius to the law of the wall

$$u^+ (Y^+, 0, 0) = \frac{1}{K} \ln (Y^+) + B$$

where $u^+ = 0$ at $Y_o^+ = e^{-KB}$

$= 0.1108$ for $K = 0.4$

$B = 5.5$.

Integrating across the boundary layer from $Y_o^+ = 0.1108$ to Y_o^+ (the edge of the boundary layer) yields

$$u^+ = \frac{1}{K} \int_{0.1108}^{Y_o^+} \frac{1}{Y^+} \left[1 - \frac{\alpha}{2} r_o^+ \left(1 - e^{2Y^+/r_o^+}\right)\right]^{\frac{1}{2}} dY^+ . \tag{32}$$

Equation (32) represents the law of the wall relation for the velocity profile accounting for pressure gradient. This relation holds throughout the boundary layer with the exception of the viscous sublayer region. Figure 3 reproduced from White's paper shows some velocity profiles obtained by integrating equation (32). The effect of positive (adverse pressure gradient) raising the curve above the incompressible log law and the effect of changes in r_o^+ with finite α are evident.

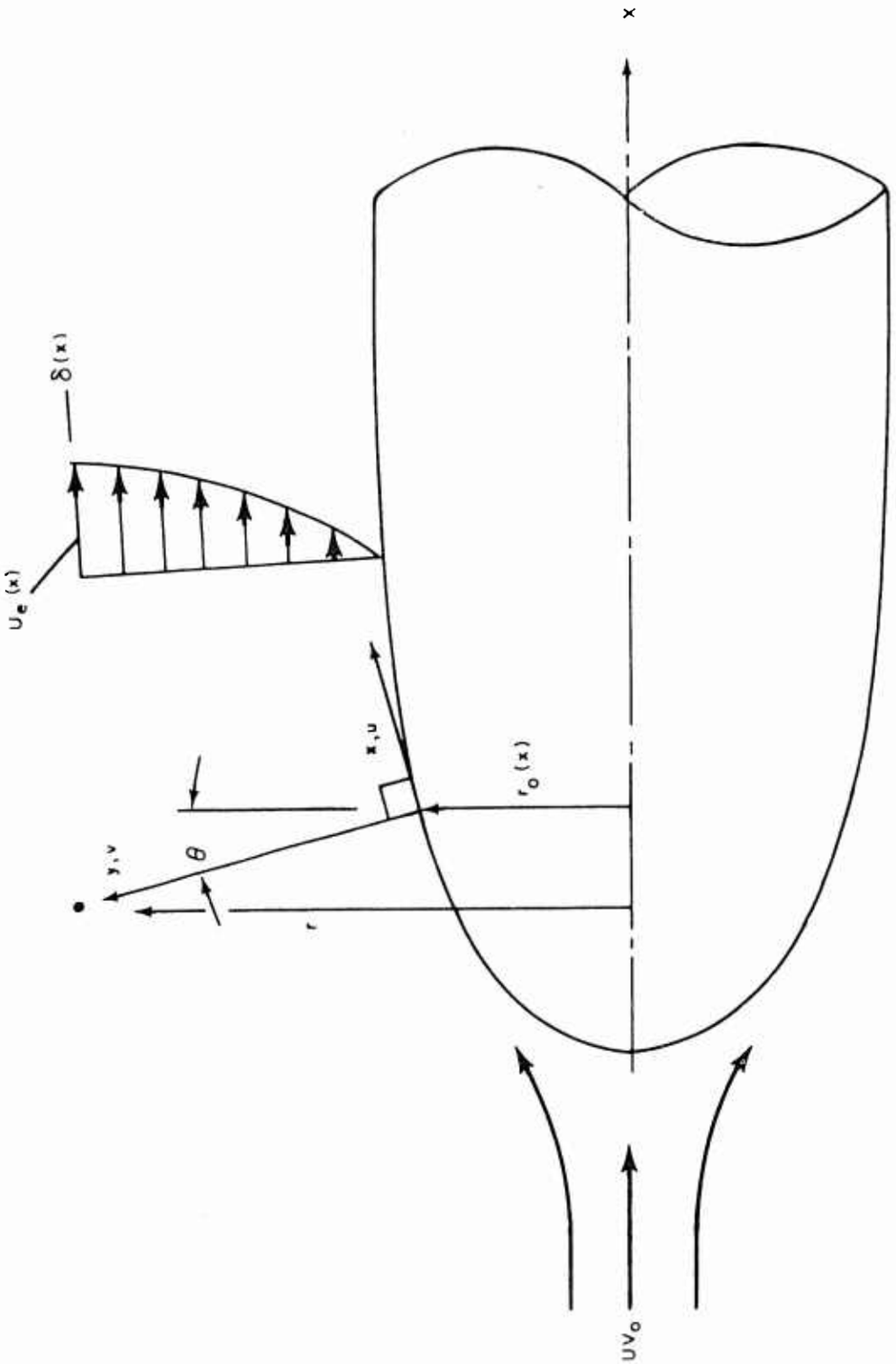

Figure 2. Coordinates for axisymmetric boundary layer flow

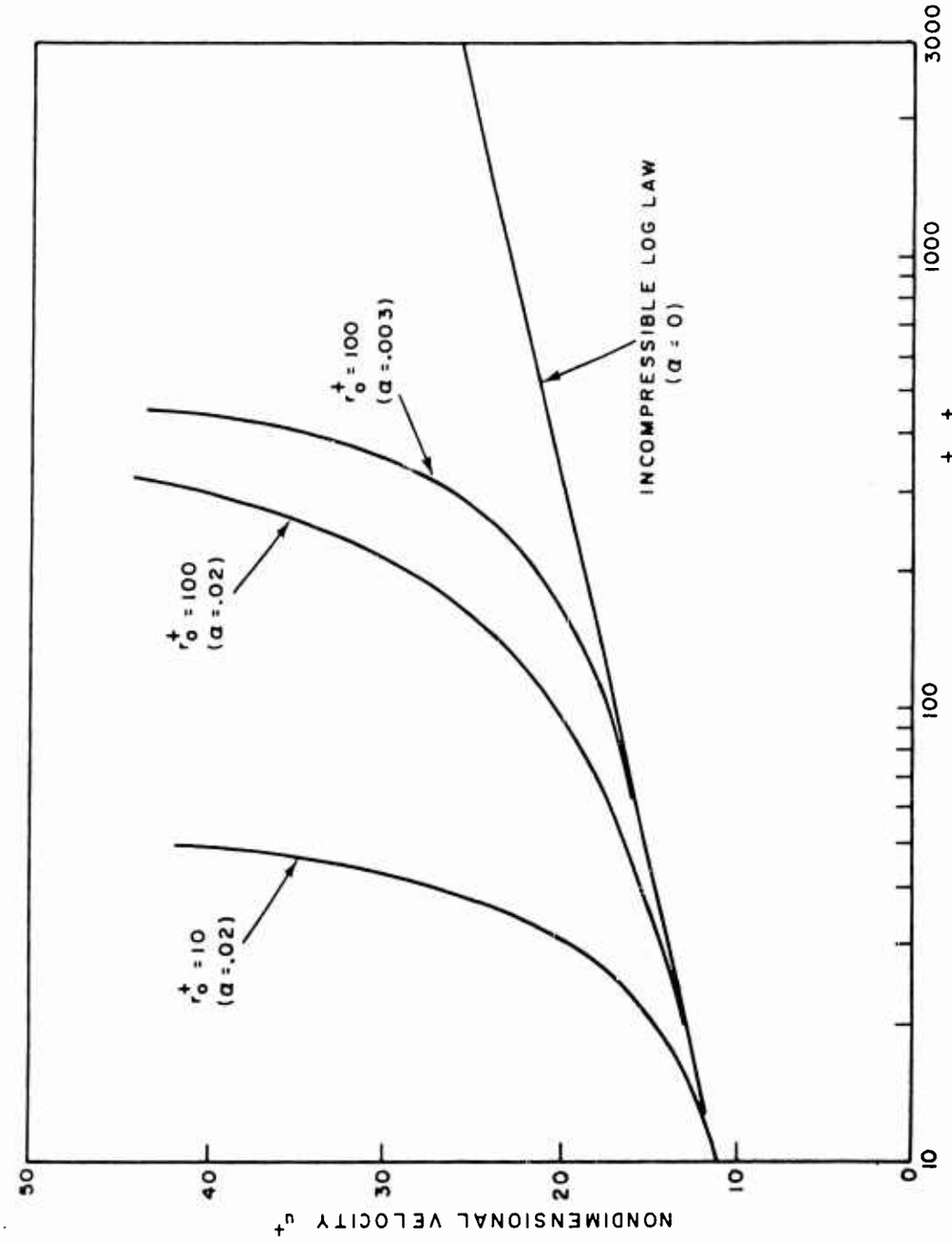

Figure 3. Some examples of the axisymmetric law - of - the - wall, computed from equations 32. (from White et al (1972))

As mentioned previously, many methods have been postulated to predict skin friction. White, F. M. et al (1972, 1973) extended an earlier integral technique developed for flat plate flows (White, F. M., 1968) to the case of thick axisymmetric boundary layer. The method concentrates on the boundary layer equations using inner law variables and is interesting in that boundary layer separation is automatically predicted. The integral technique provides for relatively simple computer solution minimizing required computer time and has been demonstrated by White, to quite accurately predict skin friction. A drawback of the method, as with most integral methods, is that thickness calculations are not very accurate. This is not a serious drawback for the intended calculations since non-dimensionalized boundary layer thickness can be applied. A priori specification of the velocity profile is required with this integral technique, as with others. The boundary layer continuity and momentum equations for turbulent axisymmetric flow are given by

$$\frac{\partial}{\partial x}(\rho u r) + \frac{\partial}{\partial y}(\rho v r) = 0 \tag{33}$$

and

$$\rho u r \left(\frac{\partial u}{\partial x}\right) + \rho v r \left(\frac{\partial u}{\partial y}\right) = - r \left(\frac{dp_e}{dx}\right) + \frac{\partial}{\partial y}(r\tau). \tag{34}$$

where x and y are normal to the body surface as shown in Figure 2. For the portions of the body to which the equations are applied, the angle θ between the normal to the surface and the normal to the body axis is small and is, therefore, neglected. Assuming the law of the wall

(32) is valid across the entire boundary layer, equations (32) through (34) form a closed system that can be solved for the skin friction. The only additional relations required for the present study are those necessary to provide a definition of the polymer wall concentration, c_w.

Appendix A presents a complete development of the equations related to this method along with the additional terms required for solution of the polymer ejection and dilution.

The resulting boundary layer equation, after considerable algebraic manipulation, is

$$\frac{d\lambda}{dx^*}\,(3\alpha H - G_1) + \frac{V'}{V}\,\lambda G_1 - \frac{\lambda^2 r_o^+}{2}\,(e^{2Y_e^+/r_o^+} - 1)$$

$$+ \frac{\lambda''}{R_L}\,\left(\frac{1}{V}\right)''\,H = -R_L V - \lambda\,\frac{dr_o^+}{dx^*}\,I \tag{35}$$

where

$$\lambda = \frac{U_e}{v^*} = \left(\frac{2}{c_f}\right)^{1/2}, \tag{36}$$

$$X^* = \frac{X}{L}, \tag{37}$$

$$V = \frac{U_e}{U_o}, \tag{38}$$

$$R_L = \frac{U_o L}{\nu}, \tag{39}$$

$$\alpha = \left(\frac{\nu_w}{\tau_w v^*}\right)\,\frac{dp_e}{dx}, \tag{40}$$

and the definition of G_1, H, and I may be found in Appendix A.

Other integral and finite difference techniques for solution of the boundary layer problem although applicable will not be reviewed since they are not of central interest to the work being presented.

Homogeneous Polymer Flow

Since the early experiments of Toms and Olroyd (1949), a large number of high molecular weight polymers have been shown to be effective drag reducers. Polysaccharides (Guar), polyethylene oxide, polyacrylamides, and sodium carboxymethyl cellulose have received most attention. The data of Hoyt and Fabula (1964) and Virk (1971) show that there is a maximum drag reduction asymptote. This asymptote, for a smooth pipe, corresponds to 80% of the friction reduction that would be attained if completely laminar flow were sustained at a given Reynolds number.

The efficiency of several of these high molecular weight polymers is evidenced in Table 1 from Hoyt (1972).

TABLE 1

Concentrations (WPPM) of Material Required to Achieve 67-Percent Drag Reduction in Pipe Flow at $R_e = 14 \times 10^3$ (from Hoyt (1972))

Guar	400
Gum Karaya	850
Polyox WSR 301	10
Polyacrylamide, Polyhall-250	20

Meyer (1966) and Elata, et al (1966) have shown that drag reduction in pipes is due to a thickening of the laminar sublayer. It was shown that the constant B in the law of the wall (6) to remain constant and equal to the Newtonian value until a critical threshold value of the shear velocity was reached (v_o^*) after which B increased logarithmically with v*

$$B = 5.5 + \gamma \ln \left(\frac{v^*}{v_o}\right) \tag{41}$$

where $\Delta B = \gamma \ln \frac{v^*}{v_o}$. (42)

White, F. M. (1968) has plotted data from several investigators and found that

$$\gamma = 2.3\, C_w^{1/2}. \tag{43}$$

Further, the data indicate a maximum value of γ of approximately 11 and a critical shear velocity, v_o^*, for the onset of drag reduction of .08 ft/sec. Many authors have described drag reduction as a "negative roughness effect" since the polymers appear to thicken the sublayer while maintaining the same slope of the u/v*vs ln $\frac{yv^*}{\nu}$ curve in the overlap region.

In the outer region, where the wake law holds, polymer additives appear to have no effect on the flow.

Nadolink (1968) demonstrated the existence of the thickened sublayer directly, using a high speed motion picture camera and a microscope.

Virk (1966) presents evidence indicating that the onset shear stress is inversely proportional to polymer molecular radius of gyration. Based on experimental data, the critical wall shear stress, τ_w^c, which must be exceeded for drag reduction to occur is given by

$$\tau_w^c = \rho(0.625 \times 10^6 \mu/R_G)^2 = \frac{\text{constant}}{R_G^2} \tag{44}$$

where R_G is the rms radius of gyration of the molecule as deduced from light scattering data.

Fabula et al (1969) have pointed out that the small value of the ratio of the polymer molecule scale to the scale of the turbulent eddier at onset indicates that individual molecules are too small by several orders of magnitude to interfere with the turbulence structure. To circumvent this problem of length scales, Fabula postulated an interaction between the time scales of the periodic molecular deformation in the viscous sublayer, given by $\dot{\gamma}/2\pi$, where $\dot{\gamma}$ is the shear rate, and a molecular characteristic relaxation time τ_1. τ_1 is determined by the Zimm or Rouse theories which relate a characteristic relaxation time of the solution, τ_1, to the solvent viscosity, μ_s, the solution viscosity, μ, the polymer molecular weight, M, temperature, T, and the concentration, C

$$\tau_1 = a \frac{(\mu-\mu_s)M}{CRT} \tag{45}$$

where a is a constant having a value between .4 and .6.

The result is a criteria for the critical wall stress for onset given by

$$2\pi(\dot{\gamma}/2\pi)\ \tau_1 = 1 \tag{46}$$

or

$$\tau_w^c = \frac{\mu}{\tau_1} = \frac{\mu RT}{a\mu_s \mu M}\ . \tag{47}$$

Equation (47) may be rewritten applying a relation between intrinsic viscosity, molecular weight and molecular dimensions resulting in

$$\tau_w^c \simeq \frac{\text{constant}}{R_G^3}\ . \tag{48}$$

Equation (48) of Fabula provides a better estimate of magnitude of onset shear stress whereas Virk's equation (44) gives a better representation when the constant is determined by a best fit of the data.

As an explanation of the effectiveness of very dilute solutions, Fabula postulated that entanglements or "blobs" of macromolecules, rather than individual molecules, are responsible for drag reduction. This explanation has also been proposed by Kowalski and Brundrett (1974). In their work, a formula has been developed connecting the size of the entangled molecules with the size of a dissipative eddy. The macromolecules entanglement hypothesis was tested to predict the so-called onset of drag reduction in pipe flows of homogeneous polymer solutions.

Darby (1972) presents a comprehensive review of drag reduction theories in which comparison of molecular hypotheses, such as Virk's time scale hypotheses, of which Fabula's and Kowalski's are examples; continuum approaches and conventional length scale boundary layer

modifications are made. The continuum mechanics approach results in the conclusion that the presence of elastic properties in dilute solutions being a sufficient criteria for drag reduction. This is accounted for by the inclusion of a dimensionless time parameter (the Deborah number), which is qualitatively the ratio of a characteristic time of the fluid to a characteristic time of the flow system. A presentation of a dozen different forms of the Deborah number is made illustrating the problems encountered with the present "state-of-the-art" of this approach.

Transition delay from laminar to turbulent flow has been reported by White and McEligot (1970) and is found to depend on where the onset shear stress is reached. If the onset shear stress occurs in the laminar flow region, a delay in transition to turbulent flow can occur.

Extension of the pipe flow data to provide insight into flow over flat plates has been successfully performed by many investigators. Granville (1971) has computed the maximum possible drag reduction on a flat plate of 80% at Reynolds numbers of 10^9. Data on flow over cylindrical bodies are somewhat sparse but evidence of 35% drag reduction by Nadolink et al (1968) for a cylindrical body dropped in a homogeneous polymer solution is representative of the results to be expected.

Polymer Ejection Studies

Practical applications of polymer solutions imply the necessity for injection whether it be for internal or external flows. Since

the polymers have been shown to effect the sublayer resulting in drag reduction, the mechanism of injection, the diffusion process and the quantities of polymers required as compared to the homogeneous flow cases treated previously are of extreme practical importance.

Two approximate methods have been used to treat diffusion patterns in turbulent shear flows. The most widely known method employs the eddy diffusivity model which assumes that the flux of the diffused matter by the turbulent fluctuations is proportional to an eddy diffusivity term, D_e, multiplied by the local concentration gradient

$$q_y = - D_e \frac{\partial c}{\partial y} . \tag{49}$$

Poreh and Hsu (1971) point out that the assumption in this model is that D_e is a function of the flow field. The fact that its value at a point can be specified regardless of the position of the source only holds true for distances from the source that are large compared to the lagrangian integral scale. Measurements made by Poreh and Cermak (1964) indicate that this characteristic holds for turbulent shear flows and the Lagrangian integral scale is of the order of 10 boundary layer thicknesses.

The second method is based on Batchelor's (1957) lagrangian similarity hypothesis. The hypothesis is used to predict the turbulent motion of particles in steady, self preserving shear flows. Cermak (1962) applied the Lagrangian similarity hypothesis to predict diffusion from a continuous point and line source. He concluded that results from application of the Lagrangian similarity hypothesis were significant for the modeling of diffusion.

Hsu (1971) and Poreh and Hsu (1971) applied the technique to predict the diffusion boundary layer growth in the intermediate, transition and final zones for polymer flows. Applying the Lagrangian similarity hypothesis, the following equations resulted describing the change of the mean vertical position $\bar{y}$, and the mean longitudinal position $\bar{x}$, for an ensemble of single particle releases

$$\frac{d\bar{y}}{d\tau} = bv^* \tag{50}$$

where b is Batchelor's constant, and

$$\frac{d\bar{x}}{d\tau} = u(\bar{y}). \tag{51}$$

Combining yields

$$\frac{d\bar{y}}{d\bar{x}} = \frac{bv^*}{u(\bar{Y})}. \tag{52}$$

Ellison (1959) estimated Batchelor's constant to be given by b = K. His analysis further suggests that $\bar{y}$, the mean position of particles at a given cross section x, is equal to $\bar{Y}$, the mean position of single particle releases when $\bar{x} = x$. The mean position of particle at any cross section x may be defined as

$$\bar{y} = \frac{\int_0^\infty cy\, dy}{\int_0^\infty c\, dy}. \tag{53}$$

By replacing y with y/δ_d where δ_d equals the value of y when C/C_{max} is .5 and c by

$$\frac{C}{C_{max}} = f\left(\frac{y}{\delta_d}\right).$$

Equation (53) may be integrated to yield

$$\bar{y} = a_1 \delta_d . \tag{54}$$

Substituting (54) into (52) results in an expression for the development of the diffusion boundary layer with distance x

$$a_1 \frac{d \delta_d}{dx} = \frac{bv^*}{u(\bar{Y})} . \tag{55}$$

Hsu (1971) has found that better agreement with data occurs if the constant b in (47) is replaced with

$$b = K(1 - \frac{\bar{Y}}{\delta}) . \tag{56}$$

Figure 4 displays a plot showing the growth of the diffusion boundary layer within the momentum boundary layer and depicting the several zones of diffusion.

The above method was applied assuming similarity in concentration profiles with those observed by Poreh and Cermak (1964) for two-dimensional turbulent mixing of ammonia gas from a wall line source. Poreh and Cermak envisioned a four-zone process which is worthy of description since the concentration profiles have come under much study as being representative for polymer diffusion. The four zones as defined by Poreh and Cermak are: (1) the initial zone - very little reliable data were obtained in this region due to very large velocity and concentration gradients. The extent of the zone (x/δ) was not determined. (2) The intermediate zone - the diffusing plume is submerged in the boundary layer, but its thickness is large compared to that of the laminar sublayer. Diffusion in this zone depends only

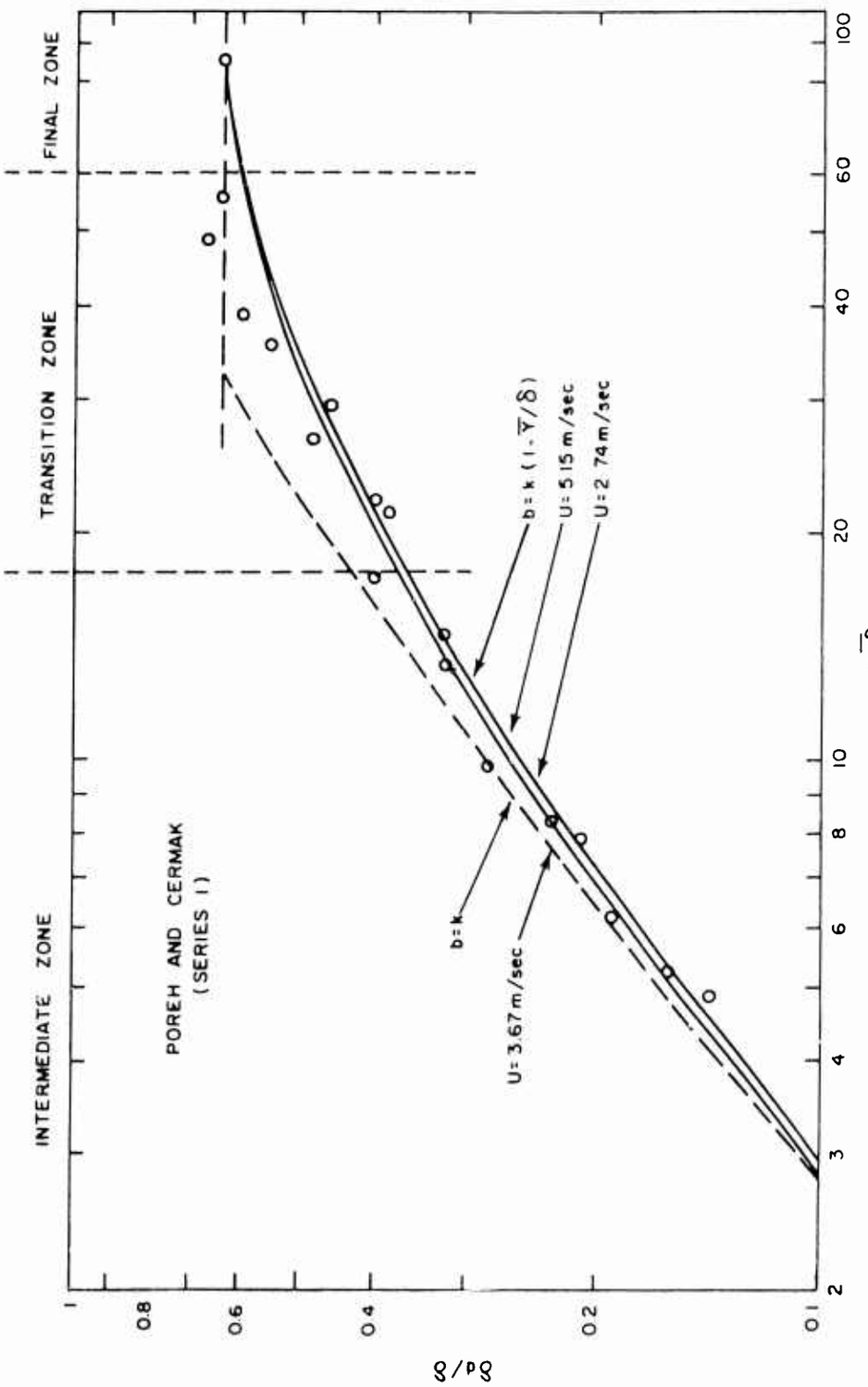

Figure 4. Growth of the diffusion boundary layer within the momentum boundary layer. (from Hsu (1971))

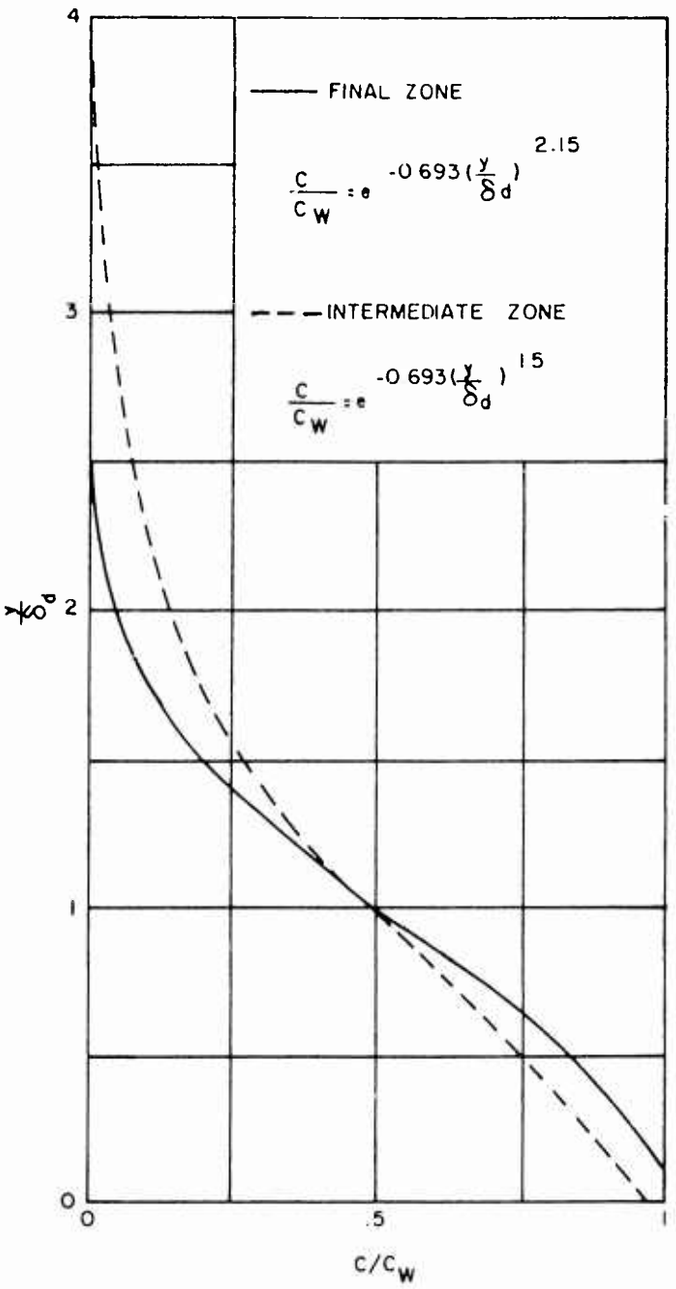

Figure 5. Concentration profiles in the intermediate and final zones

slightly on the rate of the boundary layer growth. The upper limit of the zone is about $x/\delta = 18$. (3) The transition zone - this zone provides for a decrease in the rate of growth of the diffusing plane and to gradually change the shape of the concentration profile. Within this zone $18 < \frac{x}{\delta} < 60$. Downstream of this zone, $\frac{x}{\delta} > 60$, the diffusion plane grows at the same rate as the boundary layer. (4) The final zone - diffusion is again controlled by molecular action.

Morkovin (1963) described the data taken by Poreh and Cermak as shown below:

$$\frac{c}{c_w} = e^{-0.693(y/\delta_d)^{1.5}} \qquad \text{intermediate zone} \qquad (57)$$

$$\frac{c}{c_w} = e^{-0.693(y/\delta_d)^{2.15}} \qquad \text{final zone.} \qquad (58)$$

Figure 5 displays a plot of the concentration profiles in the intermediate and final zones.

Wells (1968) suggested uniform injection through a porous wall since it raises the additive concentration to the drag reducing level in the wall region only. Using a Reynolds - Prandtl analogy to analyze the diffusion process, he calculated that distributed ejection would require 40 to 140 times less additive than slot ejection for equivalent drag reductions.

Walters and Wells (1971) conducted tests using uniform ejection of polymer solution through sintered stainless steel smooth cylinders. Fully developed turbulent flow was achieved in the test section. Concentration and velocity profiles measurements were made at

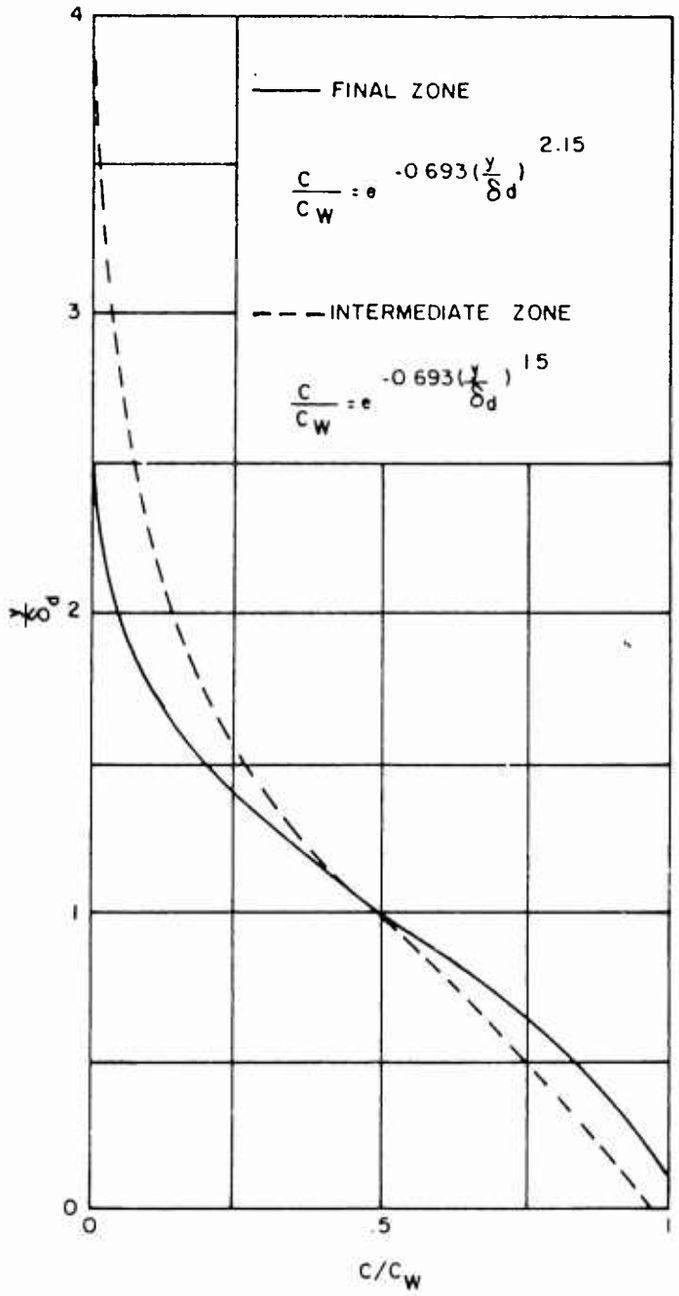

Figure 5. Concentration profiles in the intermediate and final zones

several different downstream distances. Pressure drops were also measured in the facility to give information on the friction reduction. The concentration measurements were made by using a fluorometric method. Uranine B was used as the fluorescent dye rather than several other dyes, since the laboratory apparatus could be easily decontaminated. The dye was mixed with the ejection fluid and then the tracer sample concentration measured with a fluorometer. Accuracies of the measurement instrumentation of two parts per billion are reported. The conclusions from the study are very interesting. The study showed that the porous wall approach to injection required lower quantities of additives for equivalent drag reduction than by slot ejection. For certain conditions of high polymer mass flux, a wall friction increase possibly due to the higher viscosity in this region was noted. As compared to water injection, a one or two order of magnitude reduction in total diffusivity in the ejection region was evidenced. Downstream of the ejection, an order of magnitude reduction of total diffusivity was noted along with a significant reduction in wall friction.

Latto and Shen (1970) performed an experiment of slot ejection over a flat plate positioned in a flume. Using hot film anemometry, it was found that the momentum diffusivity was less than for pure water. The velocity of injection was also found to be important. It was found to be desirable to keep the injection velocity as low as possible, and tangential to the surface.

Wetzel and Ripkin (1970) experimentally studied polymer injection into a developing boundary layer in a 9-ft-wide open channel. Polymer solutions were injected parallel to the flow near the bottom wall. Pitot tubes were located at positions 16, 28, and 40 feet downstream of the injection slot. Measurements indicated similar velocity profiles at each station. Several methods of polymer concentration determination were investigated. The fluorometric method was found to give satisfactory results. The resulting concentration profiles for water, 1000 WPPM, 2000 WPPM, and 3000 WPPM were found by the author to be in good agreement with the curves developed by Morkovin (1963) described previously.

A maximum drag reduction of 35% was achieved over 40-ft boundary length. Further, at a distance of 16 ft from the slot, greater drag reduction was attained for the low quantities ejected than for the higher. At further downstream distances, the reverse was true. The behavior was attributed to more complete mixing. Large wavering parallel streakes were evidence shortly after injection when the polymer was color dyed. The streaking was reported to be a secondary three-dimensional vortex motion superimposed on the two-dimensional flow.

Fabula and Burns (1970) invoked the negative roughness analogy to flat plat flow with polymers so that the outer layer mean velocity similarity is unaffected by friction reduction. The similarity law of mixing with polymeric friction is predicted to be the same as without polymeric friction reduction. Proceeding with this assumption, a relation for calculating the local additive concentration at downstream stations along the wall was developed. The study includes the effects

of turbulent intermittency and the similarity profile for the local additive concentration as formulated by Poreh and Cermak.

Lessmann (1970) extended this work to the case of a body of revolution with the final result:

$$Q_i C_i = 2\pi r_o \int_o^\infty \bar{u}\,\bar{c}\,\left(\frac{1 + y \cos \theta}{r_o}\right) dy \qquad (59)$$

where the terms are in accordance with Figure 2.

Wu and Tulin (1970) presented experimental data obtained by injection of various polymer concentrations along a smooth and rough flat plate. The general conclusions were that the slot ejection angle should be small with respect to the flow direction and the slot width should be comparable with the thickness of the viscous sublayer. It was also shown that a large drag reduction was obtained by ejecting the additive solution at a rate comparable to the normal viscous discharge. The choice of additive concentration of the ejected solution is governed by the length of the boundary and its roughness. These findings suggest that smaller amounts of additives are needed for injection than are usually estimated.

Tullis and Ramu (1973) studied the characteristics of mean turbulent flow in the entrance region of a rough pipe for water flow and for polymer injection into a boundary layer. A 12-inch diameter, 200-ft-long steel pipe was used for the study. Polymer was injected through a perforated wall pipe section. Drag reduction of up to 80% in the fully developed region and 90% in the inlet region were measured. Comparison between water and dilute polymeric solution injection showed that polymer concentration profiles developed slower

than that of dye in water, indicating lower diffusivity. The inlet length needed for flow to fully develop was found to be greater for polymer injected flows than for the case of no injection.

Fruman and Tulin (1974) performed a study of diffusion of a thin tangential jet of polymer solution injected into the turbulent boundary layer of a flat plate suspended in a high speed channel. Free-stream Reynolds number in the order of 3.6×10^7 were achieved. Drag measurements by reluctance force guages and wall concentrations measured by a light intensity dyed additive method were taken. The concentration distribution along the wall was found to be represented by two regions. Within the first region the wall concentration is practically constant and equal to the injected polymer concentration. In the second region, the concentration varied inversely with the distance from the injection slit. The length of this first zone was some 15 to 20 times that of water injection. The length of this first zone appears to be directly related to the thickening of the viscous sublayer, the reduction of shear stress and the decrease of molecular diffusivity. The data taken correlates well when formulated using a heat transfer analogy to the temperature distribution over a flat plate. The distribution of the wall temperature, T, as given by Seban (1960)

$$\frac{T}{T_i} = 25.0 \left(\frac{\rho_i v_i}{\rho u}\right)^{1.2} \left(\frac{x}{s}\right)^{-0.8} . \qquad (60)$$

Tulin's data for $\rho=\rho_i$ yields

$$\frac{c_w}{c_i} = 17.01 \left(\frac{v_i}{U}\right)^{1.06} \left(\frac{x}{s}\right)^{-0.711} . \qquad (61)$$

These results reported by many investigators represent clear evidence of the need for additional information regarding injection of polymers in external flows and their effect on the diffusion process. There appears to be some discrepancy in the measured concentration profiles between investigations and to the definition of the zones where the diffusion process for polymer flows varies from that of water. This will be the central thought guiding this study.

III. EXPERIMENTAL APPARATUS

The experimental apparatus used in this research consists of a clear plastic drop tank, a launcher, several test models and appropriate instrumentation and photographic equipment to measure model velocity, to deduce boundary layer thickness and to measure boundary layer concentration profiles. Figures 6 and 7 show the major elements of the experimental apparatus. The characteristic of each of the above elements is discussed below.

Drop Tank

The drop tank facility consists of a 20-ft long clear plastic cylinder 2 ft in diameter. Several viewing collars are available as noted in Figure 7 which may be positioned where desired. These viewing collars, when filled with water, minimize optical distortion due to the tank wall curvature. The liquid in the tank is continuously filtered, excepting during testing periods, to maintain high clarity. Located to either side of the tank are instrumentation platforms which may be set in any vertical position desired. A shock pad consisting of several layers of dense rubber topped with rubberized horsehair pads totalling approximately 1-ft thick is installed at the bottom to absorb the energy of models being dropped. An .062-inch diameter stainless steel wire is suspended down the center of the tank with the other end weighted to approximately 75 lbs. All models were guided down the tank by this wire. The drag of the wire on the bodies has been determined

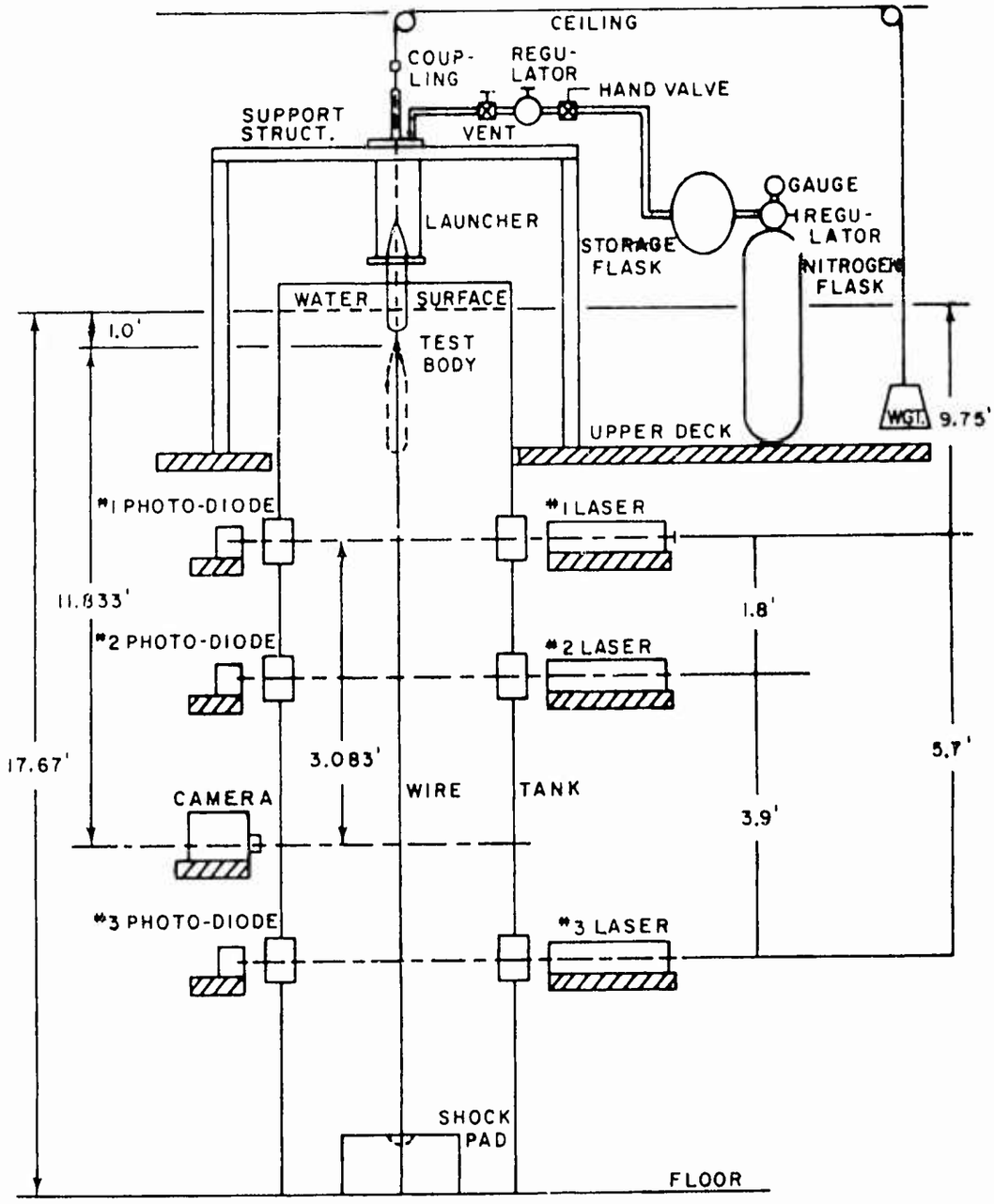

Figure 6. Experimental apparatus

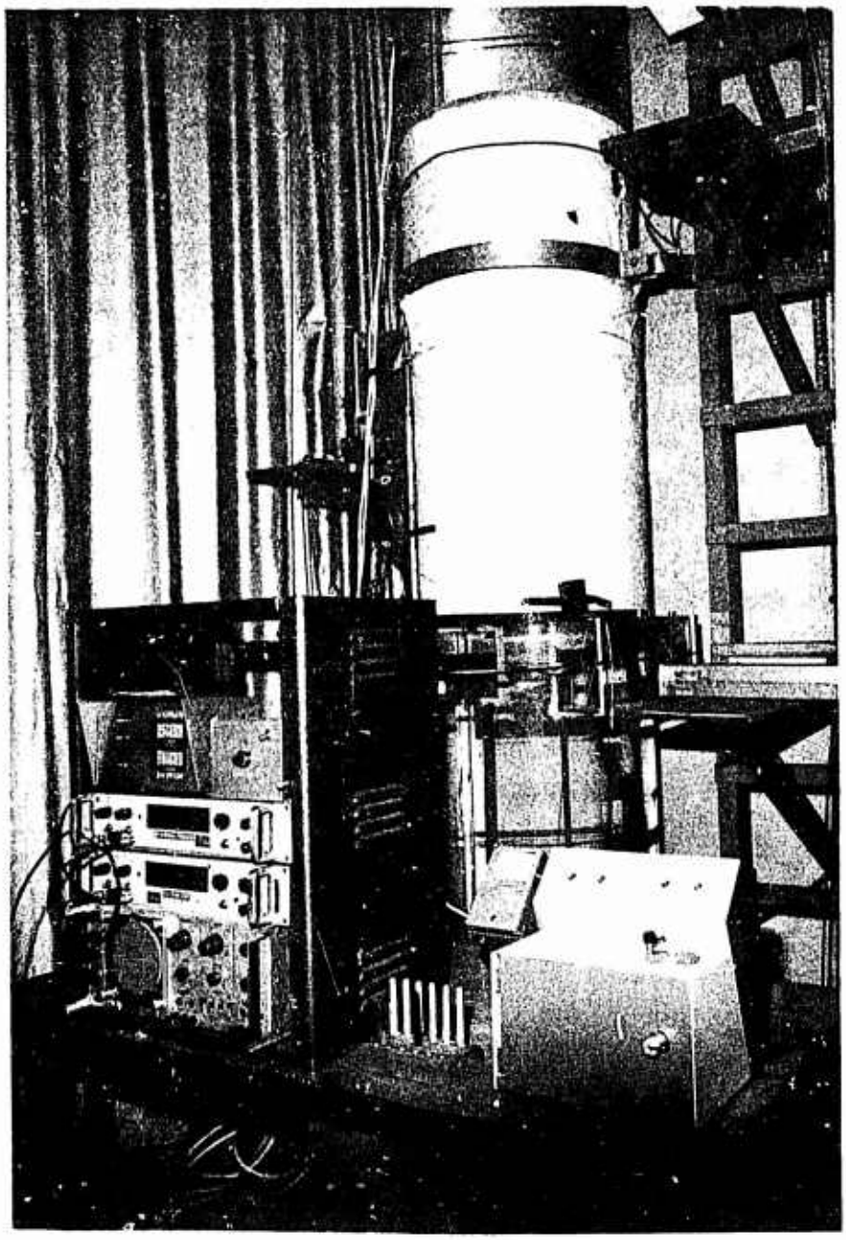

Figure 7. Experimental apparatus photograph

by a free fall sphere experiment with similar guide bearings installed in the sphere. The bearing drag force determined is approximately .1 lbs.

Launcher Assembly

A launcher was deemed necessary in order to obtain steady state velocities in the short drop tank and avoid the problem of predicting boundary layers under a transient condition. Figure 6 schematically shows the launcher components and Figure 8 displays the actual launcher used in many of the tests. As can be seen in Figure 8, the launcher is required to accelerate the test bodies very quickly in a very short distance resulting in high accelerations and, to the dismay of occupants of the building, the launcher ram must stop in a shorter distance with even higher deaccelerations.

The launching problem consists of accelerating a body of approximately 10 lbs weight, plus accelerating launcher components weighing approximately 20 lbs to a desired velocity of 30 ft/sec, the maximum velocity considered for the tests to be performed, in a distance of 24 inches. Applying the impulse momentum relation

$$\int F\,dt = \int M\,dv \tag{62}$$

where F = the force required (neglecting drag on the body)

t = time for acceleration

v = velocity

M = mass of launcher components and body under acceleration.

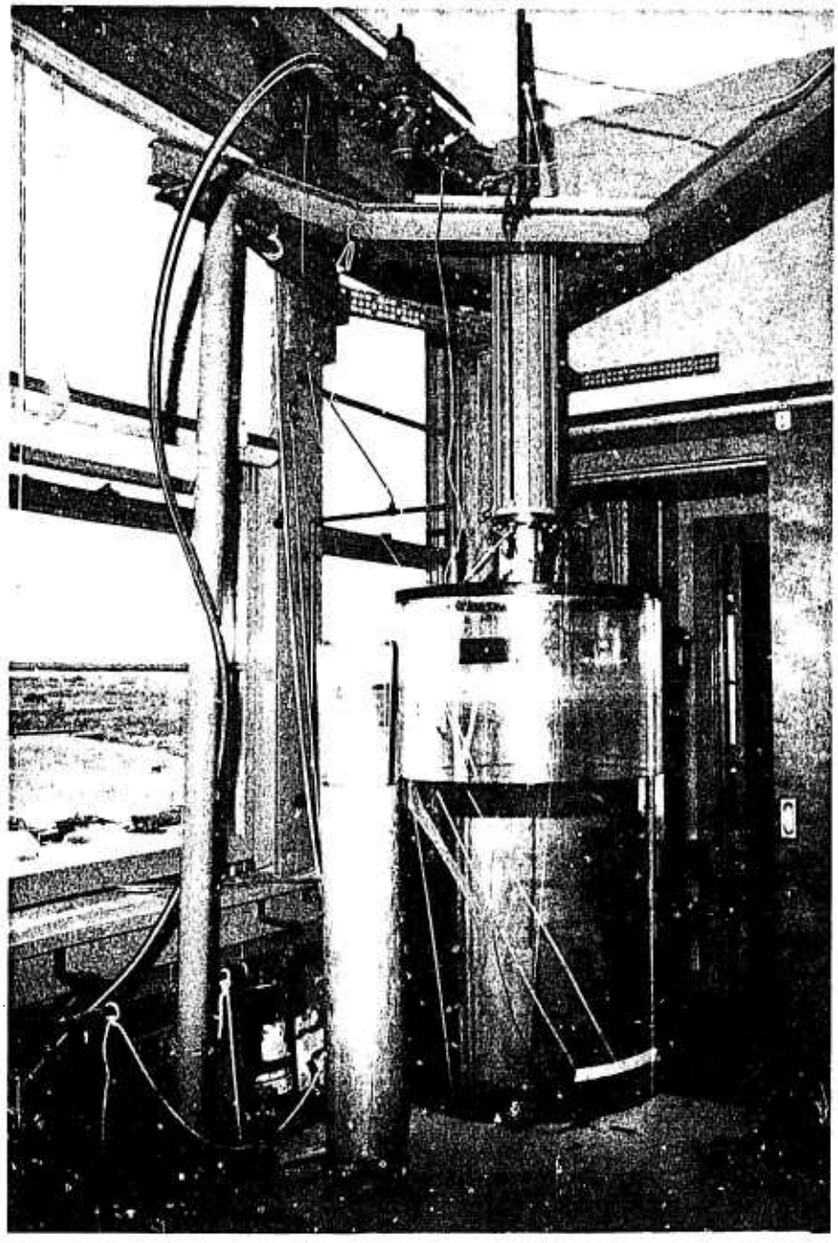

Figure 8. Launcher assembly photograph

The time for an acceleration, a, to 30 ft/sec velocity in 2 feet is given by

$$t = \frac{v}{a} . \tag{63}$$

Determining the acceleration

$$x = \frac{1}{2} at^2 = \frac{1}{2} \frac{v^2}{a} . \tag{64}$$

Rearranging and solving

$$a = \frac{1}{2} \frac{v^2}{x} = 225 \text{ ft/sec}^2 . \tag{65}$$

Substituting in (63) yields

$$t = .1333 \text{ sec} . \tag{66}$$

Integrating (62) with the established limits gives

$$t = 0 \qquad v = 0$$

$$t = .1333 \text{ sec} \qquad v = 30 \text{ ft/sec}$$

$$.1333 \, F = \frac{30}{32.2} \, (30)$$

$$F = 210 \text{ lbs.}$$

A steady force, therefore, of 210 lbs would do the job. Figure 9 is an assembly drawing of the launcher constructed. The chief components of the launcher come from a high pressure hydraulic damper cylinder normally operated at 3000 psi. For safety reasons, this was satisfying since the pressures that the cylinder would be subjected to in this work were low but the shock loads high. The overall cylinder length was about 2 feet with a working piston diameter of 4.550 in. Fitted to the end of the piston was a conical

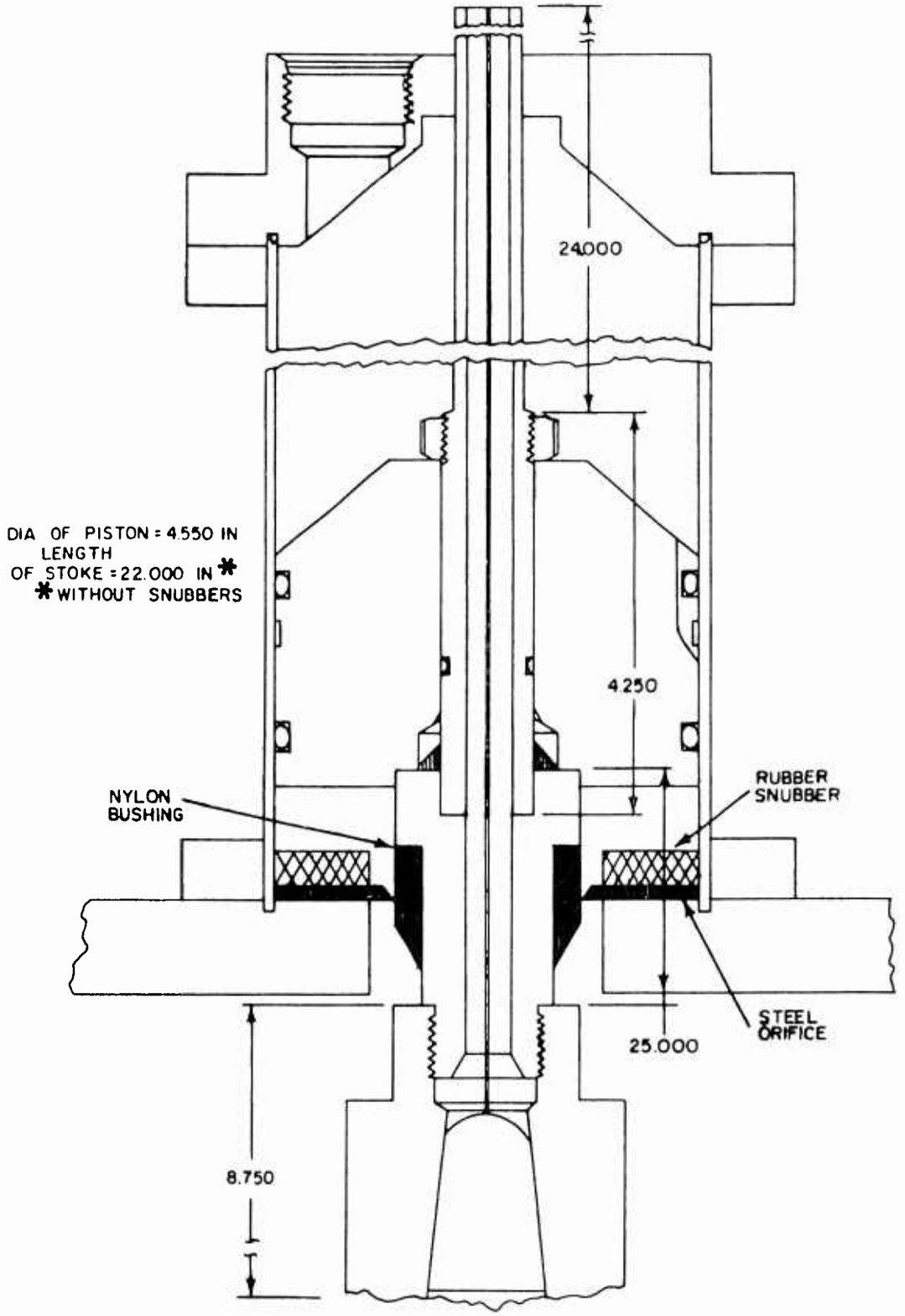

Figure 9. Launcher internal schematic

adapter which would mate with the 6^{0} tailcone of the prime test model. The total piston assembly including upper guide, piston and lower extension pieces was approximately 62 inches. All pieces were designed to minimize weight. A pressure over the piston of 14 psi should then provide the necessary acceleration force. The problem was to get the working fluid safely to the piston quickly enough.

The remainder of the launcher system, Figure 6, consisted of a high pressure nitrogen supply (2200 psi) regulated down to 150 psi, stored in a 4-cubic ft storage flask whose contents in turn were allowed to pass through a hand operated "fire" valve through a high flow low pressure regulator to the launcher itself. All pressure lines were maintained as large as possible (#12 AN) where equipments permited. The launcher chamber pressure was recorded on a Sanborn recorder so that launch velocities could be varied by varying the low pressure regulator output pressure in a predetermined fashion.

Through tests, it was found that a much higher final pressure was required to achieve 30 ft/sec ejection velocity. A final pressure of about 60 psi was required to account for the inertia of the low pressure regulator and the losses in the delivery line. The launcher has successfully been used in several hundred launches.

Velocity Measurement Instrumentation

The velocity measurement instrumentation consists of three laser photo-diode stations with known separation as shown in Figures 6 and 7. The lasers are 5 milliwatt helium neon lasers manufactured by Spectra Physics (Model 120). Lasers were used rather than a conventional light source to insure that a sharp cutoff of light by the body would occur. This was especially critical where measurements across the body length dimensions were made. The silicon photo-diodes used to detect the light cutoff were United Detector Technology, Model PIN-020A. Their response time is in the order of 5 nanoseconds, well exceeding the requirements of this investigation.

The outputs of these diodes when amplified was used to trigger two Hewlett Packard counters and a special purpose dual counter. These may be seen in Figure 6 in the instrumentation rack. The bottom instrument was only used for troubleshooting work with the equipment. The instrumentation was so arranged to allow measurement of the velocities, referring again to Figure 6, between stations 1 and 2, 2 and 3, 1 and 3, and across the body (nose to tail) at station 3. Four velocities in all were measured across a total span of 5.7 feet to less than 2 feet. For all except the last measurement, only the breaking of the light beam by the nose of the model was used to start the counters. This is rather important since although the model travelled down the center of the

tank guided by a wire, small lateral movements, especially with the 6° tapered tail model, would result in rather large unknown discrepancies in effective length of the model (where the laser intercepts the model on entrance and exit) and as a result, in the velocity measurements. Lateral motions did not seriously effect measurements taken from the nose of the model at subsequent stations since the curvature of the nose is gradual, introducing less error, and since all lasers were positioned on one side of the wire, at about .25 inches offset, resulting in approximately the same lateral offset at each station if such occurred.

Boundary Layer Thickness Measurements

The title of this section is a misnomer of sorts since actual boundary layer measurements in a drop tank experiment of this type could only be performed with extreme difficulty. Especially in the size of free falling model being tested (3-inch diameter x 25 inches long). In fact, what has been done is eject from the test bodies a visible opaque dye and photograph the body and its "boundary layer" at a given position. The assumption is that for a dilute polymer solution, the molecular diffusivity and viscosity are very close to those of the solvent. As concluded by Fabula and Burns (1970) for a far downstream case, the similarity law of mixing with polymeric friction reduction is predicted to be the same as it is without polymeric friction reduction. Two types of dyes

were used; the first, a food coloring, gave excellent results and photographic records but reduced the number of tests to 3 to 4 per day due to the resulting opaqueness of the tank. The second, phenolphthalein solution, was used as an alternative. The solution PH was kept sufficiently low, below 10, so as to not effect the polymers used (this was verified by drag reduction measurements - no velocity changes noted with or without the dye). The dye gave excellent photographic results and disappeared within seconds due to the mixing with the water and the resultant lowering of the dye PH. It is assumed for the dye as with polymers that the diffusivity would be equal to that of the solvent.

Figures 6 and 7 show the camera station. A graphic camera and Polaroid, 4" x 5" colored film was used for the photographic records. The shutter of the camera was fixed open just prior to launch and a signal from the first laser station adjustably delayed from the instrumentation console would trigger three flash units exposing the film. The adjustable delay allowed for correction for velocity changes on different tests or to photograph different segments of the body on subsequent but similar tests. Velocity of the vehicle on a run-to-run basis for the same conditions was found to be in the order of 2% allowing for accurate presetting of the delay by a calibrated vernier.

Test Models

Four axisymmetric models were constructed for use in the test program. Three of these are called the dye ejecting bodies and the fourth, the polymer ejecting body. Their purposes are different in that the dye ejecting bodies are used for drag measurements and for boundary layer photographs and the polymer ejecting body is used for polymer ejection, boundary layer concentration measurement studies. This latter body could also be used, when loaded with visible dye, for boundary layer photographic studies. The models all had a maximum diameter of three inches and an identical forebody design. In fact, the dye ejecting models all used the same forebody with replaceable tail pieces. The forebody chosen for application is a classical "half body" with a length-to-diameter ratio of 3.88. The classical half body shape is defined by placing a source, of strength m, in a uniform stream. The resulting shape is defined by the equation

$$r_h = R_o \sec \frac{\phi}{2} \tag{67}$$

where $R_o = \frac{D}{4}$

and the coordinates are defined from the source as shown in Figure 10. The body normally extends to infinity but was terminated at 11.65 inches for the models constructed. The half body was chosen for use since it presented a very streamlined, tractable shape for the prediction of pressure coefficients. The equation for the bodies, in x and r_o coordinates will be given in subsequent sections.

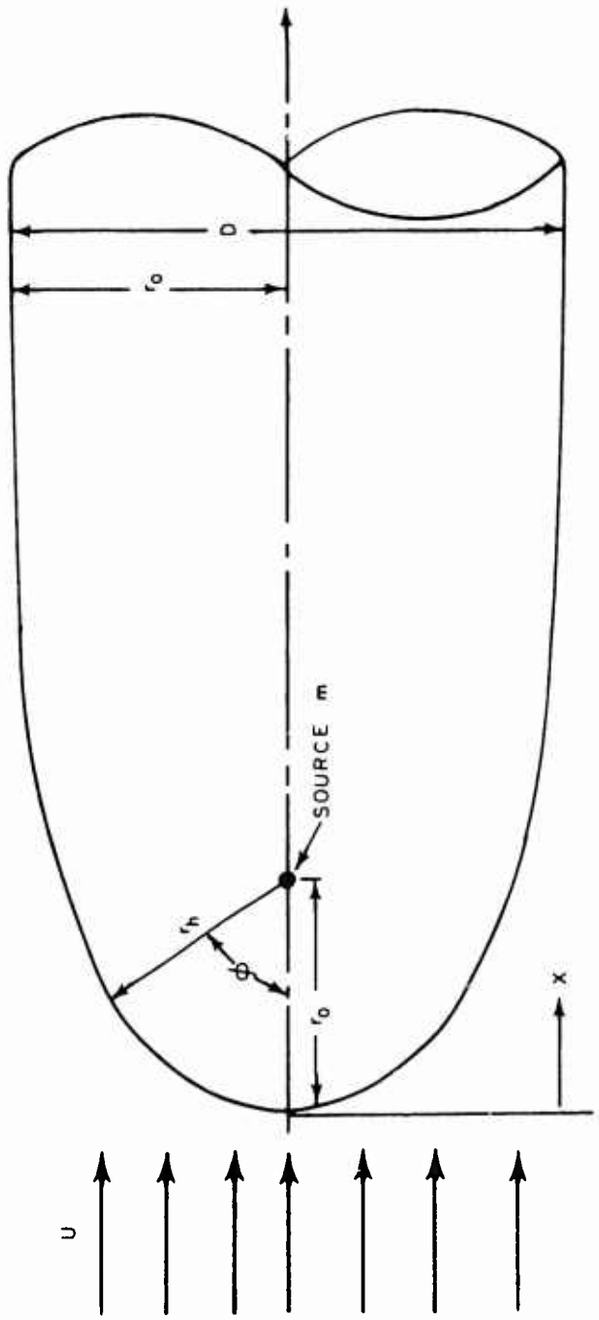

Figure 10. Half body coordinator

Dye Ejecting Bodies

Three different configurations of dye ejecting bodies were constructed. Each uses the same half body forebody discussed previously followed by a three-inch long spacer section of constant three-inch diameter. The various tail pieces were assembled to this assembly. The tail pieces constructed were a 6° tapered tail (12° included angle) terminating in a .5-inch diameter sphere, a 12° tapered tail (24° included angle) terminating in a .5-inch diameter sphere and a 3-inch diameter hemispherical tail piece. Figures 11, 12 and 13 are photographs of the three test models. The equations for the external shape of the bodies measured from the nose as shown in Figure 10 are given by:

Half Body Section

$$r_o = .079 + 4.346x - .1022x^2 + .122x^3 - 5.29x^4 \qquad (68)$$

for $0 < x \leq .981$ inches

and

$$r_o = .924 + .3296x - .0669x^2 + .000555x^3 - .000161x^4 \qquad (69)$$

for $.981 < x \leq 11.65$ inches.

Constant Diameter Section

$$r_o = 3 \text{ inches} \qquad \text{for } 11.65 < x \leq 14.65 \text{ inches} \qquad (70)$$

6° Tapered Tail

$$r_o = -.100511\,x + 2.9686$$

for $14.65 < x \leq 24.58$ inches. (71)

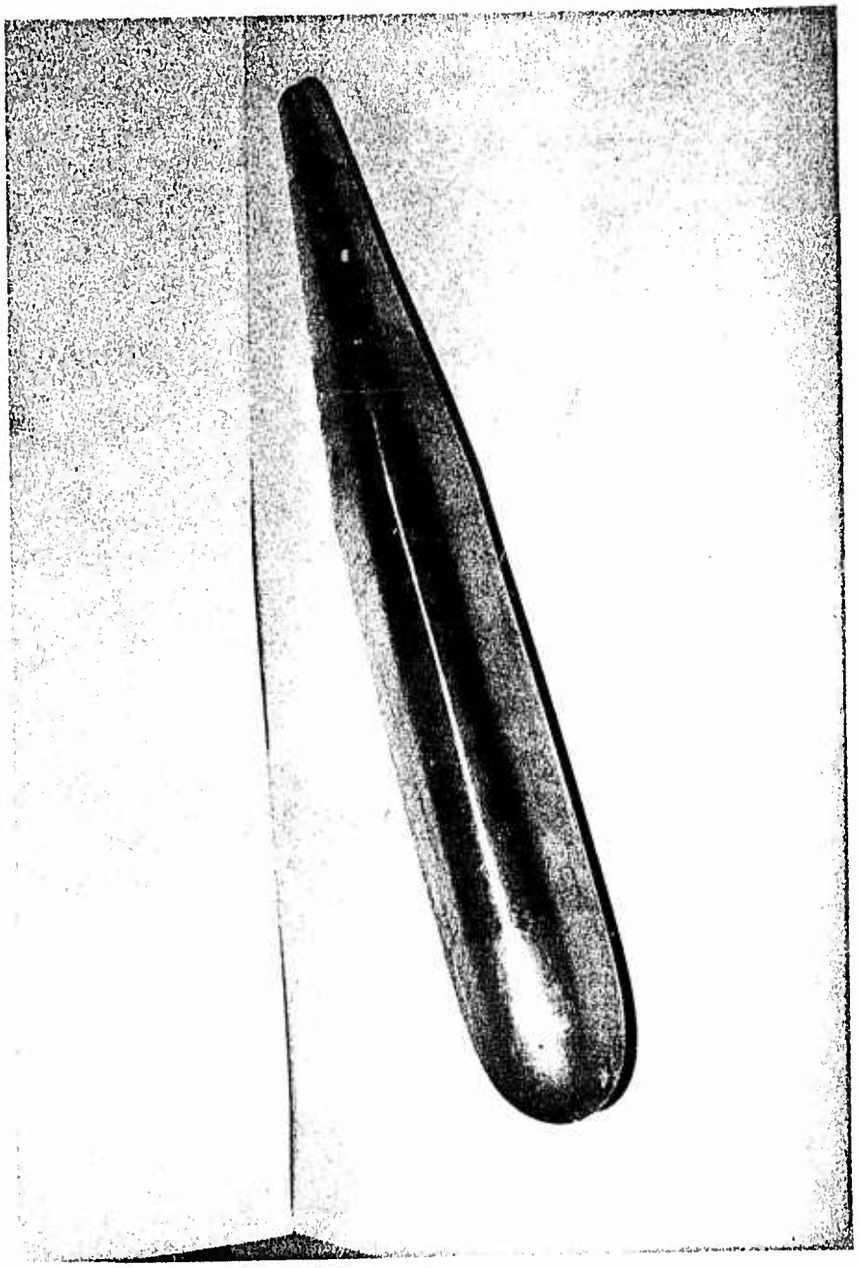

Figure 11. 6° ejecting model

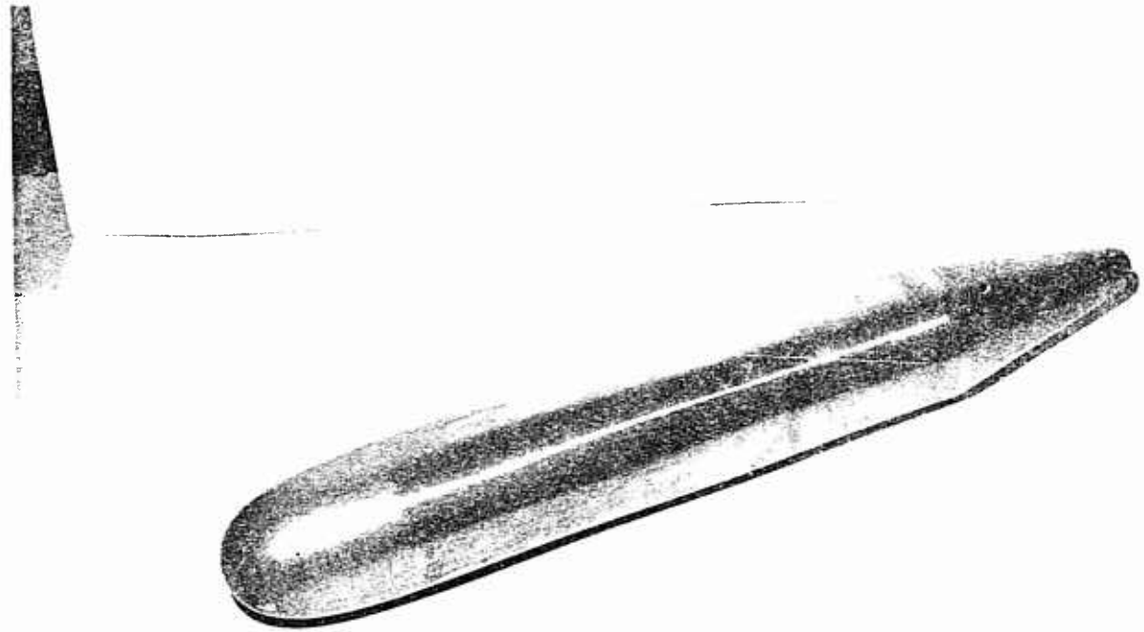

Figure 12. 12° ejecting model

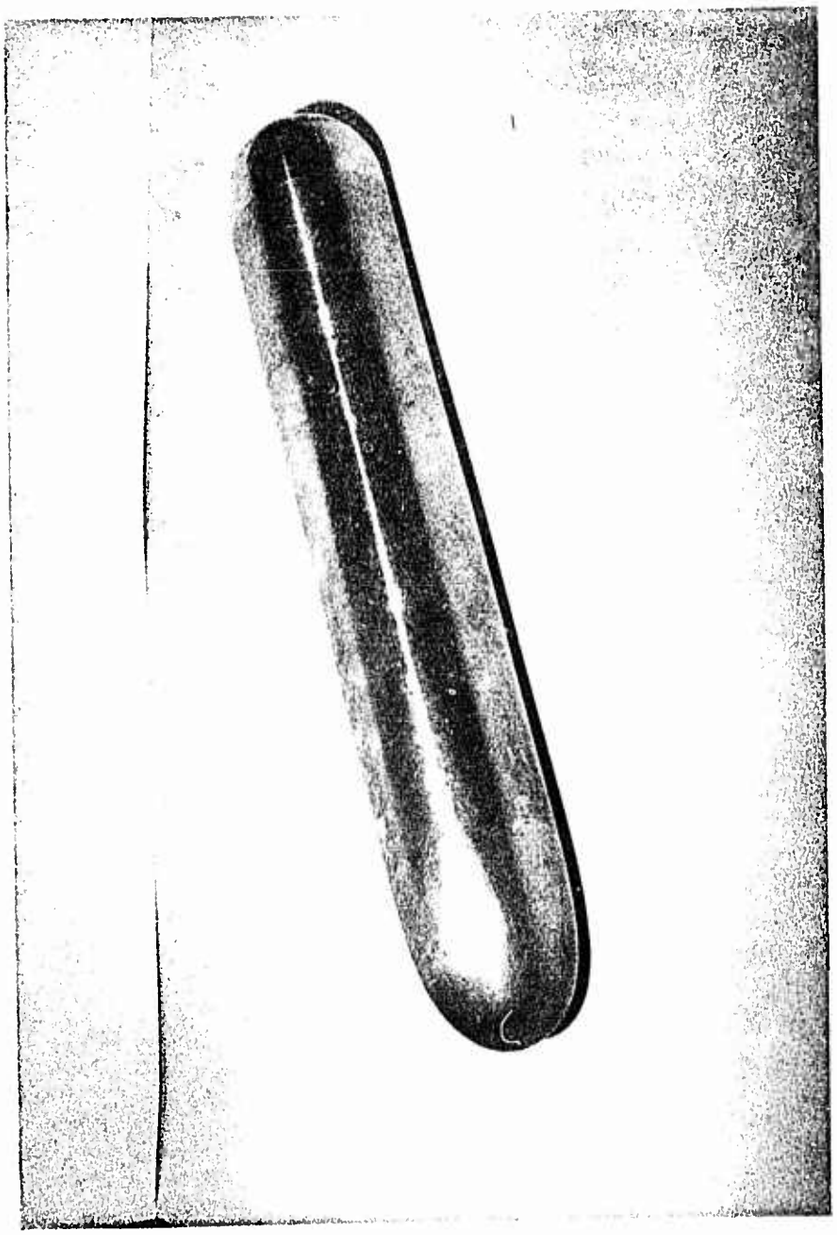

Figure 13. Hemispherical tail dye ejecting model

Hemispherical Tail for 6° Cone

$$r_o = \left[.25 - (x - 24.58)^2\right]^{\frac{1}{2}} \qquad (72)$$

for $24.58 < x \leq 25.04$.

Equations (68) through (72) described the boundary for the 6° model. The conical tail assembly was blended to the cylindrical section to remove the abrupt change in contour at that point. Continuing with the body equations:

12° Taper Tail

$$r_o = -.20842\, x + 4.6145 \qquad (73)$$

for $14.65 < x \leq 19.65$ inches.

Hemispherical Tail for 12° Cone

$$r_o = \left[.25 - (x - 24.58)^2\right]^{\frac{1}{2}} \qquad (74)$$

for $19.65 < x \leq 20.15$ inches.

Equations (68), (69), (70), (73) and (74) describe the external boundary for the 12° model.

Hemispherical Model

Constant Diameter Section

$$r_o = 3 \text{ inches} \qquad \text{for } 11.65 < x \leq 15.132 \text{ inches.} \qquad (75)$$

Hemispherical Tail

$$r_o = \left[2.25 - (x - 15.132)^2\right]^{\frac{1}{2}} \qquad (76)$$

for $15.132 < x \leq 16.632$ inches.

Equations (68), (69), (75) and (76) form the equation for the hemispherical tail model.

All bodies were constructed of aluminum and allowed for the addition of weights for matching of velocities when testing the

models under increased drag conditions. Figures 14 and 15 describe the body components and features. Referring to the figures, an explanation of the operation of the model will b . describe the function of the various pieces. The model is made ready for a launch by inserting the tank guide wire through the body guide tube, (9), the wire bears on a nylon bearing at either end of the model to minimize friction. The tail, (10), of the model is removed (separated sufficiently) and the internal cavity filled with dye. The dye ejection ports (6) being previously taped over to insure no loss of dye. The model is reassembled and the vent screw (unmarked) in the tail is removed and the model placed under the water level in the tank to back fill the cavity totally with water. The model may now be fired upon removal of the tape over the ejection holes. When fired, stagnation pressure enters the 4 stagnation ports, (1), is transmitted through the body guide tube and pressurizes the bladder, (4), forcing the dye out the four dye ejection ports located at the minimum pressure point of the forebody as determined by a potential flow program. After several tests, the bladder was found to be not necessary simplifying the operation. The stagnation ports consisted of 8, .050 inch diameter holes located on a .625 inch circle at the nose of the body. The four ejection ports were also .050 inch diameter placed on a 1.125-inch diameter circle, normal to the surface of the body. Table 2 summarizes the pertinent information about the bodies.

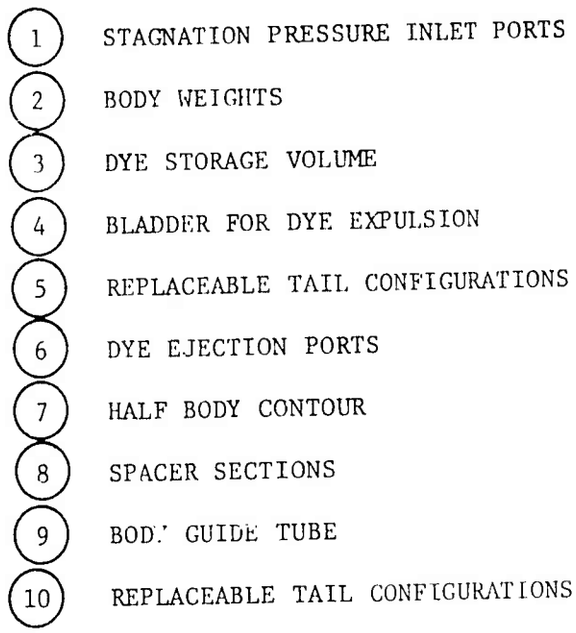

Figure 14. Dye ejecting axisymmetric body description

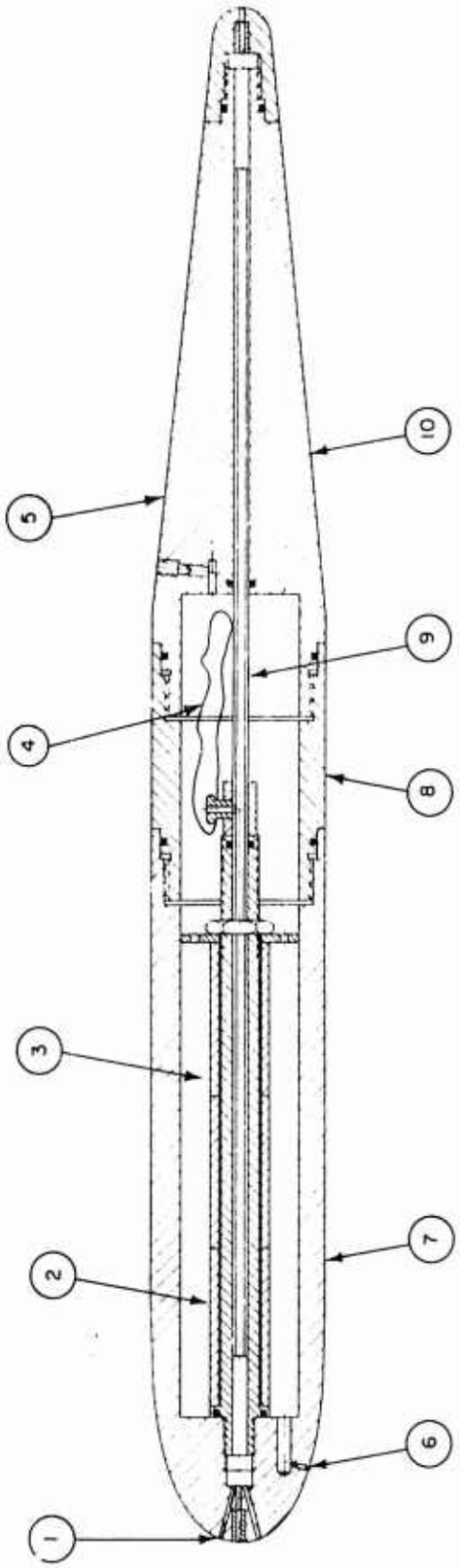

Figure 15. Dye ejecting axisymmetric body schematic

TABLE 2

Dye Ejecting Axisymmetric Body Information

	6^{o} TAIL	12^{o} TAIL	HEMISPHERICAL TAIL
LENGTH (FT)	2.0833	1.679	1.386
DIAMETER (FT)	.25	.25	.25
L/D	8.33	6.7	5.54
FRONTAL AREA (FT^2)	.0491	.0491	.0491
WEIGHT IN WATER (LBS)			
WEIGHTED	4.43	7.109	3.95
UNWEIGHTED	3.47	-	2.94

Polymer Ejecting Body

The polymer ejecting body is similar in external configuration to the 6^{o} dye ejecting body. The equations for the external shape hold for this body. The body nas been designed to perform two functions while traversing the length of the drop tank. These functions are:

1. Eject polymer or other fluids at a constant rate
2. Withdraw samples from the boundary layer at four axial stations

Figures 16 and 17 describe the various elements of the ejecting body. These elements may be viewed in assembled and disassembled form in Figures 18 and 19, respectively. The overall dimensions of the model are 25 inches in length by 3 inches in diameter. Prior to discussing the design values of the various elements, a

1. POLYMER EJECTION SCREEN
2. BOUNDARY LAYER SAMPLE TUBES
3. BOUNDARY LAYER SAMPLE COLLECTION CHAMBER
4. POLYMER SOLUTION STORAGE VOLUME
5. SUCTION PISTON FOR BOUNDARY LAYER SAMPLING
6. POLYMER EJECTOR PISTON AMBIENT PRESSURE BACKFILL VOLUME
7. POLYMER EJECTOR PISTON PRESSURIZATION AREA
8. CO_2 ORIFICE AND PUNCTURE NEEDLE
9. CO_2 SUPPLY
10. HALF BODY CONTOUR
11. VOLUME AVAILABLE FOR WEIGHT
12. POLYMER EJECTOR PISTON
13. POLYMER EJECTOR PISTON STROKE MEASUREMENT ROD
14. CO_2 SUPPLY ACTIVATION DEVICE
15. BODY GUIDE TUBE

Figure 16. Polymer ejecting axisymmetric body description

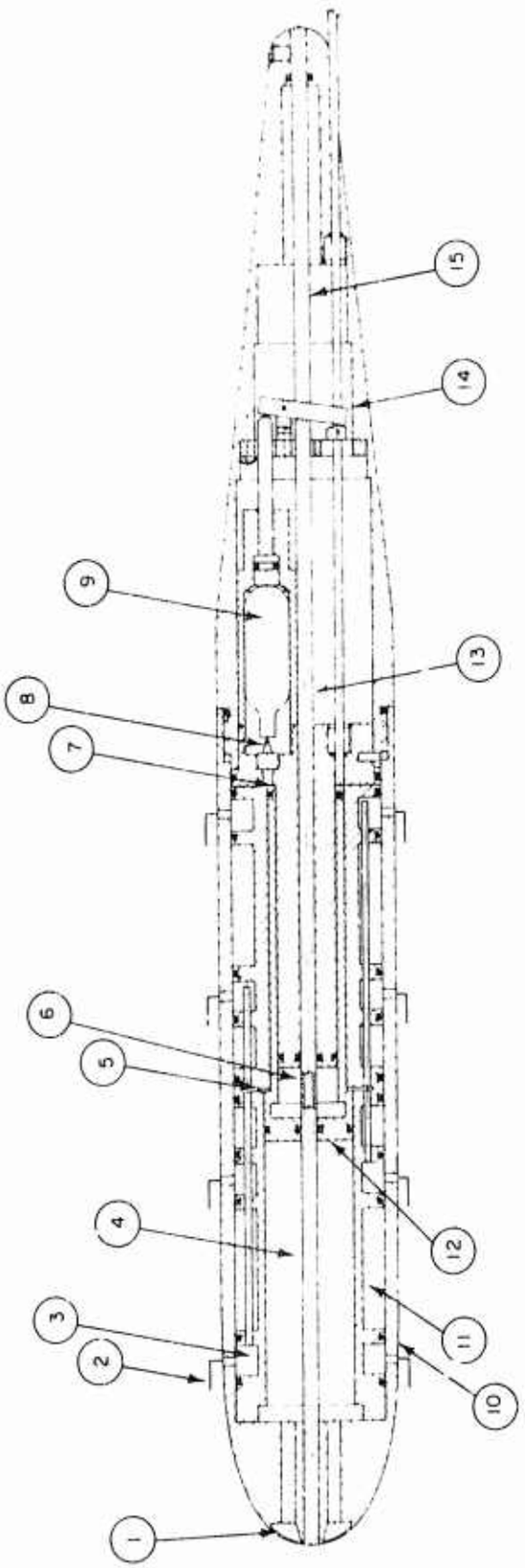

Figure 17. Polymer ejecting axisymmetric body schematic

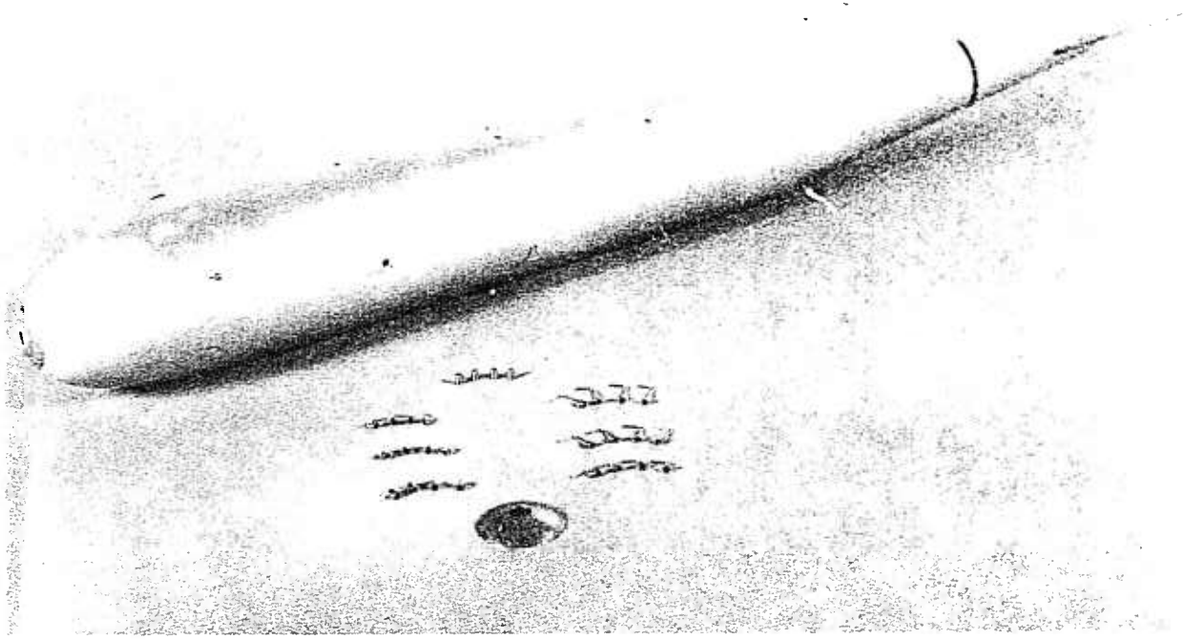

Figure 18. Polymer ejecting axisymmetric body photograph

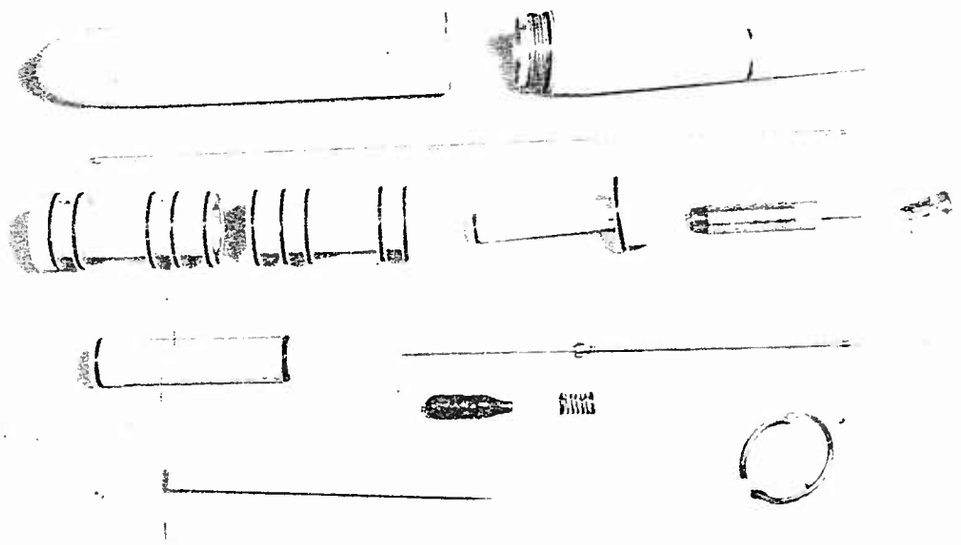

Figure 19. Polymer ejecting axisymmetric body disassembled

description of the operation of the model will serve to identify all the major components. Referring to Figures 16 and 17, the model is assembled for a launch with polymer or other fluid in the storage volume, (4), and a fresh energy source, (9), a CO_2 cartridge installed. The model is placed on the guide wire in the drop tank, (15), and inserted in the launcher. A nylon shear screw is attached through the launcher to the polymer ejector piston stroke measurement rod, (13). This rod serves to hold the model in the launcher and, upon impulsing the launcher, triggers the CO_2 supply activation device, (14), puncturing the CO_2 cartridge and releasing the constant pressure (800 psi) gas supply. The model leaves the launcher shearing the nylon screw allowing the spring loaded stroke measurement rod, (13), to bear against and follow the polymer ejector piston, (12), in its travel. The gas from the CO_2 supply passes through an orifice, (8), and pressurizes the annular piston area, (7), of the polymer ejector piston driving it forward. This action results in ejecting the polymer from the storage volume, (4), through the ejection screen, (1), and providing a suction in the annular area, (5). This area is connected to four equal sampling chambers, (3), through tubes located within 30^{o} of the arbitrarily chosen top of the model. The suction then draws either a wall sample or a sample from a probe, (2). As the piston, (12), is moving, ambient pressure, which varies from atmospheric at the surface of the tank to near 9 psi above atmospheric at the bottom of the tank, enters the guide

tube, (15), and is transmitted to the ambient pressure backfill volume, (6). Finally, at the end of the piston, (12), travel, the CO_2 gas is vented to the backfill volume chamber, (6), and out the guide tube, (15). The model at the end of a test is thoroughly vented of gas and readily handled.

The model was designed with several thoughts in mind. First, it would be desirable to eject at as low a velocity as practical so as not to disrupt the flow. Secondly, ejection in the nose stagnation region forward of the minimum pressure point would be desired to minimize the possibility of early tripping of the boundary layer to turbulent flow. The volume ejection rate should result in an annular flow of about the same dimensions as the laminar boundary layer thickness to minimize the disturbance on the flow field. The stroke and suction process should be at a constant rate. The suction process should be at a low enough rate to minimize the disturbance on the boundary layer and, for the wall suction case, to insure a sample is withdrawn near the wall and not penetrating the boundary layer too far. Finally, all processes should be completed prior to the model impacting the bottom so as not to be either ejecting or sampling under a zero velocity condition. Conversely, it is desirable to delay sampling until the boundary layer has been established at launch. This requirement was difficult to achieve and attempts discarded early in the design process. The errors introduced are less than 8% for the worse case.

The first design parameter fixed was that of deciding on the required polymer ejector volume. After deciding to keep the model as light as possible, constructing with aluminum, a guessed weight in water, based on some calculations for a hemispherical nose, a cylindrical section and a tail, of 4.43 lbs resulted for a 24-inch long body of 3-inch diameter. Assuming drag coefficients of .22 and .11, the velocity of the body was determined by the equation:

$$U = \left(\frac{W-B}{1/2\ C_D \rho A}\right)^{1/2}. \tag{77}$$

The calculated velocities for 70° water were

$U = 20.6$ ft/sec for $C_D = .22$

$U = 29.0$ ft/sec for $C_D = .11$.

The Reynolds numbers for these velocities were

$R_e = 3.9 \times 10^6$ @ $U = 20.6$ ft/sec

$R_e = 5.5 \times 10^6$ @ $U = 29.0$ ft/sec.

The laminar boundary layer thickness may be calculated using flat plate approximations and assuming a position 2 inches back along the body surface. From Schlichting (1968)

$$\frac{\delta}{x_s} = \frac{5.2}{(R_e)^{1/2}}. \tag{78}$$

Now $R_{e_x} = 3.25 \times 10^5$ $U = 20.0$ ft/sec

$R_{e_x} = 4.6 \times 10^5$ $U = 29.0$ ft/sec.

Therefore,

$\delta = 1.52 \times 10^{-3}$ ft $U = 20.0$ ft/sec.

$$\delta = 1.27 \times 10^{-3} \text{ ft} \qquad U = 29.0 \text{ ft/sec}.$$

Now, the volume flow through the annulus around the body is given by

$$Q_\delta = .6\, U\, \pi\, D\, \delta \tag{79}$$

where .6U is used as an approximation to an average velocity in the region. For the two conditions being calculated

$$Q = .0148 \text{ ft}^3/\text{sec} = 25.5 \text{ in}^3/\text{sec}$$

for U = 20.6 ft/sec

$$Q = .0174 \text{ ft}^3/\text{sec} = 29.9 \text{ in}^3/\text{sec}$$

for U = 29.0 ft/sec,

The usable tank length for model tests is about 13 ft; therefore, the time of ejection will be about

$$t_1 = \frac{18}{20.6} = .63 \text{ seconds}$$

$$t_2 = \frac{18}{29} = .448 \text{ seconds},$$

Required volumes for storage are

$$U_s = 16.0 \text{ in}^3 \qquad U = 20.6 \text{ ft/sec}$$

$$U_s = 13.4 \text{ in}^3 \qquad U = 29.0 \text{ ft/sec}$$

Comparing these volume flux rates with expected velocities from the nose, assuming a one-inch diameter ejection port with a 30% open area screen installed

$$\frac{Q_\delta}{(A_e)(.30)} = 9 \text{ ft/sec} \quad \text{for } U = 20.6 \text{ ft/sec}$$

$$\frac{Q_\delta}{(A_e)(.30)} = 10.6 \text{ ft/sec}$$

for U = 29.0 ft/sec.

These velocities are high. Velocities in the order of 5 ft/sec would be much more desirable. Reduction of velocities by 1/2 would result in a storage volume goal of about 8 cubic inches. This reduction would also result in smaller thicknesses of flow in the boundary layer as compared to the laminar layer thickness.

The effective polymer storage volume designed into the model is 8.25 in^3 with a stroke of 4.67 in. and a stroking time of .4 secs.

The ejector screen used in the model, Figure 18, was formed to the contour of the forebody nose. The screen contained 517 .024 inch diameter holes per square inch with a 24% open area. The outside diameter of the screen is 1.37 inches and the inside diameter .3 inches. The projected area is 1.4 in^2 with an open orifice area of .337 in^2. This ejection area resulted in a 5-ft per second ejection velocity.

The screen used is a No. 0 straight screen from Harrington and King Perforating Company.

The suction time was next to be determined. Since the single piston approach was decided upon, the stroke available and the stroking time for use was equivalent to that for the ejector piston, 4.67 inch and a time of .4 seconds. The suction rate for the design of the suction piston is 11.675 in^3/sec. Applying a method defined by Dowdell (1973) for correction of the measured "wall concentrations" due to the sampling process

drawing further out in the boundary layer, an estimation of a reasonable sample rate and sample probe orifice size were made. It was first decided that samples would be made at stations 3, 6, 9, and 12 inches back from the nose of the body. This selection was somewhat governed by the need in the tail for other machinery space. From a measurement standpoint, it was desirable to maximize sample size but from a correction standpoint, minimal flow velocity is desirable. As a result, four suction ports 90° apart, were located at each measurement plane. Additionally, at each subsequent plane the port locations were rotated 22° 30' so as not to be affected by the flow entering the ports in the previous plane, Figure 18. The next step was to define the approximate boundary layer thickness at the most forward probe station for the highest Reynolds number case as used before. This would give the thinnest boundary layer which is the worst case. Using a flat plate turbulent boundary layer thickness expression from Schlichting (1968)

$$\frac{\delta}{x} = \frac{0.37}{(R_e)^{1/5}} . \tag{80}$$

From (80), δ = .05 inches.

A matrix of probe sizes (inside diameter) and suction volumes were examined for the piston rates calculated, body velocities and the boundary layer thickness calculated above. This was also performed for a boundary layer thickness of .025 inches, postulated to be the thickness that might occur when polymers

were added. The result was that a .760 cubic inch suction volume and sampling tube inside diameter of .030 inches would give acceptable results. A worst case correction factor of

$$\frac{C_{\text{measured}}}{C_{w\ \text{actual}}} = .54$$

was calculated for a .025-inch thick boundary layer. This correction reduced to about .8 at a boundary layer thickness of .05 inches. Although a lower correction factor would be desirable, an ample sample volume of fluid is necessary for concentration determination. This suction rate and flush wall sample tube size had an inflow rate per tube of approximately 14 ft/sec.

The pitot probes to be used in sampling the boundary layer away from the wall were designed to minimize the effects on the flow. Two heights were chosen for measurement, .025 inches from the wall and .055 inches. These selections came about, in part, due to physical limitations. With the physical dimensions of the probes, it is difficult to get closer to the wall and with the projected boundary layer thickness for the first station, it is not desirable to get any further from the wall. These heights would allow for a reasonable three-point plot of boundary layer concentrations. Figure 20 displays the salient features of the probes. As is noted, a thin wall tubing is used which allows for flattening of the tip to .01-inch thickness. The resulting inner dimension for sampling is .004 inches high. Sampling

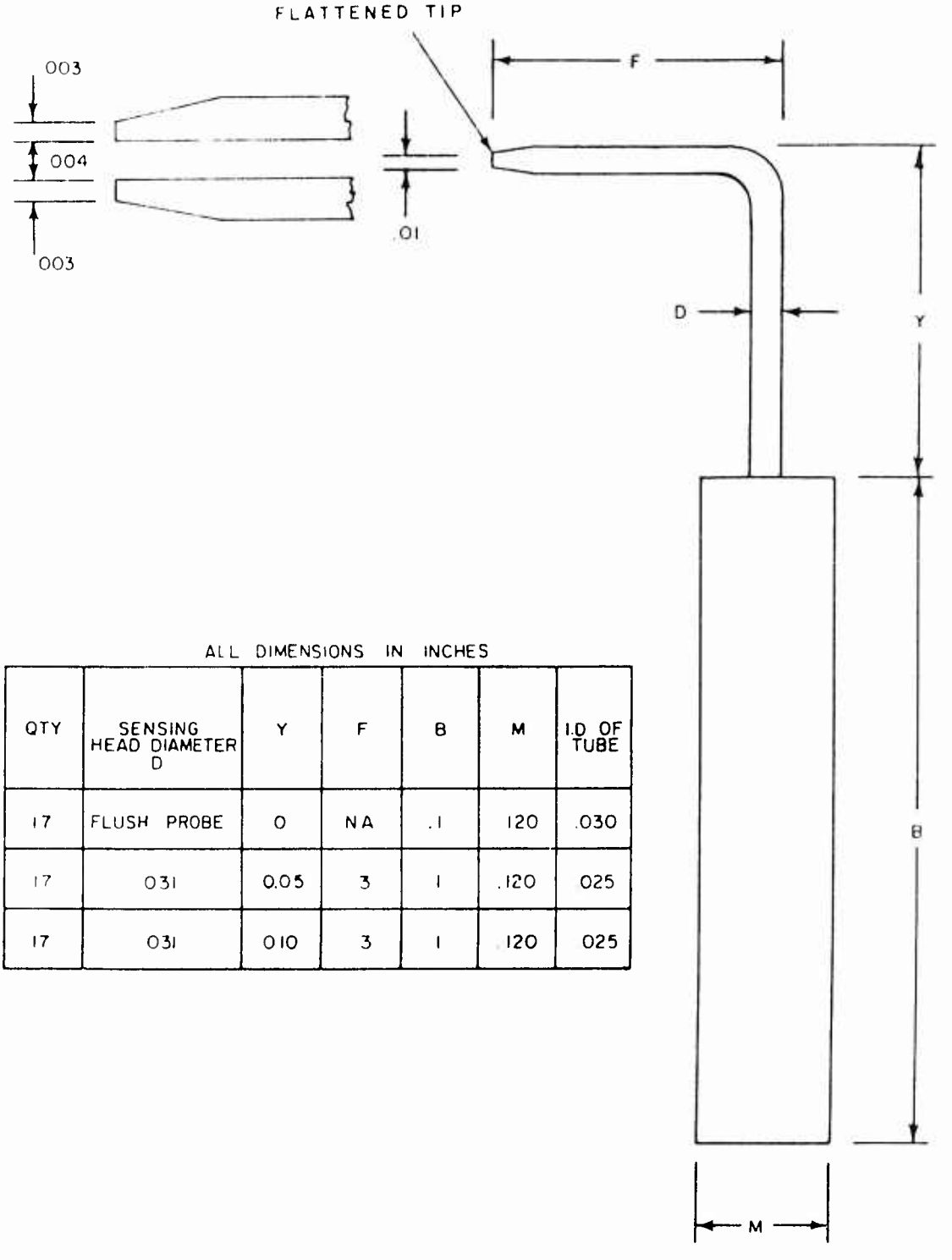

ALL DIMENSIONS IN INCHES

QTY	SENSING HEAD DIAMETER D	Y	F	B	M	I.D OF TUBE
17	FLUSH PROBE	0	NA	.1	120	.030
17	031	0.05	3	1	.120	025
17	031	010	3	1	.120	025

Figure 20. Special boundary layer probes

velocities in the tube are approximately 20 ft/sec. Sixteen probes were used in each test replacing the sixteen flush wall probes.

The model design, as can be seen from the schematic, Figure 17, contained void volumes in the suction lines which were prefilled with liquid. The void volume is 1.4316 cubic inches resulting in a sample dilution factor of .1327.

The stroking piston pressurization system consists of the carbon dioxide (CO_2) cartridge, a puncture device and an orifice. Since the goal is a constant rate ejection process, the use of a CO_2 cartridge as the gas source was chosen since the substance is stored in liquid form with a vapor pressure of 800 psi at about 65°F. Little change in the vapor pressure would occur during the use cycle as the gas is drawn off. The system was designed to minimize the free volumes in the high pressure area to insure a sufficient gas supply for the stroking process, Figure 17. The CO_2 cartridge in the final version of the model is inverted from that shown in Figure 16, with the puncturing needle placed on the opposite end also. This was done to achieve reproducibility in the stroking of the piston. Apparently, either freezing of the orifice or slight contaminants would plug the metering orifice resulting in extreme variability of stroking times. The reversal corrected the situations. The pressurization area and orifice area size for metering the CO_2 gas were

selected to provide the stroking rate previously determined. The area was somewhat governed by the desire to maximize the drop tank depth pressure balance area, (6), Figure 17. The volume in this area, besides providing for balancing of the depth pressure also minimizes the weight change during a launch by water backfilling the volume. The CO_2 piston pressurization area designed was .785 in^2 with a resultant total volume of 3.68 in^3. The orifice size was determined to achieve the .4 second stroking time. Considering that the orifice is small enough such that choked flow conditions exist, the pressure ratio across the nozzle is given by, Shapiro (1953),

$$\frac{p_2}{p_1} = \left(\frac{2}{k+1}\right)^{\frac{k}{k+1}} \tag{81}$$

Which for k = 1.29 for CO_2 gas @ 68°F yields

$$\frac{p_2}{p_1} = 0.55. \tag{82}$$

Therefore, flow will be a maximum for downstream pressures less than or equal to 440 psi with an upstream pressure of 800 psi. The flow rate is given by, Shapiro (1953)

$$\left(\frac{w}{A_1}\right)_{max.} = \sqrt{\frac{2gk}{k-1}\,(p_1\rho_g)\left[\left(\frac{2}{k+1}\right)^{\frac{2}{k-1}} - \left(\frac{2}{k+1}\right)^{\frac{k+1}{k-1}}\right]} \tag{83}$$

where ρ_g = .114 lbs/ft^3 @ 68°F.

Substituting in (83):

$$\frac{w}{A_1} = 4.28 \times 10^2 \text{ lbs/ft}^2 \text{ sec.} \tag{84}$$

Converting to match the volume flow requirements

$$\frac{Q}{A_1} = \frac{w}{\rho_g A_1} = 37.54 \times 10^2 \text{ ft/sec.} \qquad (85)$$

To achieve the 9.2 in^3/sec volume stroking rate for the pressurizing gas volume, Q must equal 9.2 in^3/sec and A_1 is determined. Substituting in (85)

$$A_1 = 1.418 \times 10^{-6} \text{ ft}^2 \qquad (86)$$

$$= 2.04 \times 10^{-4} \text{ in}^2$$

Therefore, the orifice diameter must be .016 inches. This diameter orifice has been used in the model.

The important characteristics of the 6° ejecting model as finally designed and constructed are displayed in Table 3.

TABLE 3

Characteristics of 6° Ejecting Model

Length	2.0833 ft
D	.25 ft
L/D	8.33
Weight in Water	4.46 lbs
Polymer Solution Storage Volume	8.25 in^3
Stroke	4.67 in
Stroke Time	.400 sec
Suction Volume	.760 in^3
Suction Volume Per Sampling Chamber (4 Chambers)	.19 in^3
Sample Dilution Factor	.1327
Ejection Velocity	5 ft/sec

Boundary Layer Concentration Measurements

Several methods exist for the measurement of the concentration of polymer in a sample solution. These include polarographic, turbidity, simple opaqueness and fluorometric methods. A comparison of all but the opaqueness is given in Wetzel and Ripkin (1970). The opaqueness method, which relies upon a measurement of light transmission through a portion of the boundary layer, cannot be applied to the moving body case since short time measurements and accurate body position with time would have to be known. The remaining methods are all applicable to the conditions of this study since they deal with a sample of solution. The method chosen for use is the fluorometric method. This method has been used successfully by Walters and Wells (1971), Wetzel and Ripkin (1970) and Tullis and Ramu (1973). The method consists of injecting a tracer dye into the fluid being analyzed and capturing a sample of the fluid for analysis. This assumes, of course, that the diffusion of the tracer dye is identical to that of the boundary layer mixture. A reasonable assumption as data comparing various measurement methods by Wetzel and Ripkin (1970) display. The tracer dye, which may be colorless, fluoresces when radiated with an ultraviolet source. This reradiation is measured with a photomultiplier tube and is proportional to the concentration of dye in the sample. The fluorometer used in these tests is a G. K. Turner Associates Model 111 Fluorometer.

Several tracer dyes may be used. Two prime candidates are Rhodamine-B and Uranine-B. Both are compatible with polymer solutions in that the mixture was stable and the drag characteristics were unaffected when measured in a Turbulent Flow Rheometer similar to that described in Hoyt (1966). The Rhodamine-B gives excellent results with solution concentration of 1 part in 10 inches on a weight basis but is very difficult to cleanse from the apparatus. The Uranine-B dye was readily adaptable to laboratory use and gave reproducible readings to about 1 part in 10^9 on a weight basis. This was sufficient for the experiment to be performed since the dye concentration in the solution to be ejected could be adjusted to produce samples along the body sufficiently above the background levels to give reproducible results. Calibration curves were experimentally developed for the instrument using known concentration of Uranine-B dye in the tap water to be used in the experiment. The Model 111 Fluorometer has four sensitivity settings allowing calibration curves to be drawn over a range of about 1 part per 10^6 to 1 part per 10^9, on a weight basis. For concentrations greater than the lower value, dilution prior to measurement was performed. The calibration charts for this experiment are shown in Figures 21 and 22. Approximately a 3.5 to 4.5 ml sample is required for measurement. This sample is placed in a cuvette (a small test tube) and placed in the instrument and the measurement taken.

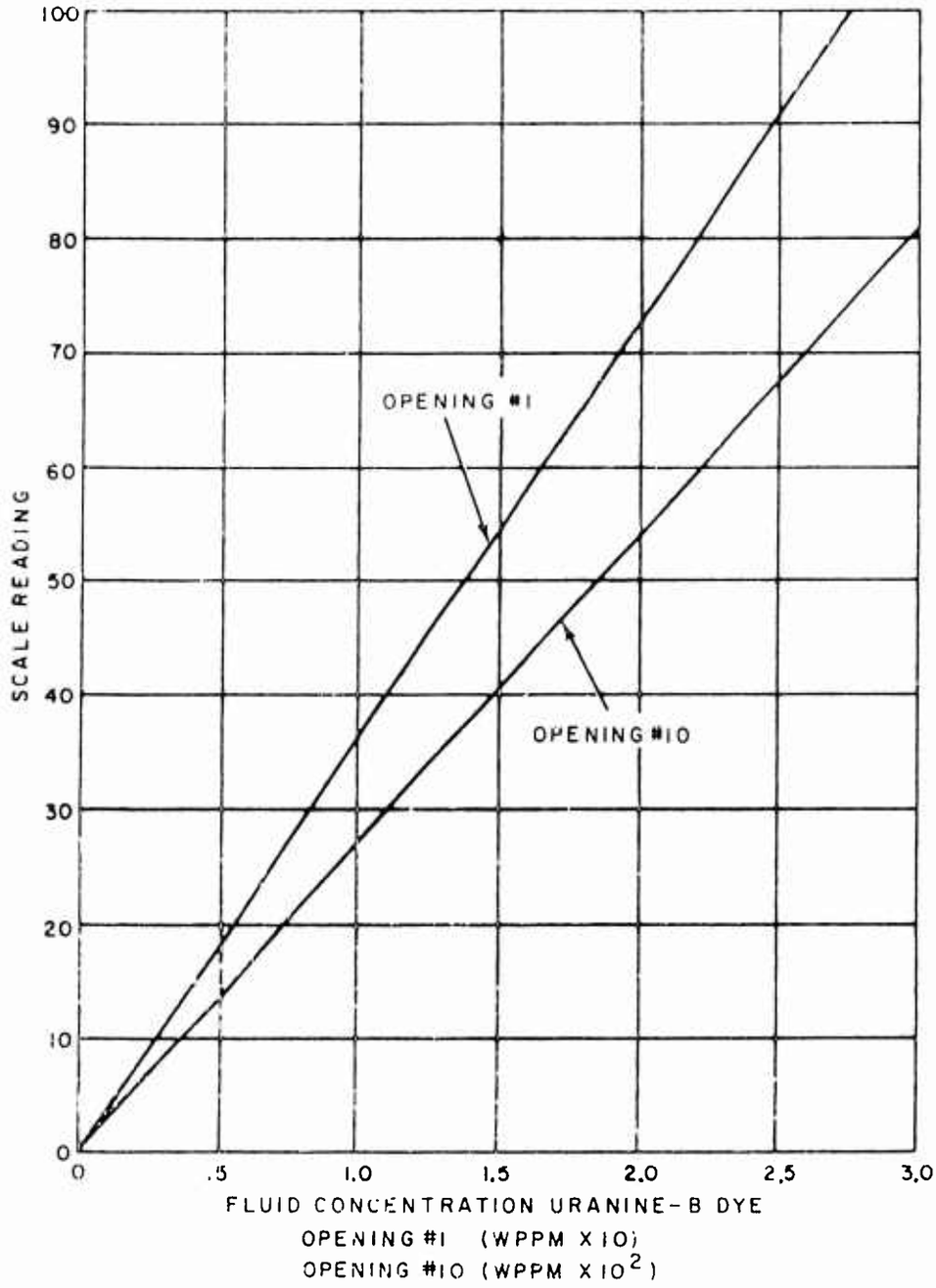

Figure 21. Calibration curves for model 111 fluorometer - openings 1 and 10

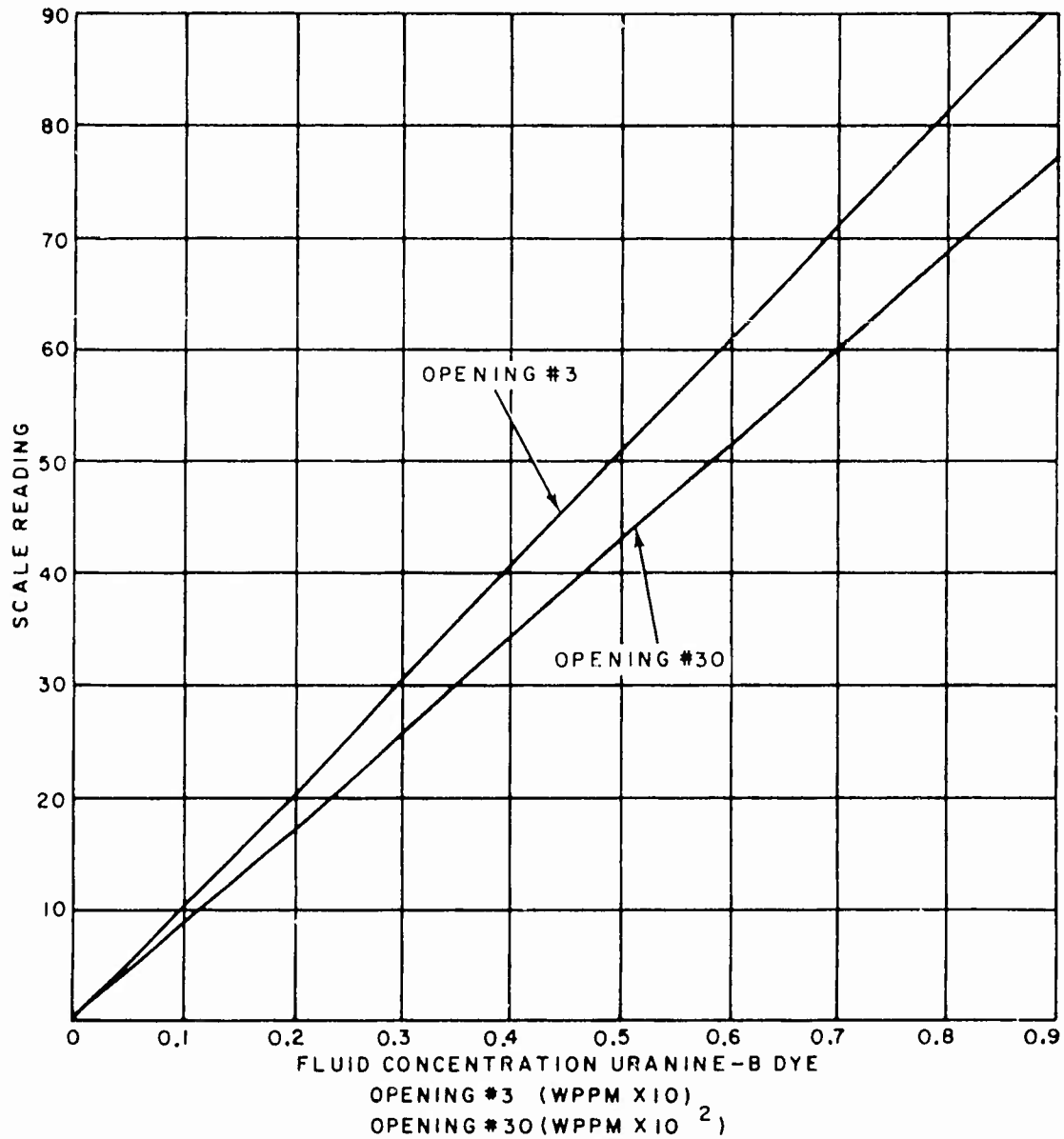

Figure 22. Calibration curves for model 111 fluorometer - openings 3 and 30

Care was taken to wipe the outside of the cuvette clean prior to measurement since fingerprints do effect the readings. Wiping with a paper towel was found to be sufficient. All samples were allowed to achieve room temperature prior to reading.

Model Calibration

Concentration Measurement Calibration

The ejecting model, as designed contained four sample collection chambers drawing samples through four flush wall or four pitot probes per sample chamber. These collection chambers are all connected by 3/32 inch inside diameter tubing to the suction piston. The transfer tubes are of unequal lengths resulting in an interesting transient analysis problem of defining the suction rate differences per sample chamber. The problem was circumvented by calibrating the model through a series of experiments. Additionally, a calibration was desirable since it was difficult to determine the exact void volume per sample chamber previously stated at 1.4316 cubic inches which resulted in a dilution factor of .1327. This resulted in a sample concentration lower than the boundary layer sample concentration. It was first thought to leave these void spaces air filled eliminating the dilution factor. Early tests showed that with the body in the tank in the vertical position, the water pressure head difference would result in a venting of the air in these chambers, since they were interconnected, out the uppermost chamber and a filling with tank water through the lower chambers. Prefilling with water, as will be

discussed later, eliminated the problem. To calibrate the model, an assembly and calibration tank was constructed. The tank is displayed in Figure 8 in the foreground having dimensions of 8-inch diameter by 3 feet height. The model is installed in the tank tail first as shown in Figure 23 and fired by pulling on a preattached lanyard. The following procedure was followed in calibrating the model. The model was assembled excepting for the half body nose and placed in the tank after connecting the lanyard to the firing rod. Tap water was placed in the tank just below the level of the polymer ejection volume completely filling all sample chamber volumes. The nose is then installed and a sample background reading of the water taken. The water was then contaminated with the Uranine-B tracer to one of three concentration levels called the Ocean Concentration. These were approximately $.3 \times 10^{-7}$, $.8 \times 10^{-7}$ and 2×10^{-7} WPPM, which were determined to result in an appropriate spread of chamber concentration levels. The model was then fired. The samples were withdrawn and measured in the Fluorometer. The samples were withdrawn by removing the model from the calibration tank, wiping the outside dry while holding in a horizontal position with the top, as defined by the position of the internal suction transfer tubes, being in the uppermost position and placing the model over individual collection trays. The samples would drain into these four separate trays for analysis. It is necessary to keep the suction transfer tubes in the uppermost position to insure no transfer of liquid between the chambers. The

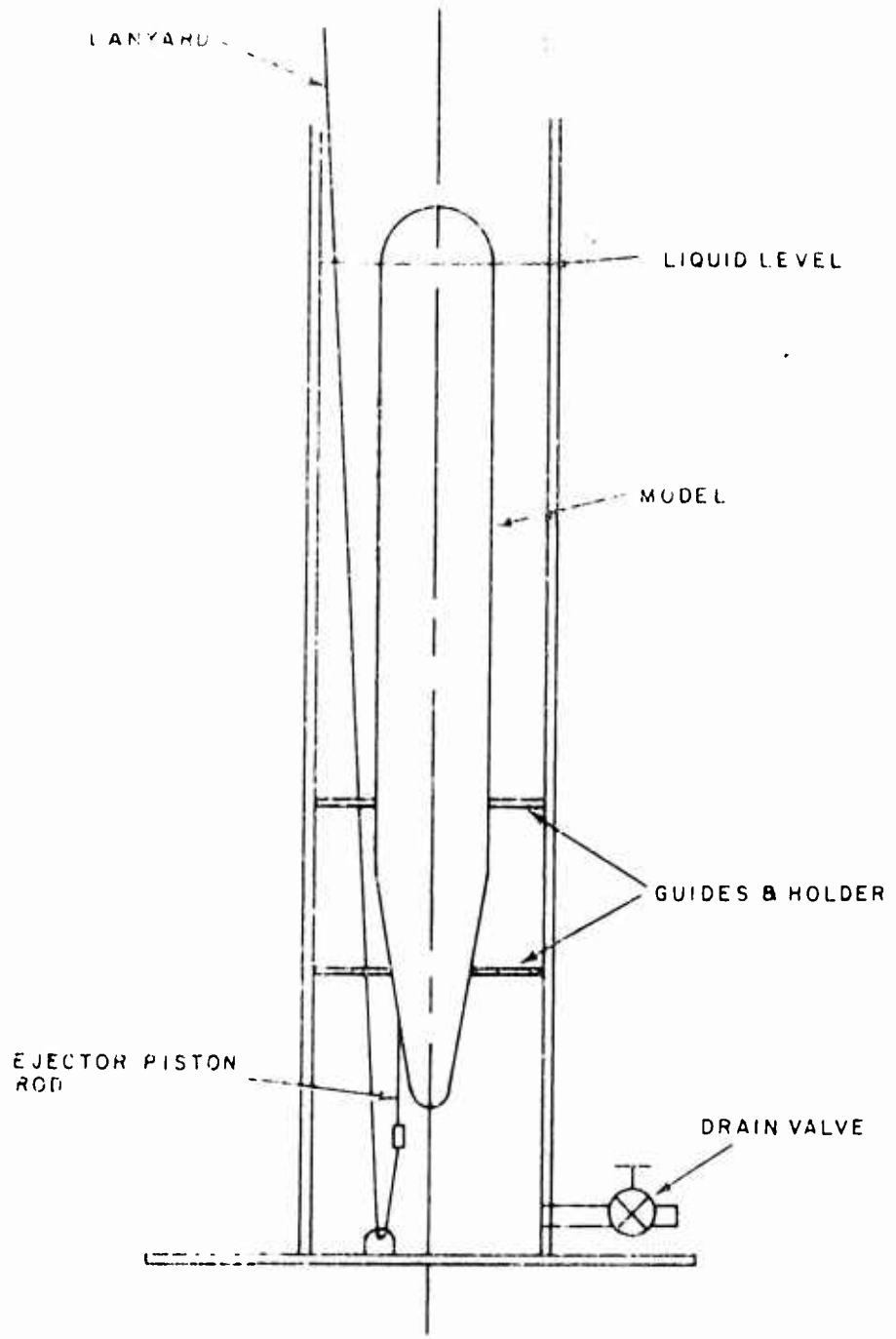

Figure 23. Assembly and calibration tank

procedure was similar for the probe case excepting that an uppermost row of probes was removed and then a bottom row to facilitate the liquid withdrawal. A minimum of four calibration tests were run at each concentration with the flush probes and also with the pitot probes. A least squares fit was performed on the data which are plotted for each sample chamber in Figures 24 through 31 for high and low chamber concentrations. Deviations of $\pm 5\%$ were noted in the data. Several tests were performed with a 50 WPPM polymer solution in the tank with no significant change in the data.

Stroking Time Verification

Verification of the stroking time was necessary to insure that the appropriate volume flow rates were being achieved. The facility shown schematically in Figure 32 was used for this purpose. To calibrate, the model was loaded with liquid and clamped to the bench. A calibration spacer was placed on the ejector follower and the rod clamped with a nylon shear screw to the facility firing arm. When fired by moving the firing arm in a counterclockwise direction and shearing the shear screw, the follower rod would move into the model following the ejector piston. The calibration spacer would interrupt the laser beam for the length of the spacer, starting the counters, discussed previously, giving a time over the known distance and the velocity of the rod. It was found, by test, that the velocity of the rod was approximately 5 times faster than the stroking time, therefore not influencing the results. A .5-inch long

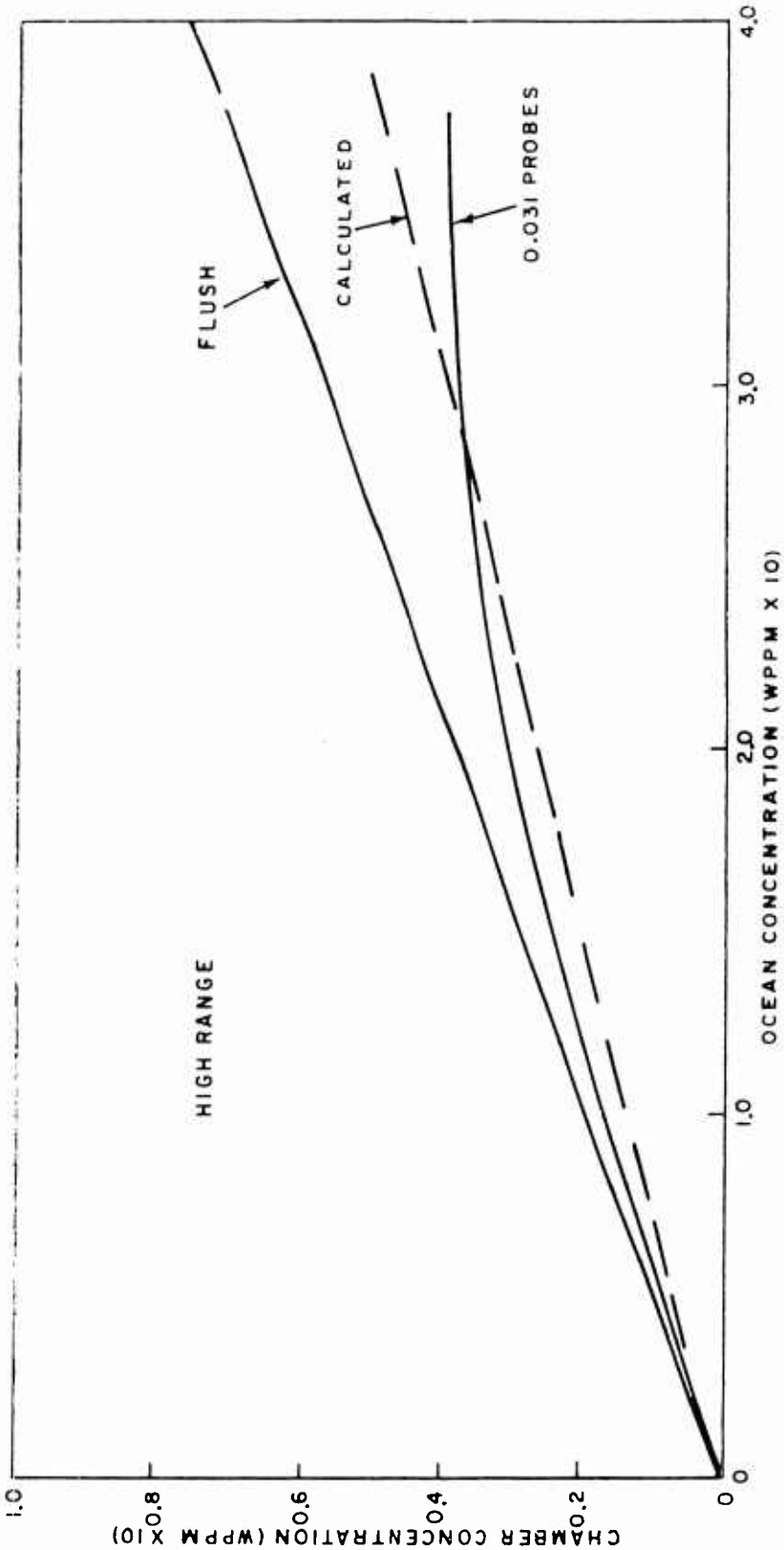

Figure 24. Chamber 1 concentration vs. ocean concentration -high range

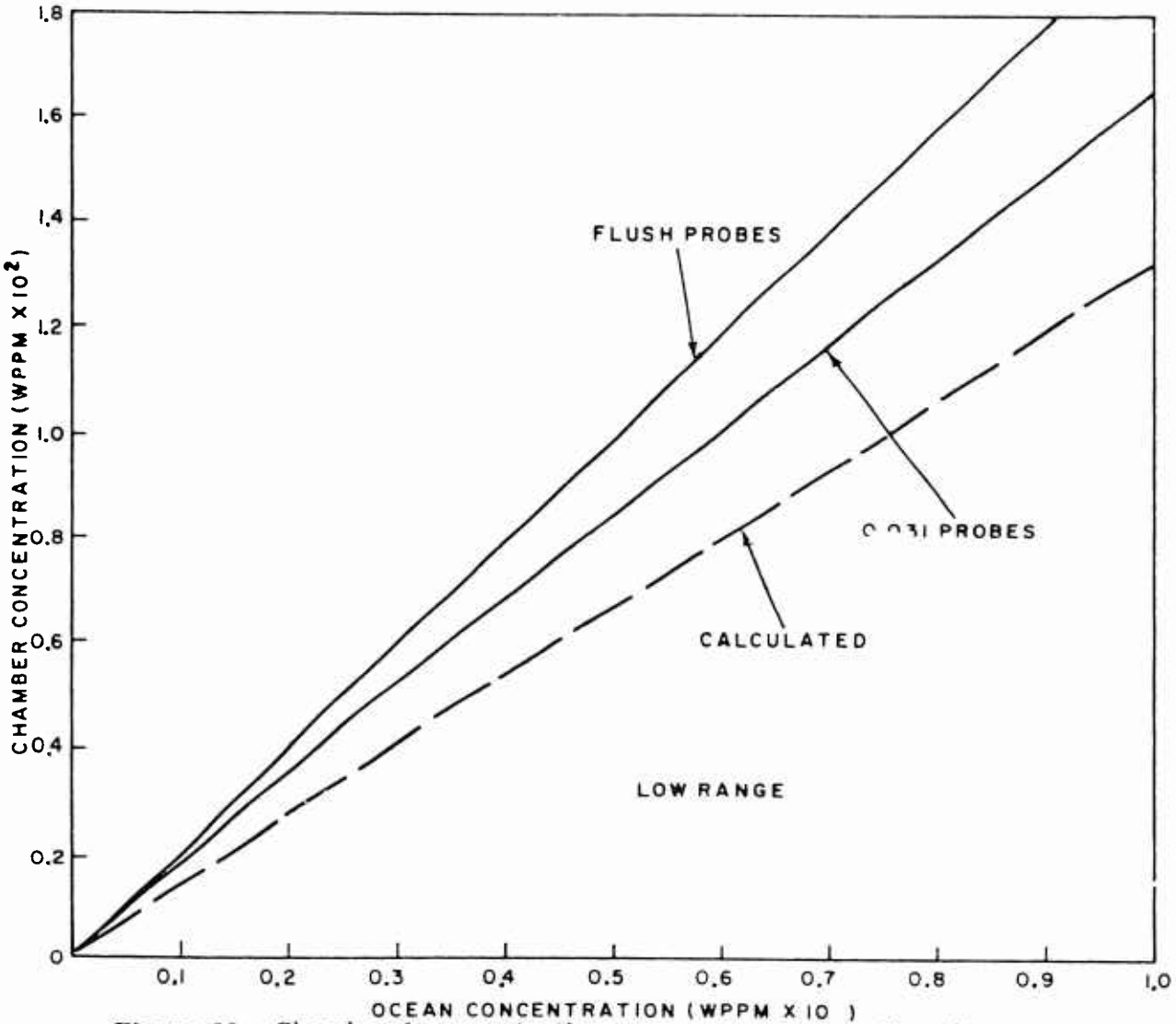

Figure 25. Chamber 1 concentration vs. ocean concentration -low range

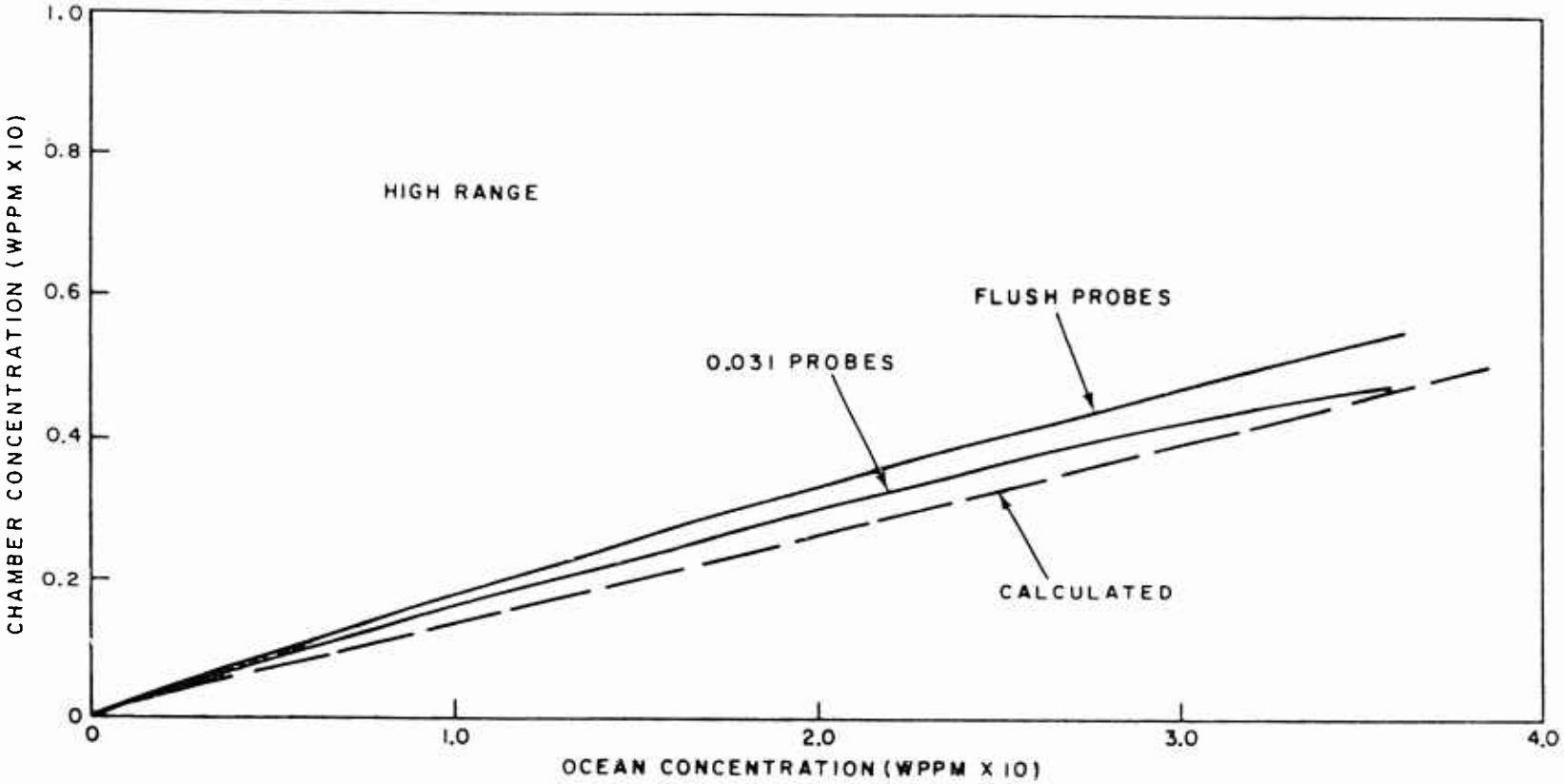

Figure 26. Chamber 2 concentration vs. ocean concentration -high range

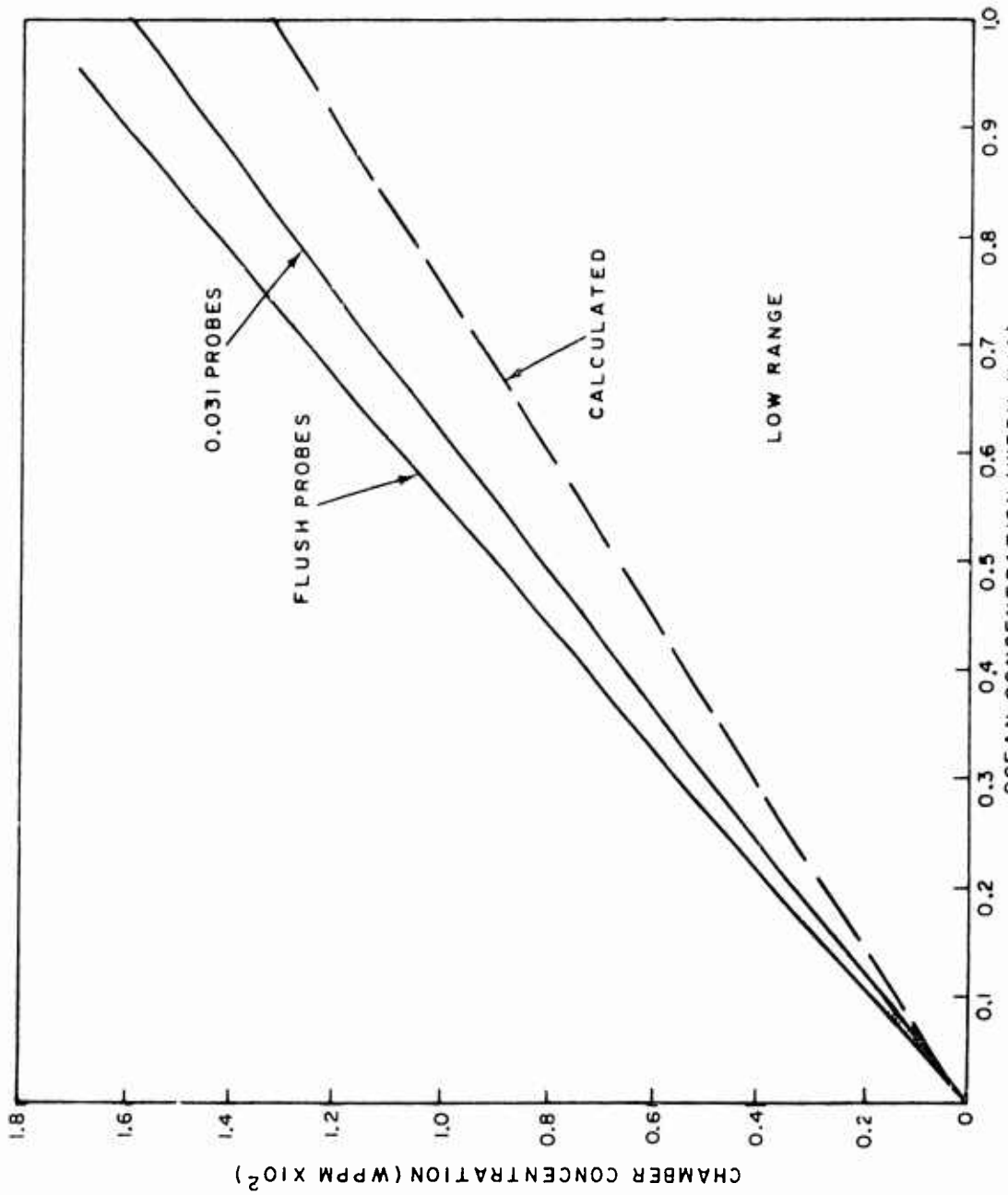

Figure 27. Chamber 2 concentration vs ocean concentration -low range

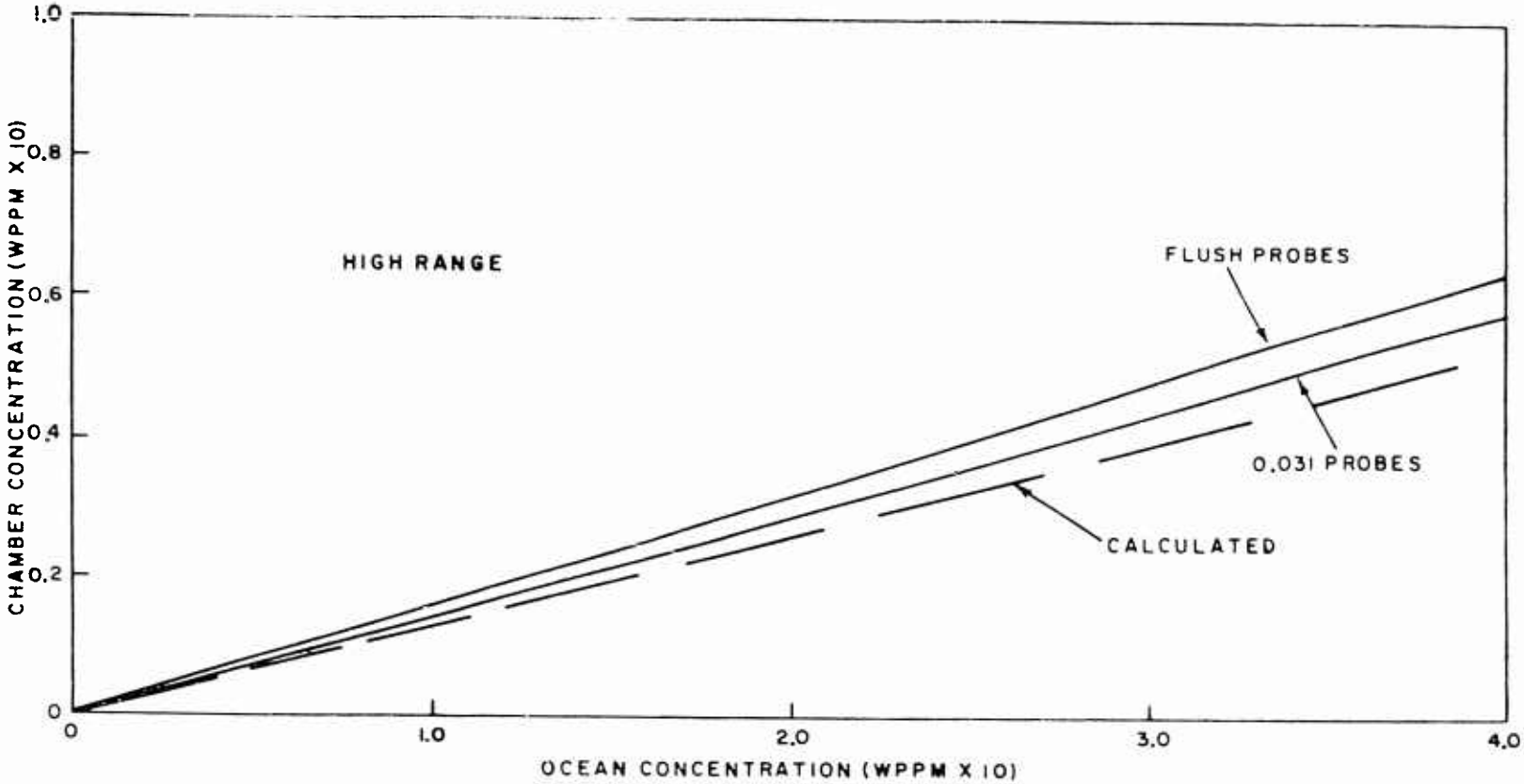

Figure 28. Chamber 3 concentration vs. ocean concentration -high range

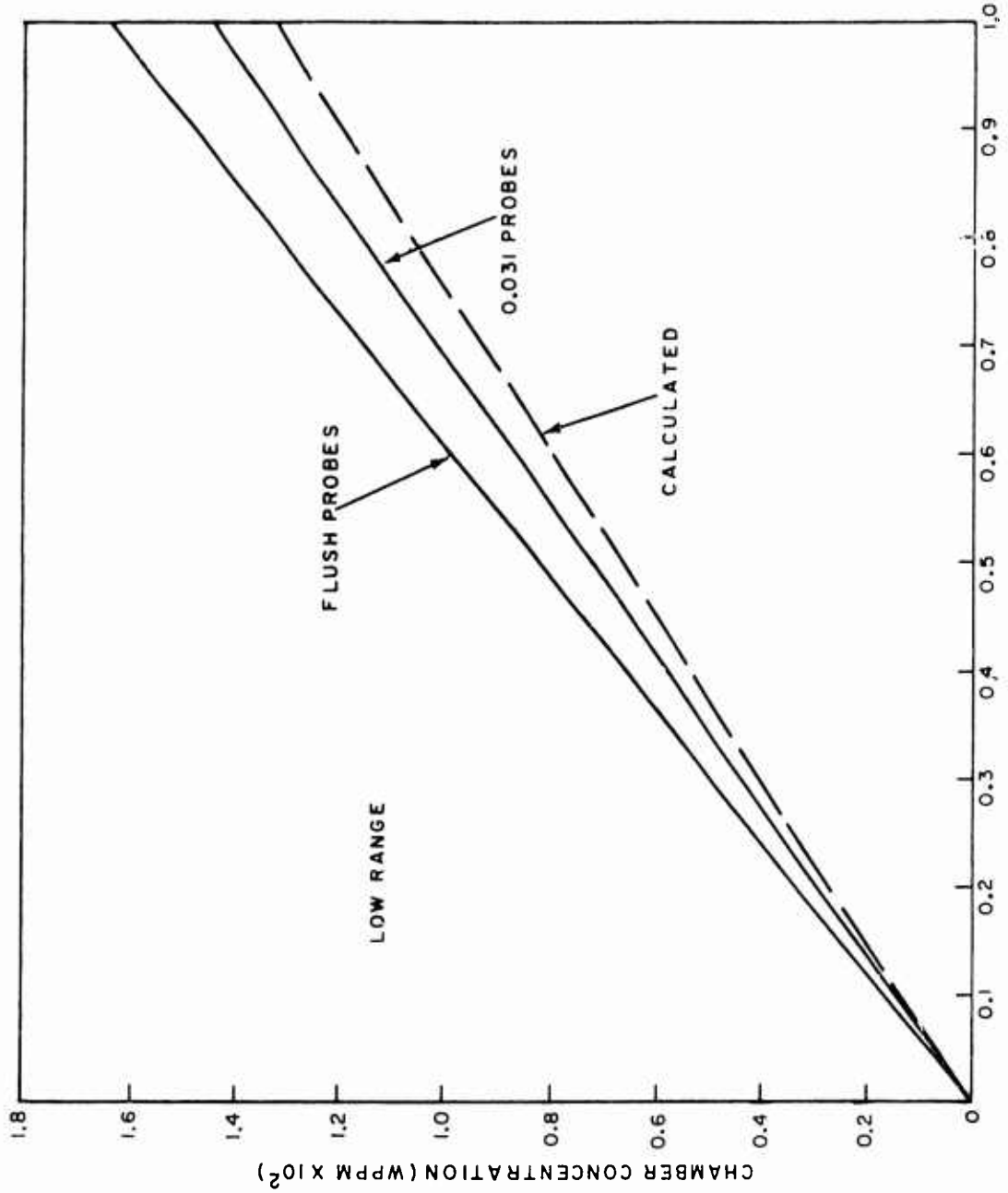

Figure 29. Chamber 3 concentration vs ocean concentration – low range

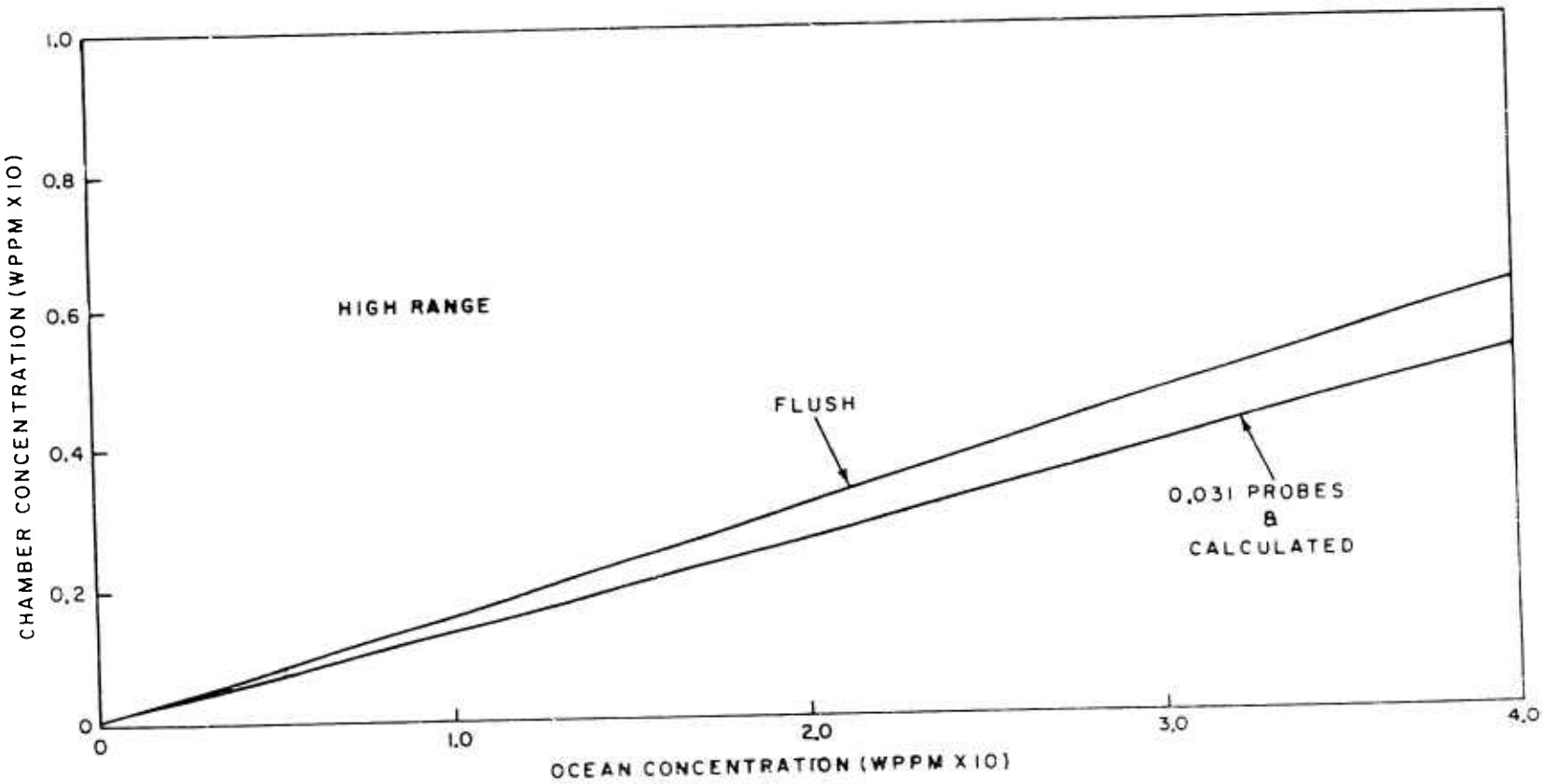

Figure 30. Chamber 4 concentration vs. ocean concentration -high range

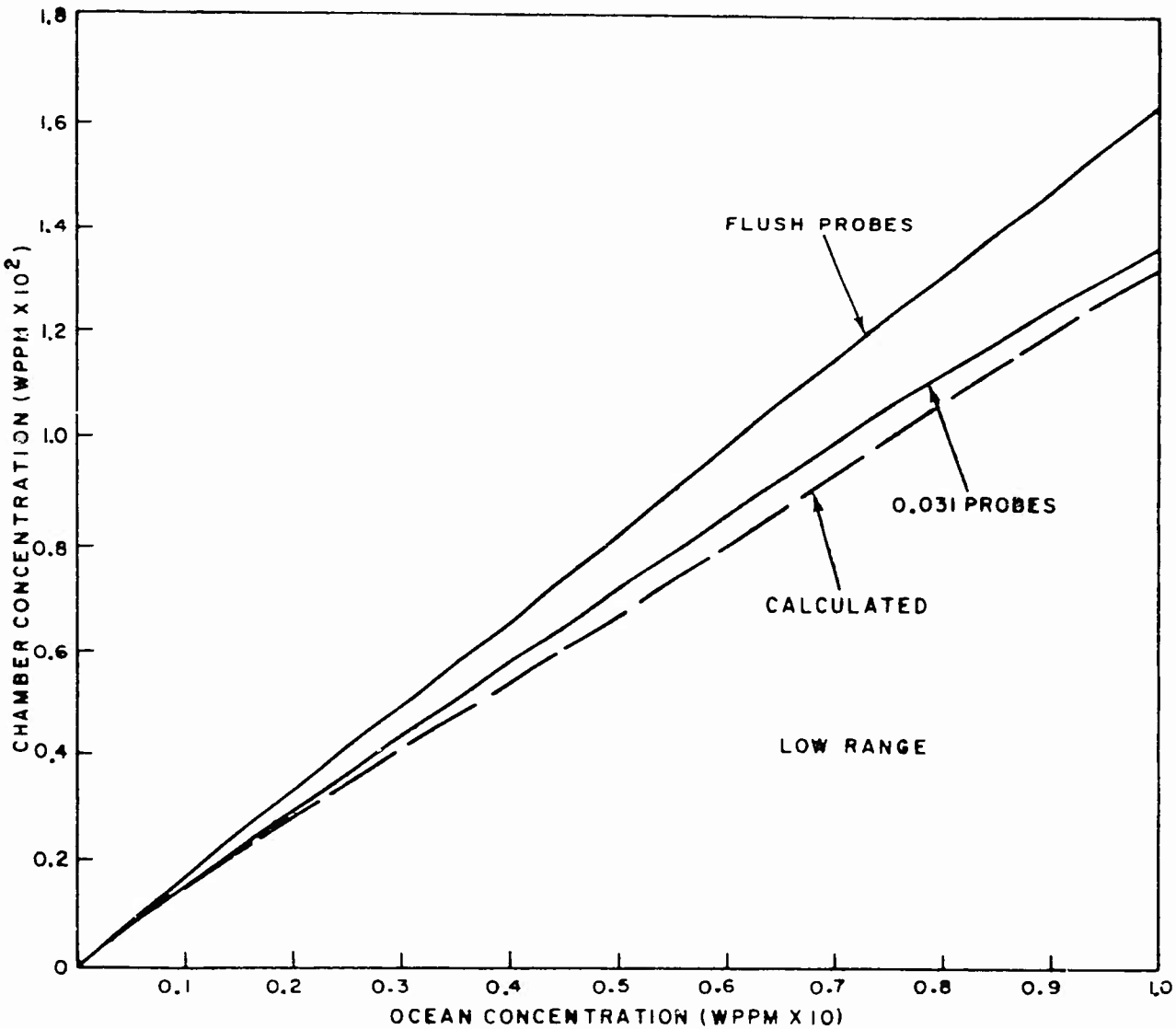

Figure 31. Chamber 4 concentration vs ocean concentration -low range

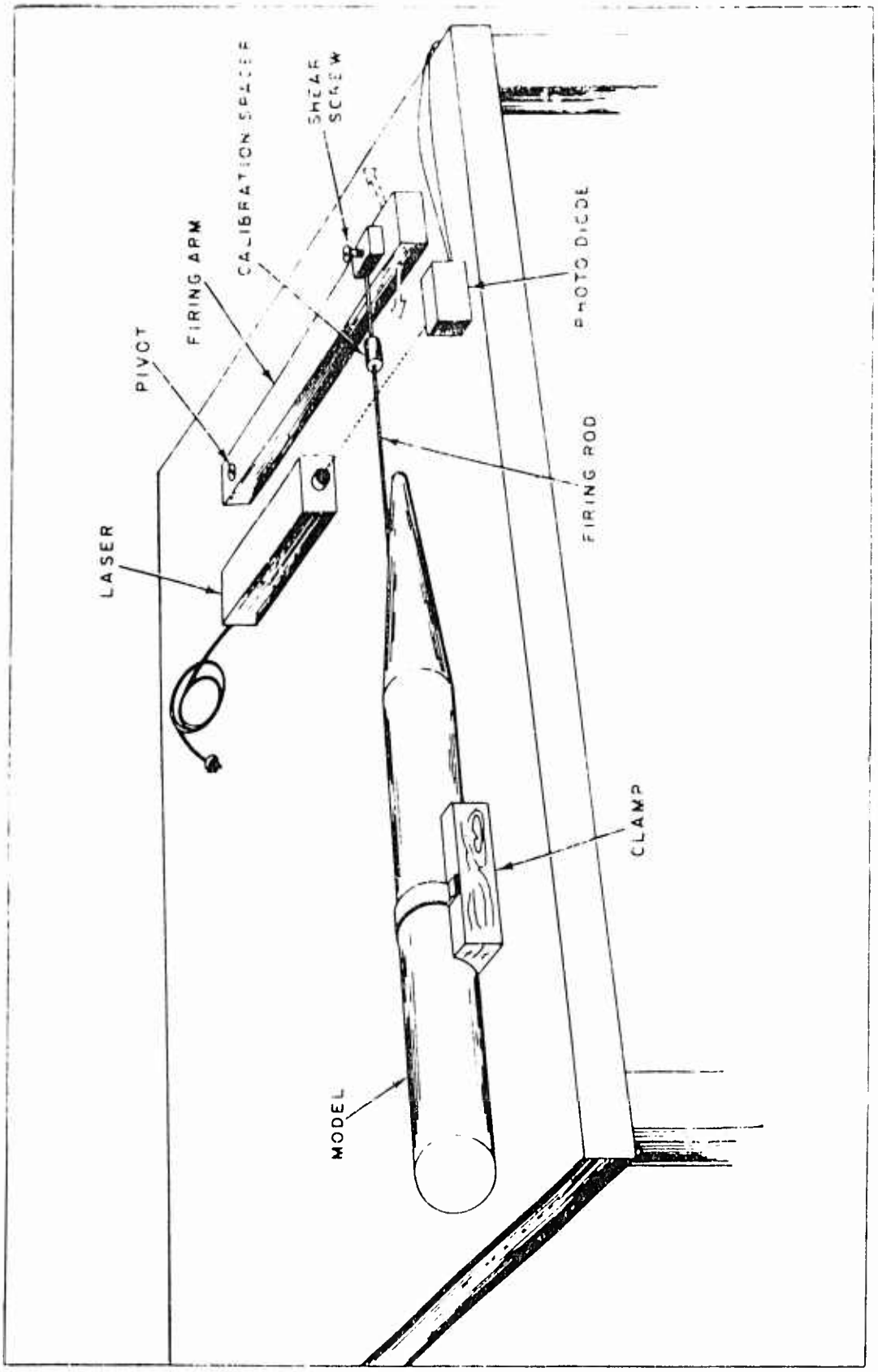

Figure 32. Stroke calibration facility

calibration spacer was used in the test and placed at several positions on the follower rod to detect any acceleration of the rod. None was evident. Nineteen calibration runs were made. The stroke rate resulting was 12.1 in/sec $\pm$6% as compared to the calculated value of 11.7 in/sec.

IV. ANALYTICAL CONSIDERATIONS

Boundary Layer Model

This section presents the analytical approach for the analysis of developing turbulent flow over an axisymmetric body for the cases of no polymer, polymer ocean and polymer injection. A model is developed for predicting growth of the boundary layer, diffusion of tracers within the boundary layer and prediction of skin friction coefficients and total drag.

From the literature review, the features of previous studies for turbulent flows can be summarized as follows:

1. A modified law of the wall type velocity profile with pressure gradient terms was developed for the thick axisymmetric boundary layer case.
2. Inner variable integral equations were developed for the thick axisymmetric boundary layer and verified for certain parameters.
3. Porous wall pipe flow studies with injection of polymers have suggested significantly reduced diffusion characteristics. This representing the ideal case of introducing polymers into the viscous sublayer.
4. External flow studies demonstrate the importance of the ejection process on polymer efficiency.

5. Far downstream dilution laws for polymer follow those for water diffusion.
6. Similarity concentration profile relations have been established for the downstream case.
7. The extent of the initial mixing zone is considerably extended by nearly a factor of 20 with polymer flows. Most investigators have obtained data in far downstream conditions only.
8. Data on concentration profiles on axisymmetric bodies are desirable to extend and/or verify dilution laws presently available.

In the analysis that follows, the velocity profile, continuity equation, momentum equation, a Lagrangian similarity hypothesis for the turbulent diffusion boundary layer growth, and a conservation of polymer equations for the intermediate and final zones of diffusion are combined to yield expressions for the growth of the turbulent boundary layer with polymer ejection. Additionally, terms are added to predict the initial zone region where molecular diffusion predominates for an optional ejection process. An alternate analytical model is postulated which would eliminate the need for the concept of an initial, intermediate and final zone concept.

Velocity Profile Relation

Equation (32) provided a relation for the law of the wall accounting for pressure gradients. Rewriting equation (32) accounting for the Meyer (1966) correction for polymers, ΔB, yields:

$$u^+ = \frac{1}{K} \int_{0.1108}^{Y_o^+} \frac{1}{Y^+} \left[1 - \frac{\alpha}{2} r_o^+ \left(1 - e^{2Y^+/r_o^+}\right) \right]^{1/2} dY^+ + \Delta B \qquad (87)$$

An alternate method for accounting of the polymer effect would be by adjustment of the mixing length constant, K. As noted by Virk (1971), a change in K by a factor of 5 is possible and in full agreement with data. This would only apply for the case of maximum drag reduction along the ultimate asymptote line, however.

Skin Friction Relations

The boundary layer continuity and momentum equations, equations (33) and (34), for turbulent axisymmetric flow

$$\frac{\partial}{\partial x} (\rho\ u\ r) + \frac{\partial}{\partial y} (\rho\ v\ r) = 0 \qquad (33)$$

and

$$\rho\ u\ r\ \left(\frac{\partial u}{\partial x}\right) + \rho\ v\ r\ \left(\frac{\partial u}{\partial y}\right) = -\ r\ \left(\frac{dp_e}{dx}\right) + \frac{\partial}{\partial y}(r\tau) \qquad (34)$$

are applied to the polymer flow case studied here.

The x derivatives must be handled by the chain rule, since each of the parameters (Y^+, α, r_o^+, C_w) in the law of the wall is a function of x. Thus, we substitute

$$\frac{\partial}{\partial x} = \frac{\partial Y^+}{\partial x}\frac{\partial}{\partial Y^+} + \frac{\partial \alpha}{\partial x}\frac{\partial}{\partial \alpha} + \frac{\partial r_o^+}{\partial x}\frac{\partial}{\partial r_o^+} + \frac{\partial C_w}{\partial x}\frac{}{\partial C_w} \qquad (88)$$

As may be noted in (88), concentration derivatives are added. It is assumed throughout that ρ_w and μ_w are constant in this analysis.

The resulting boundary layer equation, after considerable algebraic manipulation is:

$$\frac{d\lambda}{dx^*}(3\,\alpha\,H - G_1) + \frac{V'}{V}\lambda\,G_1 - \frac{\lambda^2 r_o^+}{2}(e^{2Y_e^+/r_o^+} - 1) \qquad (89)$$

$$+ \frac{\lambda^4}{R_L}\left(\frac{1}{V}\right)''H = -R_L V - \lambda\frac{dr_o^+}{dx^*}I - \lambda\frac{dc_w}{dx^*}J$$

where G, H, I, J are given in the appendix.

The prime difference between equations (89) and (35), for the polymer case, is the last term accounting for the change of concentration with x.

Appendix A presents a complete development of the equation related to this method.

Prior to solution of equations (87) and (89), it is necessary to determine a means of calculating C_w. Test (1974) applied techniques developed by Lessmann (1970), and Fabula and Burns (1970) to provide a solution for C_w. This technique satisfied the case of final zone of mixing but did not account for the development of a diffusion boundary layer in a similar

fashion to the development of a hydrodynamic boundary layer. Nevertheless, the results of the work are significant. With the application of the hypothesis suggested by Batchelor (1957), describing the development of the diffusion boundary layer and data by Poreh and Cermak (1964) and Poreh and Hsu (1971), empirical relations are developed which provide the values C_w necessary to determine the friction coefficients for the intermediate and final zone.

For the case of no polymer present, equations (87) and (89) may be solved setting all terms containing C_w equal to zero. It is only necessary, as pointed out in White (1972), to assume an initial λ_o and prescribe the flow condition (U_e, r_o) as a function of x. Additionally, for the case of operation in a polymer ocean, that is C_w is everywhere constant, all derivatives of C_w and with respect to C_w are set equal to zero and again a solution can be obtained as for the case of C_w equal to zero but instead inserting a constant value of C_w into equation (87).

Many of the previous investigators have neglected the contribution of the initial zone in the process of diffusion and resulted in good agreement with data. The suggestion being that the diffusing process with polymers is similar to that with water. This is true in the intermediate and final region of the diffusion process where molecular diffusion is not the controlling factor. Experimental methods and apparatus used significantly control the results. For the external flow case studied here, ejection in a laminar

flow region prior to transition to turbulent flow may significantly influence the process. Data by Walters and Wells (1971) and Fruman and Tulin (1974) suggest the initial zone becomes very large. It is hypothesized, here, that by injection prior to transition, the turbulence intensity levels are extremely subdued resulting in elimination of the high level mixing process associated with the turbulent eddies penetrating the viscous sublayer. When injecting into established flows, as performed by many investigators, the dampening of the turbulent intensity does occur, but not before the polymer is dispersed at a rather normal diffusion rate consistent with other fluids (water). This results in low wall concentration, rather quickly, and therefore low drag reduction efficiency. The sections that follow describe an analytical model which includes an initial zone. Figure 33 schematically describes the model.

Considering first the initial zone where molecular diffusion is presumed to predominate, an approximation to the concentration entering the turbulent transition zone is made. Writing a simplified polymer conservation relation:

$$Q_i C_i = (Q_t + Q_2)\ C_t \tag{90}$$

where Q_t and C_t are the flow rate and concentration at the transition point, respectively, and Q_2 is an initial condition correction factor. The volume flow rate Q_t is given by the mean local laminar flow velocity, $.6U_e$, at the transition position radius r_{ot} and a

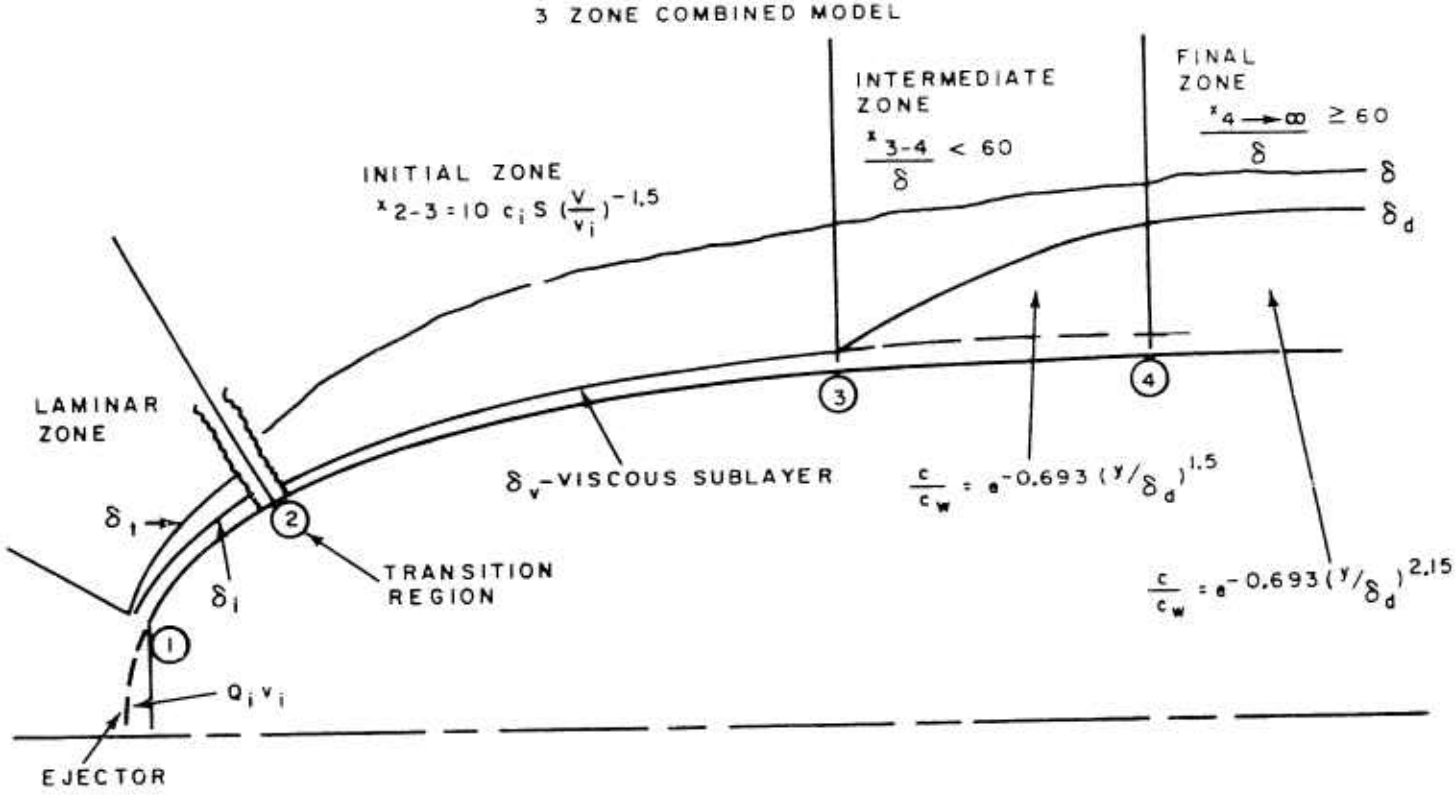

Figure 33. Schematic representation of diffusion model

laminar layer thickness, δ_t, determined from equation (78)

$$Q_t = .6U_e \, 2\pi r_o \, \delta_t . \tag{91}$$

The initial condition to the laminar flow boundary layer must be applied if the ejected volume of fluid exceeds the fluid in the laminar boundary layer at the periphery of the ejector. In equation form

$$Q_i - Q_e = Q_2$$

where Q_e is the volume flux through the laminar thickness calculated at the ejector periphery in a similar fashion to equation (91), and Q_2 is the volume flux difference which provides an "initial condition" and must be added to the boundary thickness at each station. The assumption is made that the polymer solution is uniformly mixed within this laminar layer. The local concentration at the transition point is then determined from (90). The volume flow rate into the viscous sublayer is determined by simple ratio of the thickness of the viscous sublayer height to the laminar layer height at transition.

$$Q_v = (Q_t + Q_2) \frac{\delta_v}{\delta_t} . \tag{92}$$

Approximating in this manner would tend to overpredict the flow into the viscous sublayer while underpredicting the flow in the region above the sublayer. The flow rate into the viscous region, Q_v, and the concentration, Q_t, are the parameters applied to the drag reduction and boundary layer calculations. This approxima-

mation allows for an excess quantity of fluid being introduced above the viscous sublayer. The portion of flow injected into the intermediate layer of the turbulent flow is given by

$$(Q_t + Q_2) - Q_v = Q_3. \tag{93}$$

This fluid will undergo a rapid diffusion characteristic of intermediate and far downstream diffusion as discussed earlier. The concentration of polymer at the transition point is as given previously, $C_t = \frac{Q_i\ C_i}{Q_t + Q_2}$.

Considering equation (59), the relation for this diffusion process is given by

$$Q_3 C_t = 2\pi\ (r_o + y_v)\ C_t \int_{y_u}^{\infty} u\ \frac{C}{C_t}\ (1 + \frac{y}{r_o + y_v})dy \tag{94}$$

where, for the assumption of uniform concentration in the sublayer, $C_t = C_w$ on the right side of (94). For $y_v << r_o$ equation (94) becomes

$$Q_3 C_t = 2\pi r_o\ C_w \int_{0}^{\infty} u\ \frac{C}{C_w}\ (1 + \frac{y}{r_o})dy. \tag{95}$$

Equation (95) may be integrated across the boundary layer at each x station resulting in a measure of the concentration profile above the viscous sublayer. It is suggested that this relation, (95), be solved as described in subsequent sections, as an independent solution to the two-zone diffusion process with flow and concentration inputs of Q_3 and C_t, respectively, but other boundary layer

and polymer wall concentration parameters governed by the basic initial zone calculations. This will avoid additional computer programming complexity. This calculation is only required if a measure of boundary layer concentration at particular heights in the boundary layer is desired. The extent of the initial zone has yet to be determined. Fruman and Tulin (1974) postulate a model for prediction of the extent of the initial zone for flat plates, based on an analogy to heat transfer. They show, for a near optimal ejection process, that the initial zone terminates for values of dimensionless distance greater than 8. The dimensionless distance used to correlate these data is:

$$\left[\left(\frac{U_o}{v_i}\right)^{1.5} \frac{x}{s} \frac{1}{C_i}\right] \tag{96}$$

where s is the slot width. For the axisymmetric case with nose ejection, an effective slot width may be defined as the ejection orifice area divided by the ejection circumference. For the model being applied in this study, the effective slot width is .07837 inches and C_i is replaced with C_t. No correction will be made to this relation for application to the axisymmetric case pending results of the test program. It should be reiterated that the initial zone length will normally be very small for dilute solutions of polymer as would occur if ejection were initiated in a highly turbulent region. For this type of ejection process, an intermediate and final zone model would be quite adequate.

Upon leaving the initial zone, relations for the prediction of wall concentration are required. Application of the Lagragian similarity hypothesis and the concentration similarity profiles discussed earlier coupled with the axisymmetric boundary layer relations and velocity profile provide the necessary relations.

A relation for solution of C_w in the highly turbulent flow field may be extracted by application of equations (57), (58) and (59)

$$Q_i C_i = 2\pi r_o C_w \int_0^{\infty} u \frac{\overline{C}}{C_w} \left(1 + \frac{y}{r_o}\right) dy \tag{97}$$

where, for the case of polymer flows with an initial zone, $Q_i C_i$ would be replaced with $Q_v C_t$. Changing to law of wall variables and dropping the overbars since we are dealing with average values throughout the turbulent flow field analysis

$$Q_i C_i = 2\pi r_o \nu C_w \int_0^{Y_e^+} u^+ \frac{C}{C_w} e^{2Y^+/r_o^+} dY^+. \tag{98}$$

Solving for C_w

$$C_w = \frac{Q_i C_i}{2\pi r_o \nu \int_0^{Y_e^+} u^+ \frac{C}{C_w} e^{2Y^+/r_o^+} dY^+}. \tag{99}$$

Equation (99) for polymer concentration is analogous to equation (34) for momentum. It is necessary to define a relation for C to solve equation (99) as it was necessary to develop an expression for u to solve equation (34). The similarity relations

given by equations (57) and (58) provide the needed concentration expressions

$$C/C_w = e^{-0.693\ (y/\delta_d)^{1.5}} \qquad \text{Intermediate Zone} \qquad (57)$$

and

$$C/C_w = e^{-0.693\ (y/\delta_d)^{2.15}} \qquad \text{Final Zone.} \qquad (58)$$

Within the final zone, for zero pressure gradient flows, δ_d/Y_e remains constant at 0.64. If there is a pressure gradient, data by Mellor (1966) indicate that the value of δ_d/Y_e changes to .53 in this zone.

The expression for the growth of the diffusion boundary layer, δ_d, equation (55), completes the analysis

$$a_1 \frac{d\delta_d}{dx} = \frac{b\ v^*}{u(\overline{Y})}. \qquad (55)$$

It is only necessary to determine the constant, a_1, in equation (55). Applying equation (48), changing variables and inserting a similarity concentration profile with variable exponent

$$\overline{Y} = \frac{\int_0^{\delta_d} C_w\, e^{-0.693(y/\delta_d)^{K3}}\, y/\delta_d\ d(y/\delta_d)}{\int_0^{\infty} C_w\, e^{-0.693(y/\delta_d)^{K3}}\, d(y/\delta_d)} \qquad (100)$$

which results in

$$\overline{Y} = K_2\ \delta_d = a_1\ \delta_d. \qquad (101)$$

Numerically integrating (100) for various values of K_3 between .5 and 5 yields values of K_2 which may be applied to (101) Figure 34 displays the results. Substituting (101) into (55)

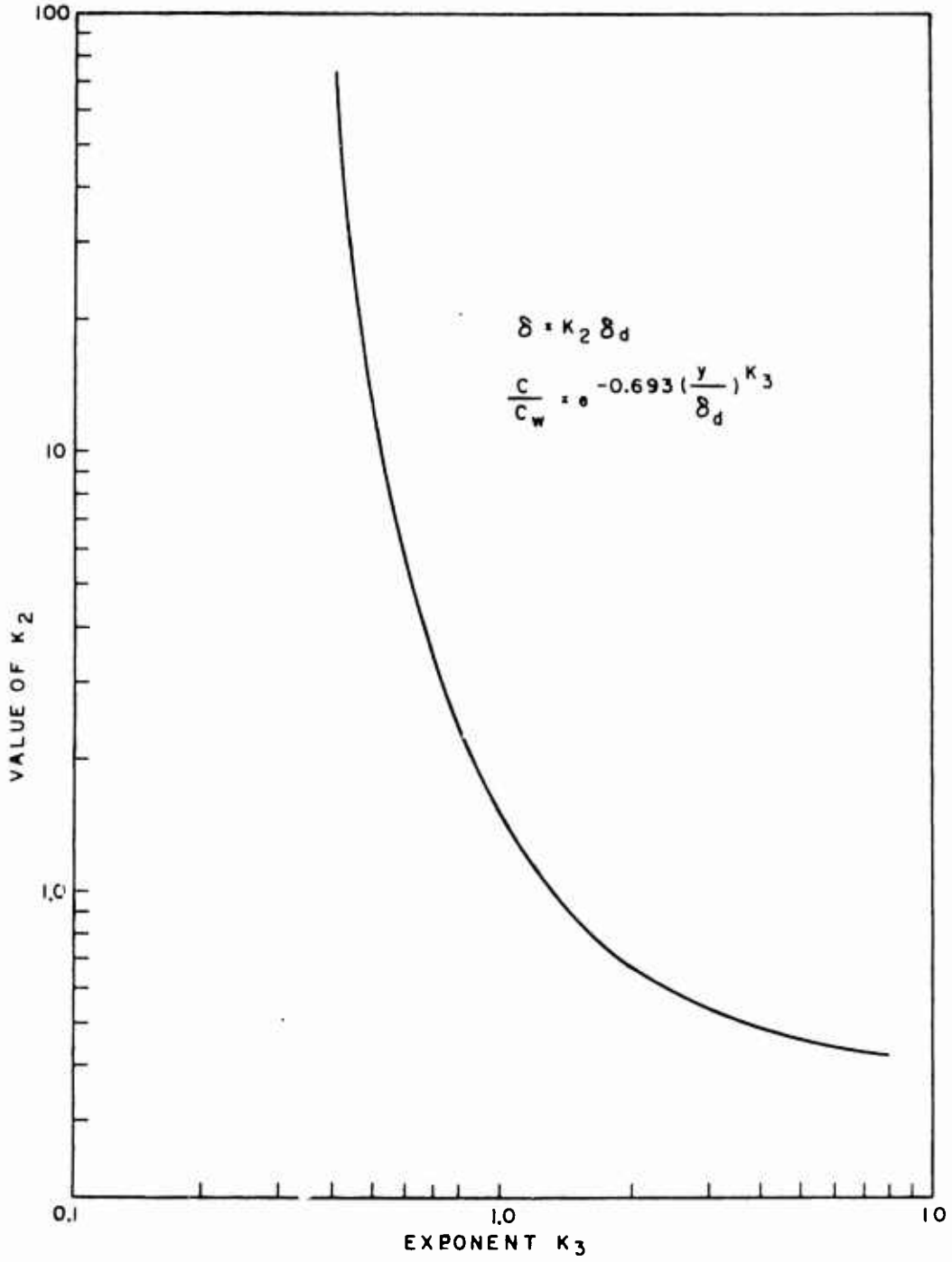

Figure 34. Value of K_2 for exponent K_3

yields a relation for δ_d

$$K_2 \frac{d\delta_d}{dx_s} = K \frac{v^*}{u_1} \tag{102}$$

where u_1 is the value of u at $K_2\delta$ and x_s, and K is the Karman constant. Virk (1971) has shown that the constant, K, used in the law of the wall varies with polymer addition resulting in an ultimate asymptote for the velocity profile in drag reduction cases. An effective value of Karman's constant may be determined. This new "constant," which is a function of ΔB, will be called K_5. The manner in which the modification of K to K_5 is determined relates to the basic equations for the velocity profiles with and without polymers, equation (87) and (32), respectively. Equating these equations

$$\frac{1}{K} \int_0^{Y_e^+} \frac{1}{Y^+} \left[1 - \frac{\alpha}{2} r_o^+ (1 - e^{2Y^+/r_o^+})\right]^{1/2} + \Delta B =$$

$$\frac{1}{K_5} \int_0^{Y_e^+} \frac{1}{Y^+} \left[1 - \frac{\alpha}{2} r_o^+ (1 - e^{2Y^+/r_o^+})\right]^{1/2} dY^+. \tag{103}$$

Solving for K_5 yields

$$K_5 = \frac{\int_0^{Y_e^+} \frac{1}{Y^+} \left[1 - \frac{\alpha}{2} r_o^+ (1 - e^{2Y^+/r_o^+})\right]^{1/2} dY^+}{\frac{1}{K} \int_0^{Y^+} \frac{1}{Y^+} \left[1 - \frac{\alpha}{2} r_o^+ (1 - e^{2Y^+/r_o^+})\right]^{1/2} dY^+ + \Delta B}. \tag{104}$$

The effect is apparent. K_5 is reduced dependent on the value of ΔB. In effect, reduction of the eddy viscosity through the mixing length is occurring. Depending on the value of u^+ and ΔB chosen, K_5 values approaching those of Virk's (1971) ultimate asymptote can be achieved. The effect of this change in K to some smaller value $K_5 = f(\Delta B)$ is to lengthen the intermediate mixing zone.

Equations (102), and (57) or (58) provide relation for the solution of C/C_w which, in turn, may be substituted into (99) yielding an expression for C_w. Equations (87) and (89), the boundary layer velocity profile and momentum equations, respectively, may then be solved. These relations apply for the intermediate and final zones of the diffusion process. Within the initial zone, equations (90) and (92) define the polymer wall concentration and flow, respectively. The equations for the intermediate and final zone are summarized below:

$$K_2 \frac{d\delta_d}{dx_s} = K_5 \frac{v^*}{u_1} \tag{102}$$

$$\frac{C}{C_w} = e^{-0.693(Y/\delta_d)^{2.15}} \qquad \text{For } x_s/Y_e > 60 \tag{58}$$

$$\frac{C}{C_w} = e^{-0.693(Y/\delta_d)^{1.5}} \qquad \text{For } x_s/Y_e < 60 \tag{57}$$

$$C_w = \frac{Q_i C_i}{2\pi r_o \nu \int_0^{Y_e^+} u^+ \frac{C}{C_w} e^{2Y^+/r_o^+} dY^+} \qquad (99)$$

$$u^+ = \frac{1}{K} \int_{0.1108}^{Y_o^+} \frac{1}{Y^+} \left[1 - \frac{\alpha}{2} r_o^+ (1 - e^{2Y^+/r_o^+})\right]^{1/2} dY^+ + \Delta B \qquad (87)$$

$$\frac{d\lambda}{dx^*} (3 \alpha H - G_1) + \frac{V'}{V} \lambda G_1 - \frac{\lambda^2 r_o^+}{2} (e^{2Y_e^+/r_o^+} - 1) \qquad (89)$$

$$+ \frac{\lambda^4}{R_L} \left(\frac{1}{4}\right)'' H = - R_L V - \lambda \frac{dr_o^+}{dx^*} I - \lambda \frac{dC_w}{dx^*} J$$

where the terms are as defined previously.

An alternate approach may be applied to attack the problem for developing flow. It is assumed the similarity expression for the concentration profile holds throughout the boundary layer. Lacking data for the effect of turbulence intensity changes in developing flow with polymer ejection, it is hypothesized that the similarity relation is functionally related to the boundary layer thickness, δ, the diffusion boundary layer thickness, δ_d, the Karman constant, K, and a distance from the inception of turbulence to the ejection slot, x_e, (set equal to 1 for cases of the ejection being at the transition to turbulent flow point or before). The exponent in the similarity expression is the controlling

parameter since it indicates the diffusion rate. The expression for the similarity profile may be written as

$$\frac{C}{C_w} = e^{-0.693\ (Y/\delta_d)^{K3}} \tag{105}$$

where $K_3 = f(\delta,\ \delta_d,\ K,\ x_e)$.

Poreh and Cermak (1964), as discussed, have empirically assigned specific zones relating downstream distance and the boundary layer thickness to establish the exponent value. It seems apparent, that in the intermediate zone, the value of the exponent should not be constant. Concentration profiles as a function of downstream distance by Walters and Wells (1971) bear this out. Rewritting (105) in terms of K_5

$$K_3 = f(\delta,\ \delta_d,\ K_5,\ x_e). \tag{106}$$

Assuming a nondimensional relationship which allows the exponent to grow as the diffusion boundary layer grows results in

$$K_3 = C\ K_5\ \frac{\delta_d}{\delta}\ \frac{x_e}{L}\ . \tag{107}$$

For final zone of diffusion where the characteristic diffusion rates of polymer and water have been shown to be the same,

$K_5 = K = .4$

$\frac{\delta_d}{\delta} = .64$ for zero pressure gradient flows

$\frac{x_e}{L} = 1$ since ejection preceeds the turbulent transition point and $K_3 = 2.15$.

Solving for C in (107) yields

$$C = 8.4 \tag{108}$$

From which (107) is defined as

$$K_3 = 8.4\ K_5\ \frac{\delta_d}{\delta}\ . \tag{109}$$

For developing polymer flows with the ejector at or preceeding the point of transition to turbulent flow (using the test model described earlier),

$K_5 = .2$

$\delta_d = .0008$ ft (for the model flow rates)

and $\delta = .003$ ft (equation (80))

the value of K_3 becomes

$K_3 = .45$

and the value of the moment, K_2, may be determined from Figure 34. The constant $K_3 = .45$ implies an extremely suppressed diffusion process, which in fact, on computation, occurs. Application of (105) with the Lagrangian similarity hypothesis for predicting the diffusion boundary layer growth would eliminate the need for a multi-zone. The exponent, K_3, would be self-adjusting throughout the boundary layer. The simple form chosen for K_3 may be incorrect. Sufficient data would be required in all diffusing zones to properly define whether the similarity profile extends to the boundary layer and to define the proper functional form. Application of this method would require integration of equation (100) rather than use of Figure 34. This is required since equation (100), although

integrated between 0 and ∞ in reality reaches final values for values nearer 4 or 5. For cases where δ_d may be small, as for much reduced diffusion, the value may become quite large and should be bounded by the viscous sublayer thickness, for $\delta_{d_{min}}$, and the boundary layer thickness for δ_{max}. This will prevent the moment, K_2, from becoming very large for low values of K_3 as implied by Figure 34. Extensive effort in pursuing this approach was not expended since the molecular diffusion coupled with the two zone model is believed to represent a sounder approach.

The equations may be solved for the skin friction distribution $C_f(x)$, the boundary layer thickness, δ, and the diffusion boundary layer thickness, δ_d. Additionally, the concentration at the wall, C_w, and at any position in the boundary layer, C, for a given polymer or tracer flow and ejection concentration and ejection rate can be determined. The initial conditions required are an estimation of λ_0, and the known flow condition U_e and r_o as functions of x. Inputs of velocity, temperature and related parameters, ejection rate and polymer concentration are required. It has been assumed that the flow becomes turbulent at the minimum pressure point and all initial conditions are determined at this point. From these input conditions, δ_{do} may be determined from a mass balance at $r_o(x)$ and δ_o may be calculated from (80). ΔB_o may be calculated from (42). An estimate for the skin friction term λ_o comes from the flat plate relation.

$$C_f = 0.0592\ R_{e_x}^{-1/5} = \frac{2}{\lambda^2}\ . \qquad (110)$$

Figures 35, 36 and 37 present the pressure coefficients vs normalized axial distance for the three bodies discussed earlier. The pressure coefficients and other flow conditions, U_e/U_o, have been determined using the Douglas-Neumann Potential Flow Program (1958) and are required for solving the previous system of equations. The total drag on the body has been determined by integrating the calculated skin friction and by integrating the pressure distribution over the body to the point of separation. As pointed out by White (1972), equation (89) provides a distinct test for separation when the coefficient $(3\alpha H - G_1)$ vanishes which causes λ to approach ∞ and C_f approaches 0. At this point, the pressure is determined and multiplied by the projected area at the radius, $r_o(x)$ of separation. Thus, both friction and form drag are accounted for. The form drag calculated in this manner may exhibit large errors due to the steepness of the calculated pressure coefficient in the tail region as seen in Figures 36 through 37. Data on pressure coefficients for similar bodies, Nadolink (1968), do not exhibit this steepness. The calculation is simple, however, and does provide an indication of the total drag.

The equations have been programmed on a Control Data Corporation Computer, CDC 3300. All numerical integrations use the standard RUNGE-KUTTA subroutine. Appendix B contains a sample of the computer program and solution for the combined model. A difficulty does occur in the formulation when a favorable pressure is encountered

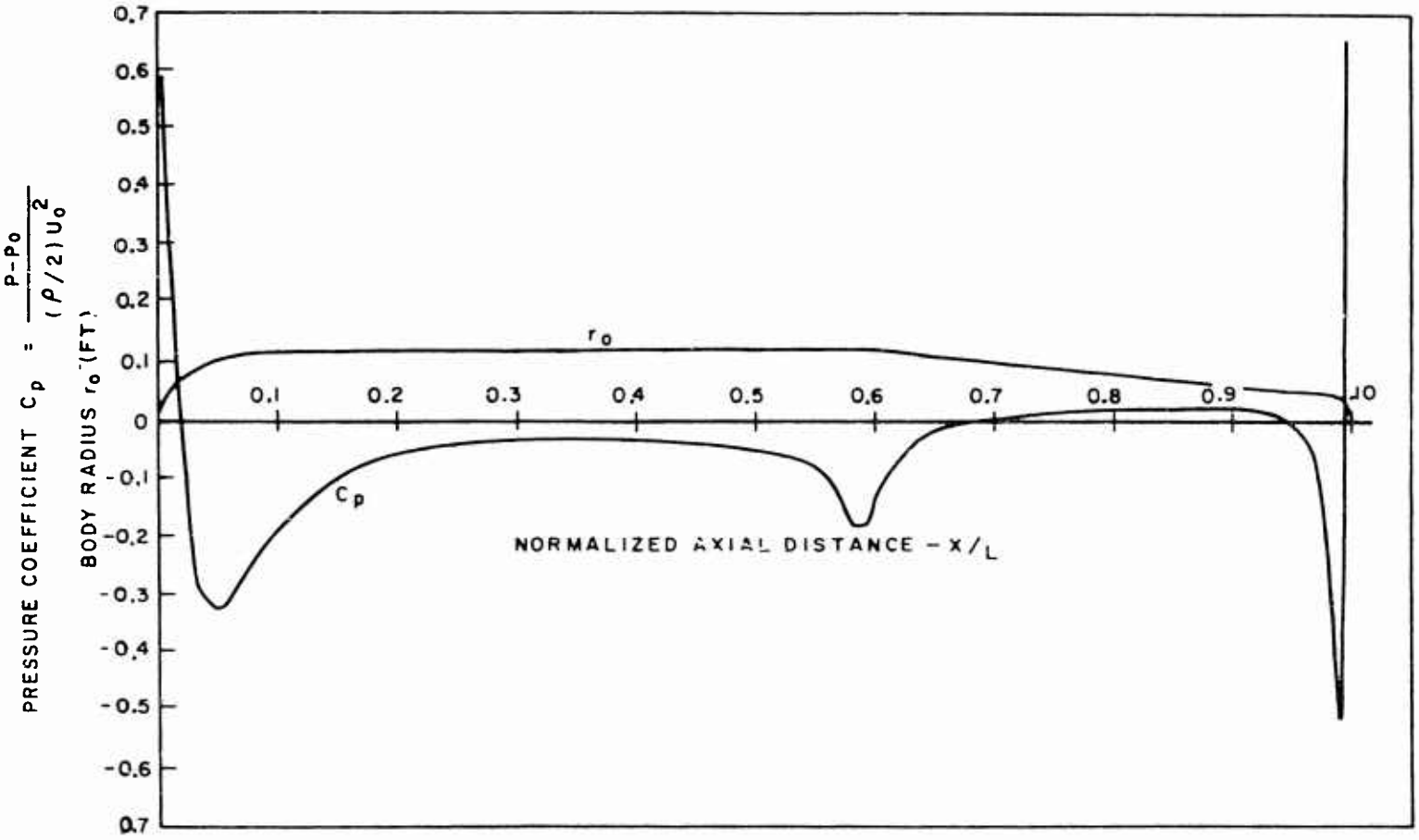

Figure 35. Calculated pressure distribution over axisymmetric body - 6° cone tail configuration

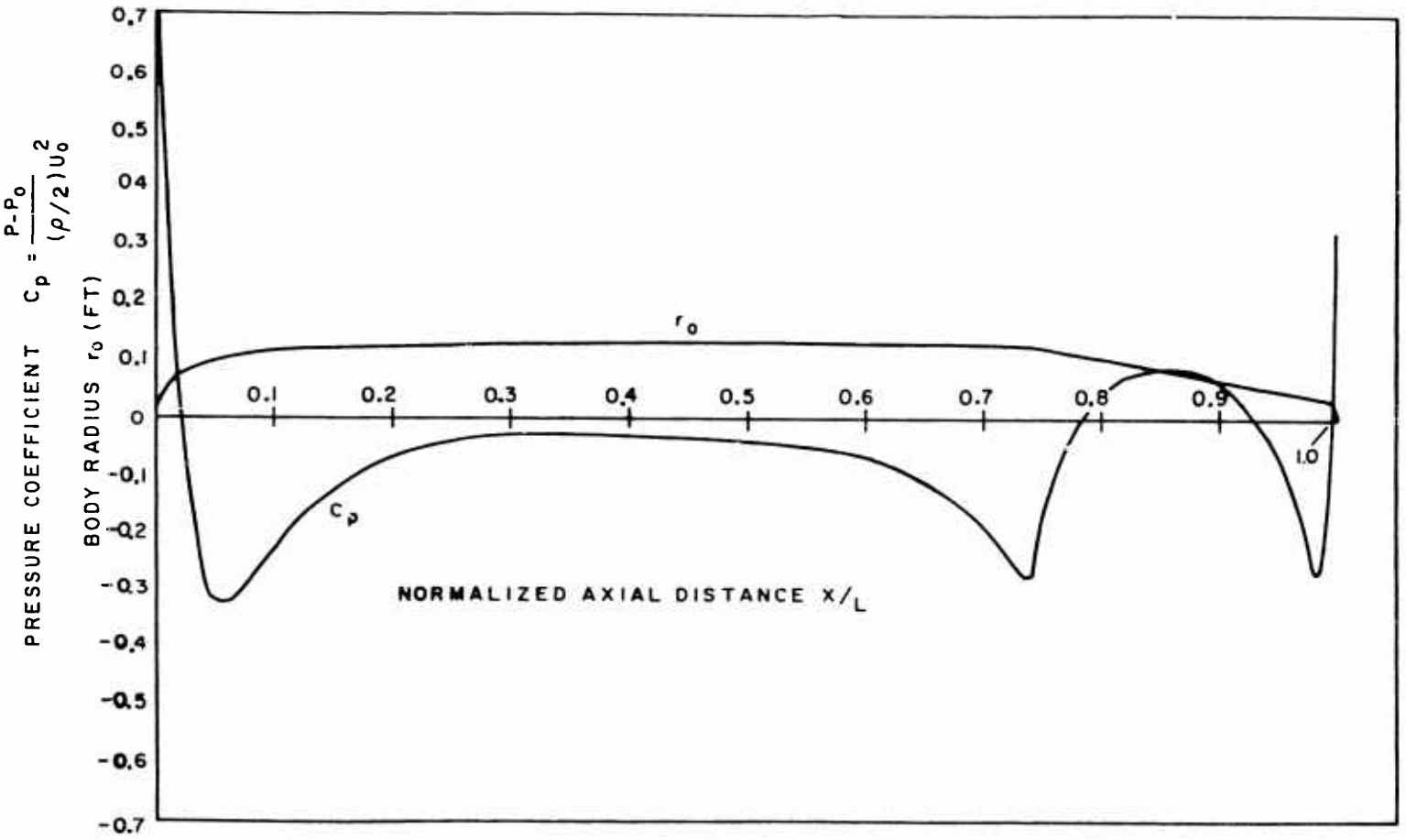

Figure 36. Calculated pressure distribution over axisymmetric body - 12° cone tail configuration

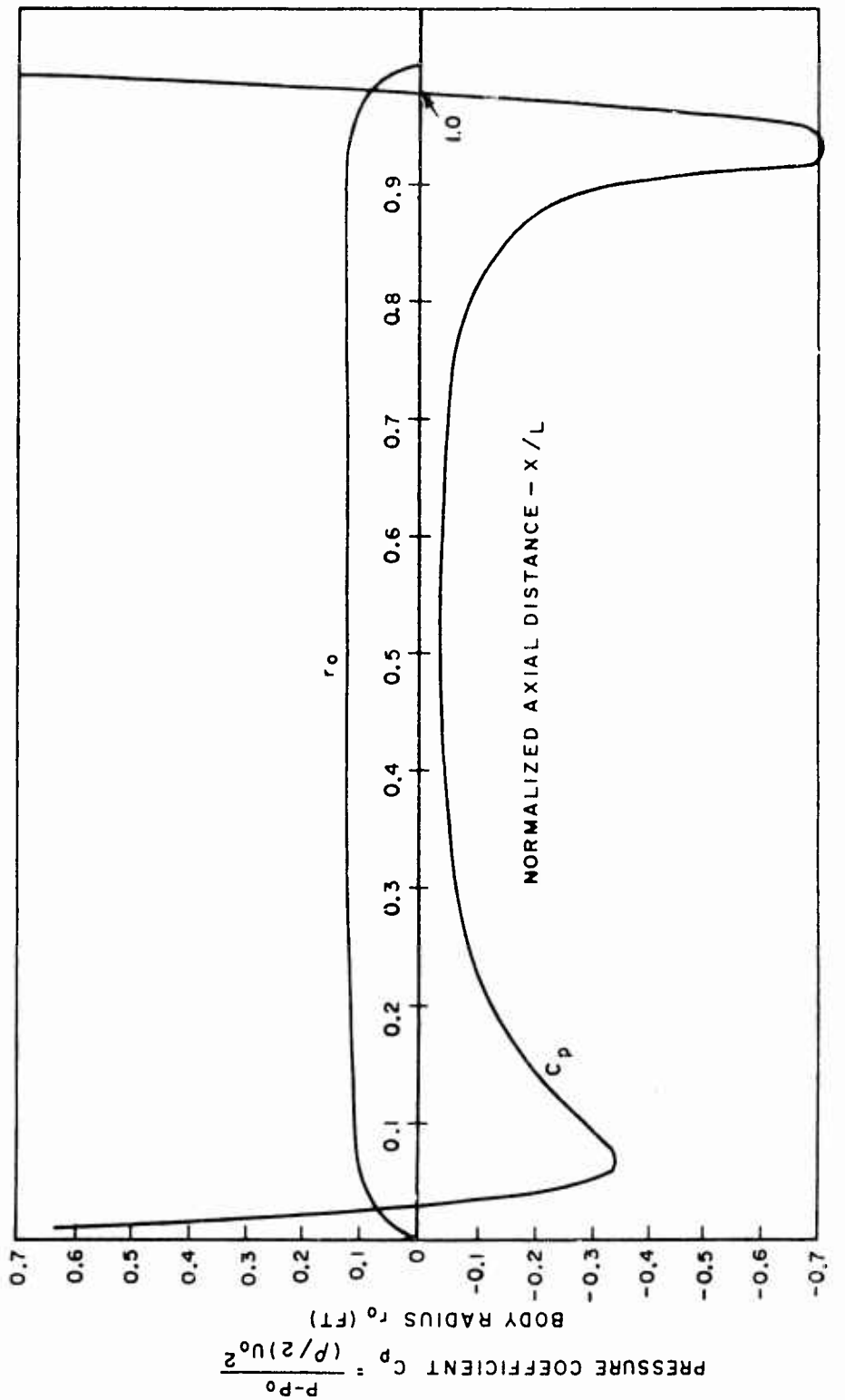

Figure 37. Calculated pressure distribution over axisymmetric body - spherical tail configuration

(negative ω). Equation (89) diverges resulting in no solution. The problem is resolved by not allowing α to become negative. This does introduce a discontinuity into the solution but recovery from the discontinuity is rapid. Two methods of solution are possible for the determination of λ in equation (89). The full equation may be used, which for small polymer wall concentration gradients $\frac{dC_w}{dx}$, provides for stable solution. For higher concentration gradients, an alternate approach is recommended. A solution for λ may be obtained neglecting the last term in equation (89). The value of λ is then corrected at each calculation interval as noted below:

$$\lambda = \lambda_{calculated} - (\Delta B_o - \Delta B) \qquad (111)$$

where ΔB_o is the previous calculated value of ΔB. In this manner, the new calculated value of λ is corrected for an updated ΔB resulting in the appropriate λ. The full equation (89) does provide a solution at the higher concentration gradients but the solution tends to become oscillatory requiring a large number of calculation points to minimize the oscillations.

The analytical model has been exercised in several different ways to test the results that may be obtained. For purposes of ease in discussing these models, they will be given specific names. First, the molecular diffusion model only contains the molecular diffusion portion of the analytical program and never switches to a higher diffusion two-zone model. The second model is called

the two zone model, the initial zone is very small and not included. This model is applicable to water diffusion or to polymer diffusion if the ejector were placed in an established turbulent flow. The third model will be called the combined model and represents the near optimal external flow process for polymer ejection, ejecting into the laminar region prior to turbulent flow transition. The postulated model, with variable K_3 is tested, in a single case, for comparison. The total model is shown schematically in Figure 33.

The calculations were all made using the 6^{o} tail model, a velocity of 27 ft/sec, an ejection rate of 20.6 in^3/sec, unless otherwise noted, and a medium temperature of $60^{o}F$. The length Reynolds number is 4.5×10^6. The primary emphasis in these calculations has been on the concentration profiles and, more specifically, wall concentration profile. It should be remembered, however, that the computer routine and analytical model allow determination of concentration throughout the boundary layer, the growth of the diffusion boundary layer within the hydrodynamic boundary layer and other boundary layer parameters. Skin friction and total drag is also determined and a comparison of the drag reduction resulting from the different diffusion processes as the three models (really one applied differently excepting the variable K_3 model) predict are compared in Table 4.

Figure 38 displays polymer wall concentration ratios vs axial distance calculated using the molecular diffusion model and the two-zone model. For comparison purposes in the drag reduction calculations, the water case for the two zone model is considered to be the baseline. This model, for water, is accurate as will be shown in subsequent sections. The molecular diffusion model presents the optimal case for drag reduction on external flows. The viscous sublayer growth is rather small over the body length, a growth of less than .001 inches over the x/L distance displayed, resulting in the flat concentration profile. The prime reason for the reduced concentration to that ejected is due to the diameter ratio from the ejection diameter to the near maximum body diameter. Since, for molecular diffusion, the concentration at the wall does not change appreciably, the single line shown applies to all polymer concentration so long as γ equals 11.5. For values of polymer concentration less than 50 WPPM, ΔB in the model would change resulting in a wall concentration variation. For this case, only v^* affects the calculations. The two zone model for 50 and 500 WPPM shows rapid dispersion of the polymer resulting in less than 1/10 the ejected concentration at about 1/2 the body length. This type of diffusion process would predict high polymer concentration or ejection rates required for reasonable drag reduction. The model would be reasonably accurate for long bodies where the initial zone is small compared to the body length.

The effect of concentration is evident with a maximum wall concentration, over the portion of the body shown exceeding that required for maximum drag reduction for ejected concentration above approximately 200 WPPM. The model, as implemented, does not include changes in viscosity for high polymer concentrations. The effects must be accounted for if large concentrations are applied.

Figure 39 displays the two-zone model compared to a data adjusted model based on data generated in the test program. Essentially, the two-zone model is reduced to a single zone model with the exponent value in the similarity expression (58) being that determined from the experimental data, .75. The effect of suppressed diffusion is apparent with concentration levels being much higher. Care must be taken in interpreting this figure, as will be discussed in the experimental section where the data is qualified. For the moment, the effect of a change in the exponent is the important factor shown here.

Figure 40 displays the variable K_3 model predicting very low diffusion and therefore high wall concentrations as compared to the two-zone model. The results are interesting warranting further development of the functional form of the K_3 function (106).

Figure 41 displays the results from the combined model compared to the two-zone model. The transition from the molecular model to the two-zone model is clearly evident as controlled by the effect of concentration on the initial zone length in equation

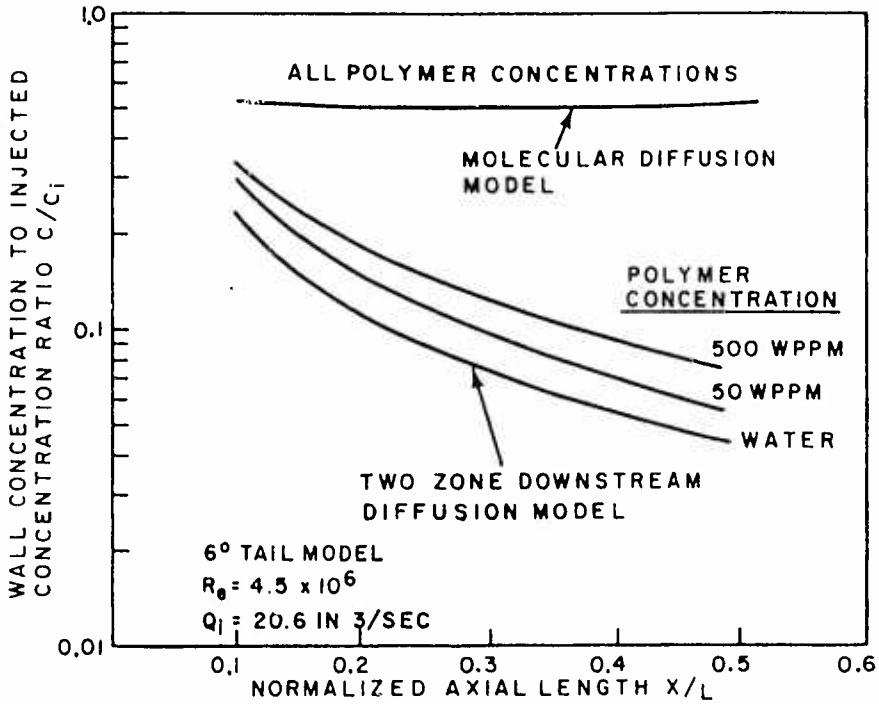

Figure 38. Comparison of predictions of wall concentration ratio of two-zone downstream diffusion model with molecular diffusion model

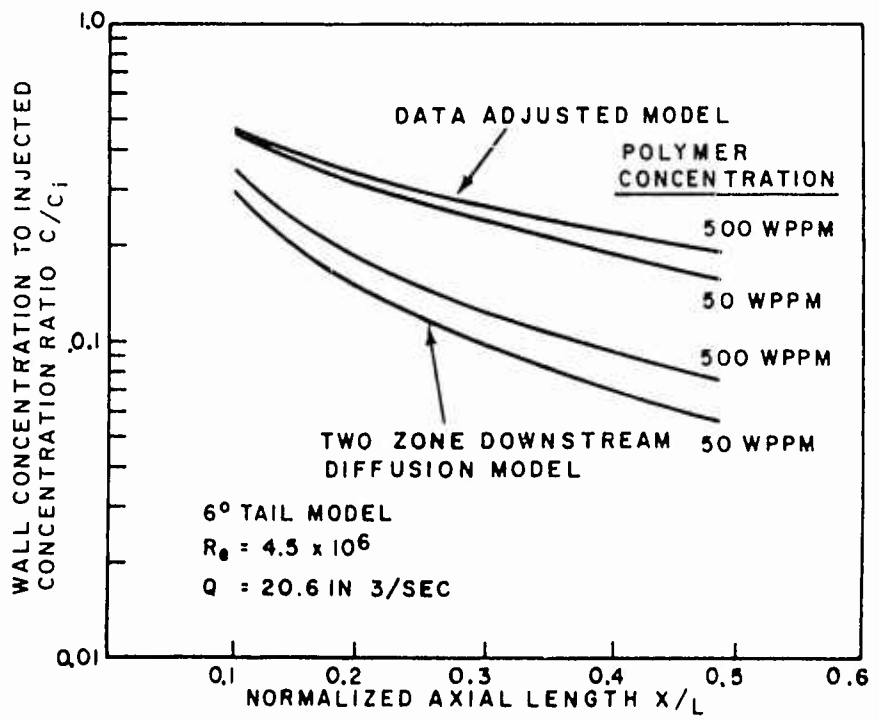

Figure 39. Comparison of predictions of wall concentration ratio of two-zone downstream diffusion model and experimental data adjusted model

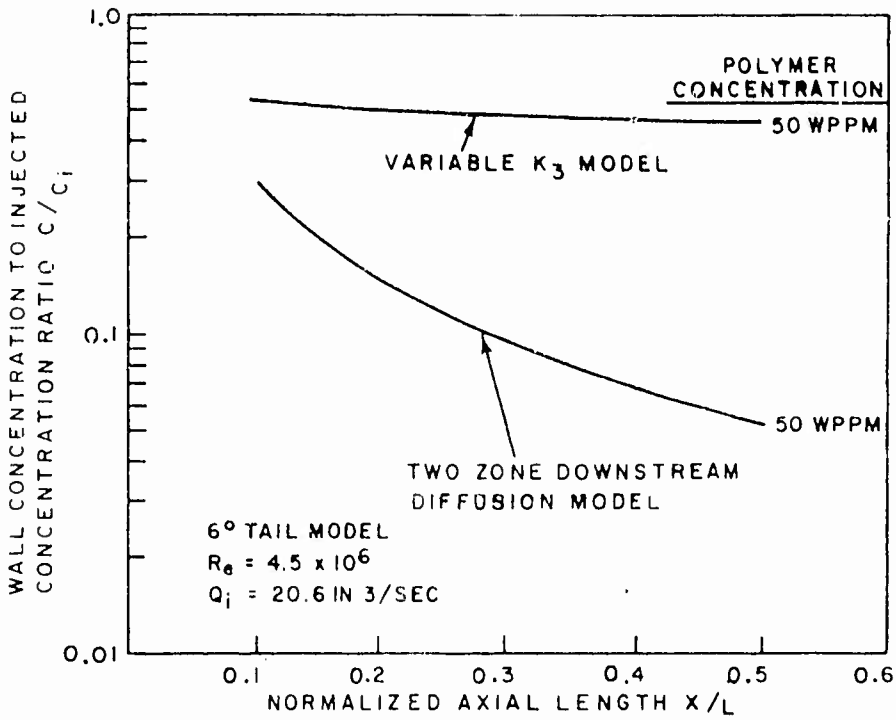

Figure 40. Comparison of predictions of wall concentration ratio of two-zone downstream diffusion model and variable K3 model

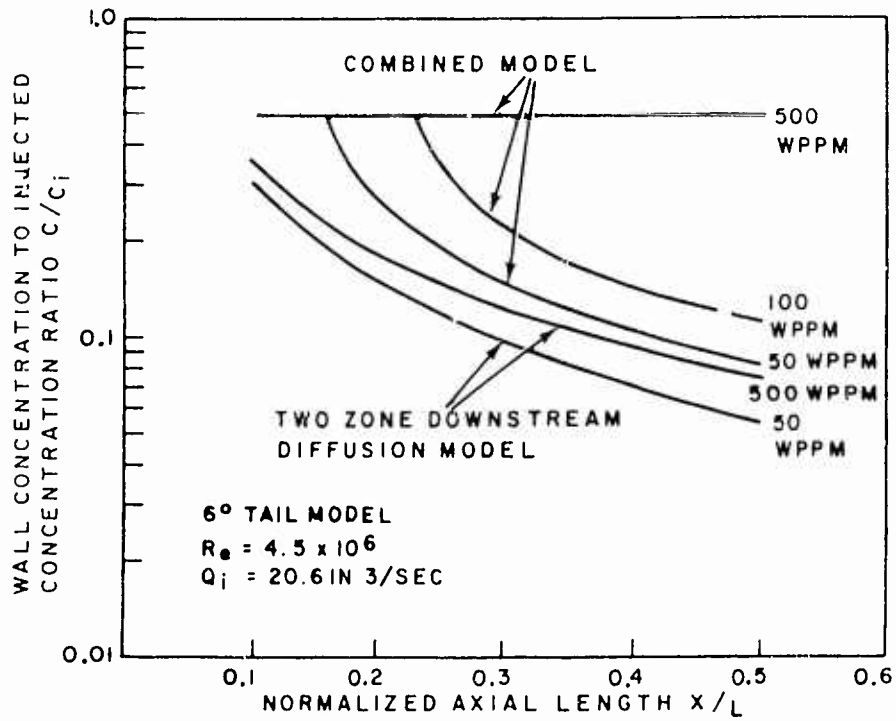

Figure 41. Comparison of predictions of wall concentration ratio of two-zone downstream diffusion model and combined model

(96) and data from Fruman and Tulin (1974). This model should adequately predict the polymer diffusion process for the initial, intermediate, and final zone of diffusion subject only to verification of the abrupt transition from the initial to intermediate zone similarity profile. Quite possibly a more gradual transition, as suggested by the variable K_3 model, would be appropriate. Figure 42 displays the effect of the ejection rate, for a fixed 50 WPPM polymer concentration, on the wall concentration ratio. The shift in the transition from the initial zone to the intermediate zone is apparent and governed by the changed ejection velocity in equation (96). Figure 43 taken from Fruman and Tulin (1974) displays wall concentration data calculated from the combined model plotted against the reduced dimensionless distance, equation (96). As may be seen, the combined model, applying the Lagrangian similarity hypothesis, results in good agreement with data obtained by Tulin.

The percent total drag reduction and percent skin friction reduction have been calculated for the cases discussed using the relations

$$\% \text{ TDR} = 100 \left(1 - \frac{D_{POLY}}{D_w}\right) \tag{112}$$

and

$$\% \text{ SFR} = 100 \left(1 - \frac{SD_{POLY}}{SD_w}\right) \tag{113}$$

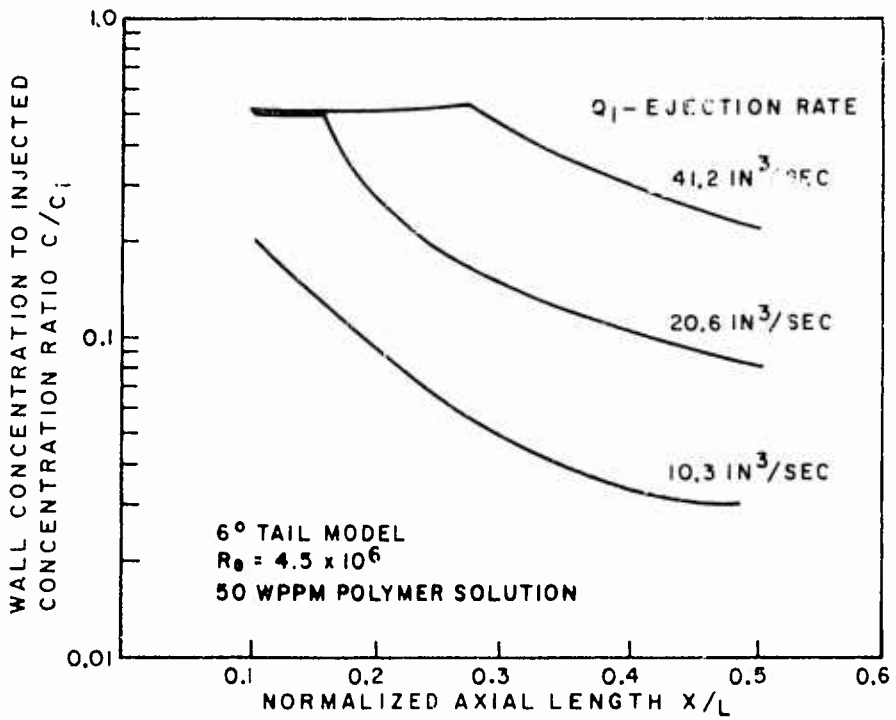

Figure 42. Effect of polymer ejection rate on wall concentration ratio - combined model - 50 WPPM polymer concentration

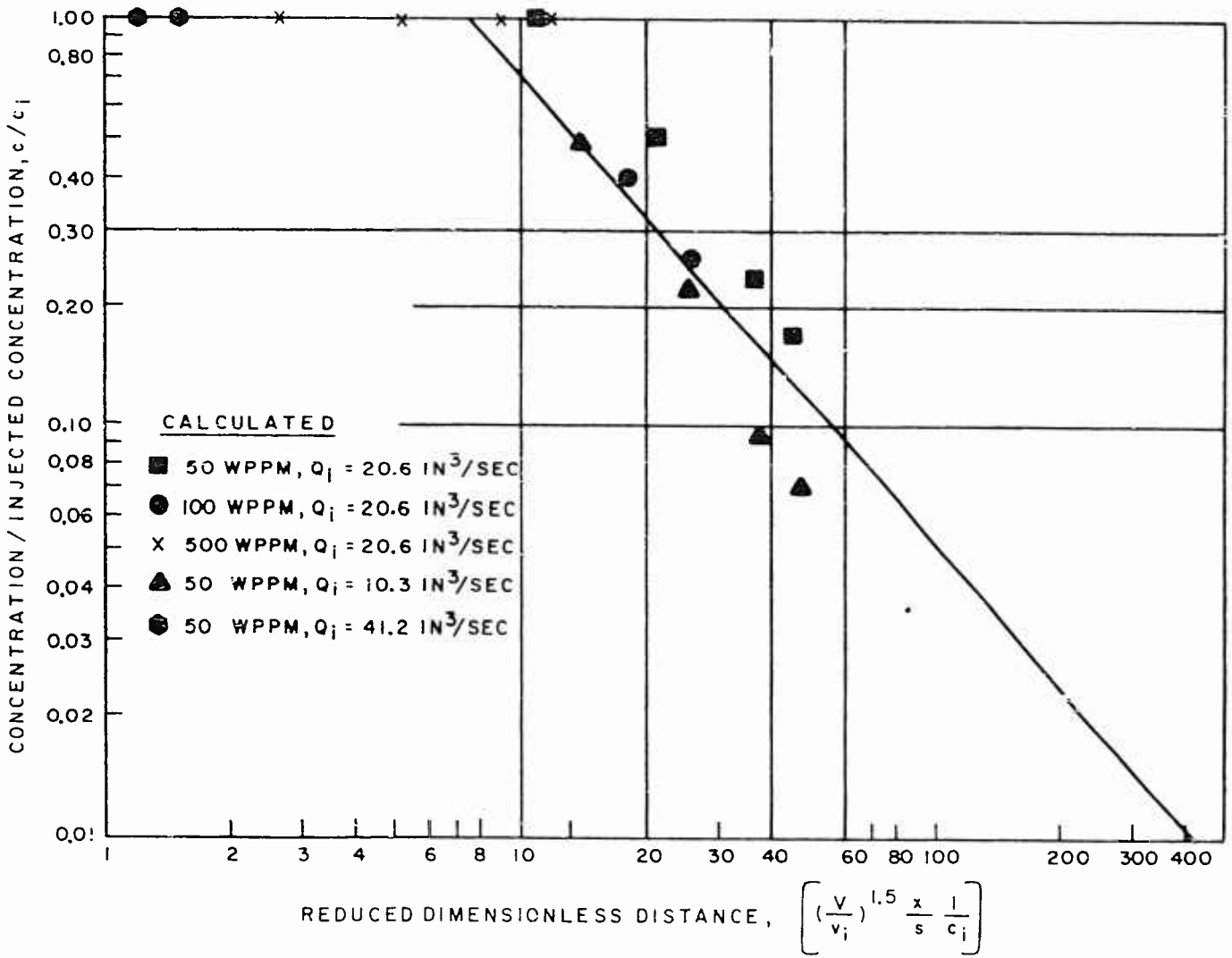

Figure 43. Dimensionless concentration vs reduced dimensionless distance (from Fruman and Tulin (1974))

where

D_{POLY} = total calculated drag with polymer ejection

D_W = total calculated drag with water ejection

SD_{POLY} = shear drag calculated with polymer ejection

SD_W = shear drag calculated with water ejection.

Table 4 lists these results. A discussion of the table will not be given since the results are as would be expected for the wall concentration shown in the previous figures.

The system of equations presented herein is believed to have several unique qualities. First, presuming that a reasonable ejection process occurs, the equations account for a change in the mixing length constant resulting in a significantly reduced diffution process. This should represent a near-optimum case for developing flow. Secondly, by maintaining the mixing length constant equal to that of water, the model represents the ejection of polymers in a fully developed turbulent flow where the similarity concentration profiles are equivalent to those of water. Thirdly, the model accounts for the initial zone of diffusion as well as the subsequent zones, which should provide an accurate prediction of the wall concentration. These beliefs will be tested in subsequent sections.

TABLE 4

Calculated Drag Reductions

Model Applied	Conditions Polymer CONC/Q_1(in^3/sec)	% TDR	% SFR
2 zone	Water/20.6	0	0
Molecular Diffusion	50,500/20.6	32.6	65
Variable K_3	50/20.6	31.2	62.3
Data Adjusted	50/20.6	27	55
	500/20.6	32	65
2 zone	50/20.6	22.6	44.6
	500/20.6	32.6	65
Combined	50/41.2	30.3	60.6
	50/20.6	24.6	50.3
	50/10.3	17.8	37.8
	100/20.6	30.1	60.4
	500/20.6	32.3	64.2

V. EXPERIMENTAL PROCEDURES

Two types of tests were performed in this research. These were: (1) polymer ocean, drag reduction and flow visualization tests and (2) polymer ejection boundary layer sampling tests. Both series made use of the full experimental apparatus but in slightly different ways. The experimental procedure for the polymer ocean tests will be discussed first.

A. Polymer Ocean Tests

General

The polymer ocean tests made use of the three dye ejecting bodies described previously and displayed in Figures 11, 12 and 13. The test series is called polymer ocean since for these tests the entire drop tank is filled with either fresh water or filled with a polymer solution. The model, therefore, is operating under conditions of uniform polymer concentration. A visible dye was ejected, by aspiration in many of the tests.

Polymer Addition

The polymer used in these tests was polyethylene oxide (Polyox-WSR-301, Union Carbide Corp.). Polyox is a long, 3 million molecular weight, water soluble polyether. Due to its considerable size and the sensitive ether linkage, the mixing of highly concentrated solutions must be undertaken with great care. A 25% by weight

polymer slurry was made up for mixture with the water in the tank. The test program called for polymer ocean concentrations of 60 WPPM to 1.25 WPPM. Since the water tank weight of water equaled 3452.5 lbs, 3452.5 x 10^{-6} lbs of polymer addition were required for each WPPM of polymer concentration desired (or 13810 x 10^{-6} lbs of 25% polymer slurry by weight). The tank was first brought to 60 WPPM concentration level, tests performed, and then drained to a predetermined level and refilled with fresh water to obtain 50 WPPM. After testing at this level, the procedure was repeated to obtain 20 WPPM and 5 WPPM. The tests requiring concentrations down to 1.25 WPPM and 2.5 WPPM were begun with a 20 WPPM concentration.

The mixing procedure consisted of premixing the preweighed 25% polymer slurry in a 25-gallon drum by slowly pouring the slurry against a wall of the drum, and spraying a high intensity fan shape spray of water on the polymer. Gentle stirring followed for approximately 1/2 hour and the mixture left to stand for 2 to 4 hours. The clear solution was then poured into the partially empty drop tank and the tank refilled. The tank was gently mixed by raising and lowering the retrieval net to insure a homogeneous mixture. Samples were taken at each concentration and measured in a Hydrat apparatus similar to that described in Hoyt (1966).

Model Preparation

The models for testing were configured in the 6° tail, 12° tail or spherical tail configuration as discussed previously. The model preparation for test was as described previously. It is repeated here for completeness. Referring to Figures 14 and 15, the model is made ready for a launch by inserting the tank guide wire through the body guide tube, (9), the wire bears on a nylon bearing at either end of the model to minimize friction. The tail, (10), of the model is removed (separated sufficiently) and the internal cavity filled with dye. The dye ejection ports, (6), being previously taped over to insure no loss of dye. The model is reassembled and the vent screw (unmarked) in the tail is removed and the model placed under the water level in the tank to back fill the cavity totally with water. The model may now be fired upon removal of the tape over the ejection holes. When fired, stagnation pressure enters the 4 stagnation ports, (1), is transmitted through the body guide tube and pressurizes the bladder, (4), forcing the dye out the four dye ejection ports located at the minimum pressure point of the forebody as determined by a potential flow program. After several tests, the bladder was found to be not necessary simplifying the operation. The tail of the model was then inserted into the launcher in preparation for launching. The launcher receptacle, as designed, mates with the 6° tail only. The other models are butted to the

launcher. The models are held in place by fishline that is tied to one side of the launcher, wrapped around the wire in front of the nose of the model and tied to the other side of the launcher. At launch, the string is severed by the forward motion. When in the ready to fire condition, all except the tail is underwater. After firing, the model is maintained on the wire in the tank, the ejection holes retaped underwater, the tail removed and the internal chamber drained and refilled with dye. The model is reassembled as before and made ready for a launch.

Launch Procedures

The launcher operation was quite simple. The low pressure regulator on the launcher was preset to some known pressure level. The hand firing valve was opened, firing the launcher. The launcher chamber pressure was recorded during this operation. The model velocity was measured at the several stations and noted for acceleration or deacceleration. The launcher pressure was then adjusted to obtain steady state velocities during the model travel down the tank. After fire, the firing valve is closed, the launcher piston chamber vented, and the firing piston retracted in preparation for the next test.

Velocity and Photographic Measurements

Little needs to be said regarding procedures here. It was only necessary to reset the counter and set the camera flash guns delay circuitry to the appropriate value. At launch, the camera shutter was held open. The appropriately delayed flash would

expose the film. Transit times through the various stations were automatically recorded.

Polymer Ocean Test Series

Two types of tests were performed. Launch tests in which the launcher was used and free drop tests, in which the model was held just underwater and allowed to gravity drop down the tank. The launch tests were all performed with the 6^{o} tail model. The free drop tests were performed with the 12^{o} tail and spherical tail model. This type of test was initiated since gross instabilities in trajectory of the models (12^{o} and spherical tail) occurred when launchings were attempted. Undoubtedly due to the launcher receptacle having a 6^{o} taper design to fit that model.

The test series are summarized in Table 5. For the launch tests, only those tests at which terminal velocity was achieved are noted. A total of 491 tests were run of which 135 tests are reported.

TABLE 5

Summary of Tests Performed
Polymer Ocean Series-Number of Tests

POLYMER CONCENTRATION PPMW	LAUNCH TESTS 60 TAIL	FREE DROP TESTS 12° TAIL	FREE DROP TESTS SPHERICAL TAIL
FRESH WATER	8	7	7
1.25	-	8	-
2.5	4	-	-
5	10	6	7
10	-	9	-
20	7	6	11
50	2	6	-
60	12	6	19

B. Polymer Ejection Tests

General

The polymer ejection tests made use of the polymer ejecting body described previously and displayed in Figure 18. In these tests, varied polymer concentrations as well as pure water all dyed with a fluorescent dye, Uranine-B, were employed. Simultaneously, either wall samples or samples at two different distances from the wall in the boundary layer were taken at four axial positions. Visible dye was also mixed with the polymer on specific tests for boundary layer photographs.

Polymer Preparation

The polymer used in this series of tests was also polyethylene oxide (Polyox-WSR-301).

The test matrix called for solutions in the 50 to 1000 PPMW range. A master solution was prepared at 2000 ppmw and diluted to the required concentration.

The master solution was prepared by sifting the premeasured polyox powder onto the surface of the carefully weighed water which was being slowly stirred by a magnetic mixing bar. After a clear solution resulted (approximately 1 hr.), the solutions were left to stand for approximately 40 hrs. to minimize the high viscoelastic effects of freshly mixed solutions, and to assure homogeneity. The master solution was kept in a dark, cool place after initial mixing to reduce the auto-oxidation problem with polyethers. When required, the proper amount was pipetted out of the master solution and diluted to the required concentration. These dilute solutions were used within 24 hrs. of the make-up time.

The uranine master solution was prepared in the same manner. Thus, when a test solution was required, the proper amount of each constituent was added to enough water to make one liter of solution. This was poured back and forth into the container ten times to assure complete mixing, and then let stand for one hour to achieve homegeneity.

A series of calibration tests with the fluorometer indicate that this procedure is adequate to obtain accurate results.

The phenolphthalein solution was also mixed with the polymer solution in the same manner as the uranine to provide a visible dye for photographic record purposes. Fluorometric readings were not taken during these tests since the slight opaqueness of the phenolphthalein resulted in erroneous fluoressence readings were attempted.

The test series conducted required polymer solutions of 5 PPMW, 10 PPMW, 20 PPMW, 50 PPMW, 500 PPMW and 1000 PPMW.

Model Preparation and Data Retrieval

The ejecting 6^{o} tail model has been previously described. The assembly for a test and the subsequent withdrawal of samples is discussed below. The model is assembled, as described previously, excepting for the half-body nose and placed in the assembly tank, Figure 23. The appropriate flush-mounted probes or boundary layers pitot tubes are installed. The installation procedure for the flush probes consists of partially inserting the flush probes, placing a small amount of wax around their periphery, heating lightly with a propane torch and pressing the probes flush with the surface. The pitot-like probes were installed in a similar fashion excepting that a feeler gauge set at either .020 inches or .050 inches, depending on probe set, was placed under the flattened tip of the probe, Figure 20. The probe area at the surface of the body

was filled with wax and flaired in with a razor blade. The height could be reasonably set within .003 inches by this method. The axial orientation was set by eye, but with the extent of the probes, .03 inches, an offset of several degrees was easily noticed and corrected.

The assembly tank was now filled with water to just below the polymer storage volume level. A background sample of the assembly tank water and drop tank water was taken at this time to correct sample fluorence readings. The solution to be ejected was then poured carefully into the polymer storage volume, Figure 17, and the halfbody nose carefully installed. The model now resides in the assembly tank, nose up, and must be transferred to the drop tank, nose down. The ejector screen was then taped with electrical tape to insure no leakage occurred on transfer to the drop tank. The guide wire was threaded through the model and the model transferred to the drop tank. The model is now inserted into the launcher receptacle and a nylon shear screw affixed through the launcher to the firing rod on the model. This holds the model in place and fires the CO_2 cartridge ejecting the polymer and withdrawing boundary samples at launch. After firing and the launcher retracted, the model is kept underwater while preparations are made to quickly wipe it dry on removal from the tank prior to placing on four separate collection trays. The model is removed from the wire, wiped dry and placed on a stand, horizontally, over

four collection trays, (keeping the top uppermost for reasons explained under the calibration section). After the samples have drained into the collection trays, the model was totally disassembled and washed prior to the next test. The chamber samples were then tested applying the fluorometric techniques described previously. The fluorometer readings were transferred to fluorescent dye concentration measurements in PPMW using the appropriate calibration curve, Figure 21 or 22, and then converted to undiluted values applying the external to internal calibration curves, Figures 24 through 31. These values, when nondimensionalized with the ejected dye concentration, represent the normalized concentration of any ejected tracer, or the polymer, at that particular station or boundary layer height under the assumption of similar diffusion qualities.

Launch Procedure

The launch procedure is the same as for the previous tests. No attempt was made to achieve terminal velocity since a significant number of tests are required to do this. The ejector type tests took approximately one hour per complete test cycle as compared to 15 minutes for the polymer ocean tests (when photographic records were desired).

Velocity and Photographic Records

The procedures for these tests were as described for the polymer ocean tests.

Polymer Ejection Test Series

The polymer ejection tests were performed with fresh water and six polymer concentrations. As previously mentioned, no attempt was made to control velocity. The test series is summarized in Table 6. The ejection rate for all tests was held constant at 20.625 in^3/sec.

TABLE 6

Summary of Tests Performed
Polymer Ejection Series-Number of Tests

POLYMER CONCENTRATION PPMW	FLUSH	PROBE HEIGHTS .020 IN.	.050 IN.	PICTURE TESTS
FRESH WATER	4	3	7	5
50	4	4	4	1
500	6	4	3	1
1000	3	-	-	2
20	1	-	-	-
10	2	-	-	-
5	2	-	-	-

VI. EXPERIMENTAL RESULTS AND DISCUSSION

A. General

The test series were directed towards providing information in several areas. These were, for the axisymmetric turbulent flow case (1) does the polymer affect the point of separation thereby affecting the form drag, (2) qualitatively, is there any change in the boundary layer characterization and lastly, (3) what is the wall concentration necessary to achieve a maximum skin friction reduction and what is the diffusion process for an ejector ejecting into the laminar nose region. A discussion of the effects of polymers on the separation region and the effects of polymer on the boundary layer characteristics will be performed simultaneously since they relate to the flow visualization portion of the study.

B. Boundary Layer Characterization and Separation Tests

Both the simple dye ejecting body and the polymer ejecting body were used in this series of tests. The mechanism of maintaining a high wall concentration was different in these tests. The dye ejecting body was operated in the drop tank with a uniform polymer concentration throughout the tank. The polymer ejecting body depended on a diffusion process for wall concentration control. Direct comparison can be made which clearly displays the effect of the polymers on the character of the boundary layer.

Brady (1973) summarized the work of Kline et al (1963) quite nicely. He states:

> "Kline et al found the 'laminar sublayer' to be made up of a regular structure of low and high velocity longitudinal streaks which meander transverse and normal to the wall. A dimensionless streak spacing $\lambda^+ = \frac{\lambda v^*}{\nu} = 76.5$ was found for zero pressure gradient. These streaks either break up or randomly burst from the sublayer into the fully turbulent region.
>
> The fully turbulent region is one of intense mixing and high dissipation of energy. Protruding from this region are intermittent large eddies -- visualized as peninsulas of turbulence.
>
> The peninsulas of turbulence which extend into the third boundary layer zone -- the outer turbulent region -- gives it a characteristic not unlike the wake behind a cylinder. It has rather large lumps of turbulence at intermittent spacings.
>
> It is clear that the driving force for the entire turbulent boundary layer is the generation of velocity streaks in the sublayer and their subsequent bursting outwards. Kline presents the results of many other investigators, as well as his own, in support of this hypothesis."

Figure 44 is a pictorial sketch of the boundary layer flow taken from Kline (1963) displaying the process quite nicely. The subsequent test results bear this process out quite well and display the effects of polymers on the process.

The first series of tests were made with the dye ejecting bodies. In this series, one or more of the four dye ejecting

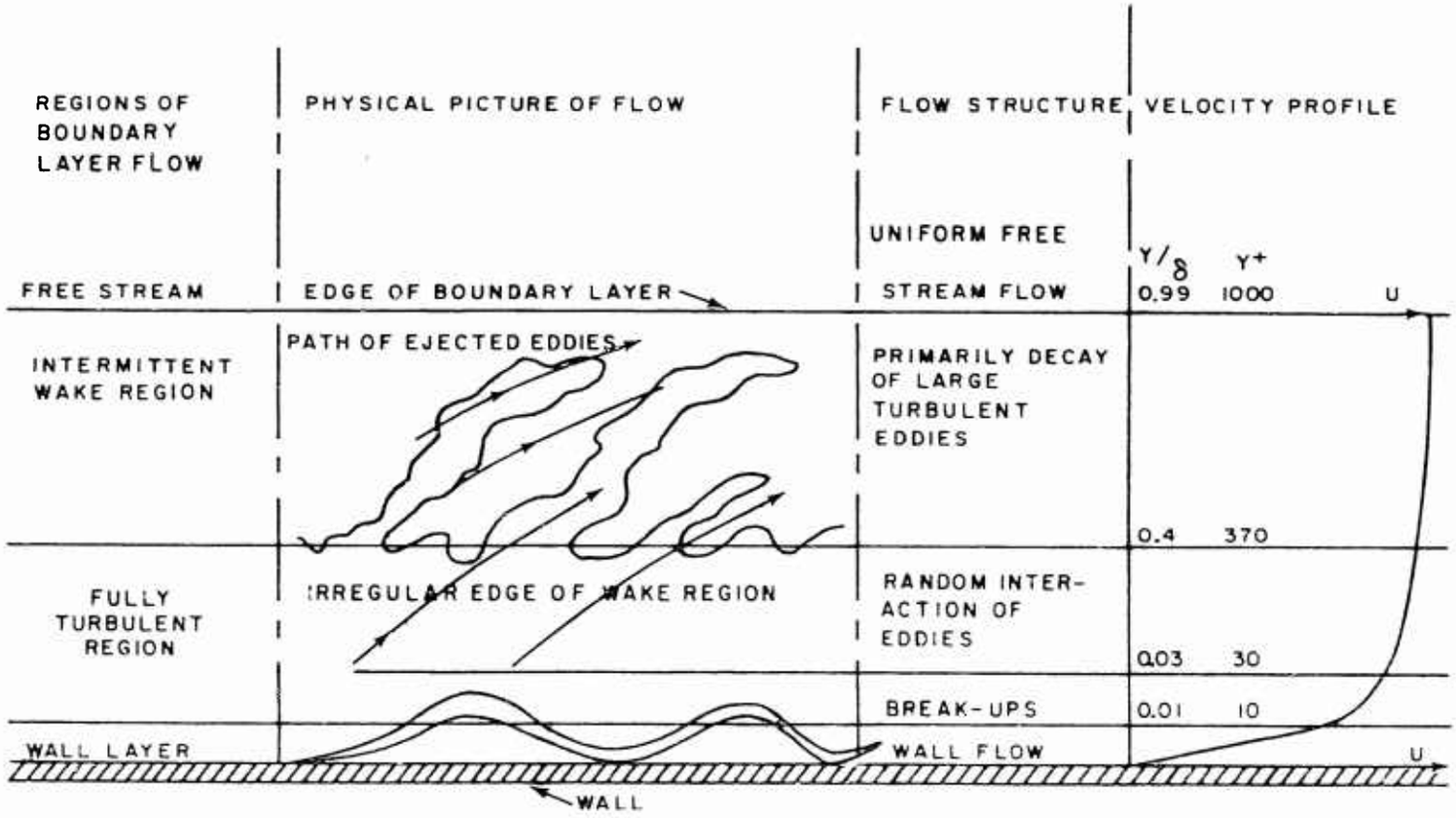

Figure 44. Pictorial sketch of boundary layer flow (from Kline, (1963))

holes was plugged to attempt to minimize tank contamination. The tests were of the launcher or free drop type depending on the tail configuration.

Figure 45 displays the boundary layer character for the 6^{o} tail configuration operating in water at a Reynold's number of 4.94×10^{6}. The highly turbulent character with the ejected eddies is clearly evident. Measurements of the boundary layer taken from this picture and others not displayed, at a mean position of the ejected eddies, is shown in Figure 46. The analytical program previously discussed was exercised to predict the boundary layer thickness. This is shown in Figure 46 also. Good agreement occurs, within 10% for this case, if one considers that the measured position was the mean of the eddies and not the tips as theorized by Kline (1963). Figure 47 presents a normalized version of this same information. Both the calculated and measured values were normalized by their respective values at $x/L = .5$. As is shown in the figure, an excellent prediction of the boundary layer shape as a function of distance down the body results for this body by the analytical routine.

A second test was performed with the 12^{o} tail configuration at a length Reynold's number of 3×10^{6} and a polymer concentration of 2.5 WPPM. The forebody portion, shown in Figure 48 displays the same character as the no-polymer case seen previously. The ejected eddy height seems somewhat larger in this case probably

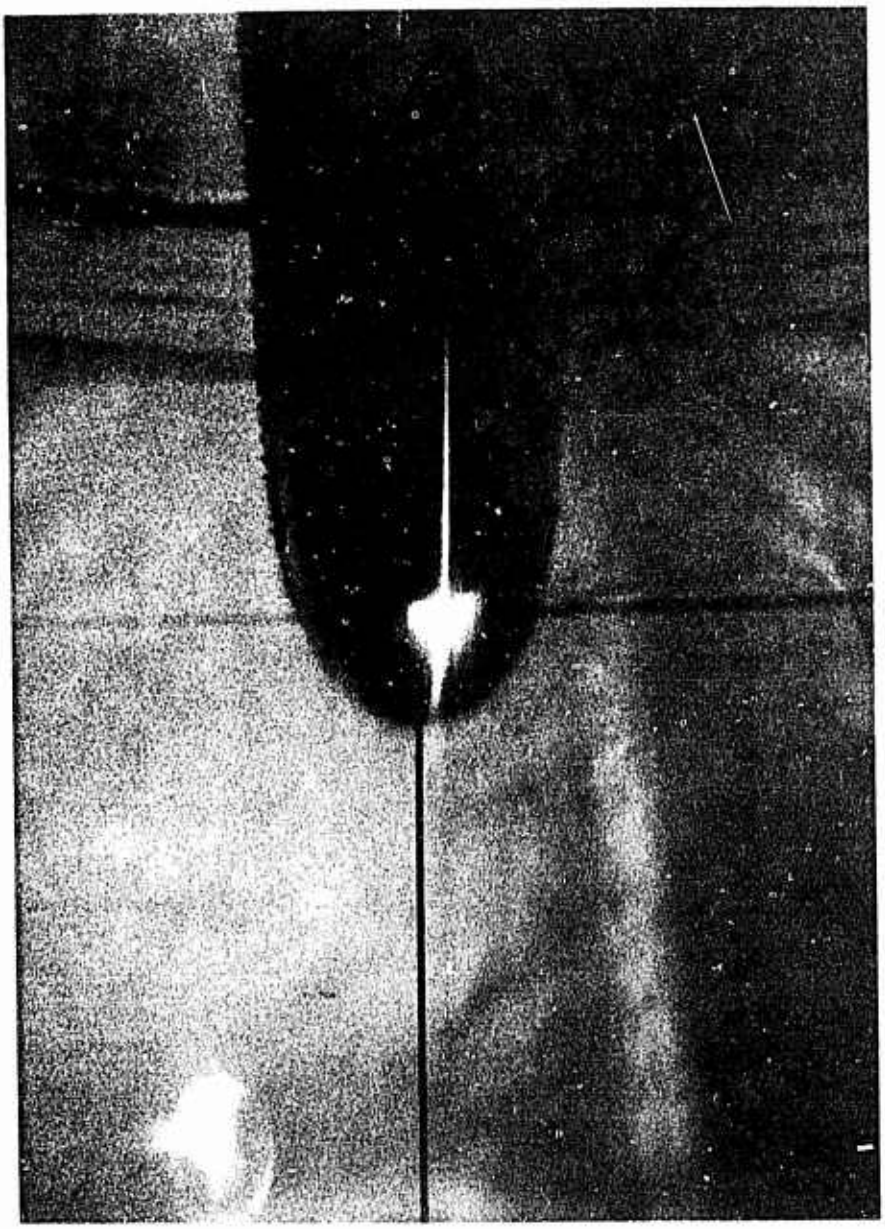

Figure 45. Photograph of dye ejection into the boundary layer - 6° tail - no polymer $R_e = 4.94 \times 10^6$

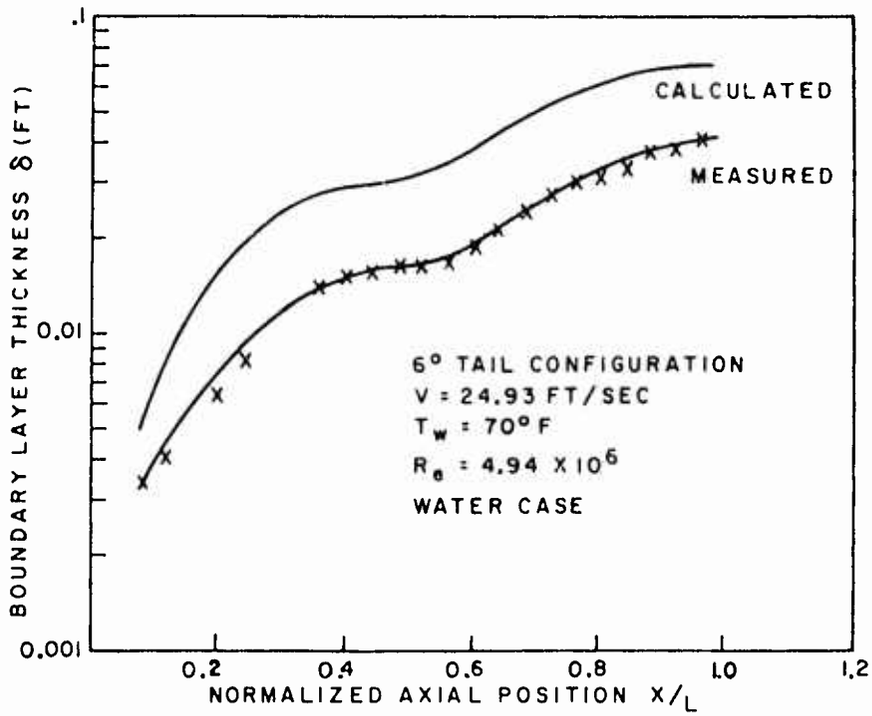

Figure 46. Boundary layer thickness vs normalized axial position - 6° tail configuration water case

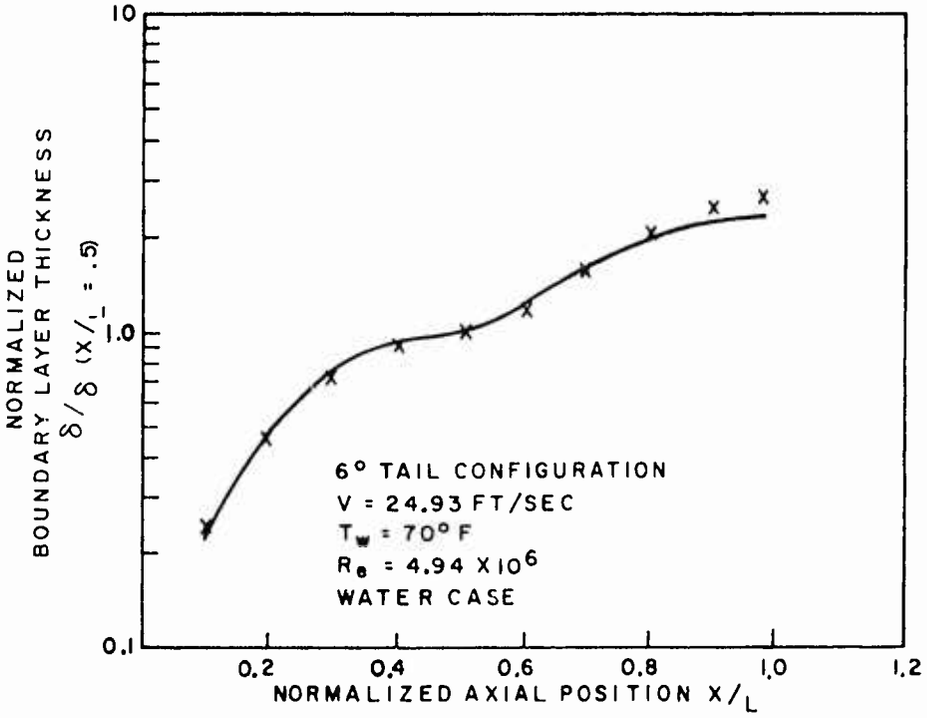

Figure 47. Normalized boundary layer thickness vs normalized axial position - 6° tail configuration water case

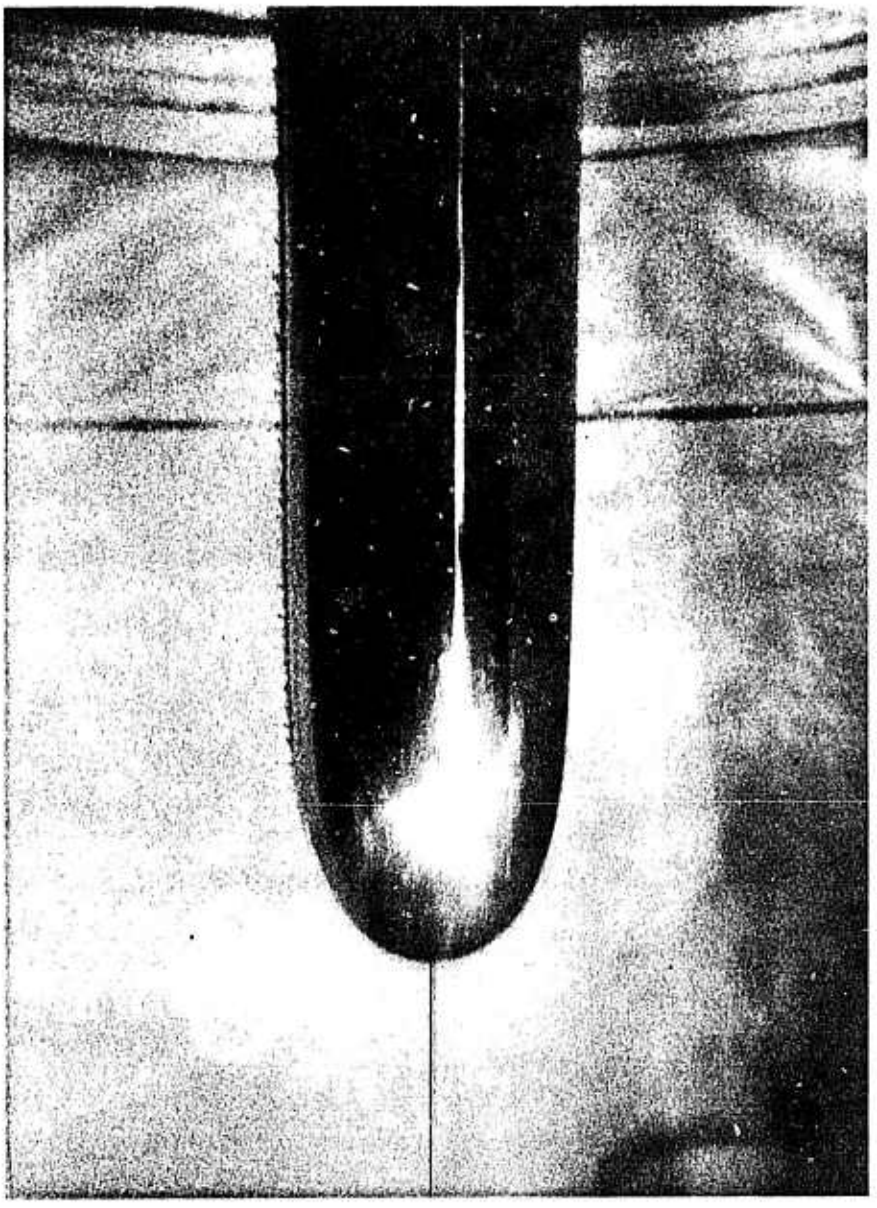

Figure 48. Photograph of dye ejection into the boundary layer - 12° tail configuration - 2.5 WPPM polymer $R_e = 3 \times 10^6$

due to the suppression of the smaller scale turbulence as displayed by White, A. Figure 49 displays the measured and calculated boundary layer thickness again using the mean eddy height for measurement purposes. The thickness measured in this test is believed to be in error (the body rotated) since the first visible position of the dye is too far for the nose. The shape of the profile should be correct, however. The normalized values are displayed in Figure 50 again showing reasonable shape agreement.

The effect of polymer suppression of the small scale turbulence was much more apparent in the tests with the polymer ejecting body. The polymer solutions used in these tests were all made up within a 24-hour period. Table 7 lists the pertinent data for this test series.

Figures 51, 52 and 53 display photographs of the polymer ejecting body ejecting visible dye and water.

Table 7

Polymer Ejecting Body - Boundary Layer Visualization and Measurement Tests - Test Parameters

POLYMER CONCENTRATION (WPPM)	VELOCITY (FT/SEC)	LENGTH REYNOLDS NUMBER
Water	26.9	5.33×10^6
50	28.33	4.67×10^6
500	29.1	5.31×10^6
1000	29.2	4.9×10^6

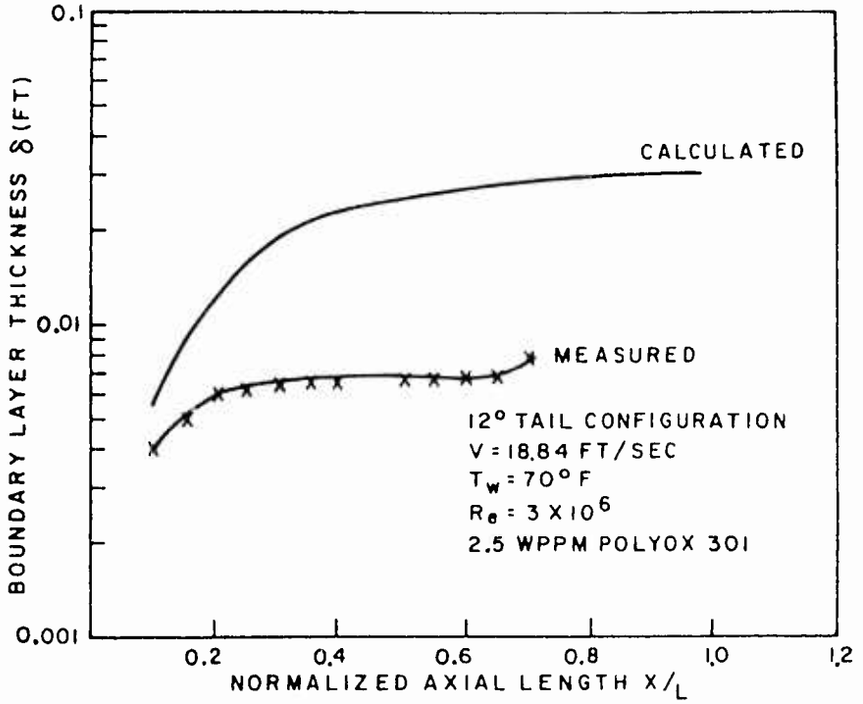

Figure 49. Boundary layer thickness vs normalized axial position - 12° tail, 2.5 WPPM polymer

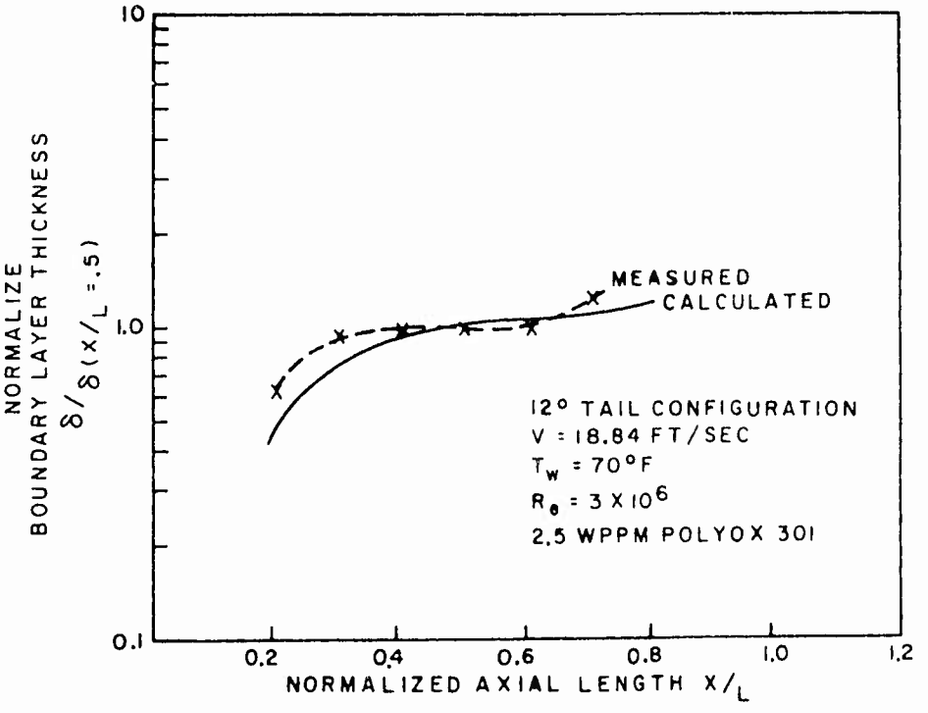

Figure 50. Normalized boundary layer thickness vs normalized axial position - 12° tail configuration, 2.5 WPPM

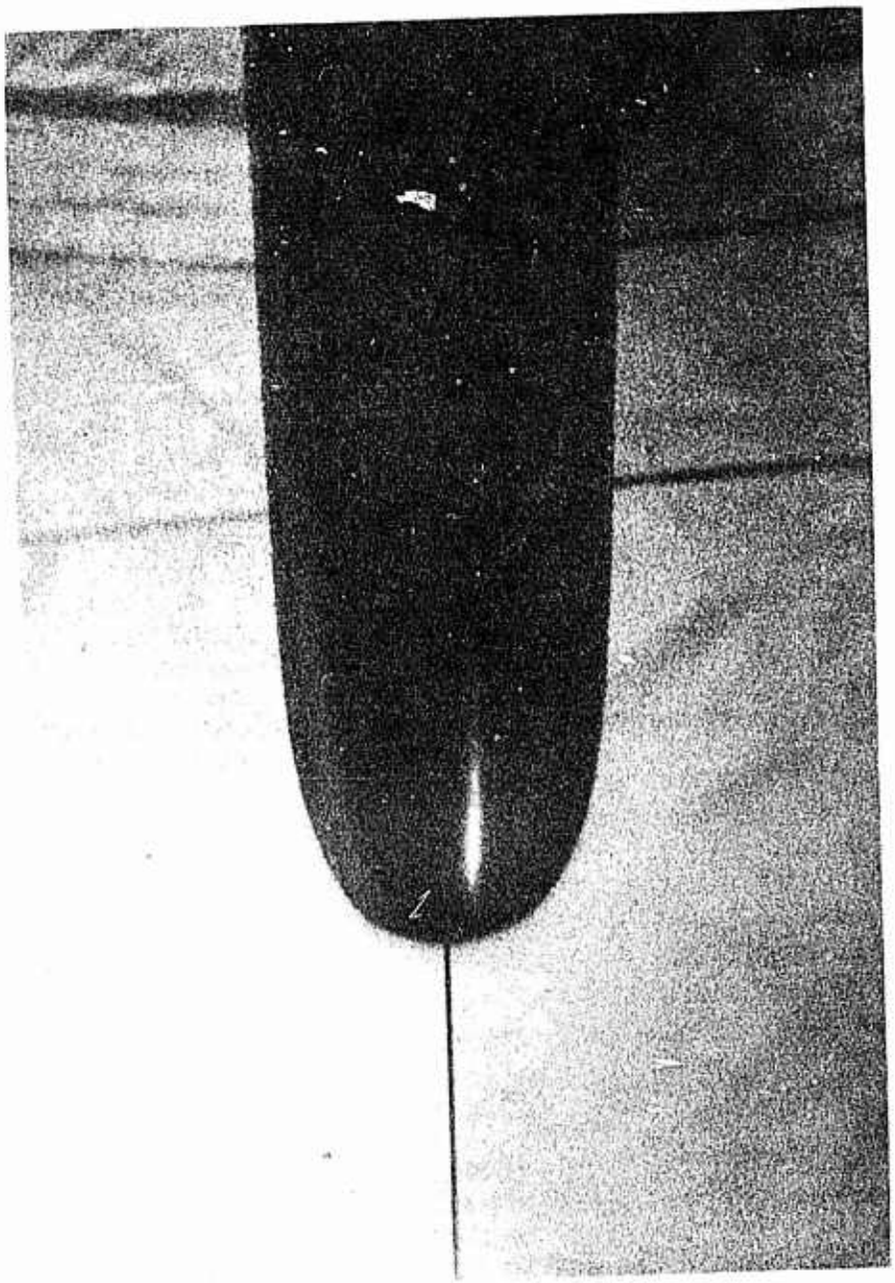

Figure 51. Photograph of polymer ejecting body - forebody view - water ejection $R_e = 5.33 \times 10^6$

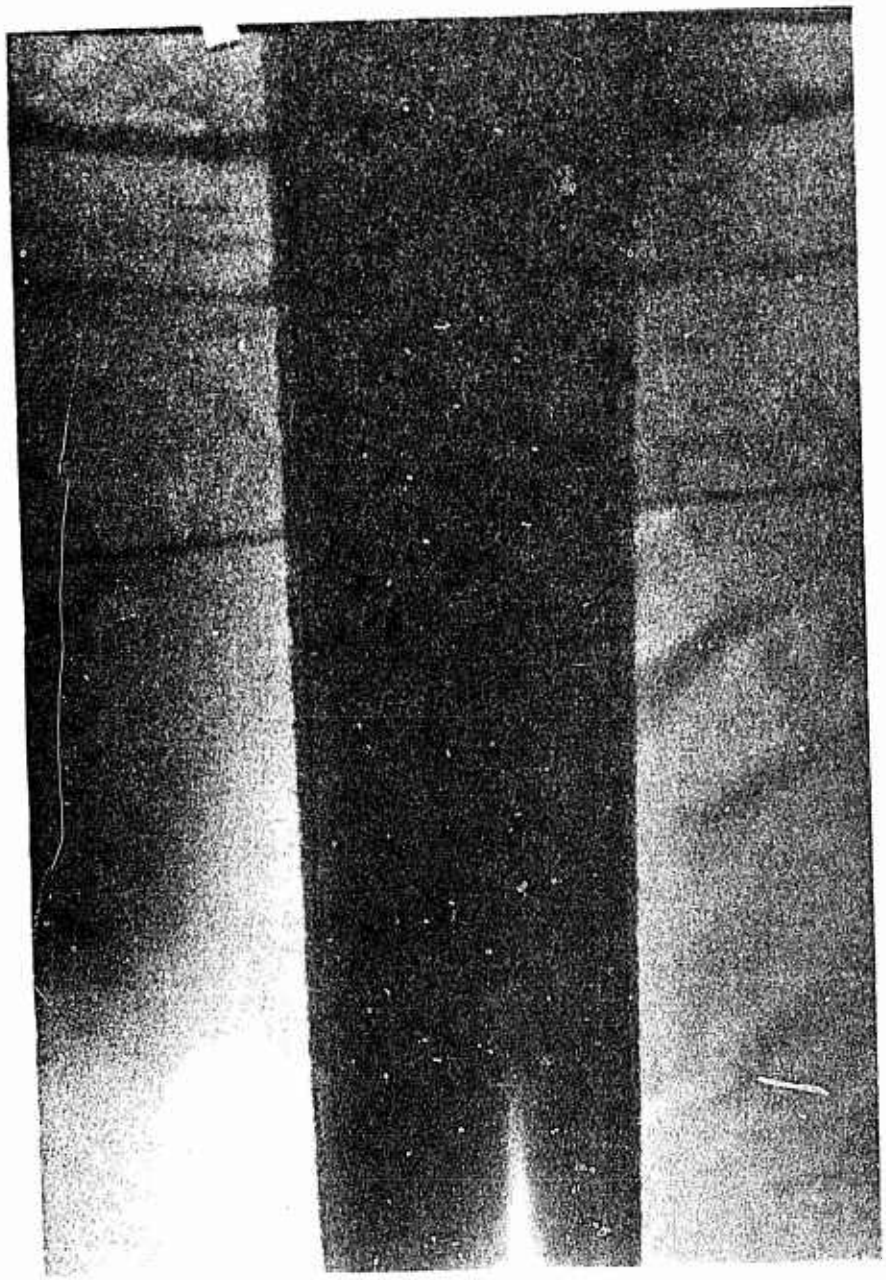

Figure 52. Photograph of polymer ejecting body - midbody view - water ejection $Re = 5.33 \times 10^6$

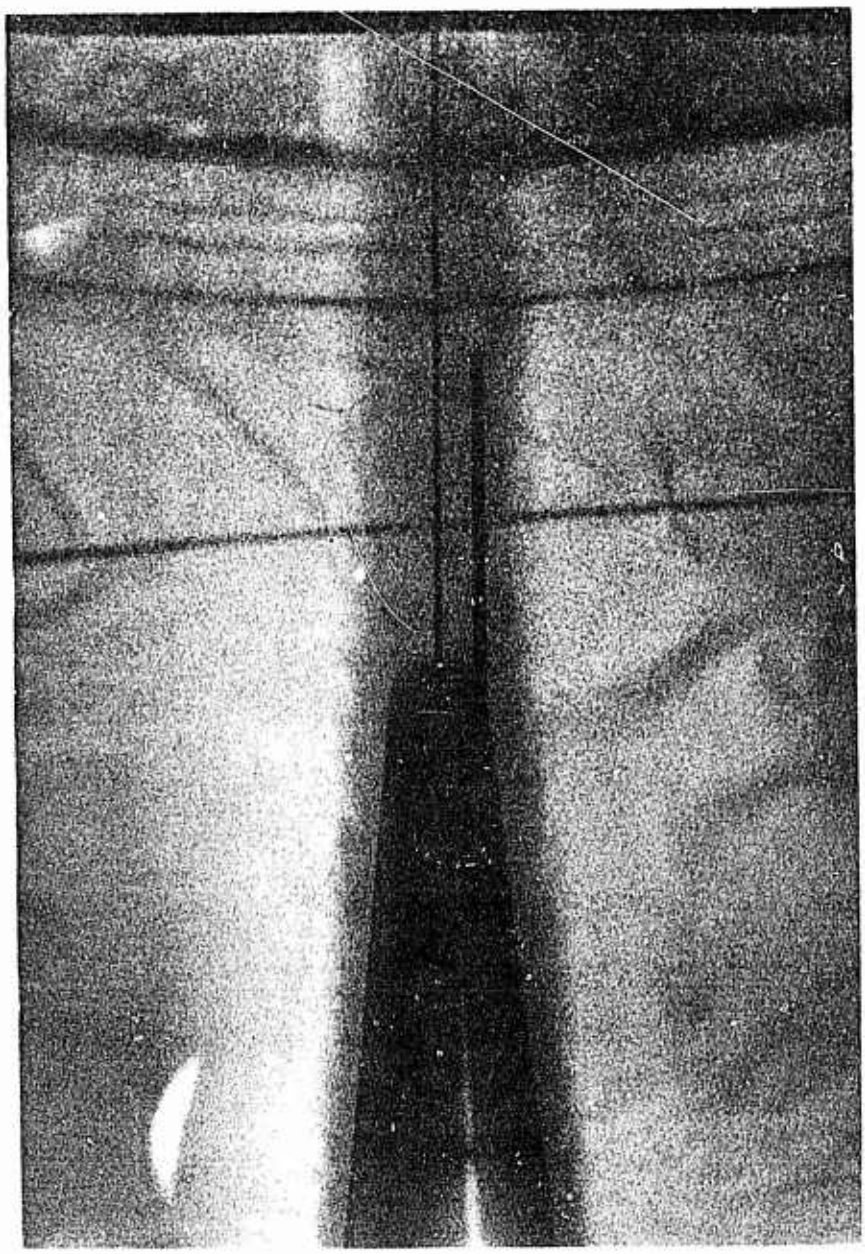

Figure 53. Photograph of polymer ejecting body - tail view - water ejection $R_e = 5.33 \times 10^6$

These views clearly show the coarse and fine scale turbulent type flow. Measurements of the boundary layer are plotted in Figure 60. Also to be noted in Figure 51 is the uniform ejection process which apparently is not seriously effecting the flow. From these views, the flow is apparently fully turbulent near the nose of the body.

The tests were repeated, this time ejecting a 50 WPPM polymer solution. Figures 54 and 55 display the results. The fine scale eddy structure is apparently missing leaving only the coarse structure. More interestingly, the boundary layer thickness has decreased a disproportionate amount in the midbody region as compared to the tail suggesting, as it should be, higher effective wall concentrations forward on the body which result in thinner boundary layers in this region and a rapid growth in the tail region. Since the boundary layer is beginning to get rather thin in the forebody region, the measurement method used should be described. Slides have been made of the figures presented in this study, these were projected on a screen such that the body diameter (3 inches) projected to about 2 feet in diameter. The resultant boundary layer thicknesses near the nose were a projected .2 inch. An overlay slide with one inch axial marks was used as an overlay (with 2 projectors to insure proper scale). This was required since the body does not reach 3 inch diameter for some distance form the nose.

The last two groups of tests in this series were with 500 WPPM and 1000 WPPM. Figures 56 and 57 show the forebody view

Figure 54. Photograph of polymer ejecting body - midbody view - 50 WPPM polymer ejection $R_e = 4.67 \times 10^6$

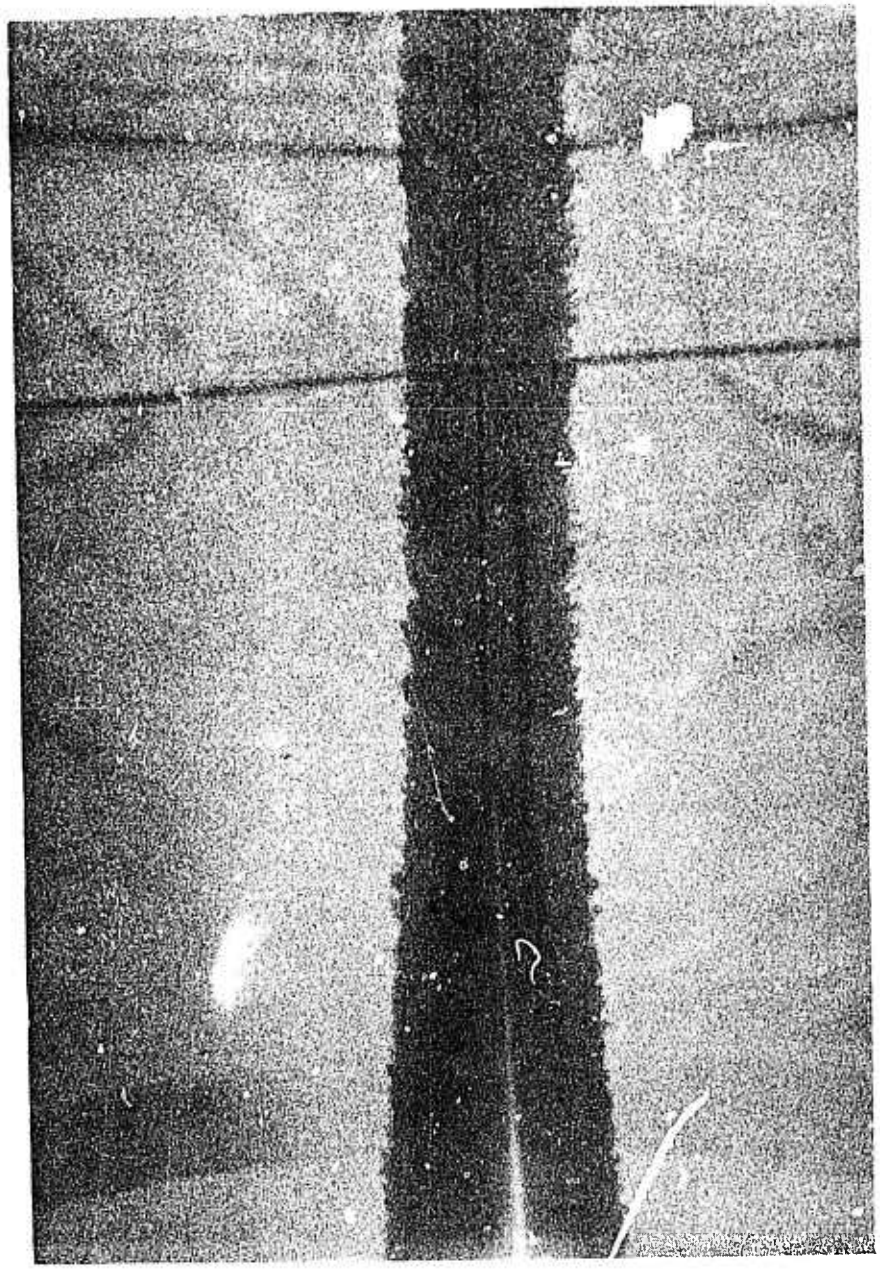

Figure 55. Photograph of polymer ejecting body - tail view - 50 WPPM polymer ejection $R_e = 4.65 \times 10^6$

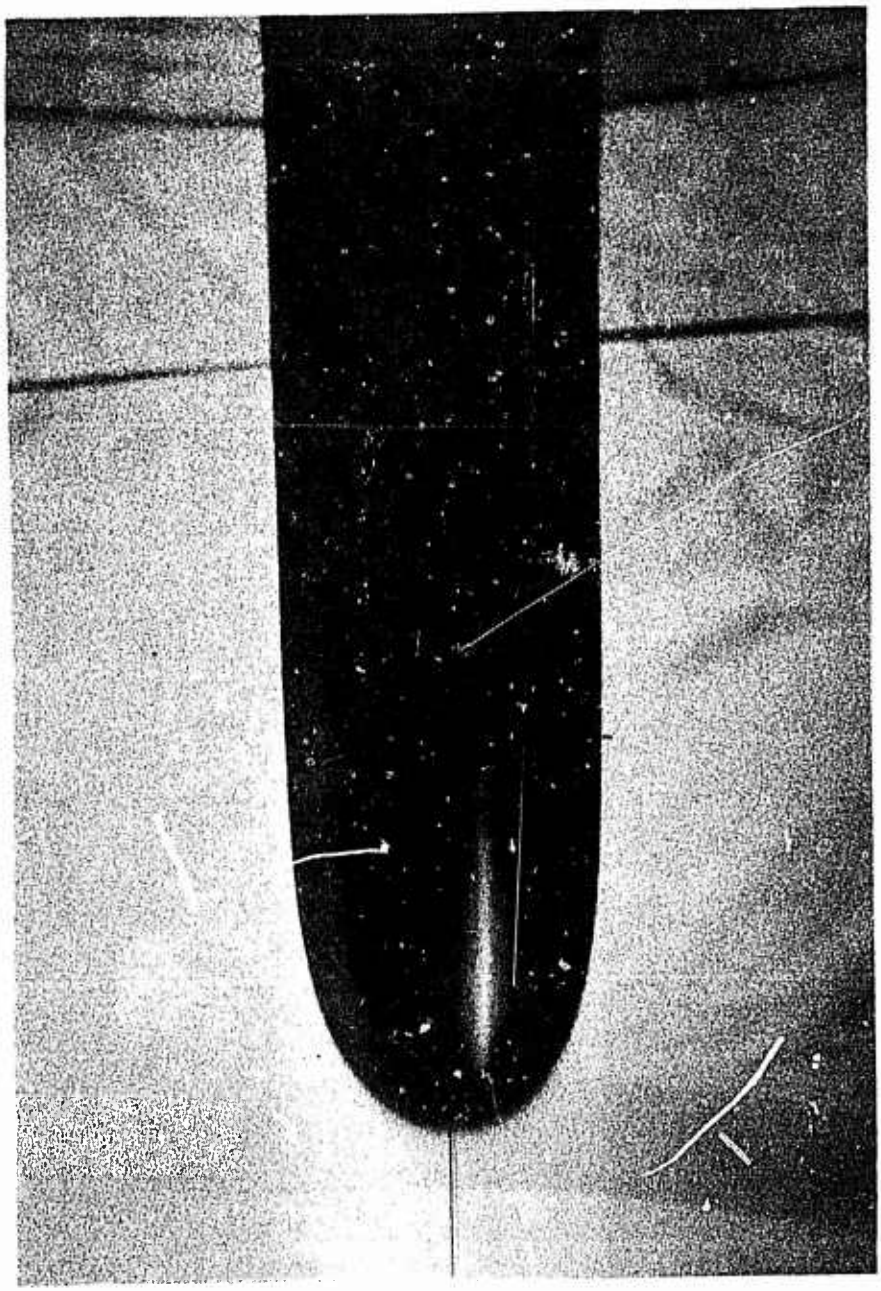

Figure 56. Photograph of polymer ejecting body - forebody view - 500 WPPM polymer ejection $R_e = 5.31 \times 10^6$

Figure 57. Photograph of polymer ejecting body - tail view - 500 WPPM polymer ejection $R_e = 5.3i \times 10^6$

and tail view for the 500 WPPM case and Figures 58 and 59 show similar views for the 1000 WPPM case. Apparently, a limit of drag reduction is being reached, presuming this may be inferred from the fact that there is little difference in the boundary layer reduction between these cases as seen in Figure 60. Moreover, an additional phenomenon is occurring. It is first noticeable in Figure 57 and readily apparent at the 1000 WPPM level of Figures 58 and 59. A significant number of streaks are evident in the flow. The approximate streak spacing is about .015 inches. The number of ejector holes is approximately 700. For the body diameter of 3 inches, the number of streaks would be about 620. Additionally, applying the dimensionless streak spacing found by Kline et al (1963) in the laminar sublayer, for a v* of approximately .6 ft/sec and viscosity of about that of water, results in a "laminar sublayer" streak spacing of the order of .015 inches. Apparently, at these concentration levels, the turbulence intensity is so damped that the streaks become well ordered and have difficulty in bursting out into the other layers of the boundary layer. It is not until the tail region that a very filamentary bursting is occuring suggestive of the long stringiness associated with elastic polymers. Even the angle of the streaks, essentially in the axial direction, are suggestive of very low energy levels bursting the streaks outward as compared to the water case. The implication of these photographs is that turbulent diffusion has ceased and a molecular

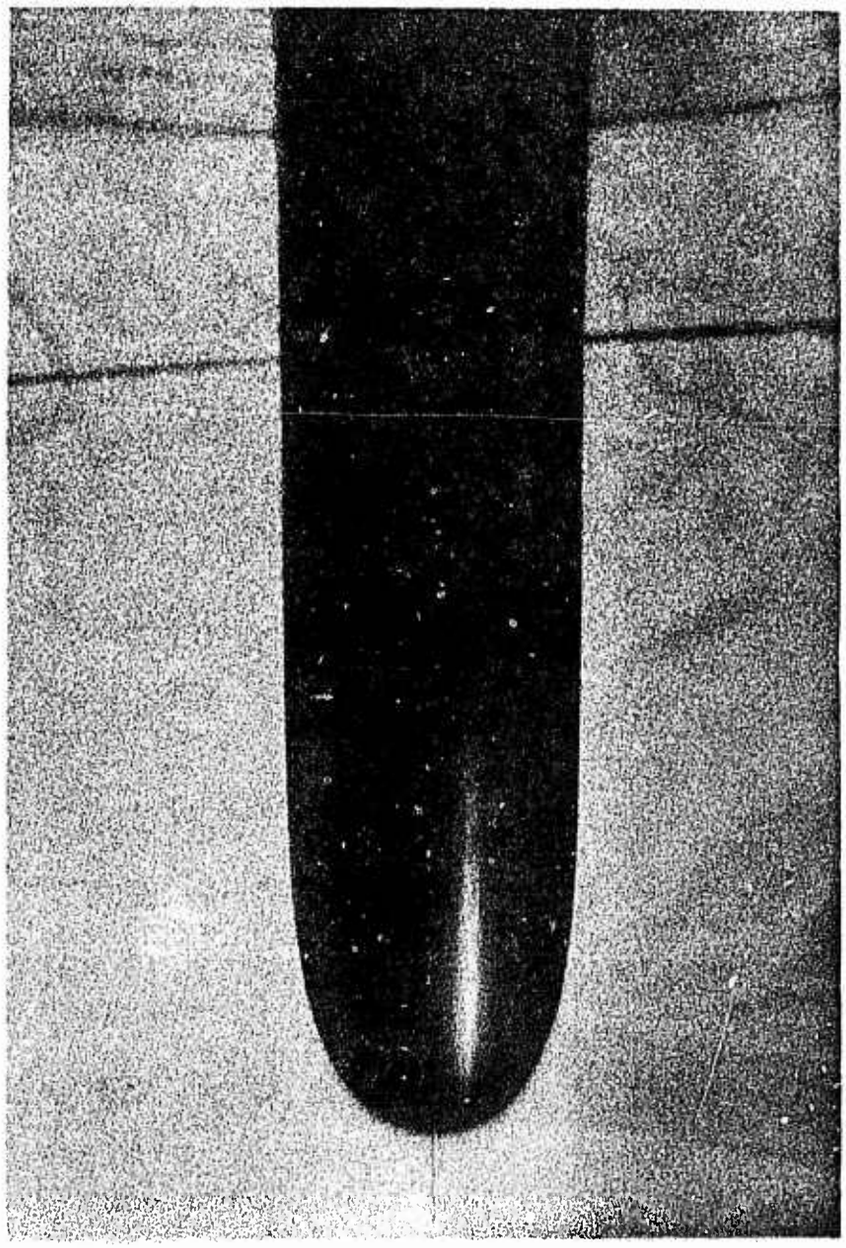

Figure 58. Photograph of polymer ejecting body - forebody view - 1000 WPPM polymer ejection $R_e = 4.9 \times 10^6$

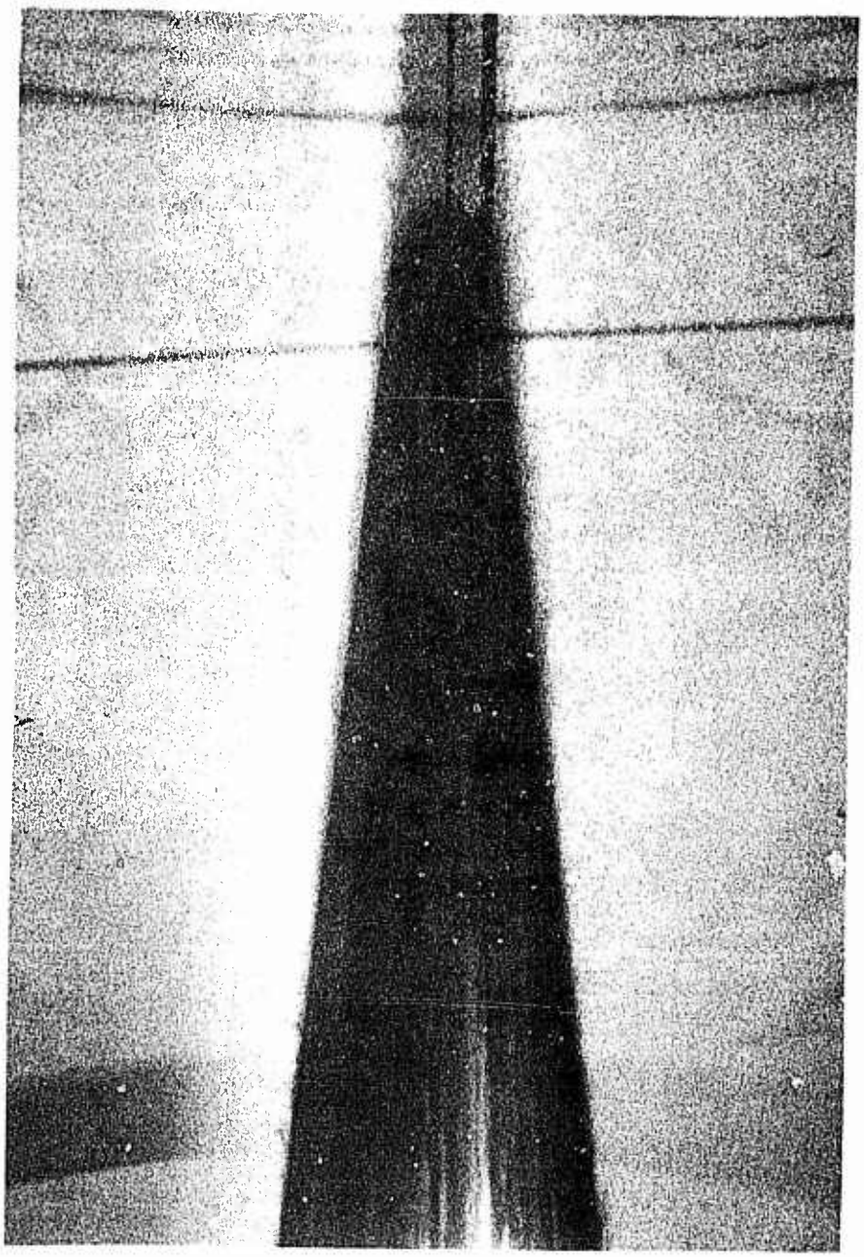

Figure 59. Photograph of polymer ejecting body - tail view - 1000 WPPM polymer ejection $R_e = 4.9 \times 10^6$

diffusion only in the sublayer is occurring. This would suggest extremely long mixing lengths. Tests by Nadolink (1968) displayed the same characteristic but for polymer ocean type tests. Figure 61 displays a normalized plot of the boundary layer growth for these tests. The polymer cases clearly show a delayed growth trend indicative of suppressed diffusion.

The last series of visual observations centered around the question of whether application of polymers effected the separation point at the tail. Several tests were run with the dye ejecting body with the hemispherical tail in fresh water and in a 20 WPPM polymer ocean. The length Reynolds number for both cases was 1.877×10^6.

Figure 62, the test with plain water, displays a thick boundary layer near the tail and a separation angle measured from the vertical of approximately 62^o to 65^o. Figure 63 displays the results of a similar test with 20 WPPM polymer concentration in the tank. The boundary layer is characteristically thin but the separation point resulting in an angular measurement of 80.6^o for either polymer case or water case. On a nondimensional basis, the computer program predicted separation at $x/L = .925$ while the data indicate $x/L = .948$ for separation. Nonetheless, the polymer, for the case tested, did not apparently change the separation point. Similar tests with the 12^o tail configuration also showed no effect on the separation point. Since sphere tests conducted by Lang and Patrick (1967) indicated that sphere

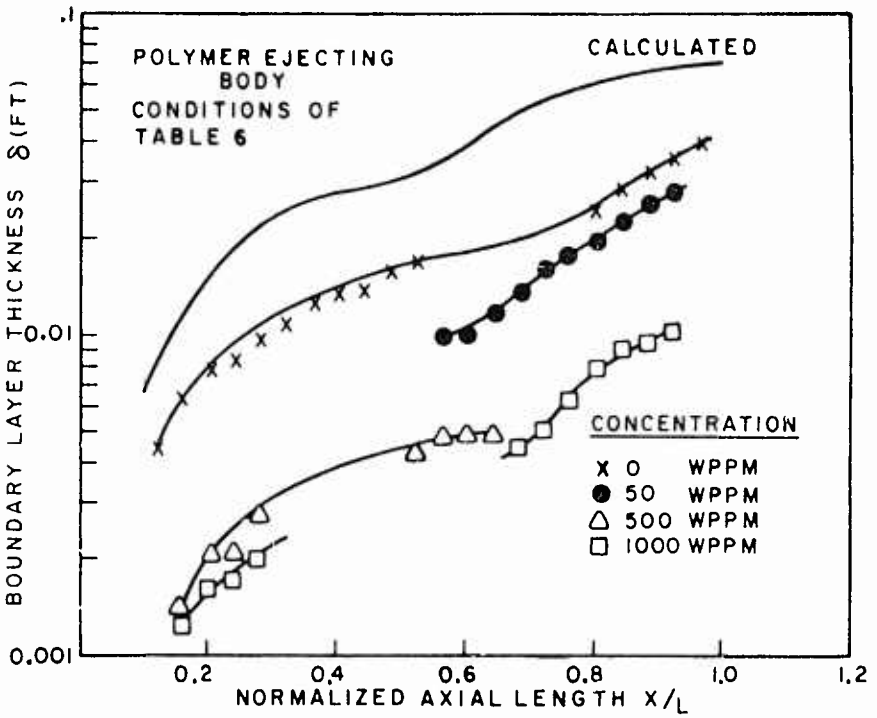

Figure 60. Boundary layer thickness vs normalized axial length - polymer ejecting body

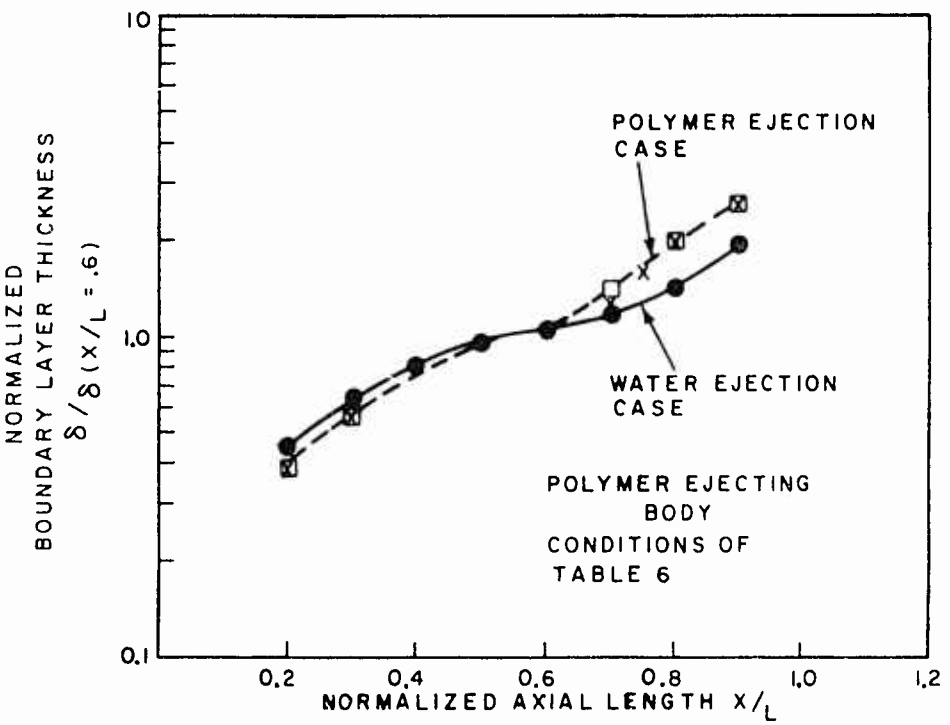

Figure 61. Normalized boundary layer thickness vs normalized axial length - polymer ejecting body

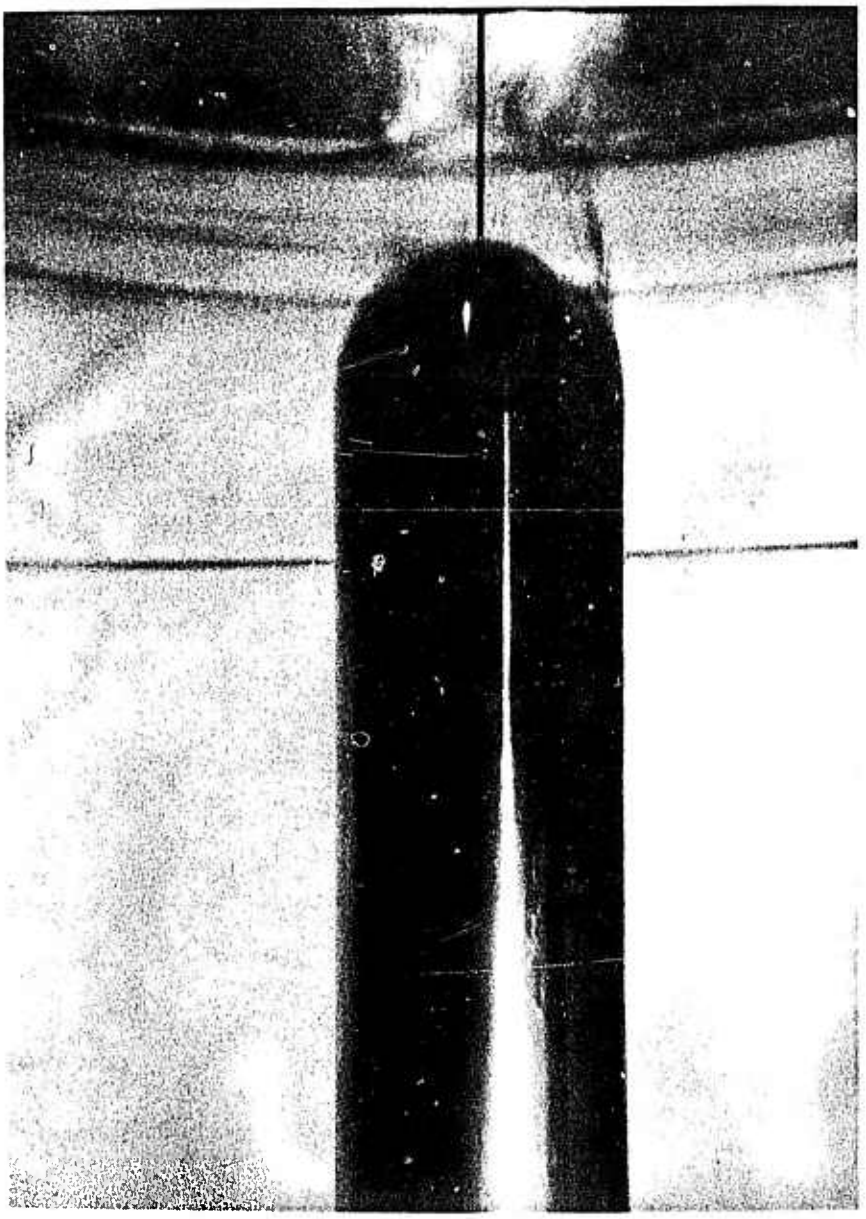

Figure 62. Photograph of dye ejecting body - 20 WPPM polymer ocean $R_e = 1.877 \times 10^6$

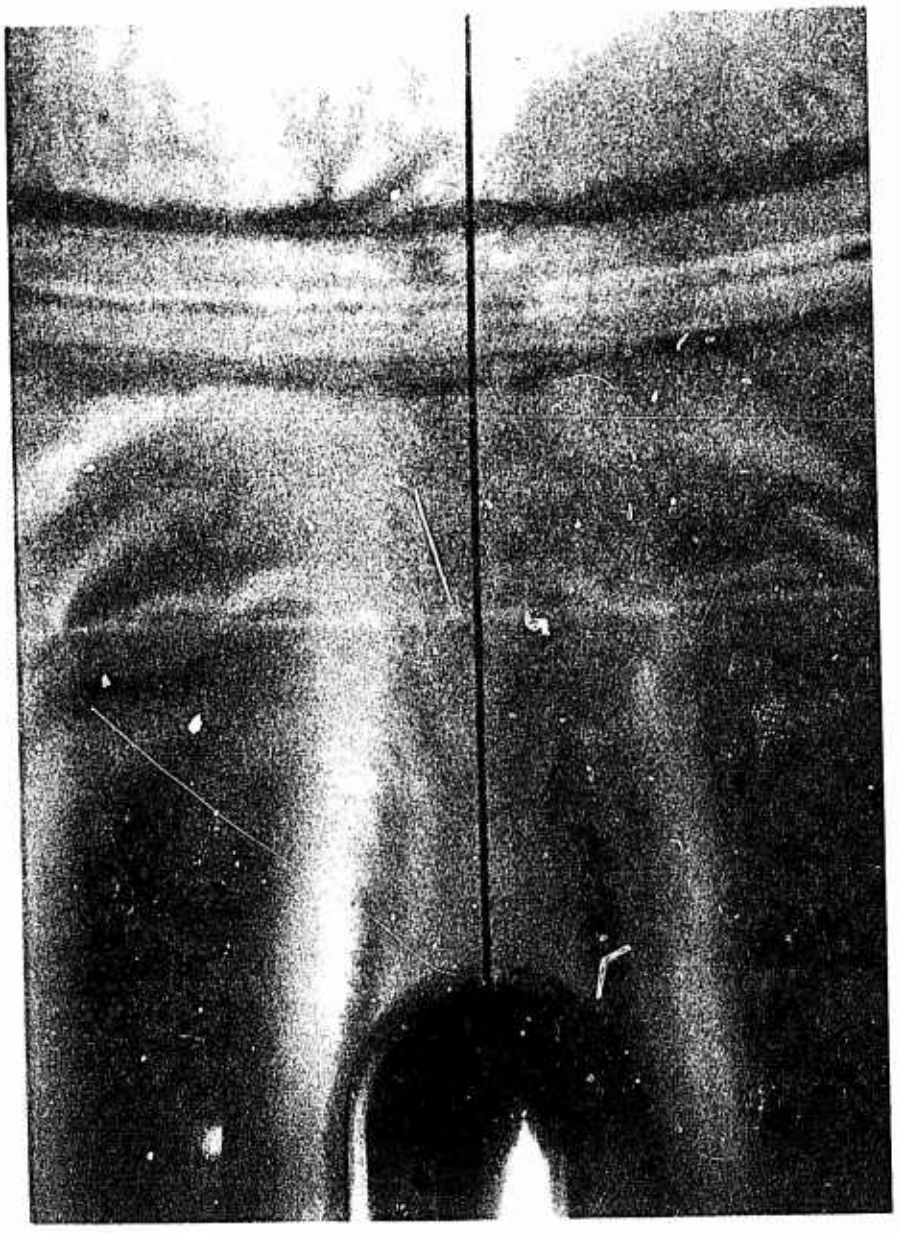

Figure 63. Photograph of dye ejecting body - spherical tail - tail view - water case $R_e = 1.877 \times 10^6$

drag was reduced by a movement of the separation point from the laminar separation point to a further back turbulent separation point. These results are not surprising for the case of a turbulent separation point initially. These results are consistent with those of Stone and Elliott (1970). Unfortunately, this small change in predicted separation point places the separation at the extreme of the negative pressure coefficient, Figure 37, resulting in a very high calculated form drag.

C. Drag Reduction Tests

The next series of tests were directed towards determining drag reduction efficiency for various polymer concentrations and tail configurations and to test the analytical model for the 6° tail case. The form drag calculation for this case are simpler due to the geometry and pressure coefficient profile. The test matrix run was as outlined in Table 5. A total drag coefficient was calculated for each series of tests using the relation

$$C_D = \frac{W - B}{1/2\ \rho\ A_f\ U_o^2} \tag{114}$$

where the frontal area, $A_f = 0.0491\ ft^2$. From the drag coefficient, C_D, the percentage total drag reduction was then calculated for each polymer concentration tested. The percentage total drag reduction is given by

$$\%\ TDR = 100\ \left(1 - \frac{C_{D_{POLY}}}{C_{D_W}}\right) \tag{115}$$

where

$C_{D_{POLY}}$ = Drag coefficient for polymer tests

C_{D_W} = Drag coefficient for water tests.

A calculation of percent skin friction reduction was also made for each test. The relation for percent skin friction reduction are.

$$\% \text{ SFR} = 100 \left(1 - \frac{C_{f_{POLY}}}{C_{f_W}}\right) \tag{116}$$

where.

$$C_f = C_D \frac{D_f}{D_t}$$

and C_D = measured drag coefficient

D_f = total shear drag analytically calculated

D_t = W-B = body weight in water.

It is noted here that D_t, the actual drag, is used in the % SFR calculation and not the total calculated drag. This is done since the skin friction as calculated by this method has been shown by White (1972) to be accurate. The addition of the term for calculating form drag is only considered to be an indicator and may be considerably in error due to the pressure coefficient inaccuracies. The 6^o tail tests were the only tests where the launcher could be used. These tests, therefore, were the only ones in this series where terminal velocities were achieved.

Extreme instabilities were noted when launch tests were attempted with the 12^o tail and spherical tail models. This is attributed to the launcher receptacle being designed to accept the 6^o tail. As

a result, the 12° tail and spherical tail were not properly guided during the launch phase. Even with the weighted guide wire, photographs of the test models travelling at angles of near 10° relative to the wire were obtained. Drag data obtained in this manner were not of any use. Additionally, velocity measurements were never achieved when this occurred since the guide wire would generally trip the lasers during the launch transient.

The free drop 12° and spherical tail tests were projected to terminal velocity using a procedure outlined in Nadolink (1968). The procedure solves the equation of motion for an accelerating body having as knowns the weight in air, the weight in water, the velocity at a particular distance and an entrained mass coefficient emperically determined and plotted in the report as a function of L/D. The procedure, because of the form of the final relation is iteratively solved for terminal drag coefficient, which will predict the velocity at the station which is being measured. From this, equation (114) is used to calculate the terminal velocity.

Tables 8, 9 and 10 present the data obtained in this series of tests as well as the percent total drag reduction and skin friction reduction calculated. Other pertinent information noted is the total drag calculated from the analytical routine for the identical test conditions. As may be noted from Table 8, the total drag predicted by the analytical routine is within 10% for the 6° tail case. Additionally, the total skin friction determined from equation (89) results in a friction drag coefficient based

TABLE 8

DATA SUMMARY 6^{o} TAIL TESTS

NUMBER OF TESTS	AVERAGE VELOCITY (FT/SEC)	POLYMER CONCEN-TRATION (WPPM)	TANK TEMP. (OF)	R_{e_L} $x10^{-6}$	C_{D_A}	% TDR	% SFR	CALC. D_f (LBS)	CALC. D_t (LBS)
8	25.1 ±3%	0	76	5.37	0.1479	-	-	2.598	4.70
4	24.64 ±2%	2.5	68	4.56	0.1202	18.73	39.8	1.508	3.60
10	26.17 ±2%	5.0	62	4.68	0.1068	27.70	49.25	1.422	3.75
7	27.14 ±2%	20.0	64	4.85	0.0991	33.00	67.1	.9206	3.35
2	26.61 ±2%	50.0	70	5.27	0.1031	30.29	68.8	.998	3.49
12	27.2 ±2%	60.0	71	5.12	0.0990	33.06	68.8	.958	3.46

LAUNCHER TESTS

L = 2.0833 FT.

A_f = 0.0491 FT^2 (FRONTAL AREA)

A_s = 1.3685 FT^2 (SURFACE AREA)

D = 0.25 FT.

W-B = 4.43 LBS. WATER TESTS (WEIGHT IN WATER)

W-B = 3.47 LBS. POLYMER TESTS (WEIGHT IN WATER)

TABLE 9

DATA SUMMARY 12^{o} Tail Tests

NUMBER OF TESTS	AVERAGE VELOCITIES (FT/SEC) V_{12}	V_{23}	V_{13}	PROJECTED TERMINAL VELOCITY (FT/SEC)	POLYMER CONCEN-TRATION (WPPM)	TANK TEMP. (OF)	R_{e_L} $x10^{-6}$	C_{D_A}	PROJECTED %TDR	%SFR	CALC. D_f (LBS)	CALC. D_t (LBS)
7	17.1	19.36	18.6	25.58	0	70	4.08	.2292	-	-	2.39	4.22
8	17.1	19.36	18.6	26.07	1.25	69	4.1	.2208	3.7	32.9	1.66	3.57
6	17.284	19.756	18.895	27.15	5	68	4.22	.2066	10.2	50.0	1.33	3.39
9	17.284	19.756	18.895	27.51	10	69	4.33	.1986	13.4	59.6	1.113	3.23
6	17.279	19.727	18.875	27.41	20	69	4.32	.1979	12.8	68	.888	2.99
6	17.359	19.813	18.986	27.92	50	69	4.39	.1928	15.9	69.2	.875	3.06
6	17.302	19.755	18.907	27.57	60	70	4.39	.1978	13.8	69.0	.863	2.99

FREE DROP TESTS

L = 1.679 FT.

A_f = 0.0491 FT^2 (FRONTAL AREA)

A_s = 1.1741 FT^2 (SURFACE AREA)

D = 0.25 FT.

W = 9.418 LBS. (WEIGHT IN AIR)

W-B = 7.109 LBS. (WEIGHT IN WATER)

TABLE 10

Data Summary Spherical Tail Tests

NUMBER OF TESTS	AVERAGE VELOCITY V_{12} (FT/SEC)	PROJECTED TERMINAL VELOCITY (FT/SEC)	POLYMER CONCEN-TRATION (WPPM)	TANK TEMP. (OF)	R_{e_L} $x10^{-6}$	C_{D_A}	%TDR	%SFR	CALC. Df (LBS)	CALC. D_t (LBS)
7	12.23	13.5	0	65	1.66	.34	-	-	.665	7.09
7	12.24	13.5	5	62	1.6	.335	1.5	44.4	.376	6.8
11	12.44	13.9	20	62	1.64	.32	6	60.4	.28	7.09
19	12.67	14.24	60	62	1.68	.305	10.3	61.8	.283	7.43

FREE DROP TESTS

L = 1.386 FT.

A_f = 0.0491 FT^2 (FRONTAL AREA)

A_s = 1.1044 FT^2 (SURFACE AREA)

D = 0.25 FT.

W = 4.9 LBS. (WEIGHT IN AIR)

W-B = 2.94 LBS. (WEIGHT IN WATER)

on surface area of C_f = .00311 which compares very favorably with that determined from the accepted formulas for flat plates of .00336 at the same length Reynolds number. The calculated skin friction coefficient is plotted in Figure 64 taken from Granville (1971). For the δ/r_o being worked with in this study and for a mild pressure gradient, a comparison is considered reasonable.

Figure 65 presents a plot of the percent total drag reduction for the various tail configurations. As noted in the figure, peak drag reductions are occurring for the 6^o and 12^o tail case at polymer concentrations of between 15 and 20 WPPM. The effect of increased form drag with the 12^o and spherical tail models results in a decreased total drag reduction since the polymer only reduces the skin friction. Figure 66 is a plot of percent skin friction reduction. This plot clearly displays the achievement of equal skin friction reduction on all the bodies tested as would be expected. Calculation of the skin friction coefficient based on surface area for the 20 WPPM case with the 6^o tail results in a C_f of .0011 at a length Reynolds number of 4.85×10^6. This point is plotted on Figure 64 and is in good agreement with the maximum drag reduction value given by Granville. Plotted on Figure 64 also are the skin friction coefficients calculated for the 12^o and spherical tail. These also are in reasonable agreement with the maximum drag reduction line as proposed by Granville.

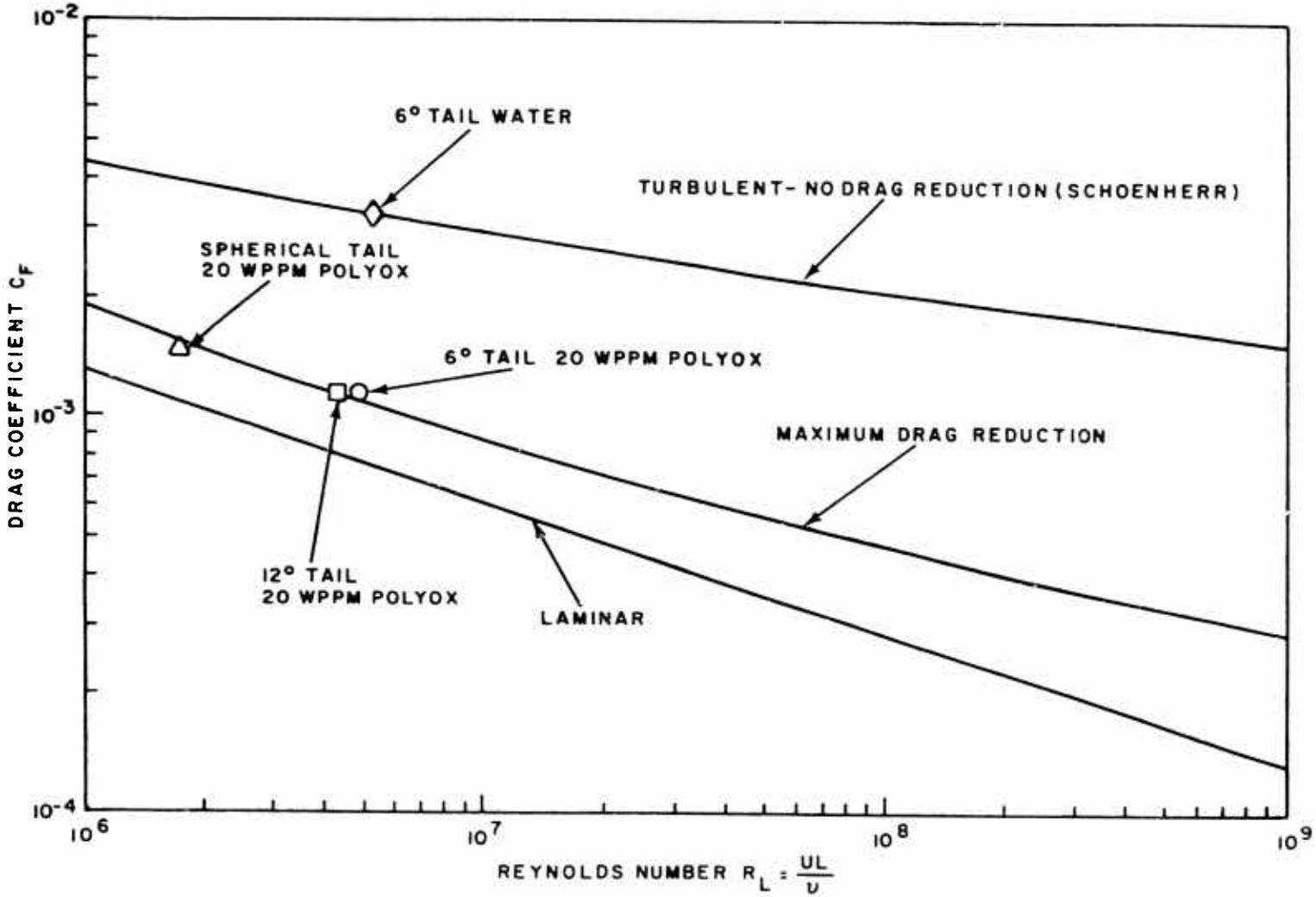

Figure 64. Drag coefficient for maximum drag reduction of flat plates (from Granville, P.S. (1971))

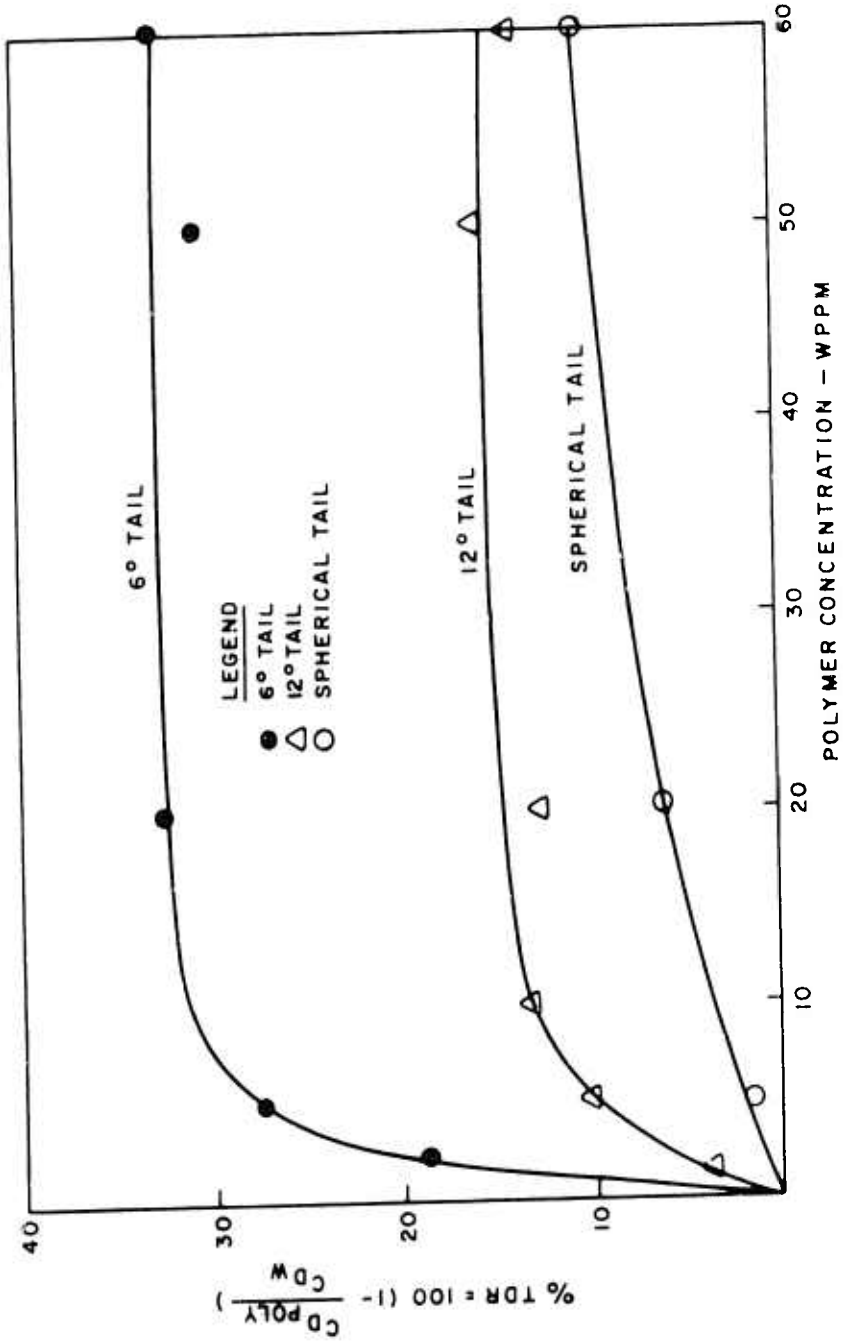

Figure 65. Percent total drag coefficient reduction vs concentration

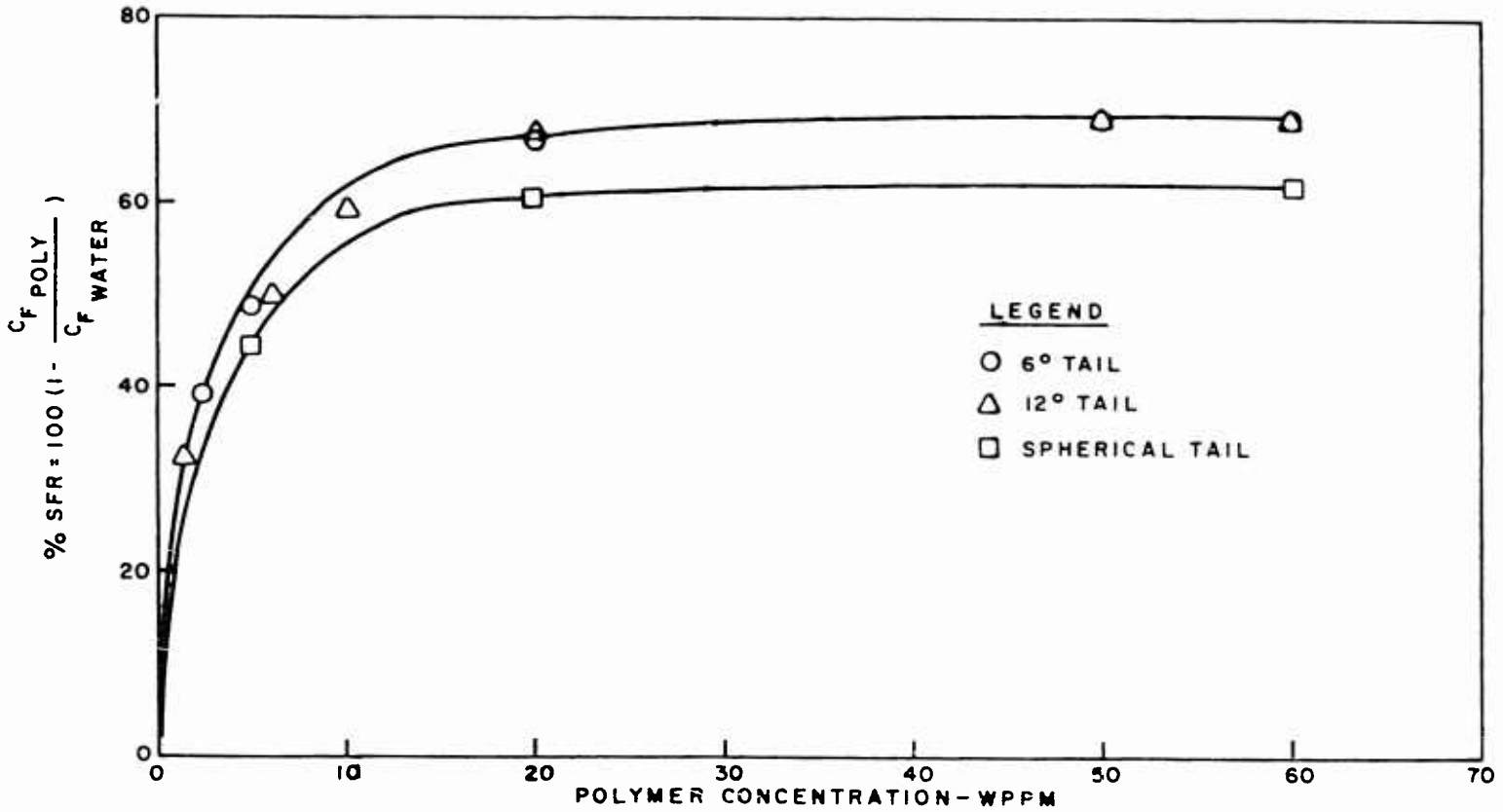

Figure 66. Percent skin friction coefficient reduction vs concentration

D. Polymer Concentration Profile Tests

The polymer ejecting body was used throughout this entire series of tests. The primary emphasis in these tests was to obtain polymer concentration measurements at the wall and at two heights in the boundary layer. These heights were selected to be .025 inches from the body to the centerline of the probes and .055 inches from the body to the probe centerline of the probes for reasons previously discussed. The probes are as described previously and shown in Figure 20. Only one stroke rate was used in these tests although other stroke rates are possible with the model through an orifice change. The stroke rate selected resulted in a volume rate of flow of 20.6 in^3/sec. Polymer concentrations of 50 and 500 WPPM of Polyox-WSR-30 were ejected and samples taken at the wall and the two probe heights. Testing with 5 WPPM, 10 WPPM, 20 WPPM and 1000 WPPM was also performed but only with the flush probes installed. Tests were also performed with fresh water dyed with the fluorescent dye to determine what differences in diffusion exist between the polymer contaminated solution being ejected and the water. All tests were run using the launcher and no attempt was made to attain terminal velocity. The tests were all made at a high enough initial velocity that near terminal velocities existed and transient characteristics were deemed to be unimportant. The tests could not be used, however, to determine drag reduction or drag coefficients. The tests went very smoothly

with only one or two failures in the entire test series when a launch was made. Velocity variations for similar tests were within one percent. Unfortunately, concentration measurements were more diverse with 10 to 15% variations not uncommon although the bulk of the data fell in a narrowband. The test operation was very procedure oriented with deviations generally resulting in an aborted attempt at a launch. The long hours spent in calibrating the model was key to the smooth test series since carefully followed procedures resulted. The test matrix run is that shown in Table 6. In general, each test series, a series being either no polymer or a specific polymer concentration, began with the flush probes installed. The .025 inch probes were next installed and finally the .055 inch probes. No intermixing of probe heights occurred, even on a per station basis. The test model functioned perfectly, as designed, with over several hundred firings being accounted for considering stroke rate calibration tests, polymer concentration tests, photographs firings and actual data gathering firings. The only malfunction occurring was in the firing rod. One of the functions of this rod was to follow the polymer ejection piston during the ejection process. A photograph of the tail region of the model could then be analyzed to reveal the position of the firing rod still external to the body. This information combined with body velocity and distance to the camera station would allow a continual check on

the stroking rate to be made. Unfortunately, the launch process proceeded to distort the rod slightly on each launch resulting in it becoming stuck and not properly following the ejection piston.

By inserting a spacer in the ejector piston volume to limit its stroke, an independent check on stroke rate was made. With the appropriate spacer size for the body velocity, camera station and stroke rate installed, a test was made with visible dye and a photograph taken. The photograph displayed several inches of the forebody free from dye while the remainder of the body uniformly covered with dye. This verified that the proper ejection rate was occurring under test conditions.

The effects of the probes on the boundary layer flow was also of concern. The rotation of subsequent sampling stations on the body was a result of this concern. Figure 67 displays a photograph of a .025 inch probe within a dyed boundary layer for a water test case. No significant distortion of the boundary layer is apparent. The velocity in this case was 20.5 ft/sec.

The results of the test series are tabulated in Tables 11, 12, 13, 14, 15, 16 and 17. Although polymer concentrations were not directly measured, the assumption that the Uranine-B in solution reacts and diffuses in the same manner, as previously discussed, allows direct translation to polymer concentration to be made. Only for the water case is the tracer concentration discussed.

Figure 67. Photograph of .025-inch probe within the boundary layer

TABLE 11

Water Ejection Test Results

SERIES	PROBE HEIGHT (IN.)	NO. OF TESTS	MEASUREMENT STATION x/L	RMS CONCENTRATION RATIO C/C_i	EJECTED CONCENTRATION C_i (WPPM)	BODY VELOCITY FT/SEC	TEMPERATURE T(°F)	R_{e_L} $x10^{-6}$
1	Flush	4	.120 .240 .360 .48	.077 .048 .051 .035	.588 .588 .588 .588	26.5 ±1% 26.5 ±1% 26.5 ±1% 26.5 ±1%	62.5 62.5 62.5 62.5	4.78 4.78 4.78 4.78
2	.025	3	.108 .228 .348 .468	.069 .045 .049 .046	1.105 1.104 1.104 1.104	25.23 ±1% 25.23 ±1% 25.23 ±1% 25.23 ±1%	65 65 65 65	4.67 4.67 4.67 4.67
3	.055	7	.108 .228 .348 .468	.0188 .0272 .0273 .0312	.560 .560 .560 .560	27.81 ±1% 27.81 ±1% 27.81 ±1% 27.81 ±1%	70 70 70 70	5.5 5.5 5.5 5.5

NOTE: Ejection Rate 20.6 in^3/sec
L = 2.0833 ft
W-B = 4.46 lbs (Weight in Water)
A_f = 0.0491 ft^2 (Frontal Area)
A_s = 1.3685 ft^2 (Surface Area)

TABLE 12

50 WPPM Ejection Test Results

SERIES	PROBE HEIGHT (IN.)	NO. OF TESTS	MEASUREMENT STATION x/L	RMS CONCENTRATION RATIO C/C_i	EJECTED CONCENTRATION (WPPM)	BODY (FT/SEC)	TEMPERATURE T(°F)	R_{e_L} $\times 10^{-6}$
4	Flush	4	.120	.507	50	27.33 ±1%	58	4.54
			.240	.42	50	27.33 ±1%	58	4.54
			.360	.406	50	27.33 ±1%	58	4.54
			.480	.490	50	27.33 ±1%	58	4.54
5	.025	4	.108	.05	50	27.0 ±1.5%	62	4.79
			.228	.075	50	27.0 ±1.5%	62	4.79
			.348	.086	50	27.0 ±1.5%	62	4.79
			.468	.098	50	27.0 ±1.5%	62	4.79
6	.055	4	.108	.0104	50	27.0 ±1%	60	4.66
			.228	.0126	50	27.0 ±1%	60	4.66
			.348	.0126	50	27.0 ±1%	60	4.66
			.468	.0366	50	27.0 ±1%	60	4.66

SEE NOTE TABLE 10

TABLE 13

500 WPPM Ejection Test Results

SERIES	PROBE HEIGHT (IN.)	NO. OF TESTS	MEASUREMENT STATION x/L	RMS CONCENTRATION RATIO C/C_i	EJECTED CONCENTRATION (WPPM)	BODY VELOCITY (FT/SEC)	TEMPERATURE $T(^{o}F)$	R_{e_L} $x10^{-6}$
7	Flush	4	.120	.45	500	28.9 ±1%	64	5.27
			.240	.45	500	28.9 ±1%	64	5.27
			.360	.555	500	28.9 ±1%	64	5.27
			.480	.54	500	28.9 ±1%	64	5.27
8	.025	4	.108	.0222	500	27.4 ±1%	60	4.73
			.228	.031	500	27.4 ±1%	60	4.73
			.348	.046	500	27.4 ±1%	60	4.73
			.468	.056	500	27.4 ±1%	60	4.73
9	.055	3	.108	.021	500	26.85	70	5.32
			.228	.0097	500	26.85	70	5.32
			.348	.02	500	26.85	70	5.32
			.468	.024	500	26.85	70	5.32

SEE NOTE TABLE 10

TABLE 14

1000 WPPM Ejection Test Results

SERIES	PROBE HEIGHT (IN.)	NO. OF TESTS	MEASUREMENT STATION x/L	RMS CONCENTRATION RATIO C/C_i	EJECTED CONCENTRATION (WPPM)	BODY VELOCITY (FT/SEC)	TEMPERATURE T(^{o}F)	R_{λ} $\times 10^{-6}$
10	Flush	3	.120	.45	1000	28.93 $\pm$2%	58	4.844
			.240	.35	1000	28.93 $\pm$2%	58	4.844
			.360	.437	1000	28.93 $\pm$2%	58	4.844
			.480	.352	1000	28.93 $\pm$2%	58	4.844

SEE NOTE TABLE 10

TABLE 15

20 WPPM Ejection Test Results

SERIES	PROBE HEIGHT (IN.)	NO. OF TESTS	MEASUREMENT STATION x/L	RMS CONCENTRATION RATIO C/C_i	EJECTED CONCENTRATION (WPPM)	BODY VELOCITY (FT/SEC)	TEMPERATURE T(^{o}F)	R_{e_L} $\times 10^{-6}$
11	Flush	1	.120 .240 .360	.39 .431 .463	20 20 20	27.2 27.2 27.2	79 79 79	6.04 6.04 6.04

SEE NOTE TABLE 10

TABLE 16

10 WPPM Ejection Test Results

SERIES	PROBE HEIGHT (IN.)	NO. OF TESTS	MEASUREMENT STATION x/L	RMS CONCENTRATION RATIO C/C_i	EJECTED CONCENTRATION (WPPM)	BODY VELOCITY (FT/SEC)	TEMPERATURE T(^{o}F)	Re_L $\times 10^{-6}$
12	Flush	2	.120	.390	10	27.1 $\pm$1%	79	6.02
			.240	.390	10	27.1 $\pm$1%	79	6.02
			.360	.355	10	27.1 $\pm$1%	79	6.02

SEE NOTE TABLE 10

TABLE 17

5 WPPM Ejection Test Results

SERIES	PROBE HEIGHT (IN.)	NO. OF TESTS	MEASUREMENT STATION x/L	RMS CONCENTRATION RATIO C/C_I	EJECTED CONCENTRATION (WPPM)	BODY VELOCITY (FT/SEC)	TEMPERATURE T(^oF)	R_{e_L} $x10^{-6}$
13	Flush	2	.120	.378	5	27.05	79	6.011
			.240	.378	5	27.05	79	6.011
			.360	.260	5	27.05	79	6.011

SEE NOTE TABLE 10

Water Ejection Test Results

Figures 68, 69 and 70 display the data obtained in test series 1, 2 and 3 of Table 10. Referring first to Figure 10, it can be noticed that for this water diffusion case, the wall dye concentration has decreased to .1 of the ejected concentration in a distance of slightly less than one body diameter. The diffusion over the next nine inches of body length near halves again the concentration level. The diffusion process is quite rapid, characteristic of turbulent mass transport. The predicted curve on this figure applies the two zone diffusion boundary layer growth model combined with the axisymmetric boundary layer model as discussed earlier. The concentration similarity profiles for water were applied for the two-zone process quite successfully.

Figure 69 displays the data from the series 2 experiment with the .025 inch probes sampling the boundary layer. Again, comparison with the model for the water case seems quite good. Although not apparent in the data, the computer solutions shows the concentration growth prior to the sampling station and then a normal decay as the dye diffuses outward in the boundary layer.

Figure 70 displaying series 3 tests with water ejection and the .055 inch probes, the rise in the concentration levels between the first and second probe stations is evident in the data and predicted by the theory.

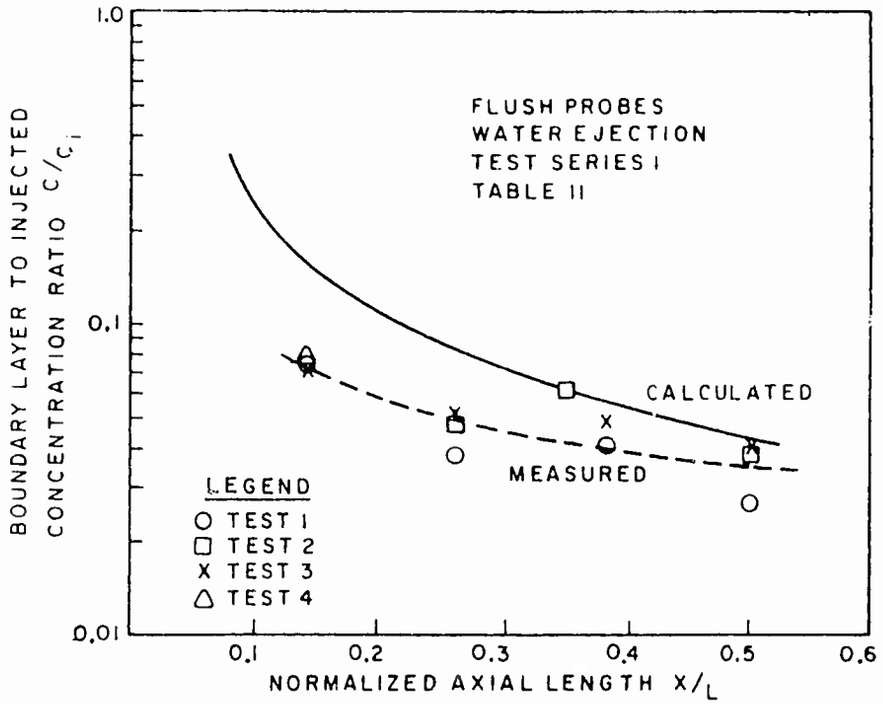

Figure 68. Boundary layer to injected concentration ratio vs normalized axial length Test Series 1

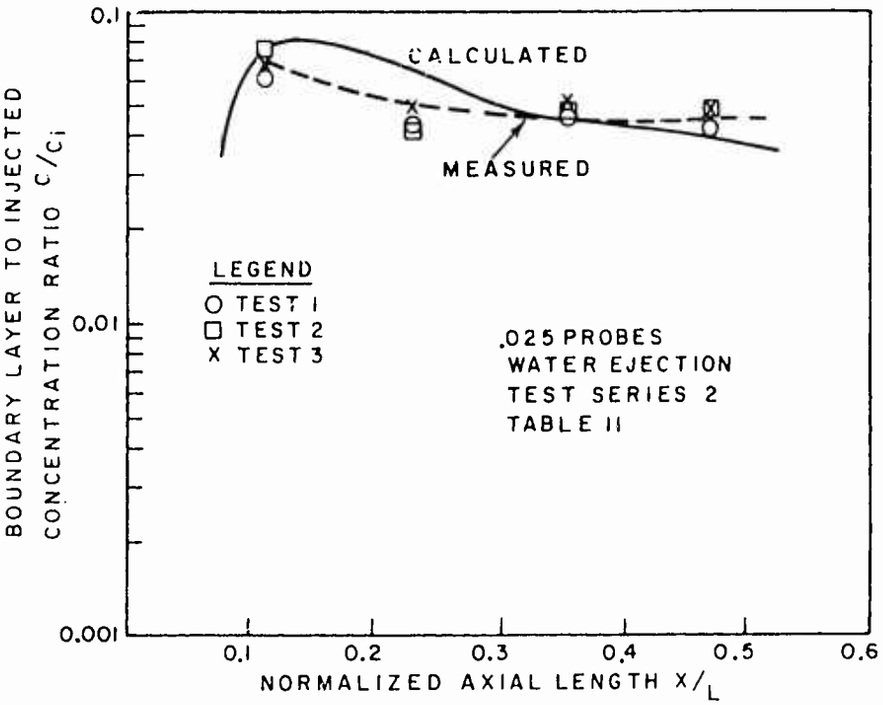

Figure 69. Boundary layer to injected concentration ratio vs normalized axial length Test Series 2

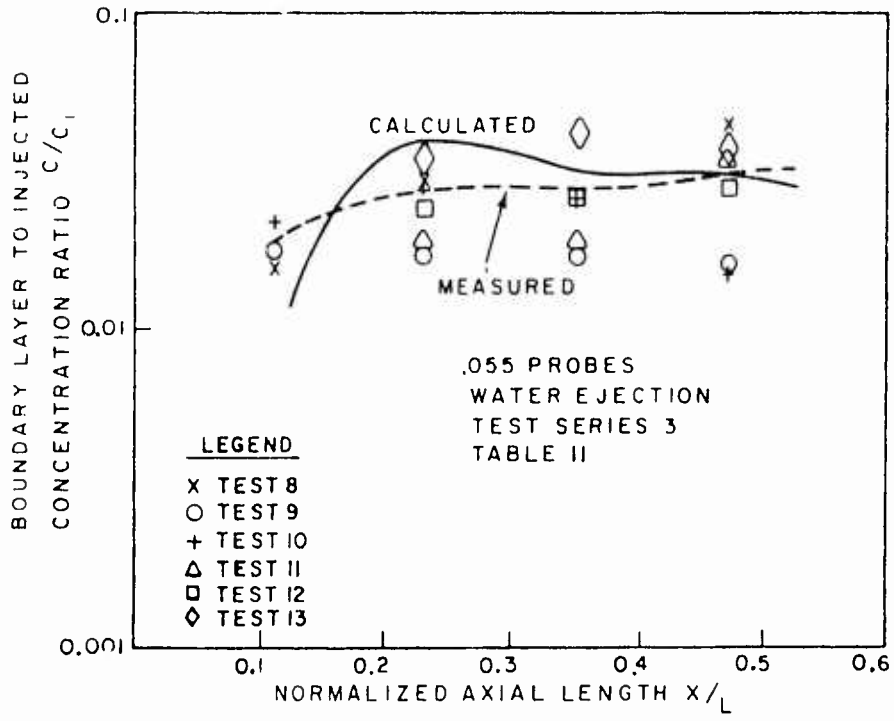

Figure 70. Boundary layer to injected concentration ratio vs normalized axial length Test Series 3

Figure 71, a composite plot of the calculated flush, .025-inch and .055-inch probes displays an interesting result. First, the increase in concentration initially for the probes away from the wall is evident. The decay in concentration as the fluorescent dye diffuses outward is as expected in the approximately constant diameter section. At x/L of approximately .6, however, the concentration ratio begins to increase. The boundary layer in this region is growing very rapidly as both the photograph for this case, Figure 53 and the calculated and measured boundary layers indicate, Figure 60. The cause of this rise is the decreasing diameter resulting in a smaller boundary layer flux area within which the tracer resides. This is a rather interesting result since in external flows one would expect a uniform decrease in concentration with length due to boundary layer growth, Figure 72 displays the growth of the diffusion boundary layer, defined as height at which the concentration is .5 of the wall concentration, within the normal boundary layer. The growth of the diffusion boundary layer is reduced as compared to the normal boundary layer in the tail region, $x/L > .6$.

Figure 73 displays a plot of the concentration profile for the first two probe stations normalized to the wall concentration. The remaining two stations were not plotted since only the .055 probe height gave a value of C/C_w different from one. A single point curve would have resulted. Table 18 provides a tabulation of the experimental data used in generating this figure. As noted in the

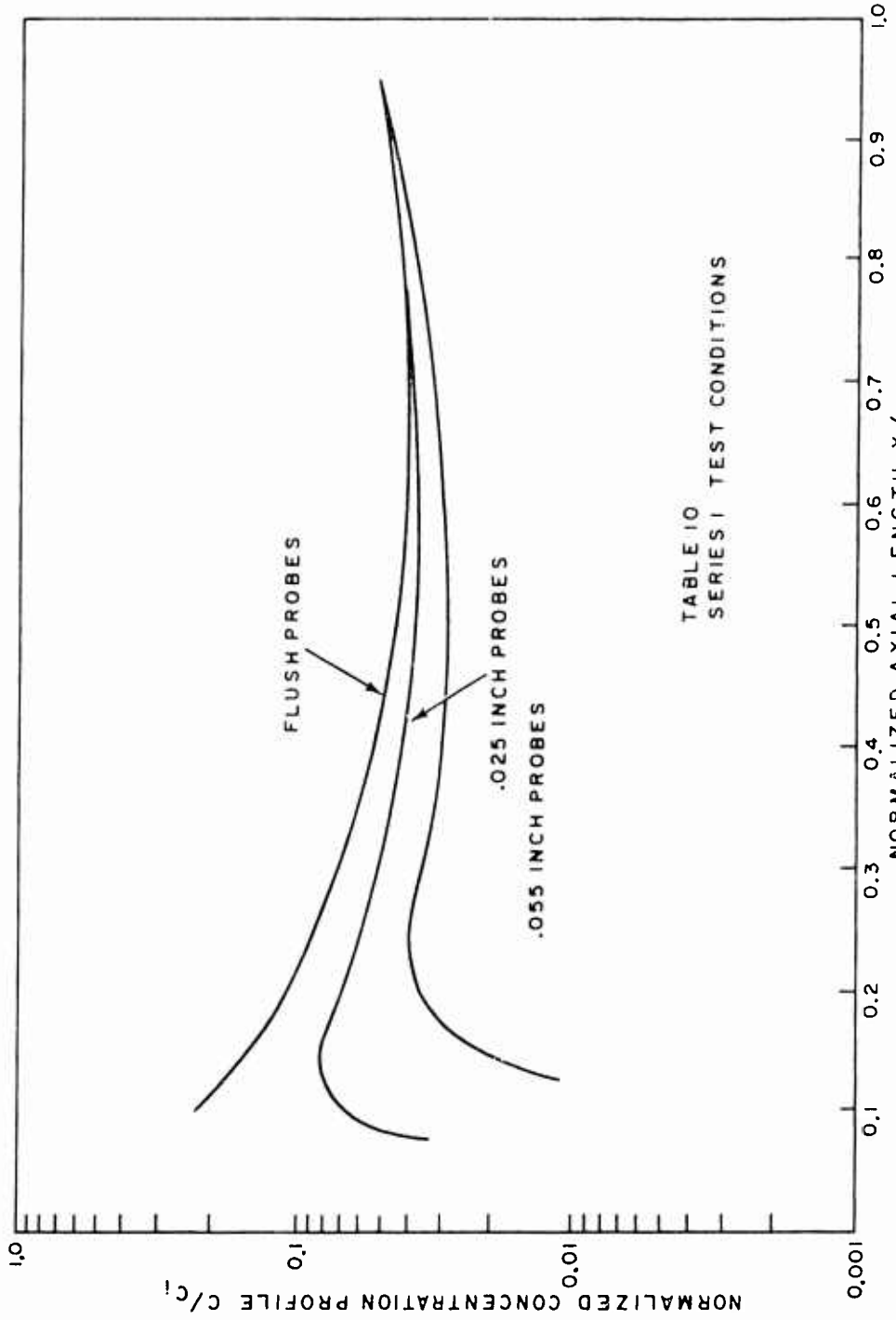

Figure 71. Calculated normalized tracer concentration vs normalized axial distance

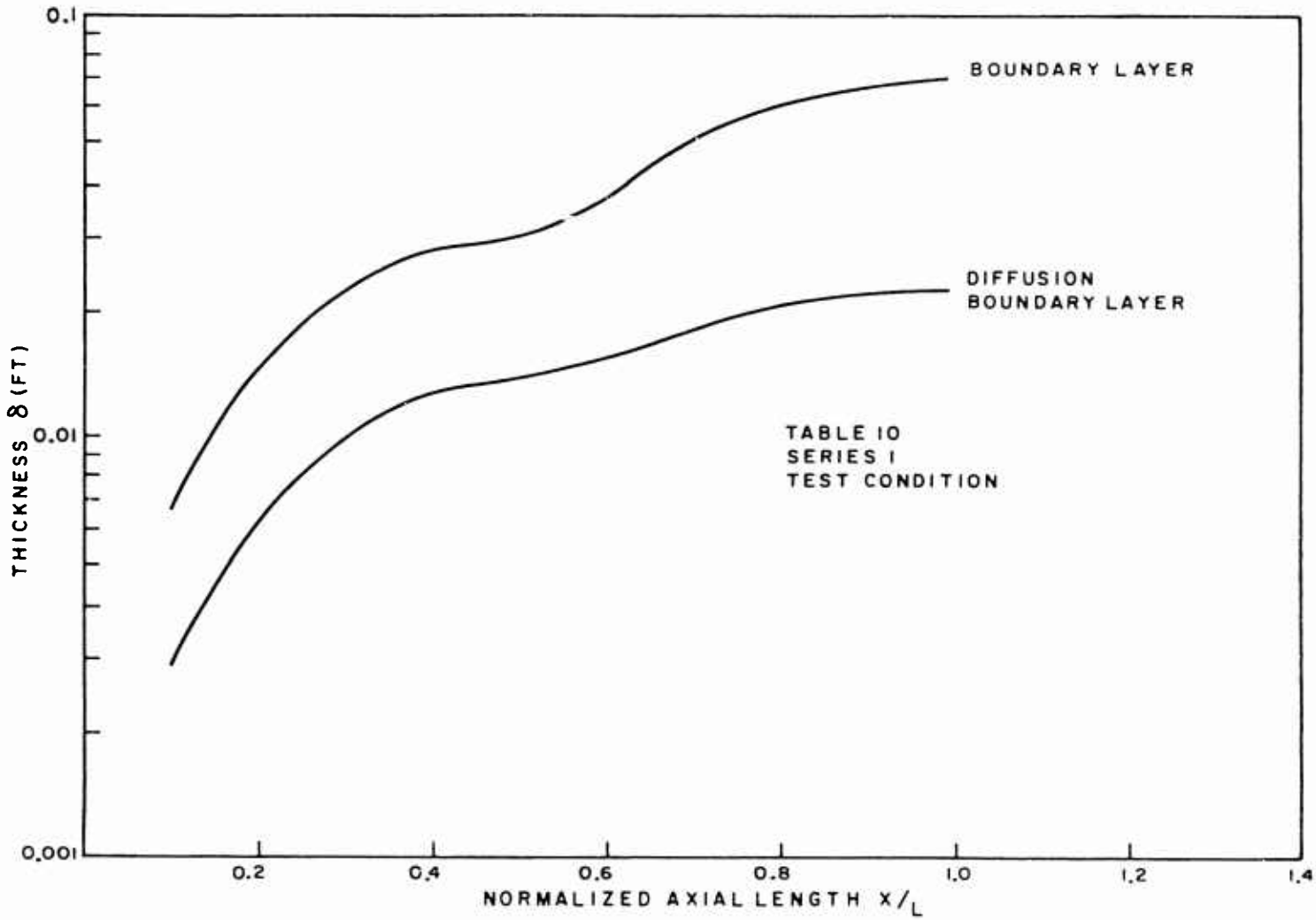

Figure 72. Calculated diffusion boundary layer and boundary layer growth vs normalized axial length

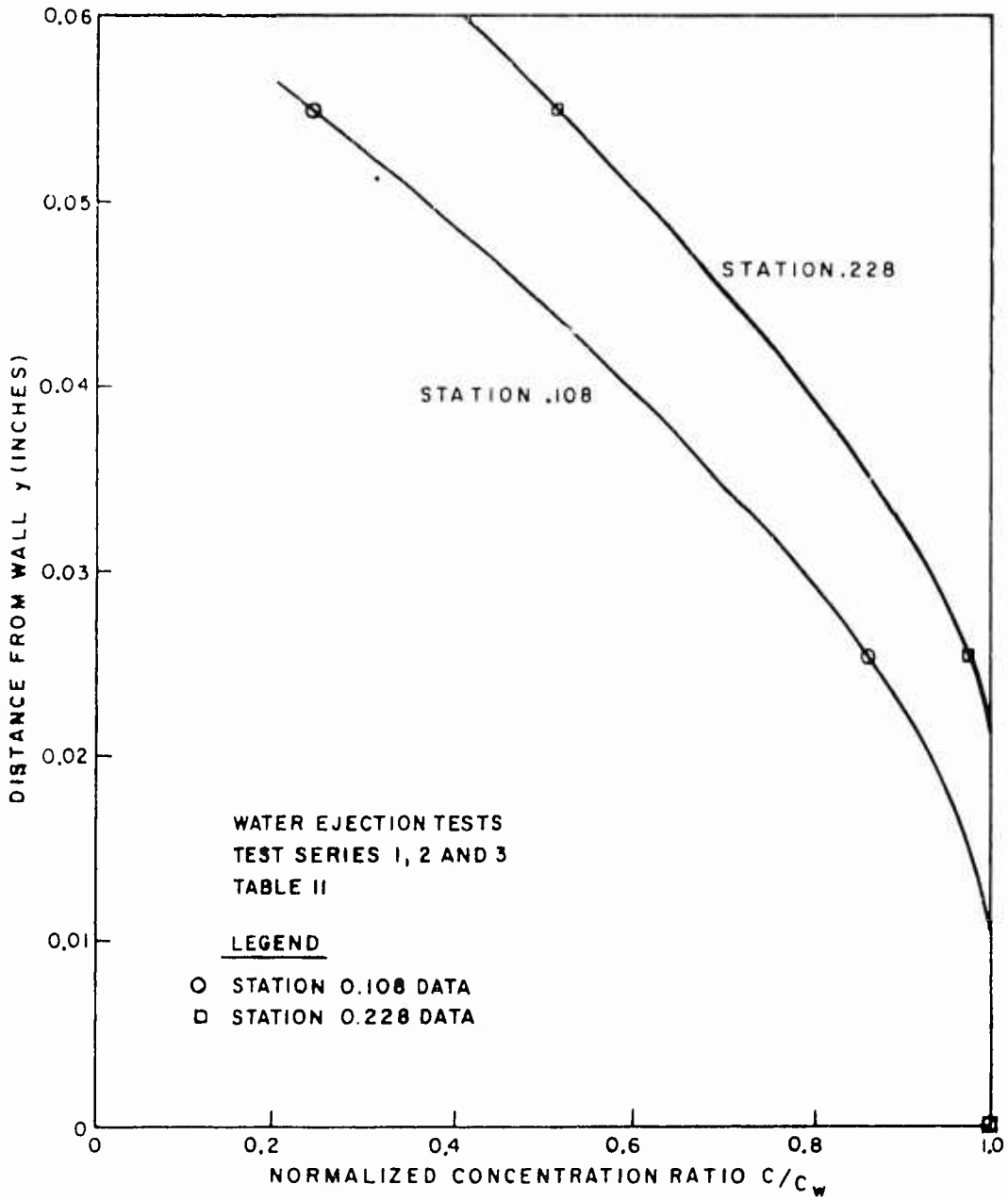

Figure 73. Distance from wall vs normalized concentration ratio water case

TABLE 18

Concentration Profile Determination
(Using Smoothed Profile)

		STATION							
		.108		.228		.348		.468	
y (IN)		C/C_i	C/C_w	C/C_i	C/C_w	C/C_i	C/C_w	C/C_i	C/C_w
	0	.082	1	.051	1	.041	1	.035	1
Water	.025	.07	.854	.051	1.48	.045	1	.045	1
	.055	.019	.23	.027	.53	.028	.68	.031	.88
	0	.49	1	.42	1	.406	1	.48	1
50 WPPM	.025	.05	.102	.075	.178	.088	.216	.095	.2
	.055	.01	.02	.012	.028	.013	.032	.034	.07
	0	.45	1	.45	1	.48	1	.57	1
500 WPPM	.025	.023	.05	.034	.076	.047	.1	.057	.1
	.055	.001	.002	.01	.02	.02	.042	.022	.04

figure, the diffusion process is quite rapid with wall concentration being approached quite far out into the boundary layer a short distance back on the body. By defining the diffusion boundary layer thickness as that value of y at which C/C_w equals .5, a normalization height is determined for plotting this data on a similarity concentration profile plot. Table 19 presents these data, along with data from subsequent tests with polymers. A comparison of these data (water case) with that from other experimentators is done on the similarity profile plot of Figure 74. The dotted line on this figure taken from Hsu (1971) has been generated from data by Poreh and Cermak (1964) and verified by Wetzel and Ripkin (1970). The equation for this line is as shown on the figure. The limited data obtained in this experiment verify, for the axisymmetric case, the applicability of this similarity profile for the downstream region. The water ejection line, although falling slightly higher resulting in a higher value of the exponent in the C/C_w relation, is in good agreement with the previous investigation. The applicability of the model in predicting the wall concentration and concentration profiles in the boundary layer seems apparent.

Polymer Ejection Test Results

Figures 75, 76 and 77 display the data obtained in test series 4, 5 and 6 of Table 12. In this series, 50 WPPM polymer concentration was ejected. The results were not as expected. At all probe stations the polymer concentration remained high indicating no diffusion occurring. As may be seen in Figure 75, the combined model

TABLE 19

Normalized Concentration Profile for
Several Concentration Ratios

		STATION											
C/C_w		.108			.228			.348			.468		
		δ_d	y	y/δ_d	δ_d	y	y/δ_d	δ_d	y	y/δ_d	δ_d	y	y/δ_d
	.1	.044			.057								
	.2	.044			.057								
Water	.4	.044	.048	1.09	.057	.0625	1.09						
	.6	.044	.039	.89	.057	.0510	.89						
	.8	.044	.029	.66	.057	.039	.68						
	.1	.0055	.1	18	.008			.0094			.0094		
	.2	.0055	.0152	2.76	.008	.022	.275	.0094	.0263	2.79	.0094	.0263	2.79
50	.4	.0055	.0078	1.42	.008	.011	1.375	.0094	.013	1.38	.0094	.013	1.38
WPPM	.6	.0055	.0037	.67	.008	.0057	.712	.0094	.0068	.723	.0094	.0068	.723
	.8	.0055	.0014	.25	.008	.0022	.275	.0094	.0028	.298	.0094	.0028	.298
	.1	.0044			.0052			.0059			.0059		
	.2	.0044	.012	2.7	.0052	.014	2.7	.0059	.0153	2.6	.0059	.0153	2.6
500	.4	.0044	.0064	1.45	.0052	.0072	1.38	.0059	.0081	1.37	.0059	.0081	1.37
WPPM	.6	.0044	.0029	.65	.0052	.0036	.69	.0059	.0004	.68	.0059	.0004	.68
	.8	.0044	.001	.23	.0052	.0014	.27	.0059	.0016	.28	.0059	.0016	.28

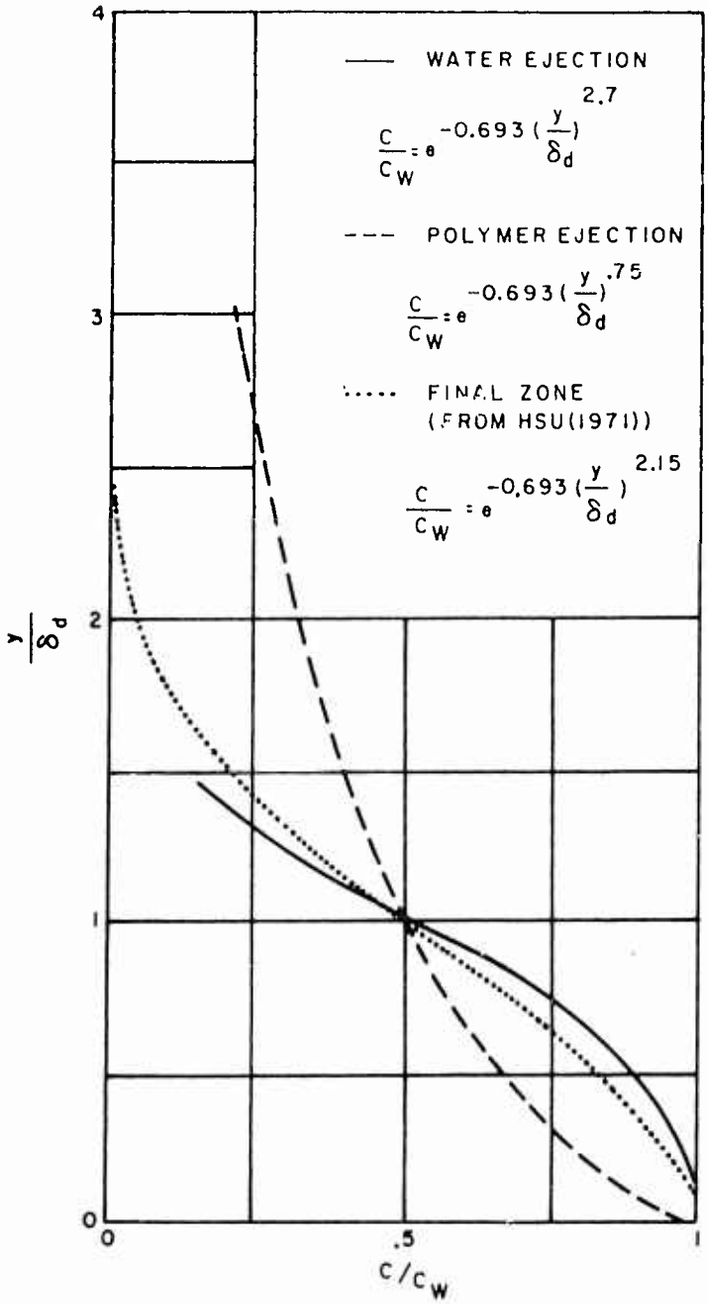

Figure 74. Concentration profiles determined for water and polymer ejection

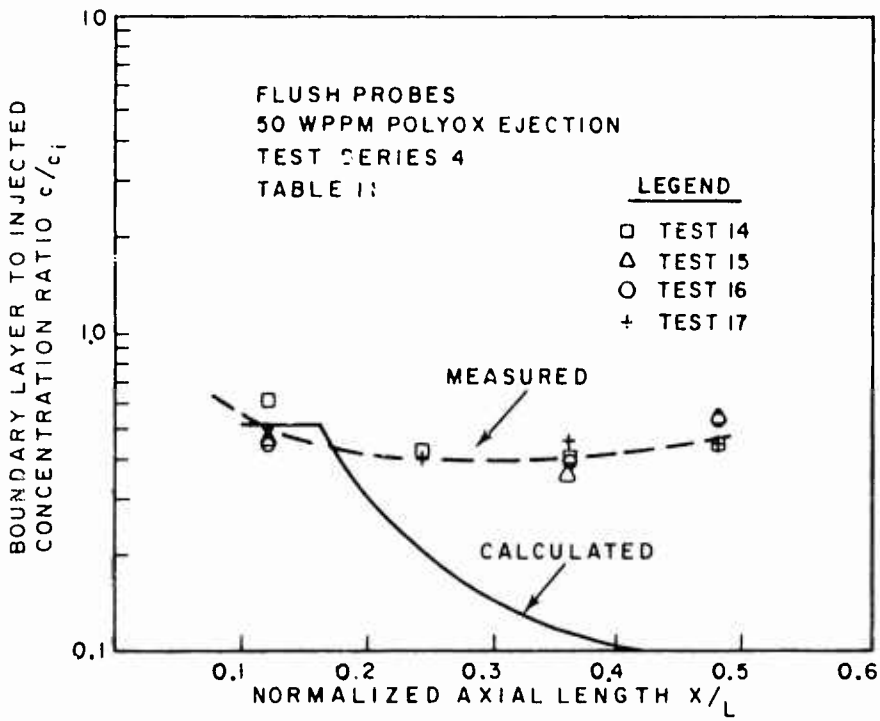

Figure 75. Boundary layer to injected concentration ratio vs normalized axial length Test Series 4

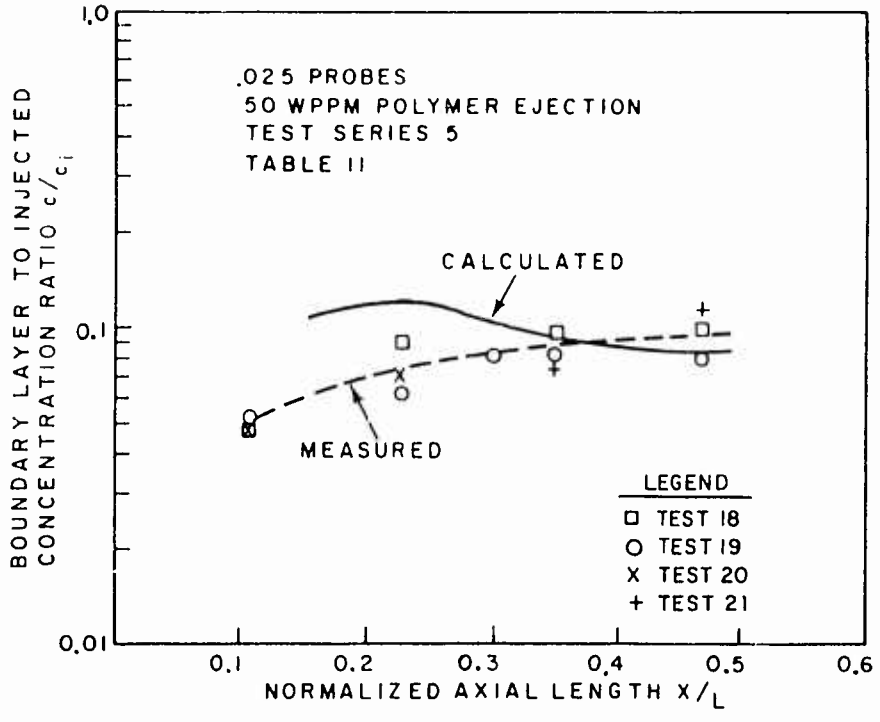

Figure 76. Boundary layer to injected concentration ratio vs normalized axial length Test Series 5

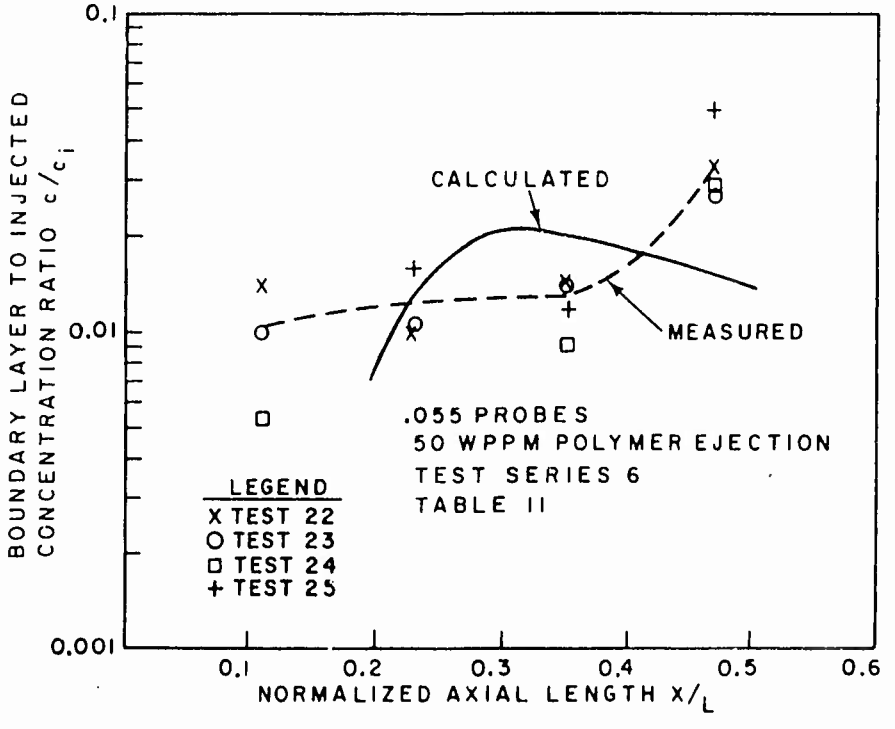

Figure 77. Boundary layer to injected concentration ratio vs normalized axial length Test Series 6

predicts a short initial zone. Figures 76 and 77 show the concentration measured with the .025-inch probes and the .055-inch probes. The experimental data display a slow build up of the concentration. The .055-inch probes which should be well outside the sublayer, display much scatter expecially at the first station. Apparently there is diffusion from the surface of the viscous layer otherwise the measured value would be much lower. The calculations do not account for diffusion from the viscous layer. There may still be some bursting occurring at this concentration level as some of the polymer in the ejection process is being hurled to regions further from the wall. The calculated values displayed in this figure show the characteristic rise and fall off of the rapid diffusion process as is predicted by the intermediate and final zone models. Figure 77 shows a sudden rise in the data at the last measurement station. Quite possibly, the end of the initial zone is being reached and the more rapid diffusion is beginning to occur.

Table 18 summarizes the concentration profile data taken for the 50 WPPM case from which Figure 78 is plotted. This figure displays the totally changed character of the concentration profile from the water case, Figure 73. Comparing, δ_d, the value of y at C/C_w equal to .5, for the water case δ_d is .044 inches at the first measurement station, while for the 50 WPPM case it is .0055 inches. (nearly a factor of 10 difference). Table 19 presents the data taken from Figure 78 from which a redefinition of the distance from the

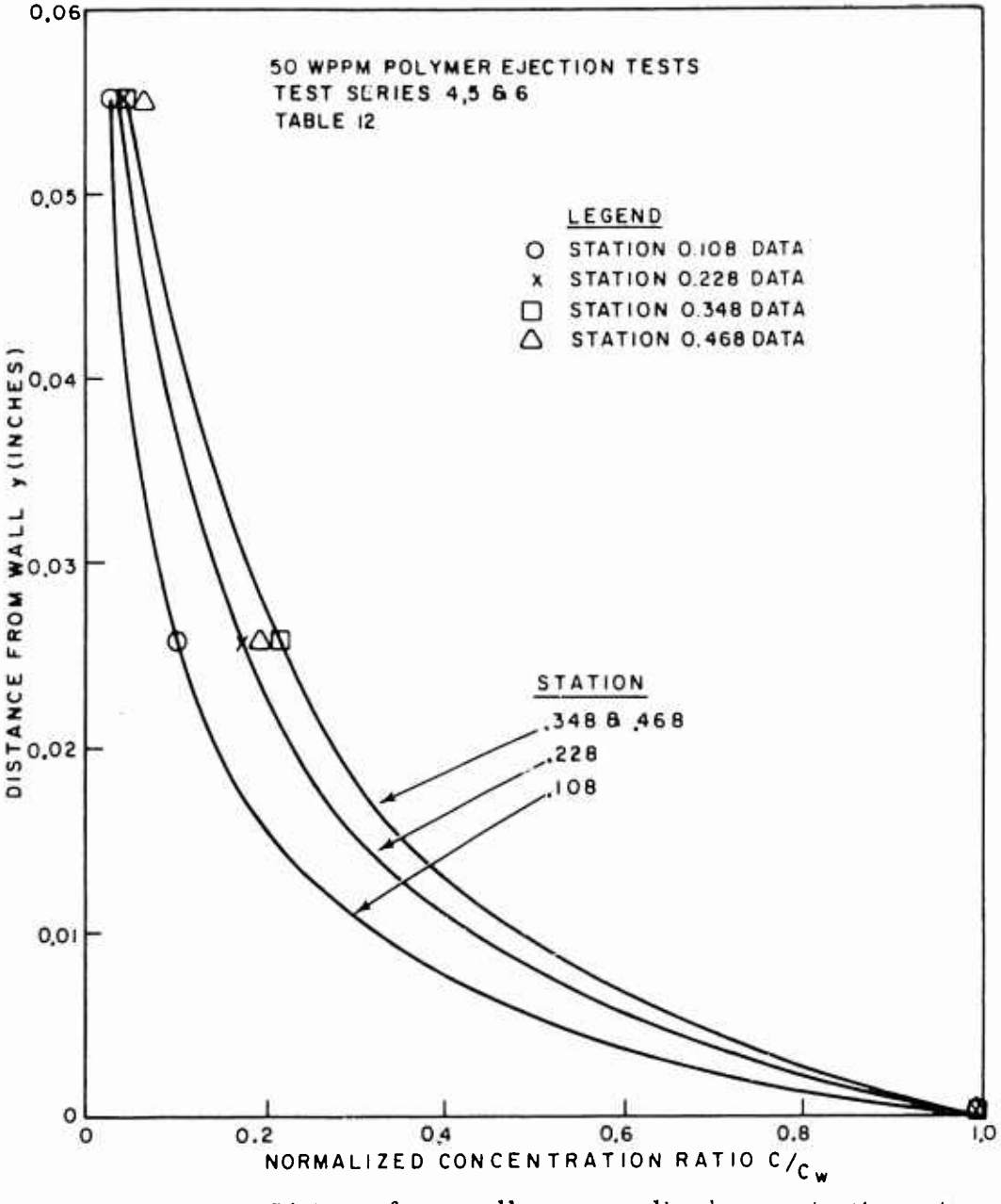

Figure 78. Distance from wall vs normalized concentration ratio 50 WPPM case

wall, y, to a nondimensional distance, y/δ_d, is made. This nondimensional height is plotted in Figure 74 and a curve fit made. The result, is a similarity profile with an exponent of .75 for all measurement stations. This exponent implies significantly reduced diffusion but not to the level which the data display. The discrepancy lies in the fitting of the curve in Figure 78. Three points are available. These are at y = .025 inches, y = .055 inches and y = 0 inches. Clearly, the curve could be drawn a number of ways which would significantly reduce the exponent value by reducing δ_d. The information demonstrating low diffusion rate is contained in the wall concentration measurement, however, so no attempt was made to match the curves to the data through the computer routine. In fact, the variable K_3 model which resulted in a steady wall concentration profile calculated an exponent value of about .15. Let it suffice that Figure 78 displays markedly reduced diffusion to that of water and recommend for future work that a probe be tested at .01-inch height. Another interesting facet of these tests were that the exponent did not change with measurement station. This implies that the diffusion rate does not change, in these tests, with downstream distance. Again this may be a function of the curve fit only since, unless only molecular diffusion is occurring, it would be expected that the diffusion rate would increase.

Figures 79, 80 and 81 present similar test results for the test series 7, 8 and 9 of Table 13. As can be seen in Figure 79, for the

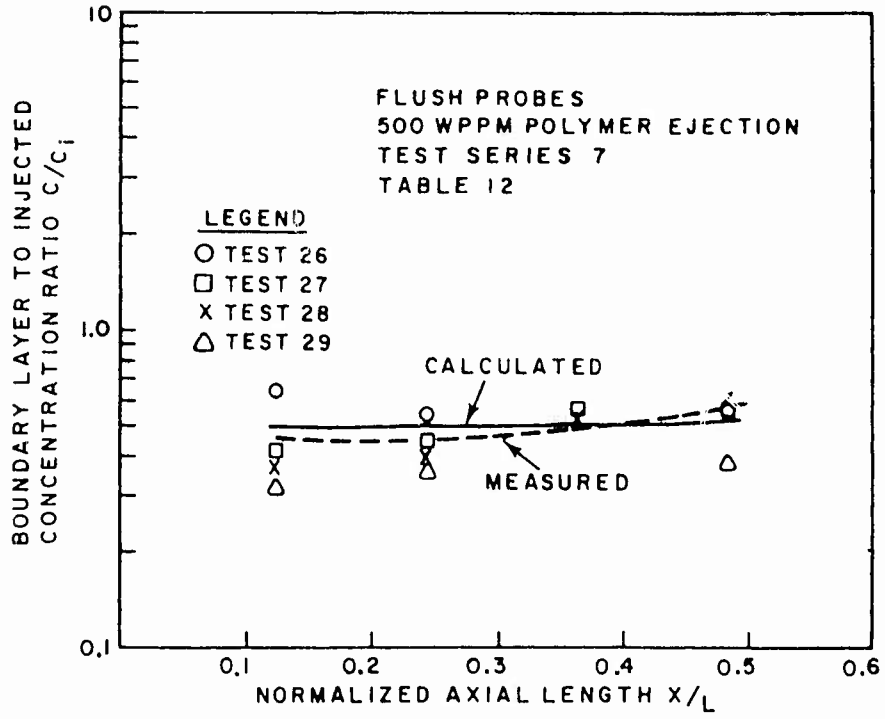

Figure 79. Boundary layer to injected concentration ratio vs normalized axial length Test Series 7

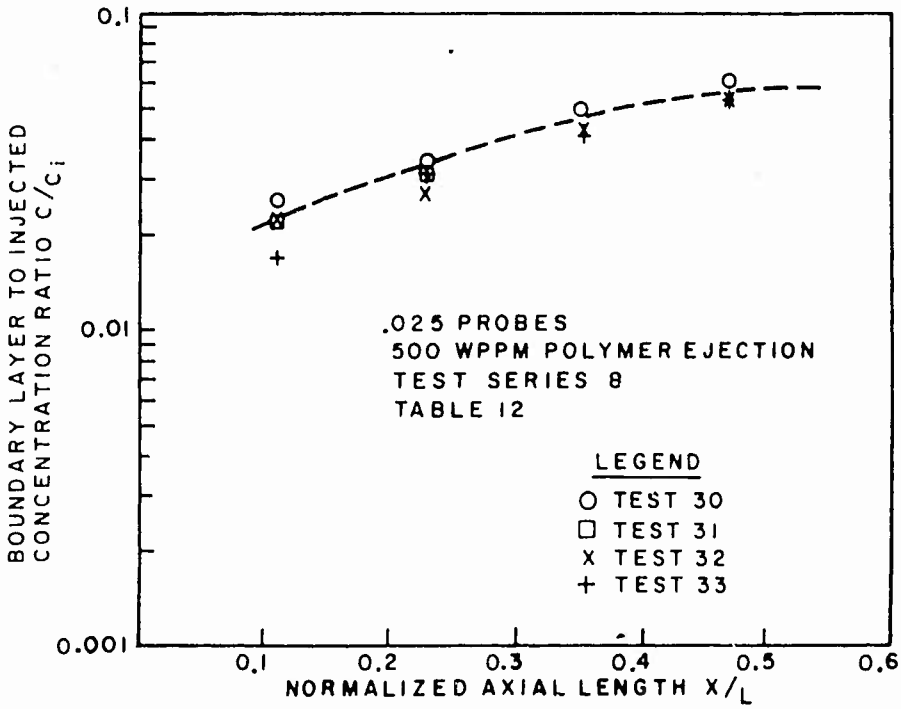

Figure 80. Boundary layer to injected concentration ratio vs normalized axial length Test Series 8

500 WPPM case, both the calculated and experimental data clearly indicate little diffusion is occurring. The .025-inch probes display the same gentle rise in concentration, Figure 80, as compared to the decay in concentration noted for the water case, Figure 69, resulting from the higher diffusion in that case. The .055-inch probes again display a slow rise with low levels indicative of low diffusion. It is interesting to note the scatter at the first station implying some anomaly in the ejection process. No calculations are evident for the concentration ratio in these probe figures since the molecular diffusion portion of the model does not incorporate a similarity concentration profile. The variable K_3 model would account for this. Before turning to a concentration profile discussion, a test, test series 10, Table 14, was performed with 1000 WPPM ejected. Figure 82 displays the results. Again a nearly constant concentration with body distance results indicating little or no diffusion. This is not surprising considering the photographs taken showing the boundary layer structure, Figures 58 and 59.

The data for the 500 WPPM series have also been normalized for plotting as concentration ratio vs height, Table 18. Figure 83 displays this plot. Again an extremely low diffusion rate is evident compared to the water case, Figure 73. The 500 WPPM case is much steeper in profile than that of the 50 WPPM case, Figure 78, implying an even greater decrease in diffusion rate. Interestingly, when the height, y, is nondimensionalized with δ_d, Table 19, the

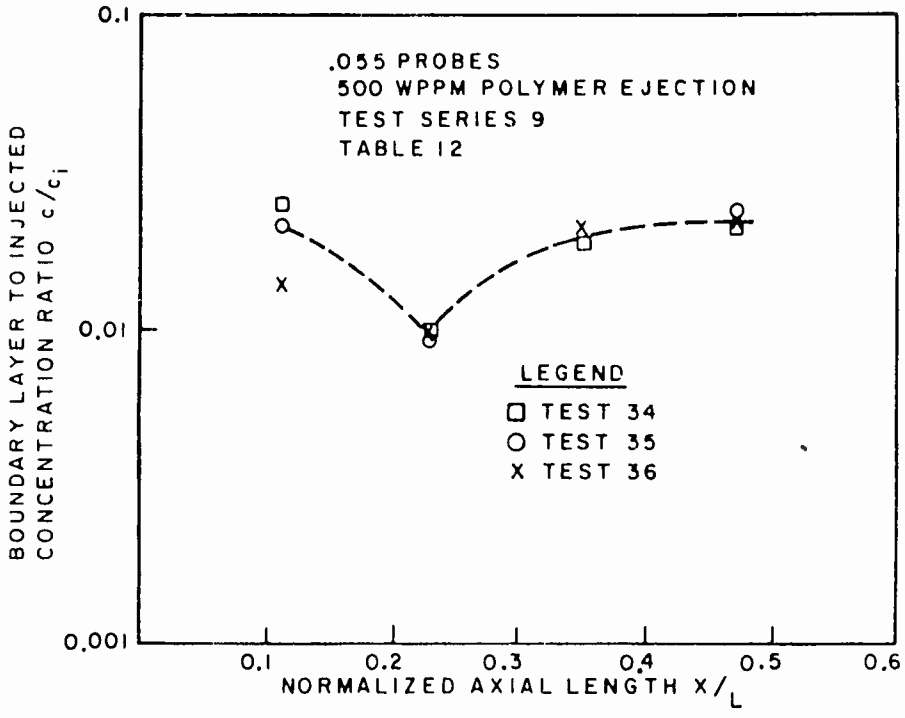

Figure 81. Boundary layer to injected concentration ratio vs normalized axial length Test Series 9

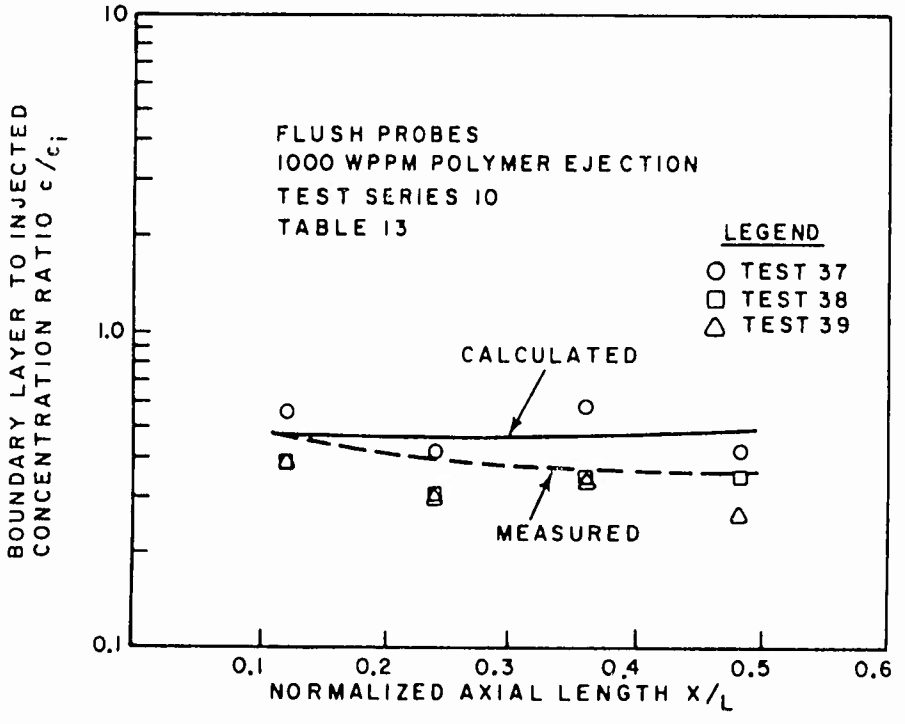

Figure 82. Boundary layer to injected concentration ratio vs normalized axial length Test Series 10

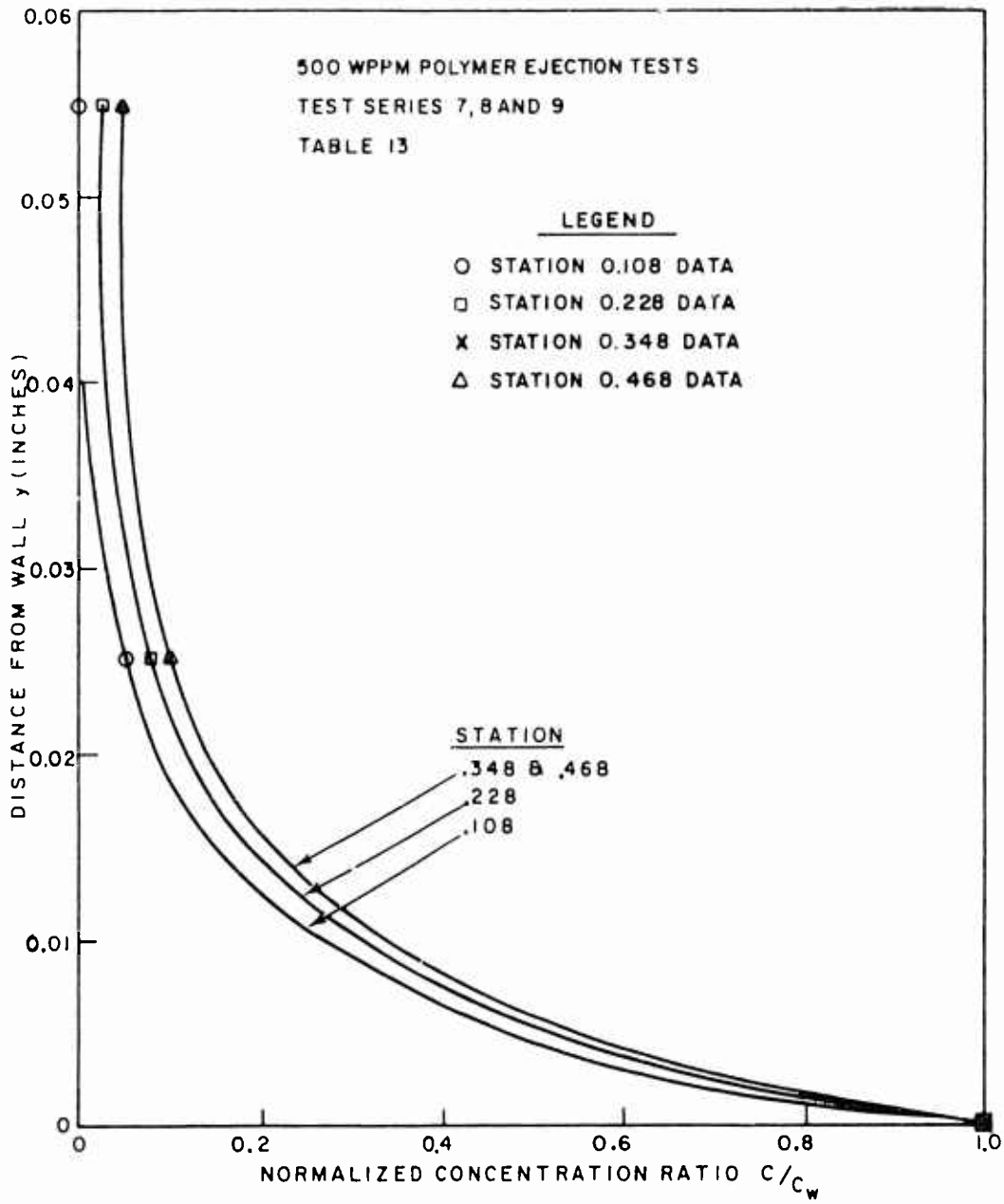

Figure 83. Distance from wall vs normalized concentration ratio 500 WPPM case

the similarity profile is the same as for the 50 WPPM case. The results are plotted in Figure 74 where the polymer ejection case applies to both the 50 WPPM and 500 WPPM test series. Again, the frailties of this plot are similar to those of Figure 78.

Additional tests were performed with reduced polymer concentrations in an attempt to define the position at which the initial diffusion zone terminated. These test results are displayed in Figure 84, for 20 WPPM polymer solution, Figure 85, 10 WPPM polymer solution and Figure 86, 5 WPPM polymer solution ejected. For both the 20 WPPM and 10 WPPM case, no drastic change to a higher diffusion rate is evident. The wall concentration to injected concentration ratio remaining about constant throughout the sampling region of the body. The 5 WPPM ejected concentration did display the result being sought. As shown in Figure 86, a definite reproducible shift to a lower concentration has occurred between the second and third sampling stations. From the flat plate data of Fruman and Tulin (1974) a projected transition to a higher diffusion process would have been projected to occur at concentration below 36 WPPM. These limited results indicate, for the axisymmetric case, a delay in transition to higher diffusion occurs at a significantly reduced concentration level.

The test series performed in this study may be compared directly with those of Fruman and Tulin (1974) if corrected for the axisymmetric influence by multiplying the concentration ratio by D_o/D_i. The

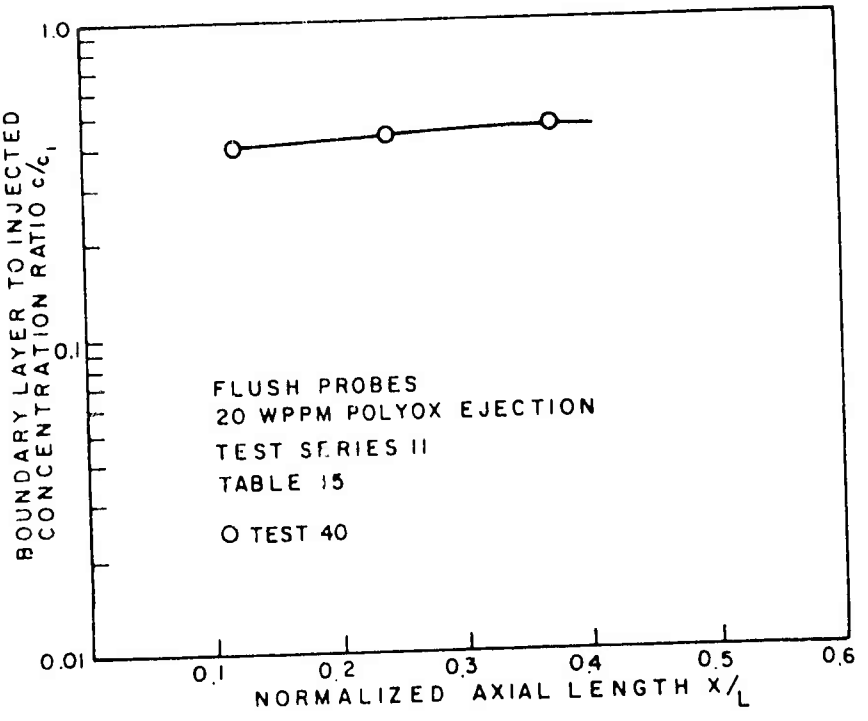

Figure 84. Boundary layer to injected concentration ratio vs normalized axial length Test Series 11

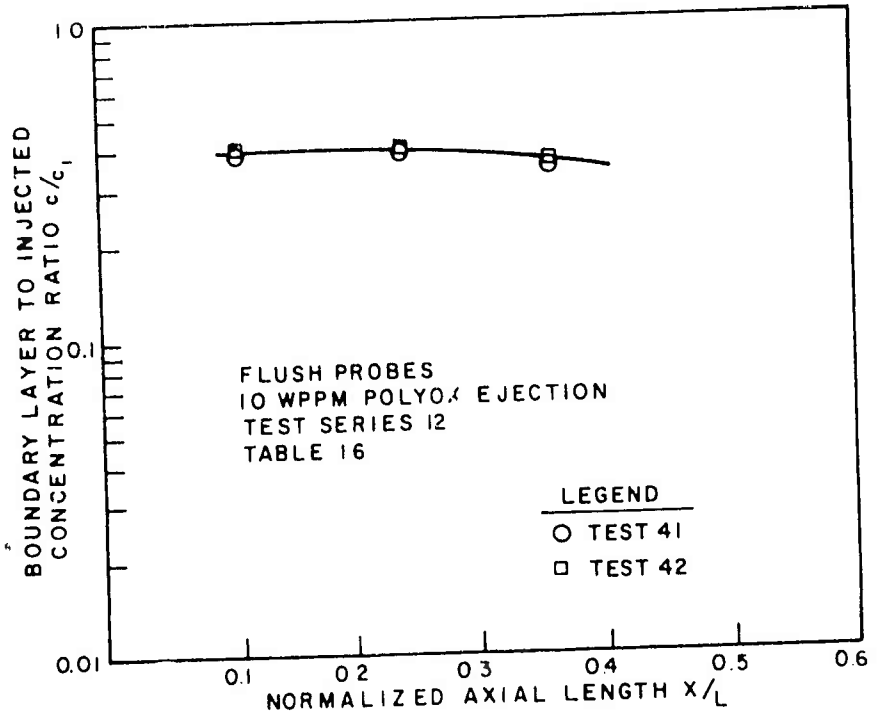

Figure 85. Boundary layer to injected concentration ratio vs normalized axial length Test Series 12

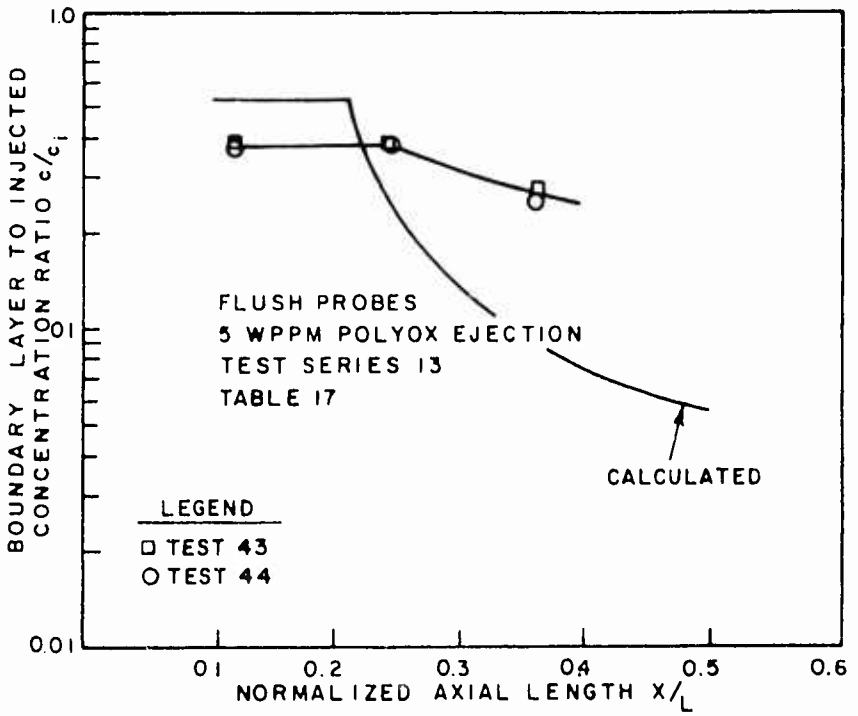

Figure 86. Boundary layer to injected concentration ratio vs normalized axial length Test Series 13

Reynolds number range for this test series was about 5 million whereas the Fruman and Tulin experiments were approximately 10 million. The ratio of ejection velocity to free stream velocity (body velocity in this case) is .185 in this study and ranges from .187 to .274 in the Fruman and Tulin experiments. Figure 87 displays a plot of the concentration to injected concentration ratio vs a dimensionless distance for a water ejected case taken from Fruman and Tulin (1974). The data from this experiment compare well. Similar plots for 1000 WPPM Figure 88, and 500 WPPM, Figure 89 show similar agreement. The data from this experiment are believed to be well qualified and displaying similar trends.

Figure 90, from Fruman and Tulin (1974), displays the departure from the initial zone of diffusion as was predicted from equation (96) from that reference. Data from this experiment are plotted on this figure. As is noted, all data for concentration fall in the initial zone region of molecular diffusion and have a corrected concentration ratio of about 1. The test series 4 data, 50 WPPM case, falls to the right of the departure from the initial zone region. The reason is suspected to be that equation (96), which applies to slot ejection, should be modified to the case of ejection into the free stream and becoming a part of the laminar boundary layer. The ejection velocity becomes meaningless for this case and should be replaced with some other velocity which may be the mean laminar flow velocity or approximately .6 of the local

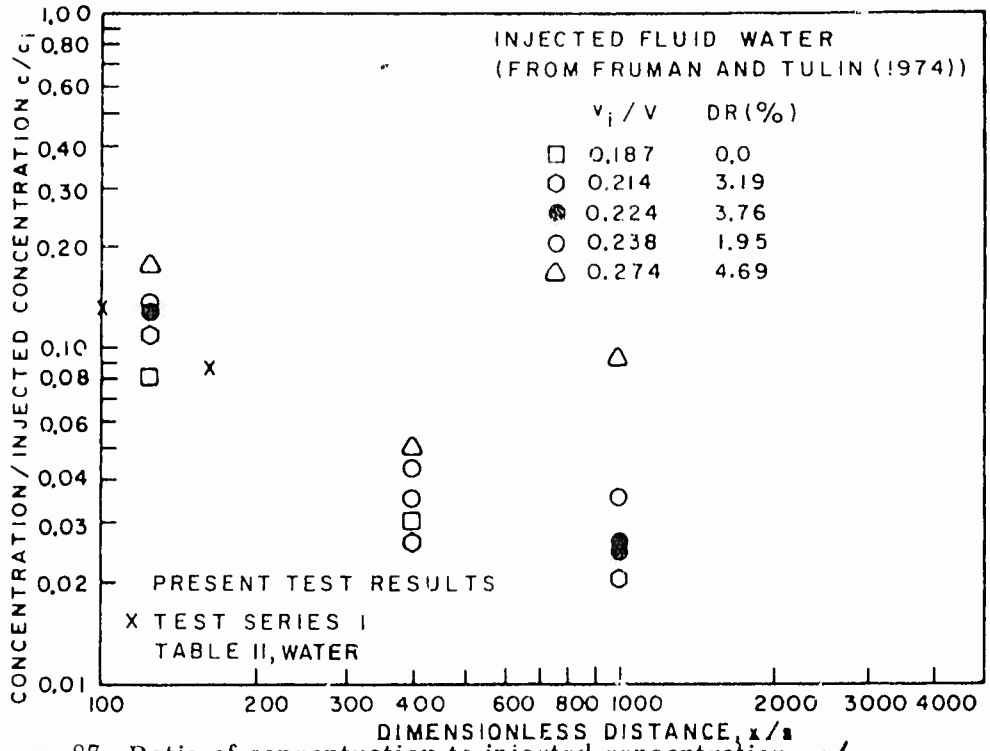

Figure 87. Ratio of concentration to injected concentration, c/c_i, vs dimensionless distance, x/s, for water injection (from Fruman and Tulin (1974))

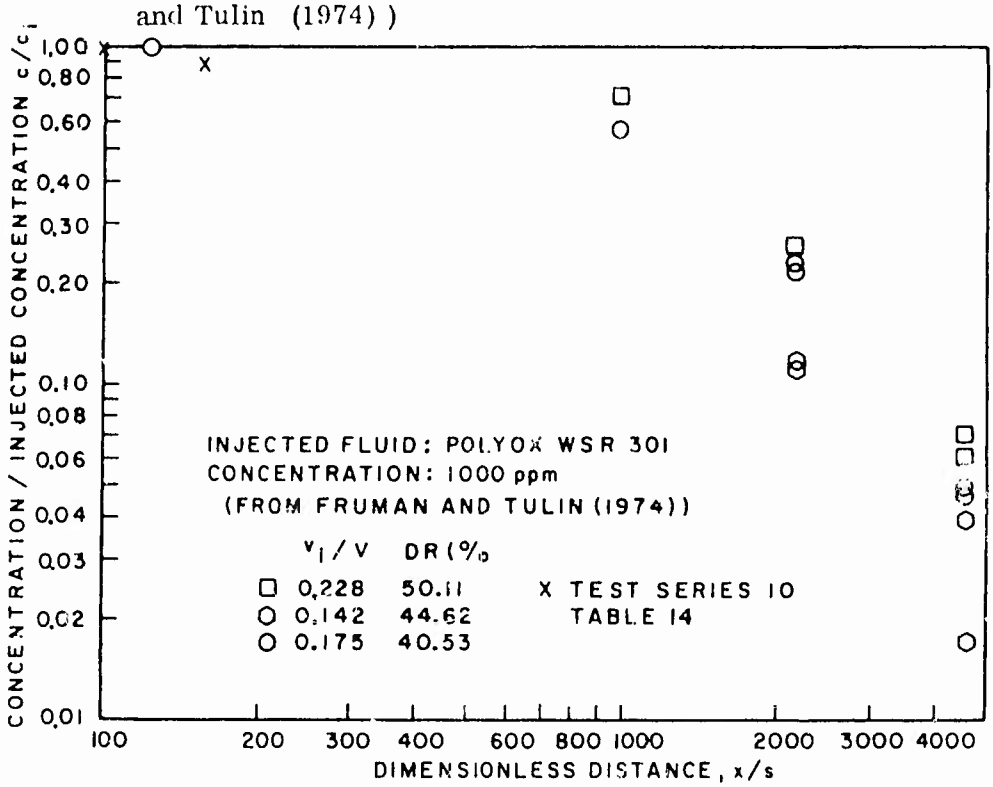

Figure 88. Ratio of concentration to injected concentration, c/c_i, vs dimensionless distance, x/s, for 1000 ppm polyox WSR 301 injection (from Fruman and Tulin (1974))

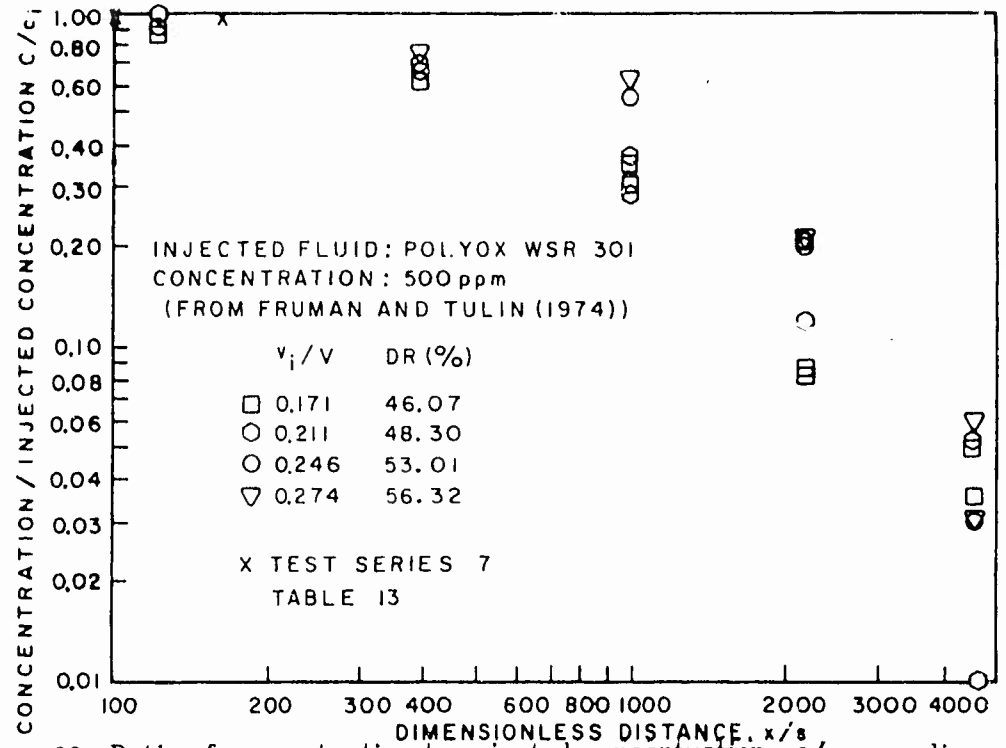

Figure 89. Ratio of concentration to injected concentration, c/c_i, vs dimensionless distance, x/s, for 500 ppm polyox WSR 301 (from Fruman and Tulin (1974))

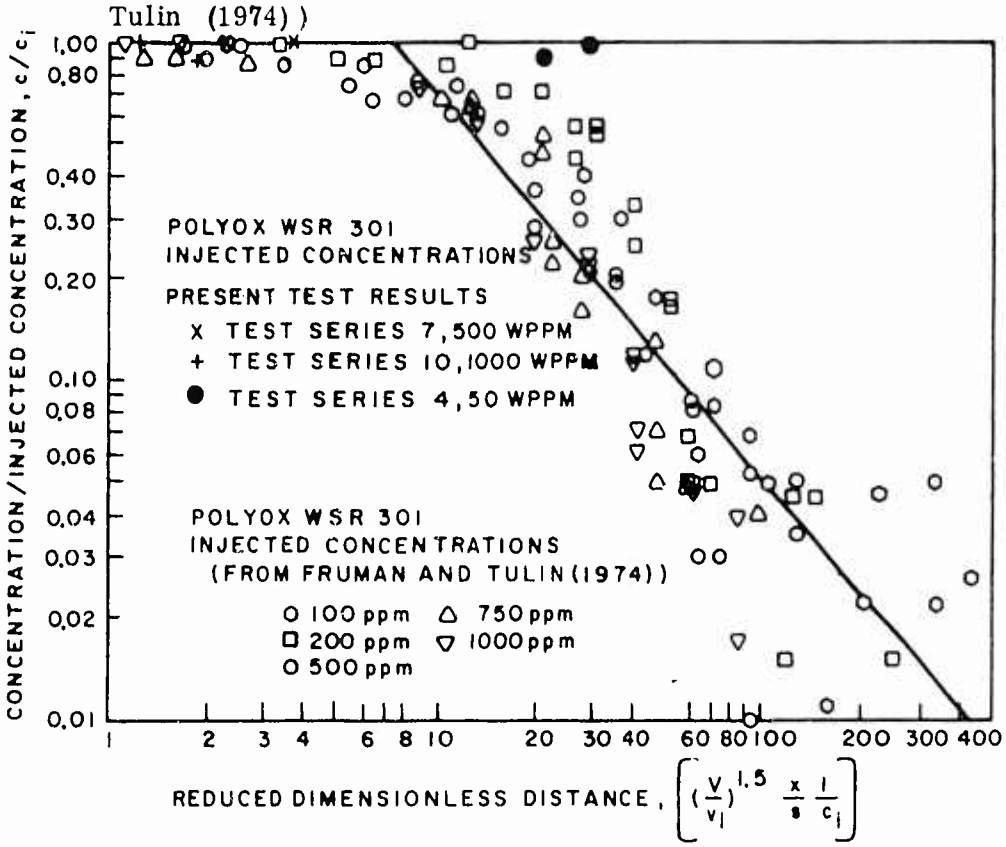

Figure 90. Dimensionless concentration vs reduced dimensionless distance (from Fruman and Tulin, (1974)).

free stream velocity. For this case, equation (96) reduces to

$$2.15 \frac{x}{s} \frac{1}{C_f} . \tag{117}$$

For the 50 WPPM case, the reduced dimensionless distance for the 50 WPPM point would now be placed at 5.87 rather than near 30 where it presently is. In fact, all the points for the present test would shift to the left indicating a large initial length as the data indicate.

Figure 91 presents the corrected experimental data plotted against the modified dimensionless distance give by equation (117). The extended initial zone compared to the flat plate experiment is apparent in this figure. The analytical model was exercised for the condition of the test shown in Figure 86 with a transfer from the initial to intermediate zone occurring at 30. The dimensionless distance given by equation (117) was used to determine the change to the intermediate diffusion zone. The calculated values are displayed in Figure 86. As may be seen, the calculated intermediate zone diffusion process is much greater than the experimental data indicate warranting further study of this zone.

The extended initial zone for the ejection method applied is significant in that no special care is needed in the ejection process. Additionally, this ejection process most likely represents the optimal case since higher ejection velocities would quickly be reduced to the mean viscous sublayer velocity through viscous drag and, for a slot ejection case, could result in flow disruption.

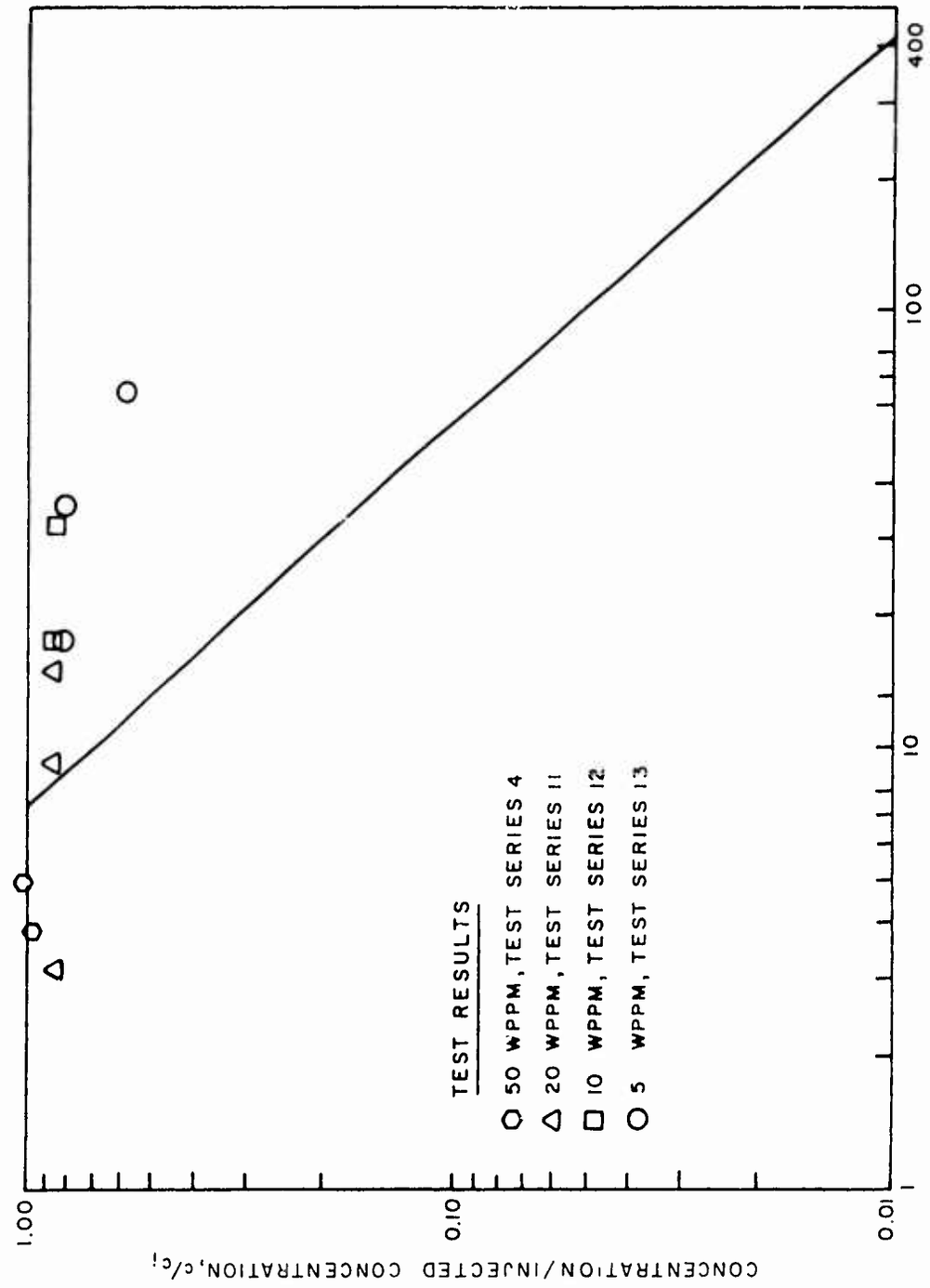

Figure 91. Dimensionless concentration vs reduced dimensionless distance - test results (from Fruman and Tulin (1974))

VII. CONCLUSIONS AND RECOMMENDATIONS

A. CONCLUSION

1. General

The object of this research was threefold: 1) to develop methods for wall concentration and drag reduction prediction for bodies of revolution with a polymer ejection process, 2) to qualitatively define the effects of polymer on boundary layers in external flows, and 3) to verify the predictive techniques by experiment. Drop tank testing was performed with several especially designed bodies of revolution. One of these bodies was capable of simultaneous ejection and boundary layer sampling at several heights in the boundary and at several axial stations. The ejection process for this model was considered optimal in that ejection occurred directly forward of the body in a laminar flow region thus affecting the developing flow region of turbulent flow. The experimental apparatus is capable of testing a wide variety of ejectors at different locations and over a range of Reynold's number to about 5×10^6. Variable ejection rates and polymer concentrations may be applied as well as boundary layer sampling at selected heights and at the wall. The drop tank facility provided a very low turbulence level apparatus in which the external flow experiment could be carried out.

2. Analytical Prediction Methods

Much of the past work in the diffusion of polymer boundary layers

has centered in the far downstream zone where the polymer attained the same diffusion characteristics as the medium. Postulates of an intermediate zone have been made but not reasonably tested for polymer cases. The case of developing flow with polymer ejection has received little attention for external flows and especially so for bodies of revolution. Predictive methods are, therefore, not well developed.

Several analytical models were developed for comparison with experimental data. The models were based upon a proven integral boundary layer analysis for thick axisymmetric boundary layers combined with a velocity profile relation accounting for pressure gradients. The models made use of a Lagrangian similarity hypothesis which predicts a diffusion boundary layer growth within the boundary layer. Two versions of the model are proposed but only one extensively used in the comparison. The first version, combined model, presently recommended as capable of accurate prediction of skin friction, polymer wall concentration and indicating total drag if provided with an experimental pressure profile, incorporates an initial diffusion zone where molecular diffusion is predomanate. Based upon a nondimensional distance, given by

$$\left(\frac{U}{v_i}\right)^{1.5} \frac{X}{S} \frac{1}{C_i} = 8 \qquad (96)$$

a change to an intermediate zone diffusion process is made. Within this region, determined by experimental data for ammonia diffusion in air to extend to $X/\delta < 60$, a similarity concentration profile exists having the form

$$\frac{C}{C_W} = e^{-0.693\ (y/\delta_d)\ K_3}$$

where the exponent is adjusted to a given value dependent on the region of diffusion. Proceeding to $X/\delta > 60$ places the diffusion process in the final zone where the second value of K_3 is applied. The Lagrangian analysis provides for the determination of, δ_d, the diffusion boundary layer. The equation for the diffusion boundary layer development incorporates the Karman constant, K, which is adjusted for the polymer flow case resulting in suppressed diffusion.

The analytical model has been compared to experimental data and found to predict proper levels of wall and concentration profiles but predicts an early increase in the diffusion process. It is hypothesized that the ejection velocity for the forward ejector, ejecting into the laminar region, is not the valid velocity for application into the non-dimensional distance relation (v_1). A mean laminar velocity is believed to be the correct velocity for this ejection process. When applied, the predictive techniques properly reproduces the experimental data. Unfortunately, only limited data are available displaying the initiation of the intermediate diffusion zone.

The second postulated model, the variable K_3 model, eliminates the need for the molecular diffusion portion of the previous model and adjusts, K_3, as a function of δ, δ_d, x/L, and c_w to account for this region. Unfortunately, insufficient data were available to perfect this model. A simplified functional relationship of K_3 was found to predict the limited experimental data

$$K_3 = C\ K_5\ \frac{\delta d}{\delta}\ \frac{x}{L}\ .$$

The combined model is considered valid for use in prediction of various flow parameters for axisymmetric bodies of revolution. The model should be exercised in several ways depending on the ejection process. If ejection occurs prior to or at the point of transition to turbulent flows, the full model should be applied. If the ejector is placed in a region of a developed turbulent boundary layer, the initial zone should be eliminated and the Karman constant reduction removed.

3. Boundary Layer Characterization and Separation Tests

Several test bodies were applied in this series of experiments covering a Reynolds number range of one to five million. One series of tests were conducted in a polymer ocean, where the drop tank was uniformly mixed to a polymer concentration level of 1.25, 2.5, 5, 10, 20, 50, and 60 WPPM using Polyox-WSR-301 polymer. In this series, models having 6^{o} tail cone, 12^{o} tail cone, and a spherical tail were tested. The photographic study displayed several interesting results. The turbulent nature of the boundary layer was apparent from the dye aspirated from these bodies at the minimum pressure point. At very low concentration levels, 2.5 WPPM, the fine structure turbulence was absent and only the large scale turbulence remained. At higher concentration, extreme boundary layer thinning occurred. Measurements of the boundary layer thickness were made from photographs and compared to computer predictions. The computer routines predicted the proper boundary layer growth shape for these tests but tended to overpredict the thickness. This was probably due to the mean height of the eddies being used for measurement purposes.

No shift in the boundary layer separation region was noted by application of the polymer. This was undoubtedly due to the large adverse pressure gradient conditions for these tail configurations. Computer predictions also indicated no shift in separation point for the test conditions.

The testing in fresh water with the polymer ejection body showed similar results but provided much better visual representations at the higher polymer concentrations. The characteristic coarse and fine scale turbulence was noted on dyed water ejection. Ejection of 50 WPPM dyed polymer solution eliminated most of the fine structure turbulence leaving only the coarse structure and somewhat the rapid boundary layer growth in the tail region. Application of 500 WPPM and 1000 WPPM of ejected polymer resulted in extremely thin boundary layers, even in the tail region with little evidence of turbulent action. In the tail region, bursting of the eddy structure is evident but with very low energy levels as evidenced by their vectors being in a near axial direction.

At the higher concentration levels, dye streaking is apparent. The streaking spacing is consistent with laminar sub layer streaks but also, for this case, agrees well with the number of ejection holes in the screen ejector in the nose of the body. In any event, turbulent mixing is not apparent at the 500 WPPM and 1000 WPPM concentrations. Boundary layer measurements were made for each case tested. A normalization of the thickness measurements shows an increased rate of growth for all concentrations tested, in the tail region. This suggests higher diffusion rates lowering the wall concentrations and reducing the subdued growth in this region.

4. Drag Reduction Tests

Drag reduction tests were performed with the 6^{o}, 12^{o}, and spherical tail bodies in a polymer ocean. The concentration levels were as discussed previously. A total drag reduction of 33% was achieved with the 6^{o} tail body at polymer concentrations of 20 WPPM and greater. This compared favorably, within 10% of calculated values. Percent skin friction reduction of near 70% were achieved, comparing well with optimal total shear drag reduction for flat plates as determined by other investigators. The maximum total drag reduction achieved with the 12^{o} tail and spherical tail bodies was less due to the reduced surface area and, therefore, increased percentage of form drag. Maximum total drag reductions of 16% and 10% were achieved respectively for the 12^{o} tail and spherical tail configuration. The skin friction reduction remained near 70% as it should. Computer predictions for total drag with the 12^{o} and spherical tail models was considerably in error due to the very large pressure coefficients predicted near the separation region for these cases from potential flow.

5. Polymer Diffusion Tests

The polymer ejecting body was applied for all tests with a fixed ejection rate of 20.6 in^{3}/sec and nominal velocity of 27 ft/sec. Wall samples and boundary layer samples at .025 inches and .055 inches were taken and analyzed applying a fluorometric technique. Testing with water ejection and 5 WPPM, 10 WPPM, 20 WPPM, 50 WPPM, 500 WPPM, and 1000 WPPM were performed. The water tests compared well with available predictive methods displaying appropriate concentration profiles as

achieved by other investigators. The tests with all polymer concentrations displayed an unexpected drastically reduced diffusion resulting in a considerably extended initial mixing zone. Application of a molecular diffusion model in this region agrees well with data. Boundary layer concentration profile data when plotted nondimensionally as y/δ_d vs c/c_w result in similarity profile exponent coefficients, K_3, of .75. It is believed, however, the value is below this since data were not obtained in the critical region of approximately .01 inches from the wall in these tests. These results are significant in that they imply significantly reduced polymer quantities may be required with proper ejection techniques. Apparently ejection into the laminar, and in this case stagnation region, of developing flow substantially reduces the turbulence levels associated with turbulent flow and reduces, therefore, diffusion. It is believed that ejection in a developed flow would result in an extremely short initial zone and rapid mixing.

6. Conclusion Summary

An experimental apparatus has been developed which allows laboratory measurement of polymer drag reduction wall concentration profiles and ejector geometries at various ejection rates on axisymmetric bodies. Experiments have displayed reduced fine scale turbulence structure with polymer and a significantly reduced diffusion process if ejection is performed upstream of the turbulent transition point. Maximum skin friction reductions were achieved. Predictive methods were developed, building on available theories, for prediction of the wall concentration on an axisymmetric body. Comparison with experiment has been performed.

B. RECOMMENDATIONS

1. The variable K_3 analytical model should be developed to more adequately describe the diffusion process. As presently configured, the model abruptly changes from molecular diffusion to a diffusion process which is believed to be too high a rate for polymer. Application of the Lagrangian approach with modified Karman constant should provide an input to the functional relationship.

2. Additional data should be obtained at boundary layer heights below the .025-inch level with this experimental model. These data are required to adequately define the concentration curves and provide the data necessary for developing the K_3 model. The variation in the similarity profile exponent, K_3, with axial length should also be defined by these data and would provide information on the intermediate and final zone similarity profile exponents.

3. Additional testing should be performed at lower concentration levels, below 50 WPPM, with the ejecting experimental model. This would clearly establish the extent of the initial mixing zone and verify the relation used for the extent of the initial zone and the hypothesis for the ejection velocity equaling a mean laminar velocity for the type of ejection process used here.

4. The experimental model should be modified for ejection into the established turbulent boundary layer region to clearly demonstrate the elimination (or drastic reduction) of the initial zone length with the

resulting high diffusion process. Significantly higher concentrations of polymers are believed to be required (higher flow rates and/or higher concentrations) for this case. Model modifications are extremely simple.

5. Drag reduction measurements should be made with this model during the ejection process. Correlations with wall concentration measurements and polymer ocean data would lend further credence to the results.

REFERENCES

Batchelor, G. K., "Diffusion in Free Turbulent Shear Flows," Cavendish Laboratory, Cambridge, 1957.

Brady, John F., "An Experimental Study of the Vibration, Noise, and Drag of a Cylinder Rotating in Water and Certain Polymer Solutions," A Dissertation for the Degree of Doctor of Philosophy, University of Rhode Island, 1973.

Cermak, J. E., "Lagrangian Similarity Hypothesis Applied to Diffusion in Turbulent Shear Flow," College of Engineering, Colorado State University, 1962.

Clauser, F. H., J. Aeronaut., vol. 21, pp. 91-180, 1954.

_____, Adv. Appl. Mech., vol. 4, pp. 1-51, 1956.

Coles, D., "The Problem of the Turbulent Boundary Layer," Journal of Applied Mathematics and Physics, Zamp, vol. V, 1954.

Coles, D., "The Law of the Wake in the Turbulent Boundary Layer," Journal of Fluid Mechanics, vol. 1 part 2, July, 1956. p. 191.

Crawford, H. R., and G. T. Pruitt , "Rheology and Drag Reduction of Some Dilute Polymer Solutions," Final Report, Contract No. N60530-6899 (NOTS), Westco Research, Dallas, Texas, July 1962.

Darby, Ronald, "A Review and Evaluation of Drag Reduction Theories," Naval Research Laboratory, Washington, D. C., June 1972.

Dowdell, Rodger, "Estimation of Downstream Ingestion Concentration Resulting from the Ejection of a Polymer Solution at the Nose of a Large Submerged Body," Naval Underwater Systems Center TM No. SB323-4364-73, 28 June 197[illegible]

Elata, C., "Reduction of Friction on Submerged Bodies by Polymer Additives," Proceedings of the 11th International Towing Tank Conference, Tokyo, 1966, p. 81.

Ellison, Y. H., "Turbulent Diffusion," Meteorology, Department of the Mechanics of Fluids, University of Manchester, 1959.

Fabula, A. G., and T. J. Burns, "Dilution in a Turbulent Boundary Layer with Polymeric Friction Reduction," Ocean Technology Department, Naval Undersea Research and Development Center, NUC TP 171, April 1970.

Fabula, A. G., J. L. Lumley and W. D. Taylor, "Some Interpretations of the Toms Effect," Annual Review of Fluid Mechanics, W. R. Sears (ed.), 1, 145 (1969)

Fruman, D. H., and M. P. Tulin, "Diffusion of a Tangential Drag-Reducing Polymer Injection on a Flat Plate at High Reynolds Numbers," Ordnance Hydroballistic Advisory Committee Meeting, October 1974.

Hoyt, J. W., "Friction Reduction as an Estimator of Molecular Weight," Polymer Letters, vol. 4, 1966, p. 713.

Hoyt, J. W., "The Effects of Additives on Fluid Friction," Naval Undersea Research and Development Center, Pasadena Laboratory, Pasadena, Calif., Freeman Scholar Lecture, 1972.

Hoyt, J. W., and A. G. Fabula, "The Effect of Additives on Fluid Friction," U.S. Naval Ordnance Test Station, Pasadena, California, 1964.

Hsu, Kuang Shen, "Diffusion of Polymers in a Developing Boundary Layer," Thesis for the Degree of Master of Science, Department of Mechanics and Hydraulics, Graduate College of the University of Iowa, January 1971.

Karman, T. Von, Nachr. Ges. Wiss. Goett. Math.-Phys. Kl., pp. 58-76, 1930.

Kline, S. J. et al, "Proceedings of 1968 Stanford Turbulent Boundary Layer Conference," 2 volumes, 1968.

Kline, S. J., P. W. Runstadler, and W. C. Reynolds, "An Experimental Investigation of the Flow Structure of the Turbulent Boundary Layer," Stanford University Department of ME Report No. MD-8, Stanford, California, 1963.

Kowalski, T., and E. Brundrett, Paper C1, "International Conference on Drag Reduction, 4-6 September 1974.

Lang, T. G., and H. V. L. Patrick, "Drag of Blunt Bodies in Polymer Solutions," Hydrodynamics Group, Research Department, U.S. Naval Ordnance Test Station, Pasadena, California, 1966.

Latto, B., and Chi Hung Shen, "Effect of Dilute Polymer Solution Injection on External Boundary Layer Phenomena," Department of Mechanical Engineering, McMaster University, Hamilton, Ontario, Canadian Journal of Chemical Engineering, vol. 48, February 1970.

Lessman, R. C., "Dilution of a Polymer Additive in a Turbulent Boundary Layer on a Body of Revolution," Naval Underwater Systems Center, Report CR 52, 15 July 1970.

Levinson, Ernie D., "A Guide to Use and Operation of G. K. Turner Model 111 Fluorometer," Naval Underwater Systems Center Technical Memorandum SB323-4406-72, 22 September 1972.

Mellor, George, L., "The Effects of Pressure Gradients on Turbulent Flow Near a Smooth Wall," Journal of Fluid Mechanics, vol 24, part 2, 1966, pp. 255-274.

Meyer, Warren A., "A Correlation of the Frictional Characteristics for Turbulent Flow of Dilute Viscoelastic Non-Newtonian Fluids in Pipes," A.I.Ch.E. Journal, May 1966

Morkovin, M. V., "On Eddy Diffusivity, Quasi-Similarity and Diffusion Experiment in Turbulent Boundary Layers," M. J. Heat Mass Transfer, vol. 8, 1963.

Mysel, K. J. "Flow of Thickened Fluids," U.S. Patent 2, 492, 173, 27 December 1949.

Nadolink, R. H., "Determination of Turbulent Velocity Distributions with Non-Newtonian Additives Using High-Speed Photomicrosoopy," Master Thesis, University of Massachusetts, 1968.

Nadolink, R. H., W. A. McNally and H. F. Dannemann, "Drag Reduction Characteristics of Streamlined Models with Polyox-WSR-301," ITN No. 3-68, Naval Underwater Weapons Research and Engineering Station, 16 January 1968.

Nikuradse, J., Ing.-Arch., vol 1, 1930 pp 306-332.

Oldroyd, J. G., Proceedings of the First International Congress on Rheology, North Holland Publishing Co., Amsterdam, 1949, p. 130.

Pasquill, F., "Lagrangian Similarity and Vertical Diffusion from a Source at Ground Level," Quarterly Journal of the Royal Meteorological Society, vol. 92, no. 392, April 1966.

Poreh, M., and J. E. Cermak, "Study of Diffusion for a Line Source Turbulent Boundary Layer," Int. J. Heat Mass Transfer, vol. 7, 1964.

Poreh, Michael, and K. S. Hsu, "Diffusion of Drag Reducing Polymers in a Turbulent Boundary Layer," HHR Report No. 125, Iowa Institute of Hydraulic Research, University of Iowa, Iowa City, Iowa, April 1971.

Prandtl, L., Z. Ver. Dtsch. Ing., vol. 77, pp. 105-114 (translated as NACA Technical Memorandum 720), 1933.

Reo, G. N. V., "The Law of the Wall in a Thick Axisymmetric Turbulent Boundary Layer," Journal of Applied Mechanics, March 1967.

Richmond, R. L., Ph.D. Thesis, California Institute of Technology, Pasadena, 1957.

Schlichting, H., Boundary Layer Theory, McGraw-Hill Book Co., New York, sixth edition, 1968.

Shapiro, A. H., Compressible Fluid Flow, The Ronald Press Co., 1953.

Stow, F. S. Jr., and J. H. Elliot, "Drag on a Tethered Ball in Solutions of Drag Reducing Polymers," Hercules Research Center, Polymer Letters, vol. 8, 1970. pp. 611-615.

Test, Frederick L., "Analytical Prediction of the Influence of Polymer Additives on the Shear Drag of Bodies of Revolution," Journal of Hydronautics, vol. 8, 1974, p. 45.

Toms, B. A., "Some Observations on the Flow of Linear Polymer Solutions Through Straight Tubes at Large Reynolds Numbers," Proceedings 1st International Congress on Rheology, 1948, vol. II, North Holland Publishing Co., Amsterdam, 1949, p. 135.

Tullis, J. P., and K. L. V. Ramu, "Viscous Drag Reduction in Developing Pipe Flow," Colorado State University, November 1973.

Virk, P. S., E. W. Merrill, H. S. Mickley, and K. A. Smith, "The Critical Wall Shear Stress for Reduction of Turbulent Drag in Pipe Flows by Poly (Ethylene Oxide) in Dilute Solution," Modern Developments in the Mechanics of Continua, Academic Press Inc., N. Y., 1966.

Virk, P.S., H.S. Mickley and K.A. Smith, "The Ultimate Asymptote and Mean Flow Structure in Toms' Phenomenon," ASME Publication, 1971.

Walters, R.R. and C.S. Wells, Jr., Effects of Distributed Injection of Polymer Solutions on Turbulent Diffusion," Report No. B-94000/1 CR-7, Advanced Technology Center, March 1971.

Wells, C.S., "An Analysis of Uniform Injection of a Drag-Reducing Fluid into a Turbulent Boundary Layer, LTV Research Center, Report No. 0-71100/8R-14, November 1968.

Wetzel, Joseph M. and John P. Ripken, Shear and Diffusion in a Large Boundary Layer Injected with Polymer Solution, University of Minnesota St. Anthony Falls Hydraulic Laboratory, Project Report No. 114, February 1970.

White, A., "Some Observations on the Flow Characteristics of Certain Dilute Macromolecular Solutions," Hendon College of Technology, London.

White, W. D., and D. M. McEligot, "Transition of Mixtures of Polymers in a Dilute Aqueous Solution," Journal of Basic Engineering Trans., ASME, series D, vol. 92, no. 3, September 1970, p. 441.

Vogel, W. M. and A. M. Patterson, "An Experimental Investigation of the Effect of Additives Injected into the Boundary Layer of an Underwater Body," Pacific Naval Laboratory, Victoria, British Columbia, Canada.

White, Frank M., "An Analysis of Flat-Plate Drag with Polymer Additives," J. Hydronautics, vol. 2, no. 4, October 1968.

White, Frank M., "Limitations on the Drag Reduction of External Bodies by Polymer Additives," AIAA Paper No. 68-127, AIAA 6th Aerospace Sciences Meeting, 1968.

White, F. M. and G. H. Christoph, "A Simple Theory for the Two-Dimensional Compressible Turbulent Boundary Layer," Transactions of the ASME, September 1972.

White, F. M., R. C. Lessmand and G. H. Christoph, "Analysis of Turbulent Skin Friction in Thick Axisymmetric Boundary Layers," University of Rhode Island, Kingston, R. I., 1972.

White, F. M., Viscous Fluid Flow, McGraw-Hill Book Co., 1974.

Wu, Jin, and Marshall P. Tulin, Drag Reduction by Ejecting Additive Solutions Into a Pure-Water Boundary Layer," Hydronautics Incorporated, Technical Report 353-7, June 1970.

Yu, Y. S., J. Ship Res., vol. 3, pp. 33-40, 1958.

APPENDIX A

SKIN FRICTION RELATIONS

The conservation of mass and the momentum equation for axisymmetric flow are given by

$$\frac{\partial}{\partial x}(\rho u r) + \frac{\partial}{\partial y}(\rho v r) = 0 \tag{A1}$$

and

$$\rho u r \left(\frac{\partial u}{\partial x}\right) + \rho v r \left(\frac{\partial u}{\partial y}\right) = - r \left(\frac{dp_e}{dx}\right) + \frac{\partial}{\partial y}(r\tau). \tag{A2}$$

White's derivation is reproduced here to show the incorporation of the polymer concentration terms.

Defining a stream function which satisfies equation (A1) to eliminate v

$$\frac{\partial \Psi}{\partial y} = \rho u r \qquad\qquad \frac{\partial \Psi}{\partial x} = - \rho v r . \tag{A3}$$

Solving (A3) for Ψ yields

$$\Psi = \int_{y_o}^{y} \rho u r \, dy . \tag{A4}$$

Rewriting in law of the wall variables

$$\Psi = \int_{y_o^+}^{y^+} \rho r v_\tau^+ \, dy^+ \tag{A5}$$

or, in terms of Y^+

$$\frac{\Psi}{\mu r_o} = \int_{0.1108}^{Y_e^+} \left(\frac{r}{r_o}\right)^2 u^+ \, dY^+ . \qquad \text{(A6)}$$

Writing equation (A2) in wall variables and substituting in equation (A3) to eliminate v

$$\rho r v^* u^+ \frac{\partial}{\partial x}(v^* u^+) - \frac{\partial \Psi}{\partial x}\frac{v^*}{\nu}\frac{\partial}{\partial y^+}(v^* u^+) = - r \frac{dp_e}{dx} + \frac{v^*}{\nu}\frac{\partial}{\partial y^+}(r\tau). \qquad \text{(A7)}$$

The x derivatives must be handled by the chain rule, since each of the parameters (Y^+, α, r_o^+, c_w) in the law of the wall is a function of x. Thus, we substitute

$$\frac{\partial}{\partial x} = \frac{\partial Y^+}{\partial x}\frac{\partial}{\partial Y^+} + \frac{\partial \alpha}{\partial x}\frac{\partial}{\partial \alpha} + \frac{\partial r_o^+}{\partial x}\frac{\partial}{\partial r_o^+} + \frac{\partial C_w}{\partial x}\frac{\partial}{\partial C_w} . \qquad \text{(A8)}$$

It is assumed throughout that ρ_w and ν_w are constant in this analysis. Differentiating u

$$u = v^*(x)\, u^+ (Y^+, \alpha, r_o^+, c_w) \qquad \text{(A9)}$$

$$\frac{d(v^* u^+)}{dx} = \left(u^+ \frac{dv^*}{dx} + v^* \frac{\partial Y^+}{dx}\frac{\partial u^+}{\partial Y^+} + v^* \frac{d\alpha}{dx}\frac{\partial u^+}{\partial \alpha} + v^* \frac{dr_o^+}{dx}\frac{\partial u^+}{\partial r_o^+} + v^* \frac{dC_w}{dx}\frac{\partial u^+}{\partial C_w}\right) \qquad \text{(A10)}$$

$$\frac{\partial(\Psi)}{\partial x} = \frac{dY^+}{dx}\frac{\partial \Psi}{\partial Y^+} + \frac{d\alpha}{dx}\frac{\partial \Psi}{\partial \alpha} + \frac{dr_o^+}{dx}\frac{\partial \Psi}{\partial r_o^+} + \frac{dC_w}{dx}\frac{\partial \Psi}{\partial C_w} . \qquad \text{(A11)}$$

Substituting in (A7)

$$\rho r v^* u^+ \Big(u^+ \frac{dv^*}{dx} + \overbrace{v^* \frac{dY^+}{dx} \frac{\partial u^+}{\partial Y^+}}^{a} + v^* \frac{d\alpha}{dx} \frac{\partial u^+}{\partial \alpha} + v^* \frac{dr_o^+}{dx} \frac{\partial u^+}{\partial r_o^+}$$

$$+ v^* \frac{dC_w}{dx} \frac{\partial u^+}{\partial C_w}\Big) - \frac{r_o}{r} \frac{v^{*2}}{\nu_w} \frac{\partial u^+}{\partial Y^+} \Big(\overbrace{\frac{dY^+}{dx} \frac{\partial \Psi}{\partial Y^+}}^{b} + \frac{d\alpha}{dx} \frac{\partial \Psi}{\partial \alpha}$$

$$+ \frac{dr_o^+}{dx} \frac{\partial \Psi}{\partial r_o^+} + \frac{dC_w}{dx} \frac{\partial \Psi}{\partial C_w}\Big) = -r \frac{dp_e}{dx} + \frac{r_o}{r} \frac{v^*}{\nu_w} \frac{\partial (r\tau)}{\partial Y^+} . \qquad (A12)$$

Terms (a) and (b) cancel using equation (A6). Multiplying out, cross multiplying by r/r_o^2 and integrating with respect to Y^+ gives

$$\rho v^* \frac{dv^*}{dx} \int_0^{Y_e^+} \frac{r^2}{r_o^2} u^{+2} \, dY^+ + \rho v^{*2} \frac{d\alpha}{dx} \int_0^{Y_e^+} \frac{r^2}{r_o^2} u^+ \frac{\partial u^+}{\partial \alpha} \, dY^+$$

$$+ \rho v^{*2} \frac{dr_o^+}{dx} \int_0^{Y_e^+} \frac{r^2}{r_o^2} u^+ \frac{\partial u^+}{\partial r_o^+} \, dY^+ + \rho v^{*2} \frac{dc_w}{dx} \int_0^{Y_e^+} \frac{r^2}{r_o^2} u^+ \frac{\partial u^+}{\partial c_w} \, dY^+$$

$$- \frac{v^{*2}}{r_o \nu_w} \frac{d\alpha}{dx} \int_0^{Y_e^+} \frac{\partial \Psi}{\partial \alpha} \frac{\partial u^+}{\partial Y^+} \, dY^+ - \frac{v^{*2}}{r_o \nu_w} \frac{dr_o^+}{dx} \int_0^{Y_e^+} \frac{\partial \Psi}{\partial r_o^+} \frac{\partial u^+}{\partial Y^+} \, dY^+$$

$$- \frac{v^{*2}}{r_o \nu_w} \frac{dc_w}{dx} \int_0^{Y_e^+} \frac{\partial \Psi}{\partial c_w} \frac{\partial u^+}{\partial Y^+} \, dY^+ = - \frac{dp_e}{dx} \int_0^{Y_e^+} \frac{r^2}{r_o^2} \, dY^+ \frac{v^*}{\nu_w} \int_{\tau_w}^{0} d(r\tau). \qquad (A13)$$

Where the integral of the last term is $- \frac{v^*}{\nu_w} r_o \tau_w$ and the term

$$\frac{dp_e}{dx} \int_0^{Y_e^+} \left(\frac{r}{r_o}\right)^2 dY^+ = - \rho_w U_e \frac{dU_e}{dx} \int_0^{Y_e^+} \left(\frac{r}{r_o}\right)^2 dY^+ \qquad (A14)$$

may be simplified by substituting in e^{2Y^+/r_o^+} for $(\frac{r}{r_o})^2$ and integrated resulting in

$$- \rho_w U_e \frac{dU_e}{dx} \frac{r_o^+}{2} (e^{2Y_e^+/r_o^+} - 1). \qquad (A15)$$

Rearranging (A13) yields

$$\rho v^* \frac{dv^*}{dx} \int_0^{Y_e^+} e^{2Y^+/r_o^+} u^{+2} dY^+ + \rho v^* \frac{d\alpha}{dx} \int_0^{Y_e^+} \{e^{2Y^+/r_o^+} u^+ \frac{\partial u^+}{\partial \alpha}$$

$$- \frac{1}{\rho \nu r_o} \frac{\partial \Psi}{\partial \alpha} \frac{\partial u^+}{\partial Y^+} \} dY^+ + \rho v^{*2} \frac{dr_o^+}{dx} \int_0^{Y_e^+} \{e^{2Y^+/r_o^+} u^+ \frac{\partial u^+}{\partial r_o^+}$$

$$- \frac{1}{\rho \nu r_o} \frac{\partial \Psi}{\partial \alpha} \frac{\partial u^+}{\partial Y^+} \} dY^+ + \rho v^{*2} \frac{dc_w}{dx} \int_0^{Y_e^+} \{e^{2Y^+/r_o^+} u^+ \frac{\partial u^+}{\partial c_w}$$

$$- \frac{1}{\rho \nu r_o} \frac{\partial \Psi}{\partial c_w} \frac{\partial u^+}{\partial Y^+} \} dY^+ = \rho U_e \frac{dU_e}{dx} \frac{r_o^+}{2} (e^{2Y_e^+/r_o^+} - 1) - \frac{v^*}{\nu} \tau_w. \qquad (A16)$$

Dividing by ρ and remembering that $\rho\nu = \mu$ yields

$$v^* \frac{dv^*}{dx} G_1 + v^{*2} \frac{d\alpha}{dx} H + v^{*2} \frac{dr_o^+}{dx} I + v^{*2} \frac{dc_w}{dx} J$$

$$= U_e \frac{dU_e}{dx} \frac{r_o^+}{2} (e^{2Y_e^+/r_o^+} - 1) - \frac{v^*}{\nu} \tau_w. \qquad (A17)$$

Where

$$C_1 = \int_0^{Y_e^+} e^{2Y^+/r_o^+} u^{+2}\, dY^+ \tag{A18}$$

$$H = \int_0^{Y_e^+} \{e^{2Y^+/r_o^+} u^+ \frac{\partial u^+}{\partial \alpha} - \frac{1}{\mu r_o} \frac{\partial \Psi}{\partial \alpha} \frac{\partial u^+}{\partial Y^+} \}\, dY^+ \tag{A19}$$

$$I = \int_0^{Y_e^+} \{e^{2Y^+/r_o^+} u^+ \frac{\partial u^+}{\partial r_o^+} - \frac{1}{\mu r_o} \frac{\partial \Psi}{\partial r_o^+} \frac{\partial u^+}{\partial Y^+}\}\, dY^+ \tag{A20}$$

$$J = \int_0^{Y_e^+} \{e^{2Y^+/r_o^+} u^+ \frac{\partial u^+}{\partial c_w} - \frac{1}{\mu r_o} \frac{\partial \Psi}{\partial c_w} \frac{\partial u^+}{\partial Y^+}\}\, dY^+. \tag{A21}$$

Defining dimensionless parameters

$$X^* = \frac{X}{L}$$

$$V = \frac{U_e}{U_o}$$

$$\lambda = \frac{U_e}{v^*} = \left(\frac{2}{c_f}\right)^{\frac{1}{2}} = \frac{VU_o}{v^*}.$$

Rewriting terms of equation (A17) with these nondimensional parameters

$$v^* = \frac{VU_o}{\lambda} = \frac{U_e}{\lambda}$$

$$\frac{1}{L}\frac{dv^*}{dx^*} = \frac{d(U_e/\lambda)}{dx^*} = \frac{1}{L}\left(\frac{U_o}{\lambda}\frac{dV}{dx^*} - \frac{U_o V}{\lambda^2}\frac{d}{dx^*}\right)$$

$$\alpha = \left(\frac{\nu_w}{\tau_w v^*}\right) \frac{dp_e}{dx} = -\frac{\nu_w}{v^{*3}} U_e \frac{dU_e}{dx}$$

$$\alpha = -\frac{\nu_w}{v^{*2}} \lambda \frac{dU_e}{dx} = \frac{\nu_w}{U_e^2} \lambda^3 \frac{dU_e}{dx} = -\frac{\nu_w}{U_o V^2} \lambda^3 \frac{dV}{dx} = -\frac{\nu_w}{U_o L} \frac{\lambda^3}{v^2} \frac{dV}{dx}$$

now $R_O = \frac{U_o L}{\nu}$.

Therefore,

$$\alpha = -\frac{\lambda^3}{R_L V^2} \frac{dV}{dx^*}$$

but $-\frac{1}{V^2} \frac{dV}{dx^*} = \left(\frac{1}{V}\right)'$

where ' denotes first derivative with respect to x*, resulting in

$$\alpha = \frac{\lambda^3}{R_L} \left(\frac{1}{V}\right)'.$$

Finally

$$\frac{1}{L} \frac{d\alpha}{dx^*} = \frac{1}{L} \left[\frac{3\lambda^2}{R_L} \left(\frac{1}{V}\right)' \frac{d\lambda}{dx^*} + \frac{\lambda^3}{R_L} \left(\frac{1}{V}\right)''\right].$$

Substituting in (A-17)

$$\frac{U_o V}{L\lambda} \left(\frac{U_o}{\lambda} V'\right. - \frac{U_o V}{\lambda^2} \frac{d}{dx^*}) G_1 + \frac{V^2 U_o^2}{L\lambda^2} \frac{3\lambda^2}{R_L} \left(\frac{1}{V}\right)' \frac{d\lambda}{dx^*}.$$

Multiply through by λ and rearranging setting $\alpha = \frac{\lambda^3}{R_L} \left(\frac{1}{V}\right)'$

$$\frac{d\lambda}{dx^*}\,(3\alpha H - G_1) + \frac{V'}{V}\,\lambda\,G_1 - \frac{\lambda^2 r_o^+}{2}\,(e^{2Y_e^+/r_o^+} - 1) \tag{A22}$$

$$+ \frac{\lambda^4}{R_L}\left(\frac{1}{V}\right)''\,H = 1\,R_L V - \lambda\,\frac{dr_o^+}{dx^*}\,I - \lambda\,\frac{dc_w}{dx^*}\,J \tag{A22}$$

where G, H, I, J are given by

$$G_1 = \int_0^{Y_e^+} e^{2Y^+/r_o^+}\,u^+\,dY^+ \tag{A23}$$

$$H = \int_0^{Y_e^+} \{e^{2Y^+/r_o^+}\,u^+\,\frac{\partial u^+}{\partial \alpha} - \frac{1}{\mu r_o}\,\frac{\partial \Psi}{\partial \alpha}\,\frac{\partial u^+}{\partial Y^+}\}\,dY^+ \tag{A24}$$

$$\frac{\partial u^+}{\partial \alpha} = \int_0^{Y_e^+} \frac{r_o^+\,(e^{2Y^+/r_o^+} - 1)}{4KY^+\left[1 + \frac{\alpha}{2}\,r_o^+\,(e^{2Y^+/r_o^+} - 1)\right]^{1/2}}\,dY^+ \tag{A25}$$

$$\frac{1}{\mu r_o}\,\frac{\partial \Psi}{\partial \alpha} = \int_0^{Y_e^+} e^{2Y^+/r_o^+}\,\frac{\partial u^+}{\partial \alpha}\,dY^+ \tag{A26}$$

and

$$\frac{\partial u^+}{\partial Y^+} = \frac{1}{KY^+}\left[1 + \frac{\alpha}{2}\,r_o^+\,(e^{2Y^+/r_o^+} - 1)\right]^{1/2} \tag{A27}$$

$$I = \int_0^{Y_e^+} e^{2Y^+/r_o^+}\,u^+\,\frac{\partial u^+}{\partial r_o^+} - \frac{1}{\mu r_o}\,\frac{\partial \Psi}{\partial r_o}\,\frac{\partial u^+}{\partial Y^+}\,dY^+ \tag{A28}$$

where

$$\frac{\partial u^+}{\partial r_o^+} = \int_0^{Y_e^+} -\frac{1}{2KY^+} \frac{\left[-\frac{\alpha}{2} + \frac{\alpha}{2} e^{2Y^+/r_o^+} - \frac{\alpha Y^+}{r_o^+} e^{2Y^+/r_o^+}\right]}{\left[1 - \frac{\alpha}{2} r_o^+ (1 - e^{2Y^+/r_o^+})\right]^{1/2}} dY^+$$

$$= \int_0^{Y_e^+} \frac{\alpha}{4KY^+} \frac{\left[(1 - e^{2Y^+/r_o^+}) + \frac{Y^+}{2r_o^+} e^{2Y^+/r_o^+}\right]}{\left[1 + \frac{\alpha}{2} r_o^+ (e^{2Y^+/r_o^+} - 1)\right]^{1/2}} dY^+ \qquad \text{(A29)}$$

and

$$\frac{1}{\mu r_o} \frac{\partial \Psi}{\partial r_o^+} = \frac{\partial}{\partial r_o^+} \int_0^{Y^+} e^{2Y^+/r_o^+} u^+ dY^+$$

$$= \int_0^{Y^+} \left\{-\frac{2Y^+}{r_o^{+2}} e^{2Y^+/r_o^+} u^+ + e^{2Y^+/r_o^+} \frac{\partial u^+}{\partial r_o^+}\right\} dY^+ \qquad \text{(A30)}$$

$$J = \int_0^{Y_e^+} \left\{e^{2Y^+/r_o^+} u^+ \frac{\partial u^+}{\partial c_w} - \frac{1}{\mu r_o} \frac{\partial \Psi}{\partial c_w} \frac{\partial u^+}{\partial Y^+}\right\} dY^+ \qquad \text{(A31)}$$

where

$$\frac{\partial u^+}{\partial c_w} = \frac{2.3}{2(c_w)^{1/2}} \ln \frac{v^*}{v_o^+} = \frac{1.15}{c_w} \ln \frac{v^*}{v_o^+} \qquad \text{(A32)}$$

and

$$\frac{1}{\mu r_o} \frac{\partial \Psi}{\partial c_w} = \int_0^{Y^+} e^{2Y^+/r_o^+} \frac{\partial u^+}{\partial c_w} dY^+. \qquad \text{(A33)}$$

APPENDIX B

COMPUTER PROGRAM SAMPLES

BOUNDARY

JOB ACCOUNTING INFORMATION

NAME=BOUNDARY ACCT=G4511489

DATE=05/21/75 EDITION=4M TIME-ON=10/11/05 TIME-OFF=10/46/18
MAPS ED=01

TIME USED
COMP=00/08/31.667
CHAN=00/00/17.344

FACILITIES NOT USED
CORE=002
SCR =002
LINE=527
CARD=0

POLYMER CONCENTRATION 5 WPPM

$$\left(\frac{U_o}{.6U_o}\right)^{1.5} \frac{x}{s} \frac{1}{C_i} = 30$$

DIFFUSION + $\bar{C}_t$ MODEL

COMBINED MODEL

ANSI FORTRAN(2.3)/MASTER   INTEGER WORD SIZE = 2 , * OPTION IS OFF , O OPTION IS   OFF   05/21/75   PAGE 001

```
      PROGRAM C3LRML
      COMMON ROPLUS(200),RO(200),XLAMDA(200),DROPDXS(200),VX(200),
     1VXD1(200),VINVP(200),VINVPP(200),XLSTAR(200),ALPHA,AK,RHO,XNU,W,
     2N,RL,XLAMDAC,X1,G1,H,XJ,IER,I,CF(200),VSTARE,ROPLUSE,UEX(200),YPLU
     3S,UPLUS,YPLUSC,STEP,VOSTAR,VSTARIN,UI,DELTAD,JDELTA,XCHECK,CDCW,CW
     4,OI,CI,U1PLUS,DELR,DCWDXS(200),YE,JPOLY,GAMMA,DISPLAC,THOMENT,CAPT
     5,AXL(200),YPMAX,M1,DELY,CW0,AK2,AK5,AK3,ICHECK,YPLUSV,C8AR,C2PAR,
     6DV,YPLUS35
      DIMENSION XL(200)        ,VINV(200),VXD2(200),RX(200),VSTAR(200),
     1Y(11),DERY(10),AUX(8,10),PRMT(5),XLSTARC(3),ROPLUSC(3),DROPDXC(3),
     2CWSC(3),DCWDXSC(3),         SAREA(200),CWS(200),CP(200),SDRAG(2
     300),PDRAG(200),DELPLUS(200)
      EXTERNAL RMLAYER,MOUTPUT
      PRINT 34
34    FORMAT(*  AXIAL-X   SURF-X   S-AREA   XLSTAR      RO      VX   PDR
     1AG   LAMDA      CP     SDRAG       DELY          RO,        DEL,
     2  ALPHA    T*)
7     FORMAT(/,2F12.6,F12.9,2F12.6,2F12.1,F12.6,2F11.6,I5,3I4)
9     FORMAT(F12.2,3F12.8,2F6.2,3F12.6,3F11.6)
100   FORMAT(*          AXLDL          LAMDA         ALPHA          AK2       VSTA
     1RE      ROPLUSE        YPLUS        DELTAD      DISPLAC       THOMENT  THETF
     2IER    M    I*,/,*       XCHECK            CF           AXL               VX
     3 AK3    AK5         CWDCT          SDRAG          PDRAG    DELY(I+1)        DE
     4LR*)
333   FORMAT(4F9.5 ,5F8.3,2F10.4,2F12.1,F11.5,I4)
20    FORMAT(F12.9,12X,F12.9,12X)
      RHO=1.9386
      AK=0.4
      XNU=1.253E-5
      VOSTAR=0.08
      CI=5.0
      OI=20.19/1728.0
      TOSAREA=0.0
      CW=30.0
      XCHECK=0.0
      U0=27.33
      CONST=-3.14159/2.0*RHO*U0**2
      CONSTS=RHO*3.14159
      NREAD=3
      NDATA=100
      ISTART=35
      ISTART2=100
      READ(2,20)(AXL(I),I=1,NDATA)
      READ(2,20)(RO(I),I=1,NDATA)
      READ(2,20)(VINV(I),I=1,NDATA)
      READ(2,20)(CP(I),I=1,NDATA)
C
      DO 1 I=1,NDATA
      AXL(I)=AXL(I)/12.0
      RO(I)=RO(I)/12.0
      IF(I.GT.1) GO TO 21
      AXL0=0.0
      R00=0.0
      XL0=0.0
21    XL(I)=SQRT((AXL(I)-AXL0)**2 + (RO(I)-R00)**2) + XL0
      XL0=XL(I)
```

```
LN 0057          AXL0=AXL(I)
LN 0058          R00=R0(I)
LN 0059          SAREA(I)=(XL(I)-XL(I-1))*(R0(I)+R0(I-1))*3.14159
LN 0060          VX(I)=    VINV(I)
LN 0061          UEX(I)=VX(I)*U0
LN 0062          RX(I)=UEX(I)*XL(I)/XNU
LN 0063          IF(I.LE.(ISTART-1)) GO TO 22
LN 0064          CF(I)=0.451/(ALOG(0.056*RX(I)))**2
LN 0065          GO TO 23
LN 0066    22    CF(I)=0.664/SQRT(RX(I))
LN 0067    23    SDRAG(I)=RHO/2.*(CF(I)+CF(I-1))/2.0*((UEX(I)+UEX(I-1))/2.0)**2*
LN 0068         1SAREA(I) +SDRAG(I-1)
LN 0069          XLAMDA(I)=SQRT(2.0/CF(I))
LN 0070          VSTAR(I)=UEX(I)/XLAMDA(I)
LN 0071          ROPLUS(I)=R0(I)*VSTAR(I)/XNU
LN 0072    1     CONTINUE
LN 0073          TL=XL(NDATA)
LN 0074          RL=U0*TL/XNU
LN 0075          DO 30 I=1,NDATA
LN 0076          XLSTAR(I)=XL(I)/TL
LN 0077    30    CONTINUE
LN 0078    C        CALCULATE FIRST AND SECOND DERIVATIVES OF VELOCITY DATA
LN 0079    C        OBTAINED FROM DOUGLAS-NEUMAN PROGRAM
LN 0080          CALL DGT3(XL,VX,VXD1,NDATA,IER)
LN 0081          CALL DGT3(XL,VXD1,VXD2,NDATA,IER)
LN 0082          CALL DGT3(XLSTAR,ROPLUS,DROPOXS,NDATA,IER)
LN 0083          DO 33 I=1,NDATA
LN 0084          VINVP(I)=-1.0*VXD1(I)/(VX(I)*VX(I))
LN 0085          VINVPP(I)=2.0*VXD1(I)/(VX(I)**3) -1.0*VXD2(I)/(VX(I)*VX(I))
LN 0086          ALPHA=(XLAMDA(I)**3)*VINVP(I)/RL
LN 0087          PDRAG(I)=CONST*(CP(I)+CP(I-1))/2.0*(R0(I)**2-R0(I-1)**2)+PDRAG(I-1
LN 0088         1)
LN 0089          IF(I.LE.(ISTART-1)) GO TO 24
LN 0090          DELPLUS(I)=0.37*XL(I)*VSTAR(I)/(XNU*RX(I)**0.20)
LN 0091          GO TO 25
LN 0092    24    DELPLUS(I)=5.0*XL(I)*VSTAR(I)/(XNU*SQRT(RX(I)))
LN 0093    25    CONTINUE
LN 0094          DELY=R0(I)*(EXP(DELPLUS(I)/ROPLUS(I))-1.0)*12.0
LN 0095          TOSAREA=SAREA(I) + TOSAREA
LN 0096          PRINT 333,AXL(I),XL(I),TOSAREA ,XLSTAR(I),R0(I),VX(I),PDRAG(I),
LN 0097         1XLAMDA(I),CP(I),SDRAG(I),DELY,ROPLUS(I),DELPLUS(I),ALPHA,I
LN 0098    33    CONTINUE
LN 0099          PRINT 332
LN 0100    332   FORMAT(1H1)
LN 0101          PRINT 100
LN 0102    C        SET INITIAL CONDITIONS FOR ITERATION PROCEDURE
LN 0103          XLAMDAC=45.0
LN 0104          VSTARE=UEX(ISTART)/XLAMDAC
LN 0105          U1=25.0
LN 0106          DELY=R0(ISTART)*(EXP(DELPLUS(ISTART)/ROPLUS(ISTART))-1.0)
LN 0107          DELP=25.0
LN 0108          U1PLUS=U1/VSTARE
LN 0109          YPLUSC=0.37*XL(ISTART)*VSTARE/(XNU*RX(ISTART)**0.20)
LN 0110          YPMAX=YPLUSC
LN 0111          YE=YPLUSC*XNU/VSTARE
LN 0112          ROPLUSE=R0(ISTART)*VSTARE/XNU
```

```
LN 0113          ALPHA=XLAMDAC**3*VINVP(ISTART)/RL
LN 0114          IXX=0
LN 0115          Q2=0.6*VX(ISTART-1)*U0*6.2832*R0(ISTART-1,*DELPLUS(ISTART-1)*XNU/
LN 0116         1VSTAR(ISTART-1)
LN 0117          Q16=0.6*UEX(16)*6.2832*R0(16)*DELPLUS(16)*XNU/VSTAR(16)
LN 0118          QC=QI-Q16
LN 0119          IF(QC.LT.0.0) QC=0.0
LN 0120          C2BAR=QI*CI/(Q2+QC)
LN 0121          DELC34=QC/(.6*VX(34)*U0*6.2832*R0(34))
LN 0122          DELPC=DELC34*VSTAR(34)/XNU
LN 0123     C
LN 0124          DO 2 I=ISTART,ISTART2
LN 0125          XX=(XL(I+1)-.16570)/.00653
LN 0126          XXX=(U0/(U0*0.6))**1.5*XX/CI
LN 0127          M1=0
LN 0128          IF(I.LT.(ISTART+3)) GO TO 5
LN 0129          J=I-3
LN 0130          DO 6 K=1,3
LN 0131          J=J+1
LN 0132          XLSTARC(K)=XLSTAR(J)
LN 0133          R0PLUSC(K)=R0PLUS(J)
LN 0134     6    CONTINUE
LN 0135          CALL DGT3(XLSTARC,R0PLUSC,DR0PDXC,NREAD,IERT)
LN 0136          DR0PDXS(I)=DR0PDXC(2)
LN 0137     5    CONTINUE
LN 0138     C       SET VALUES FOR RUNGE-KUTTA-GILL INTEGRATION OF SYSTEM OF
LN 0139     C       EQUATIONS TO COMPUTE G1,H AND XI
LN 0140          ICHECK=0
LN 0141          M=1
LN 0142          N=0
LN 0143          STEP=0.5
LN 0144          NDIM=8
LN 0145          XNDIM=NDIM
LN 0146          WEIGHT=1.0/XNDIM
LN 0147          DO 40 JK=1,NDIM
LN 0148          Y(JK)=0.0
LN 0149     40   CONTINUE
LN 0150          PRMT(1)=0.1108
LN 0151          GO TO 94
LN 0152     92   PRMT(1)=YPLUS
LN 0153     94   PRMT(2)=YPLUSC
LN 0154          PRMT(3)=STEP
LN 0155          PRMT(4)=5.0E-2
LN 0156          PRMT(5)=0.0
LN 0157          DO 41 JK=1,NDIM
LN 0158          DERY(JK)=WEIGHT
LN 0159     41   CONTINUE
LN 0160          CALL RKGS(PRMT,Y,DERY,NDIM,IHLF,BDLAYER,NOUTPUT,AUX)
LN 0161          IF(YPLUS.LT.(0.99*YPLUSC)) GO TO 92
LN 0162          CHEXSEP=3.0*ALPHA*H-G1
LN 0163          IF(CHEXSEP.GE.0.0) GO TO 90
LN 0164          DELYV=R0(ISTART)*(EXP(YPLUSV/R0PLUSE)-1.0)
LN 0165          IF(IXX.EQ.0) QV=(Q2+QC)*DELYV*VSTAR(35)/(XNU*(DELPLUS(34)+DELPC))
LN 0166          IXX=1
LN 0167          IF(XXX.GT.30.0) GO TO 102
LN 0168          CW=YPLUS35*C2BAR/YPLUSV
```

```
LN 0169          DELTAD=(YPLUSV      )*XNU/VSTARE
LN 0170    102   CONTINUE
LN 0171          AK5=(YPLUS-DELB)*AK/UPLUS
LN 0172          IF(XCHECK.LT.60.0) AK3=1.5
LN 0173          IF(XCHECK.GT.60.0) AK3=2.15
LN 0174          IF(AK3.GT.2.0) AK2=.64
LN 0175          IF(AK3.LT.2.0) AK2=.84
LN 0176    C        INTERGRATE EQUATION TO DETERMINE DELTAD
LN 0177          IF(XXX.LT.30.0) GO TO 101
LN 0178          M=4
LN 0179          PRMT(1)=XL(I)
LN 0180          PRMT(2)=XL(I+1)
LN 0181          PRMT(3)=(XL(I+1)-XL(I))/5.0
LN 0182          PRMT(4)=5.0E-2
LN 0183          PRMT(5)=0.0
LN 0184          NDIM=1
LN 0185          Y(1)=DELTAD
LN 0186          DERY(1)=1.0
LN 0187          CALL RKGS(PRMT,Y,DERY,NDIM,IHLF,BDLAYER,HOUTPUT,AUX)
LN 0188    101   CONTINUE
LN 0189    C
LN 0190    C        SOLVE EQUATION FOR LAMDA WITH PREVIOUS ASSUMED LAMDA
LN 0191          M=3
LN 0192          PRMT(1)=XLSTAR(I)
LN 0193          PRMT(2)=XLSTAR(I+1)
LN 0194          PRMT(3)=(XLSTAR(I+1)-XLSTAR(I))/5.0
LN 0195          PRMT(4)=5.0E-2
LN 0196          PRMT(5)=0.0
LN 0197          NDIM=1
LN 0198          IF(I.EQ.ISTART) XLAMDA(I)=45.0
LN 0199          Y(1)=XLAMDA(I)
LN 0200          DERY(1)=1.0
LN 0201          CALL RKGS(PRMT,Y,DERY,NDIM,IHLF,BDLAYER,HOUTPUT,AUX)
LN 0202          IF(I.EQ.ISTART) DELBO=DELB
LN 0203          XLAMDAC=XLAMDAC-(DELBO-DELB)
LN 0204    C
LN 0205    C        WITH LAMDA JUST COMPUTED(NEW POINT) RECOMPUTE ALPHA,V*,AND R0*
LN 0206    C        TO SOLVE FOR U* AT NEW POINT
LN 0207          IF(VINVP(I+1).GT.0.0) GO TO 43
LN 0208          VINVP(I+1)=0.0
LN 0209          VINVPP(I+1)=0.0
LN 0210          UEX(I+1)=UEX(I)
LN 0211          VX(I+1)=VX(I)
LN 0212          VXD1(I+1)=0.0
LN 0213    43    CONTINUE
LN 0214          ALPHA=XLAMDAC**3*VINVP(I+1)/RL
LN 0215          CHEXSEP=3.0*ALPHA*H-G1
LN 0216          IF(CHEXSEP.GE.0.0) GO TO 90
LN 0217          VSTARE=UEX(I+1)/XLAMDAC
LN 0218          ROPLUSF=R0(I+1)*VSTARE/XNU
LN 0219    C        INTEGRATE EQUATION FOR U* STOPPING WHEN U*=LAMDA (JUST COMPUTED)
LN 0220    C        THIS DETERMINES BOUNDARY LAYER THICKNESS FOR COMPUTED LAMDA
LN 0221          M=5
LN 0222          N=0
LN 0223          STEP=0.5
LN 0224          Y(1)=0.0
```

```
LN 0225          Y(2)=0.0
LN 0226          Y(3)=0.0
LN 0227          PRMT(1)=0.1108
LN 0228          GO TO 54
LN 0229    52    PRMT(1)=YPLUS
LN 0230    54    PRMT(2)=YPLUSC*100.0
LN 0231          PRMT(3)=STEP
LN 0232          PRMT(4)=5.0E-2
LN 0233          PRMT(5)=0.0
LN 0234          NDIM=3
LN 0235          DERY(1)=0.33
LN 0236          DERY(2)=0.33
LN 0237          DERY(3)=0.34
LN 0238          CALL RKGS(PRMT,Y,DERY,NDIM,IHLF,BDLAYER,HOUTPUT,AUX)
LN 0239          IF(UPLUS.LT.(0.99*XLAMDAC)) GO TO 52
LN 0240    C
LN 0241          XLAMDA(I+1)=XLAMDAC
LN 0242          ROPLUS(I+1)=ROPLUSF
LN 0243          CF(I+1)=2.0/(XLAMDAC**2)
LN 0244          SDRAG(I+1)=CONSTS*(CF(I)+CF(I+1))/2.0*((UEX(I)+UEX(I+1))/2.0)**2*
LN 0245         1(XL(I+1)-XL(I))*(RO(1)+RO(I+1))/2.0 + SDRAG(I)
LN 0246          DELY=RO(I+1)*(EXP(YPLUS/ROPLUSE  )-1.0)
LN 0247          RDISPLAC=(DISPLAC*U0/XNU)
LN 0248          DEN=DELY*VSTARE/XNU
LN 0249          II=I+1
LN 0250          YPLUSC=YPLUS
LN 0251          YPMAX=YPLUSC
LN 0252          UIPLUS=U1/VSTARE
LN 0253          YE=YPLUSC*XNU/VSTARE
LN 0254          XCHECK=(XL(I+1)-.16570)/YE
LN 0255          AXLDL=AXL(I)/AXL(NDATA)
LN 0256          RATIO=DELTA0/YE
LN 0257          DELR0=DELB
LN 0258    C        INTEGRATE EQUATION 5 TO DETERMINE CW
LN 0259          IF(XXX.LT.30.0) GO TO 200
LN 0260          N=2
LN 0261          JDELTA=0
LN 0262          N=0
LN 0263          STEP=0.5
LN 0264          Y(1)=0.0
LN 0265          Y(2)=0.0
LN 0266          PRMT(1)=0.1108
LN 0267          GO TO 201
LN 0268    202   PRMT(1)=YPLUS
LN 0269    201   PRMT(2)=YPLUSC
LN 0270          PRMT(3)=STEP
LN 0271          PRMT(4)=5.0E-2
LN 0272          PRMT(5)=0.0
LN 0273          NDIM=2
LN 0274          DERY(1)=0.5
LN 0275          DERY(2)=0.5
LN 0276          CALL RKGS(PRMT,Y,DERY,NDIM,IHLF,BDLAYER,HOUTPUT,AUX)
LN 0277          IF(YPLUS.LT.(0.99*YPLUSC)) GO TO 202
LN 0278    200   CONTINUE
LN 0279          CWDCI=CW/CI
LN 0280          DELYV=RO(I+1)*(EXP(YPLUSV/ROPLUSE)-1.0)
```

```
ANSI FORTRAN(2,3)/MASTER     INTEGER WORD SIZE = 2 , * OPTION IS  OFF , 0 OPTION IS  OFF    05/21/75        PAGE 006

LN 0281          PRINT 7,AXLOL,XLAMDAC,ALPHA,CZBAR,VSTARE,XXX    ,YPLUS,DELTAD,
LN 0282         1DISPLAC,TMOMENT,IHLF,IER,M,II
LN 0283          PRINT 9,XCHECK,CP(I+1),AXL(I+1),VX(I+1),OV ,AKS,CWDCI,SDRAG(I+1),
LN 0284         1PDRAG(I+1),DELY,DELB,GAMMA
LN 0285          CWO=CW
LN 0286        2 CONTINUE
LN 0287          GO TO 80
LN 0288       90 PRINT 91
LN 0289       91 FORMAT(*       SEPARATION HAS OCCURRED - CALCULATE FORM DRAG*)
LN 0290          PDRAG(I)=PDRAG(I)-CONST*CP(I)*RO(I)**2
LN 0291          GO TO 84
LN 0292       80 PRINT 81
LN 0293       81 FORMAT(*            END OF BODY OR DATA POINTS PROVIDED*)
LN 0294       84 DRAG=SDRAG(I)+PDRAG(I)
LN 0295          PRINT 83,DRAG
LN 0296       83 FORMAT(13H TOTAL DRAG =,F12.4)
LN 0297          END

        USASI FORTRAN DIAGNOSTIC RESULTS FOR CALBDL

        NO ERRORS
```

```
ANSI FORTRAN(2,3)/MASTER     INTEGER WORD SIZE = 2 , * OPTION IS  OFF , 0 OPTION IS   OFF     05/21/75        PAGE 001

 LN 0001           SUBROUTINE RDLAYER(X,Y,DERY)
 LN 0002           COMMON ROPLUS(200),R0(200),XLAMDA(200),DROPDXS(200),VX(200),
 LN 0003          1VXD(200),VINVP(200),VINVPP(200),XLSTAR(200),ALPHA,AK,RHO,XNU,W,
 LN 0004          2N,RL,XLAMDAC,XI,G1,H,XJ,IER,I,CF(200),VSTARF,ROPLUSE,UEX(200),YPLU
 LN 0005          3S,UPLUS,YPLUSC,STEP,VOSTAR,VSTARIN,DI,DELTAD,JDELTA,XCHECK,CDCW,CW
 LN 0006          4,QI,CI,U1PLUS,DELR,DCWDXS(200),YE,JPOLY,GAMMA,DISPLAC,TMOMENT,CAPT
 LN 0007          5,AXL(200),YPM4X,M1,DELY,CW0,AK2,AK5,AK3,ICHECK,YPLUSV,CWAP,C2BAR,
 LN 0008          6QV,YPLUS35
 LN 0009           DIMENSION Y(10),DERY(10)
 LN 0010     C        THIS SUBROUTINE IS USED TO WRITE EQUATIONS TO BE SOLVED
 LN 0011           IF(M.EQ.4) GO TO 10
 LN 0012           IF(M.EQ.3) GO TO 3
 LN 0013           EXV=EXP(2.0*X/ROPLUSE)
 LN 0014           IF(M.EQ.6) GO TO 78
 LN 0015           EXV1=1.0-EXV
 LN 0016           CHEXSQT=1.0-ALPHA*ROPLUSE/2.0*EXV1
 LN 0017           TERM1=SQRT(CHEXSQT)
 LN 0018           TERM2=TERM1/(AK*X)
 LN 0019     C        REMOVE THE ENCLOSED CARDS FOR NO POLYMER CASES
 LN 0020           IF(M.EQ.2) GO TO 77
 LN 0021           IF(M.EQ.5) GO TO 66
 LN 0022           SQCW=SQRT(CW)
 LN 0023           GAMMA=2.3*SQCW
 LN 0024           AL=ALOG(VSTARE/VOSTAR)
 LN 0025     C        REMOVE THE ENCLOSED CARDS FOR POLYMER OCEAN CASE
 LN 0026           IF(GAMMA.GT.11.5) GO TO 4
 LN 0027           JPOLY=0
 LN 0028           GO TO 5
 LN 0029     C        REMOVE THE ENCLOSED CARDS FOR POLYMER OCEAN CASE
 LN 0030     4     JPOLY=1
 LN 0031           GAMMA=11.5
 LN 0032     5     CONTINUE
 LN 0033           DELB=ALOG(VSTARE/VOSTAR)*GAMMA
 LN 0034           IF(DELB.GT.28.0) DELB=28.0
 LN 0035           DIRUCW=1.15*AL/SQCW
 LN 0036           IF(JPOLY.EQ.1) DIRUCW=0.0
 LN 0037           GO TO 77
 LN 0038     77    TERM3=R0(I)/DELTAD*(EXP(X/ROPLUSE)-1.0)
 LN 0039           CDCW=EXP(-0.693*TERM3**AK3)
 LN 0040     78    CONTINUE
 LN 0041           CW=1.0/Y(2)
 LN 0042           GAMMA=2.3*SQRT(CW)
 LN 0043           IF(GAMMA.GT.11.5) GAMMA=11.5
 LN 0044           DELB=ALOG(VSTARE/VOSTAR)*GAMMA
 LN 0045           IF(DELB.GT.28.0) DELB=28.0
 LN 0046           UPLUS=Y(1) + DELB
 LN 0047           EXVU=EXV*UPLUS
 LN 0048     C        EQUATIONS TO SOLVE FOR U+ AND CW
 LN 0049           DERY(1)=TERM2
 LN 0050           DERY(2)=6.2832*R0(I)*XNU*EXVU*CDCW/(C2BAR*QV)
 LN 0051           RETURN
 LN 0052     C        SYSTEM OF EQUATIONS TO SOLVE FOR G1,H AND XI
 LN 0053     C        TERM2=D(G+)/D(Y+)
 LN 0054     C        Y+=X
 LN 0055     C        U+=Y(1) + DELB
 LN 0056     C        G1=Y(2)
```

```
LN 0057     C         D(U+)/D(ALPHA)=Y(3)
LN 0058     C         D(PSI)/D(ALPHA)=Y(4)
LN 0059     C         H=Y(5)
LN 0060     C         D(U+)/D(R0+)=Y(6)
LN 0061     C         D(PSI)/D(R0+)=Y(7)
LN 0062     C         XI=Y(8)
LN 0063     73    DERY(1)=TERM2
LN 0064           UPLUS=Y(1) + DELB
LN 0065           EXVU=EXV*UPLUS
LN 0066           DERY(2)=EXVU*UPLUS
LN 0067           DERY(3)=-R0PLUSE  /2.0*EXV1/(2.0*AK*X*TERM1)
LN 0068           DERY(4)=EXV*Y(3)
LN 0069           DERY(5)=EXVU*Y(3)-Y(4)*TERM2
LN 0070           DERY(6)=ALPHA*(EXV1-EXV*2.0*X/R0PLUSE  )/(4.0*AK*X*TERM1)
LN 0071           DERY(7)=-2.0*X/(R0PLUSE**2)*EXVU + EXV*Y(6)
LN 0072           DERY(8)=EXVU*Y(6)-Y(7)*TERM2
LN 0073           RETURN
LN 0074     C        EQUATION TO SOLVE FOR LAMDA
LN 0075     C        XLAMDAC=Y(1)
LN 0076     3     EXV=EXP(2.0*YPLUS/R0PLUSE)
LN 0077           DERY(1)=(-RL*VX(I)-Y(1)*DR0PDXS(I)*XI-Y(1)**4/RL*VINVPP(I)*H-VXD1(
LN 0078          1I)/VX(I)*Y(1)*(G1-Y(1)**2*R0PLUSE/2.0*(EXV-1.)))/(3.0*ALPHA*H-G1)
LN 0079           RETURN
LN 0080     C        EQUATION TO SOLVE FOR DELTAD
LN 0081     C        DELTAD=Y(1)
LN 0082     10    DERY(1)=AK5/AK2*(1.0-AK2*Y(1)/YE)*VSTARE/U1
LN 0083           RETURN
LN 0084     C        CBAR=Y(1)
LN 0085     78    DERY(1)=6.7832*R0(I)*XNU*EXV*X/(C2*AR*DV)
LN 0086           RETURN
LN 0087     66    DERY(1)=TERM2
LN 0088           TERM4=Y(1)*VSTARE/UEX(I+1)
LN 0089           DERY(2)=(1.0-TERM4)*EXV*XNU/VSTARE
LN 0090           DERY(3)=DERY(2)*TERM4
LN 0091           RETURN
LN 0092           END
```

USASI FORTRAN DIAGNOSTIC RESULTS FOR BOLAYER

NO ERRORS

UNREFERENCED STATEMENT LABELS

00072

```
LN 0001          SUBROUTINE HOUTPUT(X,Y,DERY,IHLF,NDIM,PRMT)
LN 0002          COMMON RPLUS(200),RO(200),XLAMDA(200),DRDPDXS(200),VX(200),
LN 0003         1VXD(200),VINVP(200),VINVPP(200),XLSTAR(200),ALPHA,AK,RHO,YNU,M,
LN 0004         2N,PL,XLAMDAC,XI,GI,H,XJ,IER,I,CF(200),VSTARE,RPLUSE,UEX(200),YPLU
LN 0005         3S,UPLUS,YPLUSC,STEP,VOSTAR,VSTARIN,UI,DELTAO,JDELTA,ICHECK,CDCW,CW
LN 0006         4,QI,CI,UIPLUS,DELR,DCWDXS(200),YE,JPOLY,GAMMA,DISPLAC,TMOMENT,CAPT
LN 0007         5,AXL(200),YPMAX,MI,DELY,CWO,AK2,AK5,AK3,ICHECK,YPLUSV,CHAR,C2BAR,
LN 0008         6QV,YPLUS35
LN 0009          DIMENSION Y(10),DERY(10),PRMT(5)
LN 0010    C         THIS SUBROUTINE IS USED TO RECORD COMPUTED VALUES FROM RKG
LN 0011          IF(N.EQ.4) GO TO 40
LN 0012          IF(N.EQ.3) GO TO 3
LN 0013          IF(N.EQ.2) GO TO 4
LN 0014          IF(N.EQ.5) GO TO 4
LN 0015          IF(N.EQ.6) GO TO 44
LN 0016          UPLUS=Y(1) * DELR
LN 0017          GI=Y(2)
LN 0018          H=Y(5)
LN 0019          XI=Y(8)
LN 0020          YPLUS=X
LN 0021          IF(ICHECK.EQ.1) GO TO 31
LN 0022          IF(YPLUS.LT.UPLUS) GO TO 31
LN 0023          ICHECK=1
LN 0024          YPLUSV=YPLUS
LN 0025          IF(I.EQ.35) YPLUS35=YPLUSV
LN 0026          IF(I.EQ.36) YPLUS35=YPLUSV
LN 0027    31    CONTINUE
LN 0028          IF(N.EQ.1) GO TO 10
LN 0029          IF(N.EQ.2) GO TO 11
LN 0030          IF(N.EQ.3) GO TO 12
LN 0031          IF(N.EQ.4) GO TO 13
LN 0032          IF(N.EQ.5) GO TO 2
LN 0033          IF(YPLUS.LE.20.0) GO TO 2
LN 0034          N=1
LN 0035          PRMT(5)=1.0
LN 0036          STEP=5.0
LN 0037          GO TO 2
LN 0038    10    IF(YPLUS.LE.200.0) GO TO 2
LN 0039          N=2
LN 0040          PRMT(5)=1.0
LN 0041          STEP=10.0
LN 0042          GO TO 2
LN 0043    11    IF(YPLUS.LE.500.0) GO TO 2
LN 0044          N=3
LN 0045          PRMT(5)=1.0
LN 0046          STEP=25.0
LN 0047          GO TO 2
LN 0048    12    IF(YPLUS.LE.1000.0) GO TO 2
LN 0049          N=4
LN 0050          PRMT(5)=1.0
LN 0051          STEP=50.0
LN 0052          GO TO 2
LN 0053    13    IF(YPLUS.LE.2000.0) GO TO 2
LN 0054          N=5
LN 0055          PRMT(5)=1.0
LN 0056          STEP=100.0
```

```
LN 0057          GO TO 2
LN 0058    3     CONTINUE
LN 0059          XLAMDAC=Y(1)
LN 0060          GO TO 2
LN 0061    44    YPLUS=X
LN 0062          CBAR=1.0/Y(1)
LN 0063          CW=CBAR
LN 0064          GO TO 61
LN 0065    4     CONTINUE
LN 0066          YPLUS=X
LN 0067          IF(M.EQ.5) GO TO 60
LN 0068    C        REMOVE THE ENCLOSED CARDS FOR NO POLYMER CASES
LN 0069          CW=1.0/Y(2)
LN 0070          DELYC=RO(1)*(EXP(YPLUS/ROPLUSE  )-1.0)
LN 0071          C=CW0*CDCW
LN 0072          IF(M1.EQ.0) GO TO 110
LN 0073          IF(M1.EQ.1) GO TO 111
LN 0074          GO TO 100
LN 0075    110   IF(DELYC.GE.0.030/12.0) GO TO 112
LN 0076          GO TO 100
LN 0077    112   C030DCI=C/CI
LN 0078          M1=1
LN 0079          PRINT 103,C030DCI
LN 0080    103   FORMAT(9H C030DCI=,F7.4)
LN 0081          GO TO 100
LN 0082    111   IF(DELYC.GE.0.100/12.0) GO TO 113
LN 0083          GO TO 100
LN 0084    113   C100DCI=C/CI
LN 0085          PRINT 102,C100DCI
LN 0086    102   FORMAT(9H C100DCI=,F7.4)
LN 0087          M1=2
LN 0088    100   CONTINUE
LN 0089          GAMMA=2.3*SQRT(CW)
LN 0090          IF(GAMMA.GT.11.5) GAMMA=11.5
LN 0091          DELB=ALOG(VSTARE/VOSTAR)*GAMMA
LN 0092          IF(DELB.GT.28.0) DELB=28.0
LN 0093          IF(JDELTA.EQ.1) GO TO 30
LN 0094          YECHECK=YPLUS*XNU/VSTARE
LN 0095          IF(YECHECK.LT.(AK2*DELTAD)) GO TO 30
LN 0096          JDELTA=1
LN 0097          U1=UPLUS*VSTARE
LN 0098    30    CONTINUE
LN 0099    C        REMOVE THE ENCLOSED CARDS FOR NO POLYMER CASES
LN 0100    60    UPLUS=Y(1) + DELB
LN 0101          IF(M.EQ.2) GO TO 61
LN 0102          DISPLAC=Y(2)
LN 0103          YMOMENT=Y(3)
LN 0104          IF(UPLUS.GE.(0.99*XLAMDAC)) PRNT(5)=1.0
LN 0105    61    CONTINUE
LN 0106          IF(N.EQ.1) GO TO 20
LN 0107          IF(N.EQ.2) GO TO 21
LN 0108          IF(N.EQ.3) GO TO 22
LN 0109          IF(N.EQ.4) GO TO 23
LN 0110          IF(N.EQ.5) GO TO 2
LN 0111          IF(YPLUS.LE.20.0) GO TO 2
LN 0112          N=1
```

```
LN 0113          PRMT(5)=1.0
LN 0114          STEP=5.0
LN 0115          GO TO 2
LN 0116    20    IF(YPLUS.LE.200.0) GO TO 2
LN 0117          N=2
LN 0118          PRMT(5)=1.0
LN 0119          STEP=10.0
LN 0120          GO TO 2
LN 0121    21    IF(YPLUS.LE.500.0) GO TO 2
LN 0122          N=3
LN 0123          PRMT(5)=1.0
LN 0124          STEP=25.0
LN 0125          GO TO 2
LN 0126    22    IF(YPLUS.LE.1000.0) GO TO 2
LN 0127          N=4
LN 0128          PRMT(5)=1.0
LN 0129          STEP=50.0
LN 0130          GO TO 2
LN 0131    23    IF(YPLUS.LE.2000.0) GO TO 2
LN 0132          N=5
LN 0133          PRMT(5)=1.0
LN 0134          STEP=100.0
LN 0135          GO TO 2
LN 0136    40    DELTAD=Y(1)
LN 0137          IF(DELTAD.GT.(AK2*DELY)) DELTAD=AK2*DELY
LN 0138    2     CONTINUE
LN 0139          IF(IHLF.LT.11) GO TO 70
LN 0140          PRINT 71
LN 0141    71    FORMAT(*   IHLF IS GREATER THAN 10  *)
LN 0142    70    CONTINUE
LN 0143          RETURN
LN 0144          END
```

USASI FORTRAN DIAGNOSTIC RESULTS FOR HOUTPUT

NO ERRORS

```
SSS*LGO
```

AXIAL-X	SURF-X	S-AREA	XLSTAR	RO	VX	PDRAG	LAMDA	CP	SDRAG	DELY	RO*	DEL*	ALPHA	I
0.00001	0.00109	0.00000	0.00050	0.061	0.016	0.001	4.306	1.000	0.0000	0.0164	8.8	7.1	-1.09733	1
0.00037	0.00761	0.00018	0.00352	0.008	0.122	0.129	11.644	0.985	0.0000	0.0107	173.8	19.3	-0.35960	2
0.00108	0.01339	0.00056	0.00618	0.013	0.213	0.394	15.417	0.955	0.0001	0.0105	402.3	25.6	-0.26898	3
0.00201	0.01835	0.00105	0.00847	0.018	0.291	0.720	18.032	0.915	0.0003	0.0104	641.2	29.9	-0.21956	4
0.00287	0.02195	0.00150	0.01014	0.022	0.343	1.006	19.652	0.882	0.0005	0.0105	827.2	32.6	-0.19763	5
0.00405	0.02614	0.00213	0.01207	0.026	0.404	1.378	21.383	0.837	0.0008	0.0105	1060.5	35.5	-0.18542	6
0.00553	0.03064	0.00292	0.01415	0.030	0.471	1.813	23.112	0.779	0.0012	0.0105	1331.3	38.4	-0.16489	7
0.00680	0.03405	0.00359	0.01572	0.033	0.516	2.157	24.285	0.733	0.0016	0.0106	1536.6	40.3	-0.15125	8
0.00820	0.03749	0.00434	0.01731	0.036	0.562	2.509	25.408	0.685	0.0022	0.0106	1749.6	42.2	-0.14295	9
0.00974	0.04097	0.00517	0.01892	0.039	0.606	2.863	26.476	0.633	0.0028	0.0107	1967.5	44.0	-0.13430	10
0.01141	0.04448	0.00607	0.02054	0.042	0.649	3.211	27.498	0.578	0.0035	0.0107	2189.2	45.6	-0.12502	11
0.01322	0.04804	0.00706	0.02218	0.046	0.691	3.549	28.468	0.523	0.0043	0.0108	2411.4	47.3	-0.13462	12
0.01517	0.05167	0.00813	0.02386	0.049	0.744	3.867	29.531	0.447	0.0052	0.0108	2670.9	49.0	-0.10582	13
0.01726	0.05530	0.00928	0.02554	0.052	0.769	4.156	30.286	0.409	0.0063	0.0110	2856.2	50.3	-0.08274	14
0.01947	0.05900	0.01051	0.02724	0.055	0.805	4.428	31.136	0.352	0.0075	0.0111	3076.0	51.7	-0.09284	15
0.02188	0.06279	0.01184	0.02899	0.057	0.839	4.670	31.955	0.296	0.0088	0.0112	3292.1	53.0	-0.05251	16
0.02442	0.06663	0.01327	0.03077	0.060	0.877	4.874	32.792	0.231	0.0102	0.0113	3520.9	54.4	-0.08769	17
0.02711	0.07055	0.01478	0.03258	0.063	0.909	5.035	33.564	0.174	0.0118	0.0114	3734.1	55.7	-0.07586	18
0.02995	0.07454	0.01640	0.03442	0.066	0.939	5.156	34.304	0.119	0.0136	0.0115	3940.0	56.9	-0.07037	19
0.03296	0.07862	0.01813	0.03630	0.069	0.968	5.233	35.028	0.064	0.0155	0.0117	4143.3	58.1	-0.06445	20
0.03614	0.08279	0.01997	0.03823	0.071	0.993	5.266	35.718	0.013	0.0175	0.0118	4336.0	59.3	-0.05839	21
0.03949	0.08707	0.02193	0.04021	0.074	1.018	5.255	36.393	-0.037	0.0197	0.0120	4523.5	60.4	-0.05316	22
0.04302	0.09146	0.02401	0.04223	0.077	1.040	5.202	37.041	-0.082	0.0221	0.0121	4700.4	61.5	-0.04721	23
0.04673	0.09597	0.02622	0.04432	0.079	1.060	5.109	37.670	-0.124	0.0246	0.0123	4868.4	62.5	-0.04210	24
0.05065	0.10062	0.02857	0.04646	0.082	1.078	4.977	38.279	-0.163	0.0273	0.0125	5026.3	63.5	-0.03746	25
0.05476	0.10541	0.03107	0.04867	0.084	1.095	4.810	38.874	-0.199	0.0302	0.0127	5175.3	64.5	-0.03266	26
0.05910	0.11036	0.03373	0.05096	0.087	1.109	4.611	39.449	-0.230	0.0332	0.0129	5312.1	65.5	-0.02760	27
0.06367	0.11549	0.03636	0.05333	0.089	1.121	4.385	40.008	-0.257	0.0365	0.0131	5437.4	66.4	-0.02350	28
0.06849	0.12081	0.03957	0.05579	0.091	1.132	4.135	40.556	-0.281	0.0399	0.0134	5552.5	67.3	-0.01901	29
0.07357	0.12635	0.04278	0.05834	0.093	1.140	3.867	41.086	-0.299	0.0435	0.0136	5653.3	68.2	-0.01492	30
0.07893	0.13212	0.04621	0.06101	0.096	1.147	3.584	41.610	-0.315	0.0473	0.0139	5744.3	69.1	-0.01112	31
0.08461	0.13817	0.04988	0.06380	0.098	1.151	3.293	42.118	-0.325	0.0513	0.0142	5820.4	69.9	-0.00717	32
0.09062	0.14451	0.05381	0.06673	0.100	1.154	2.997	42.620	-0.331	0.0555	0.0145	5885.3	70.7	-0.00419	33
0.09700	0.15118	0.05803	0.06981	0.102	1.155	2.701	43.117	-0.335	0.0599	0.0148	5937.8	71.6	-0.00110	34
0.10380	0.15823	0.06257	0.07305	0.103	1.155	2.409	21.087	-0.334	0.0721	0.0544	12362.3	530.4	0.00016	35
0.11105	0.16570	0.06747	0.07651	0.105	1.154	2.125	21.181	-0.331	0.0933	0.0565	12505.7	547.4	0.00052	36
0.12508	0.18004	0.07709	0.08314	0.108	1.144	1.663	21.339	-0.310	0.1340	0.0606	12662.1	577.0	0.00071	37
0.13539	0.19052	0.08428	0.08797	0.110	1.141	1.380	21.452	-0.302	0.1637	0.0634	12775.4	599.1	0.00092	38
0.14178	0.19698	0.08877	0.09096	0.111	1.136	1.228	21.514	-0.291	0.1870	0.0652	12803.0	611.5	0.00120	39
0.14854	0.20382	0.09357	0.09412	0.112	1.131	1.086	21.576	-0.280	0.2012	0.0671	12821.9	624.4	0.00123	40
0.15572	0.21106	0.09869	0.09746	0.113	1.126	0.953	21.640	-0.268	0.2214	0.0691	12830.7	637.7	0.00121	41
0.16335	0.21874	0.10417	0.10101	0.114	1.121	0.829	21.705	-0.256	0.2427	0.0712	12835.0	651.8	0.00123	42
0.17151	0.22695	0.11007	0.10480	0.115	1.115	0.715	21.771	-0.242	0.2653	0.0735	12824.7	666.4	0.00126	43
0.18025	0.23573	0.11643	0.10885	0.116	1.109	0.611	21.840	-0.229	0.2893	0.0759	12808.2	681.6	0.00122	44
0.18966	0.24518	0.12332	0.11321	0.116	1.102	0.516	21.910	-0.215	0.3147	0.0785	12782.6	698.1	0.00120	45
0.19984	0.25538	0.13081	0.11793	0.117	1.096	0.431	21.984	-0.201	0.3419	0.0812	12749.1	715.4	0.00117	46
0.21534	0.27091	0.14231	0.12510	0.118	1.086	0.329	22.090	-0.180	0.3827	0.0854	12685.8	741.7	0.00110	47
0.23457	0.29017	0.15668	0.13399	0.119	1.076	0.236	22.215	-0.158	0.4323	0.0905	12605.6	772.9	0.00097	48
0.25692	0.31255	0.17352	0.14432	0.120	1.066	0.161	22.352	-0.137	0.4887	0.0964	12509.9	809.2	0.00085	49
0.28338	0.33902	0.19359	0.15655	0.121	1.057	0.101	22.504	-0.116	0.5538	0.1033	12399.3	851.5	0.00072	50
0.31538	0.37103	0.21801	0.17133	0.122	1.047	0.056	22.675	-0.097	0.6304	0.1115	12274.4	901.9	0.00059	51
0.35508	0.41074	0.24850	0.18966	0.123	1.038	0.023	22.871	-0.078	0.7230	0.1215	12135.4	963.4	0.00045	52
0.40603	0.46168	0.28783	0.21319	0.123	1.030	-0.001	23.101	-0.062	0.8383	0.1341	11980.8	1040.9	0.00033	53
0.47427	0.52993	0.34074	0.24470	0.124	1.023	-0.017	23.377	-0.047	0.9880	0.1507	11808.0	1142.3	0.00022	54
0.57122	0.62689	0.41621	0.28947	0.124	1.018	-0.027	23.719	-0.036	1.1932	0.1738	11612.8	1281.9	0.00013	55
0.72130	0.77696	0.53339	0.35877	0.124	1.014	-0.033	24.163	-0.028	1.4987	0.2087	11387.2	1489.6	0.00004	56
0.92322	0.97889	0.69141	0.45201	0.125	1.015	-0.037	24.657	-0.030	1.8940	0.2544	11196.3	1759.1	-0.00008	57
1.01230	1.06796	0.76120	0.49314	0.125	1.018	-0.037	24.842	-0.036	2.0645	0.2741	11145.9	1875.1	-0.00019	58
1.09563	1.15129	0.82649	0.53162	0.125	1.025	-0.037	25.015	-0.051	2.2233	0.2922	11148.6	1988.9	-0.00063	59
1.17897	1.23463	0.89178	0.57011	0.125	1.052	-0.037	25.215	-0.106	2.3850	0.3090	11342.3	2129.0	-0.00256	60
1.21194	1.26761	0.91759	0.58533	0.124	1.086	-0.019	25.338	-0.179	2.4518	0.3140	11633.4	2220.0	0.00007	61
1.21340	1.26906	0.91873	0.58601	0.124	1.086	-0.012	25.341	-0.179	2.4548	0.3144	11624.4	2221.7	0.00020	62
1.21485	1.27052	0.91987	0.58668	0.124	1.086	-0.004	25.343	-0.178	2.4578	0.3147	11615.5	2223.4	0.00020	63
1.21630	1.27197	0.92100	0.58735	0.124	1.085	0.003	25.345	-0.178	2.4609	0.3151	11606.6	2225.0	0.00020	64

1.21776	1.27343	0.92214	0.58802	0.124	1.085	0.011	25.347	-0.178	2.4639	0.3154	11597.7	2226.7	0.00020	65
1.21921	1.27488	0.92327	0.58869	0.124	1.085	0.018	25.349	-0.178	2.4669	0.3157	11588.8	2228.4	0.00020	66
1.22067	1.27634	0.92441	0.58937	0.124	1.085	0.025	25.352	-0.178	2.4699	0.3161	11579.9	2230.1	0.00020	67
1.22212	1.27779	0.92554	0.59004	0.124	1.085	0.033	25.354	-0.177	2.4729	0.3164	11571.0	2231.8	0.00020	68
1.22357	1.27925	0.92668	0.59071	0.124	1.085	0.040	25.356	-0.177	2.4759	0.3168	11562.1	2233.4	0.00020	69
1.22503	1.28070	0.92781	0.59138	0.124	1.085	0.047	25.358	-0.177	2.4789	0.3171	11553.2	2235.1	0.00020	70
1.22648	1.28216	0.92894	0.59205	0.124	1.085	0.054	25.360	-0.177	2.4819	0.3175	11544.3	2236.8	0.00020	71
1.22793	1.28362	0.93007	0.59273	0.124	1.085	0.062	25.363	-0.177	2.4849	0.3178	11535.4	2238.4	0.00018	72
1.22939	1.28507	0.93120	0.59340	0.124	1.085	0.069	25.365	-0.176	2.4879	0.3181	11526.9	2240.1	0.00045	73
1.24405	1.29979	0.94258	0.60019	0.122	1.067	0.179	25.355	-0.139	2.5175	0.3228	11232.9	2232.6	0.00330	74
1.28125	1.33717	0.97087	0.61744	0.119	1.035	0.393	25.344	-0.070	2.5880	0.3344	10558.6	2228.2	0.00199	75
1.32292	1.37905	1.00153	0.63679	0.114	1.021	0.518	25.386	-0.042	2.6608	0.3461	10035.5	2256.2	0.00086	76
1.36458	1.42093	1.03108	0.65613	0.110	1.013	0.591	25.432	-0.026	2.7293	0.3578	9574.9	2292.7	0.00055	77
1.40625	1.46280	1.05954	0.67547	0.106	1.007	0.633	25.462	-0.015	2.7942	0.3696	9143.0	2331.3	0.00040	78
1.44792	1.50468	1.08689	0.69481	0.102	1.003	0.653	25.533	-0.006	2.8557	0.3817	8728.5	2372.0	0.00031	79
1.48958	1.54656	1.11314	0.71414	0.098	1.000	0.659	25.584	0.000	2.9141	0.3941	8326.2	2413.6	0.00025	80
1.53125	1.58843	1.13828	0.73348	0.093	0.997	0.654	25.633	0.005	2.9694	0.4070	7932.5	2455.7	0.00021	81
1.57292	1.63031	1.16233	0.75282	0.089	0.995	0.641	25.685	0.010	3.0219	0.4205	7545.4	2498.0	0.00018	82
1.66583	1.70359	1.20175	0.78666	0.082	0.992	0.605	25.771	0.018	3.1071	0.4458	6881.6	2572.4	0.00016	83
1.72917	1.78735	1.24268	0.82533	0.074	0.989	0.550	25.866	0.021	3.1943	0.4783	6138.9	2657.4	0.00010	84
1.81250	1.87110	1.27920	0.86400	0.065	0.988	0.489	25.959	0.025	3.2713	0.5166	5410.9	2742.8	0.00004	85
1.89583	1.95485	1.31131	0.90268	0.057	0.988	0.431	26.051	0.025	3.3383	0.5636	4699.3	2830.6	-0.00021	86
1.97917	2.03861	1.33902	0.94135	0.048	0.987	0.400	26.159	0.006	3.3963	0.6242	4027.3	2936.8	-0.00298	87
2.03492	2.09464	1.35509	0.96723	0.043	1.066	0.475	26.357	-0.136	3.4322	0.6668	3779.4	3142.4	-0.02190	88
2.05131	2.11112	1.35944	0.97484	0.041	1.197	0.569	26.617	-0.432	3.4437	0.6833	4032.4	3435.4	-0.02559	89
2.05464	2.11453	1.36031	0.97641	0.040	1.229	0.629	26.676	-0.510	3.4463	0.6848	4062.9	3505.6	-0.01371	90
2.05798	2.11800	1.36118	0.97801	0.039	1.231	0.719	26.685	-0.517	3.4490	0.6738	3972.6	3515.4	0.00536	91
2.06131	2.12157	1.36205	0.97956	0.038	1.214	0.832	26.658	-0.474	3.4514	0.6899	3791.9	3483.5	0.01939	92
2.06464	2.12529	1.36292	0.98138	0.037	1.179	0.952	26.600	-0.390	3.4542	0.7145	3532.4	3415.0	0.03264	93
2.06798	2.12919	1.36380	0.98319	0.035	1.126	1.060	26.508	-0.269	3.4565	0.7512	3197.9	3308.8	0.04751	94
2.07131	2.13336	1.36467	0.98511	0.032	1.054	1.133	26.373	-0.112	3.4587	0.8075	2790.3	3159.8	0.06810	95
2.07464	2.13792	1.36554	0.98721	0.029	0.960	1.140	26.179	0.079	3.4605	0.9004	2310.2	2957.4	0.09208	96
2.07798	2.14307	1.36641	0.98959	0.025	0.836	1.048	25.893	0.302	3.4620	1.0786	1757.1	2681.8	0.13510	97
2.08131	2.14930	1.36728	0.99246	0.020	0.664	0.818	25.415	0.559	3.4631	1.5621	1123.0	2278.4	0.22827	98
2.08423	2.15666	1.36804	0.99587	0.013	0.439	0.475	24.549	0.808	3.4637	4.3416	504.4	1697.6	0.51481	99
2.08589	2.16561	1.36852	1.00000	0.004	0.144	0.170	22.215	0.979	3.4638	26027.9939	58.7	773.1	3.80983	100

AXLDL XCHECK	LAMDA CF	ALPHA AXL	AK2 VX	VSTARF AK3 AK5	ROPLUSE CWDCT	YPLUS SDRAG	DELTAD PDRAG	DISPLAC DELY(FT)	TMOMENT DELR	IHLF	IER	M	I
0.049762	45.328239	0.005098835	2.668415	0.695523	-0.0	190.1	0.000716	0.002209	0.000816	-1	0	5	36
-0.00	0.00097340	0.11105000	1.15356160	0.02 0.18	0.533683	0.085768	2.125157	0.003481	24.968212	11.500000			
0.053239	29.494467	0.001873319	2.668415	1.060455	0.9	340.1	0.000452	0.001586	0.000949	-1	0	5	37
3.57	0.00229905	0.12508250	1.14443997	0.02 0.28	0.533683	0.100115	1.663428	0.004094	8.125280	3.757116			
0.059966	31.226543	0.002845797	2.668415	0.998725	1.6	320.1	0.000297	0.001726	0.000979	-1	0	5	38
6.18	0.00205108	0.13539250	1.14111760	0.02 0.27	0.533683	0.114896	1.379818	0.004090	9.709989	3.757116			
0.064909	31.145520	0.003634808	2.668415	0.997160	2.1	310.1	0.000315	0.001661	0.000945	0	0	5	39
8.03	0.00206176	0.14177750	1.13637260	0.02 0.28	0.533683	0.123571	1.228142	0.003966	9.484663	3.757116			
0.067970	31.268379	0.003741714	2.668415	0.988859	2.5	320.1	0.000316	0.001725	0.000984	-1	0	5	40
9.40	0.00204559	0.14854000	1.13135842	0.02 0.28	0.533683	0.132732	1.085711	0.004130	9.478769	3.757116			
0.071212	31.323606	0.003683294	2.668415	0.982398	3.0	330.1	0.000318	0.001784	0.001021	0	0	5	41
10.77	0.00203839	0.15572000	1.12595151	0.02 0.28	0.533683	0.142380	0.952781	0.004290	9.447362	3.757116			
0.074654	31.383330	0.003716161	2.668415	0.975931	3.5	340.1	0.000320	0.001843	0.001058	-1	0	5	42
12.15	0.00203064	0.16335000	1.12067213	0.02 0.28	0.533683	0.152567	0.829271	0.004451	9.422734	3.757116			
0.078312	31.452698	0.003801948	2.668415	0.968495	4.0	340.1	0.000322	0.001861	0.001067	-1	0	5	43
13.92	0.00202169	0.17150750	1.11459087	0.02 0.28	0.533683	0.163374	0.715408	0.004486	9.397919	3.757116			
0.082223	31.517379	0.003675822	2.668415	0.961243	4.6	350.1	0.000325	0.001927	0.001107	0	0	5	44
15.35	0.00201340	0.19025000	1.10852047	0.02 0.28	0.533683	0.174855	0.611186	0.004655	9.369180	3.757116			
0.086414	31.574858	0.003583555	2.668415	0.954006	5.2	360.1	0.000327	0.001994	0.001147	-1	0	5	45
14.80	0.00200608	0.18966250	1.10218037	0.02 0.28	0.533683	0.187106	0.516477	0.004827	9.340944	3.757116			
0.090926	31.637428	0.003486544	2.668415	0.946531	5.9	380.1	0.000330	0.002106	0.001219	-1	0	5	46
17.82	0.00199815	0.19983750	1.09571175	0.02 0.28	0.533683	0.200225	0.431139	0.005141	9.312548	3.757116			
0.095804	31.730785	0.003267495	2.668415	0.935588	6.9	400.1	0.000332	0.002236	0.001300	-1	0	5	47
19.63	0.00198641	0.21533500	1.08624016	0.02 0.28	0.533683	0.219955	0.328905	0.005482	9.282995	3.757116			
0.100234	31.811469	0.002856733	2.668415	0.924602	8.2	430.1	0.000336	0.002423	0.001476	-1	0	5	48
21.35	0.00197634	0.23456500	1.07621522	0.02 0.28	0.533683	0.244057	0.235899	0.005974	9.239308	3.757116			
0.112453	31.881936	0.002472128	2.668415	0.914028	9.7	460.1	0.000340	0.002615	0.001536	-1	0	5	49
23.28	0.00196762	0.25692250	1.06626371	0.02 0.28	0.533683	0.271645	0.160613	0.006476	9.194929	3.757116			
0.123171	31.961067	0.002066930	2.668415	0.903430	11.4	500.1	0.000344	0.002865	0.001693	0	0	5	50
24.99	0.00195789	0.28338500	1.05651504	0.02 0.28	0.533683	0.303777	0.101297	0.007139	9.151713	7116			
0.135858	32.041215	0.001652269	2.668415	0.893193	13.5	575.1	0.000348	0.003291	0.001873	0	0	5	51
25.45	0.00194810	0.31537750	1.04716371	0.02 0.28	0.533683	0.341986	0.055994	0.008341	9.107894	3.757116			
0.151105	32.110297	0.001252639	2.668415	0.883822	16.1	625.1	0.000352	0.003614	0.002178	0	0	5	52
27.65	0.00193973	0.35508250	1.03841134	0.02 0.29	0.533683	0.388648	0.022585	0.009191	9.065078	3.757116			
0.170230	32.202456	0.000892453	2.668415	0.874496	19.5	700.1	0.000356	0.004080	0.002479	-1	0	5	53
29.51	0.00192864	0.40602750	1.03040331	0.02 0.29	0.533683	0.447570	-0.001020	0.010451	9.025452	3.757116			
0.194654	32.318328	0.000580099	2.668415	0.865415	24.0	800.1	0.000360	0.004701	0.002885	-1	0	5	54
31.44	0.00191484	0.47427000	1.02337254	0.02 0.29	0.533683	0.525205	-0.016900	0.012144	8.985597	3.757116			
C030DCI= 0.1675													
C100DCI= 0.0000													
0.227377	32.472457	0.000323272	2.668415	0.856458	30.4	925.1	0.001433	0.005495	0.003408	0	0	2	55
34.08	0.00189670	0.57122500	1.01761055	0.02 0.29	0.314020	0.633645	-0.027027	0.014300	6.832547	2.881984			
C030DCI= 0.1967													

C100DCI= 0.0165

0.273851 30.689579 0.000072295 2.668415 0.902782 40.3 1200.1 0.003273 0.005895 0.003955 0 0 2 56
36.70 0.00212348 0.72130000 1.01375769 0.02 0.31 0.134422 0.809565 -0.033055 0.017823 4.569655 1.885596
C030DCI= 0.1046
C100DCI= 0.0368

0.345799 28.813009 0.000000000 2.668415 0.961579 53.6 1450.1 0.005762 0.005486 0.003970 0 0 2 57
43.04 0.00240909 0.92322500 1.01375769 0.02 0.33 0.071550 1.076038 -0.036990 0.020403 3.420704 1.375682
C030DCI= 0.0611
C100DCI= 0.0275

0.442604 27.856804 0.000000000 2.668415 0.994586 59.5 1600.1 0.006830 0.005081 0.003821 0 0 2 58
44.76 0.00257731 1.01230000 1.01375769 0.02 0.35 0.058214 1.205491 -0.037359 0.021879 3.127361 1.240868
C030DCI= 0.0512
C100DCI= 0.0267

0.485307 27.726855 0.000000000 2.668415 0.993248 65.0 1700.1 0.007801 0.005183 0.003939 0 0 2 59
46.23 0.00260153 1.09563333 1.01375769 0.02 0.35 0.050707 1.331284 -0.037359 0.023249 2.924174 1.158100
C030DCI= 0.0455
C100DCI= 0.0264

0.525258 27.674446 0.000000000 2.668415 1.001140 70.4 1800.1 0.008746 0.005342 0.004090 0 0 2 60
47.45 0.00261139 1.17896667 1.01375769 0.02 0.36 0.045121 1.457904 -0.037359 0.024693 2.760478 1.092451
C030DCI= 0.0406
C100DCI= 0.0243

0.565209 27.565392 0.000083954 2.668415 1.076511 72.6 1700.1 0.009118 0.004572 0.003492 0 0 2 61
55.68 0.00263210 1.21194375 1.08578310 0.02 0.36 0.041063 1.511401 -0.018933 0.021448 2.709080 1.042173
C030DCI= 0.0370
C100DCI= 0.0222

0.581019 27.622109 0.000261632 2.668415 1.074201 72.7 1550.1 0.009133 0.004210 0.003189 0 0 2 62
61.02 0.00262130 1.21339738 1.08568250 0.02 0.36 0.041872 1.514452 -0.011540 0.019461 2.733359 1.052383
C030DCI= 0.0400
C100DCI= 0.0233

0.581716 27.695724 0.000263778 2.668415 1.071247 72.8 1600.1 0.009154 0.004351 0.003302 0 0 2 63
59.03 0.00260738 1.21485102 1.08558190 0.02 0.36 0.044055 1.516989 -0.004159 0.020198 2.805752 1.079474
C030DCI= 0.0397
C100DCI= 0.0236

0.582413 27.765316 0.000265421 2.668415 1.068463 72.9 1600.1 0.009169 0.004406 0.003338 0 0 2 64
58.95 0.00259433 1.21630465 1.08548130 0.02 0.36 0.041595 1.519511 0.003208 0.020256 2.718691 1.048898
C030DCI= 0.0375
C100DCI= 0.0225

0.583109 27.685417 0.000263581 2.668415 1.071447 73.0 1600.1 0.009183 0.004344 0.003297 0 0 2 65
59.20 0.00260932 1.21775828 1.08538070 0.02 0.36 0.041471 1.522032 0.010562 0.020196 2.717558 1.047334
C030DCI= 0.0374
C100DCI= 0.0225

0.583806 27.687172 0.000263680 2.668415 1.071280 73.1 1600.1 0.009197 0.004346 0.003299 0 0 2 66
59.27 0.00260899 1.21921192 1.08528010 0.02 0.36 0.041444 1.524558 0.017902 0.020200 2.716525 1.046999
C030DCI= 0.0373
C100DCI= 0.0225

0.584503 27.689345 0.000263791 2.668415 1.071096 73.2 1600.1 0.009212 0.004349 0.003301 0 0 2 67
59.33 0.00260858 1.22066555 1.08517950 0.02 0.36 0.041419 1.527082 0.025229 0.020205 2.715500 1.046673
C030DCI= 0.0373
C100DCI= 0.0225

0.585200 27.691139 0.000263892 2.668415 1.070928 73.3 1600.1 0.009226 0.004351 0.003302 0 0 2 68
59.40 0.00260824 1.22211918 1.08507890 0.02 0.36 0.041393 1.529603 0.032543 0.020209 2.714480 1.046343
C030DCI= 0.0373
C100DCI= 0.0225

```
   0.585897   27.692938 0.000263992   2.668415   1.070759       73.4      1600.1   0.009240   0.004353   0.003304   0   0   2  69
     59.47  0.00260791  1.22357282 1.08497830  0.02  0.36   0.041367   1.532123   0.039843   0.020214   2.713466   1.046016
C030DCI= 0.0373
C100DCI= 0.0225

   0.586594   27.694745 0.000264093   2.668415   1.070590       73.5      1600.1   0.009254   0.004355   0.003305   0   0   2  70
     59.54  0.00260757  1.22502645 1.08487770  0.02  0.36   0.041341   1.534640   0.047131   0.020218   2.712459   1.045691
C030DCI= 0.0373
C100DCI= 0.0225

   0.587291   27.696557 0.000264194   2.668415   1.070420       73.6      1600.1   0.009268   0.004357   0.003307   0   0   2  71
     59.61  0.00260722  1.22644008 1.08477710  0.02  0.36   0.041316   1.537154   0.054404   0.020222   2.711458   1.045369
C030DCI= 0.0373
C100DCI= 0.0226

   0.587988   27.689766 0.000232425   2.668415   1.070584       73.7      1650.1   0.009283   0.004464   0.003397   0   0   2  72
     57.88  0.00260850  1.22793372 1.08467650  0.02  0.36   0.040985   1.539667   0.061665   0.020902   2.700750   1.041180
C030DCI= 0.0370
C100DCI= 0.0224

   0.588685   27.773469 0.000592401   2.668415   1.067282       73.8      1400.1   0.009297   0.003865   0.002899   0   0   2  73
     68.10  0.00259280  1.22938715 1.08460000  0.02  0.36   0.042791   1.542171   0.068746   0.017581   2.756326   1.063872
C030DCI= 0.0410
C100DCI= 0.0242

   0.589381   29.756109 0.005340861   2.668415   0.980269       74.7       825.1   0.009499   0.002815   0.001964   0   0   2  74
    107.53  0.00225880  1.24405417 1.06728883  0.02  0.36   0.052505   1.565295   0.178814   0.011015   2.952975   1.178456
C030DCI= 0.0486
C100DCI= 0.0189

   0.596413   32.509683 0.034193978   2.668415   0.869772       77.2      1400.1   0.007049   0.005800   0.004068   0   0   2  75
     58.08  0.00189236  1.28125000 1.03461429  0.02  0.36   0.071717   1.612262   0.393451   0.021987   3.286484   1.377285
C030DCI= 0.0627
C100DCI= 0.0319

   0.614245   31.538117 0.001657875   2.668415   0.884611       80.0      1900.1   0.007530   0.007870   0.005709   0   0   2  76
     45.08  0.00201075  1.32291667 1.02081801  0.02  0.36   0.062048   1.658011   0.518314   0.030343   3.078585   1.281078
C030DCI= 0.0546
C100DCI= 0.0277

   0.634220   30.438123 0.000940009   2.668415   0.909404       82.7      2100.1   0.008054   0.008070   0.006009   0   0   2  77
     43.38  0.00215971  1.36458333 1.01282654  0.02  0.36   0.058587   1.704132   0.590950   0.033089   3.025919   1.244842
C030DCI= 0.0522
C100DCI= 0.0282

   0.654196   30.111665 0.000656661   2.668415   0.914239       85.5      2200.1   0.008582   0.008478   0.006366   0   0   2  78
     42.02  0.00220577  1.40625000 1.00729045  0.02  0.36   0.056603   1.749994   0.632617   0.034877   2.980709   1.223575
C030DCI= 0.0509
C100DCI= 0.0290

   0.674171   29.917633 0.000493284   2.668415   0.916406       88.2      2400.1   0.009108   0.009201   0.006997   0   0   2  79
     40.80  0.00223448  1.44791667 1.00317231  0.02  0.36   0.055008   1.794418   0.653401   0.038720   2.941275   1.206215
C030DCI= 0.0499
C100DCI= 0.0297

   0.694147   29.760458 0.000389682   2.668415   0.918293       91.0      2500.1   0.009536   0.009636   0.007381   0   0   2  80
     40.48  0.00225814  1.48958333 0.99995651  0.02  0.36   0.053672   1.837240   0.659357   0.040830   2.907804   1.191484
C030DCI= 0.0491
C100DCI= 0.0303

   0.714122   29.638516 0.000321462   2.668415   0.919643       93.8      2600.1   0.010164   0.010081   0.007777   0   0   2  81
     40.16  0.00227676  1.53125000 0.99732409  0.02  0.36   0.052591   1.878410   0.654412   0.043074   2.880085   1.179415
C030DCI= 0.0484
C100DCI= 0.0309
```

```
   0.734098   29.536992 0.000270414   2.668415   0.920745      96.5      2600.1   0.010688   0.010242   0.007919   0   0   2  82
     41.39  0.00229244  1.57291667  0.99509798  0.02  0.36  0.051784   1.917880   0.641246   0.043420   2.859310   1.170334
C0300CI= 0.0482
C1000CI= 0.0334

   0.754073   29.407042 0.000204562   2.668415   0.921956      101.3      2700.1   0.011578   0.010938   0.008568   0   0   2  83
     41.91  0.00231274  1.64583333  0.99202367  0.02  0.36  0.051308   1.982763   0.604807   0.046288   2.847606   1.164917
C0300CI= 0.0480
C1000CI= 0.0343

   0.789030   29.274011 0.000145113   2.668415   0.923630      106.9      2800.1   0.012576   0.011857   0.009333   0   0   2  84
     42.69  0.00233381  1.72916667  0.98932822  0.02  0.36  0.051338   2.050327   0.549613   0.049721   2.850629   1.165289
C0300CI= 0.0484
C1000CI= 0.0355

   0.828981   29.122874 0.000056628   2.668415   0.926748      112.4      3000.1   0.013554   0.013745   0.010965   0   0   2  85
     42.04  0.00235810  1.81250000  0.98754404  0.02  0.36  0.052090   2.110928   0.488813   0.056257   2.875392   1.177794
C0300CI= 0.0496
C1000CI= 0.0372

   0.868932   28.768118 0.000000000   2.668415   0.938177      117.9      2800.1   0.014524   0.013242   0.010590   0   0   2  86
     47.84  0.00241661  1.89583333  0.98754404  0.02  0.36  0.053294   2.165057   0.431288   0.052910   2.922963   1.187274
C0300CI= 0.0508
C1000CI= 0.0403

   0.908883   28.750506 0.000000000   2.668415   0.938751      123.4      2800.1   0.015421   0.014828   0.011947   0   0   2  87
     50.11  0.00241957  1.97916667  0.98754404  0.02  0.36  0.056354   2.212357   0.399970   0.056334   3.006475   1.220897
C0300CI= 0.0538
C1000CI= 0.0419

   0.948834   28.759980 0.000000000   2.668415   0.938442      127.1      2700.1   0.015999   0.015731   0.012681   0   0   2  88
     53.50  0.00241798  2.03491625  0.98754404  0.02  0.36  0.058550   2.239807   0.475150   0.056538   3.064080   1.244451
C0300CI= 0.0560
C1000CI= 0.0452

   0.975561   28.787255 0.000000000   2.668415   0.937553      128.2      2700.1   0.016162   0.016456   0.013284   0   0   2  89
     53.91  0.00241340  2.05131083  0.98754404  0.02  0.36  0.058350   2.247225   0.569083   0.057775   3.057661   1.242322
C0300CI= 0.0559
C1000CI= 0.0438

   0.983420   28.773406 0.000000000   2.668415   0.938004      128.4      2700.1   0.016195   0.016669   0.013472   0   0   2  90
     54.03  0.00241572  2.05464417  0.98754404  0.02  0.36  0.058463   2.248711   0.628625   0.058224   3.061225   1.243527
     SEPARATION HAS OCCURRED - CALCULATE FORM DRAG
TOTAL DRAG =      4.7738
```

DISTRIBUTION

Addressee	No. of Copies
Chief of Naval Material (MAT-0313, 03L4)	2
Office of Naval Research (Code 438-Dr. R. Cooper; Code 472-Mr. G. Neece)	2
Office of Naval Research, Branch Office, Boston (Attn: Dr. A. Wood)	1
Naval Sea Systems Command (SEA-034, 037, 037C, 08, 425, 2052, PMS-393, PMS-393-A3, PMS-395) (SEA-035 Dr. T. Peirce, 035 Dr. McKinney)	9 2
Naval Air Systems Command (AIR-52032 - Mr. P. Stone)	1
Naval Ship Engineering Center (NSEC-6101, 6103, 6110, 6101E, 6111, 6114D, 6136 (Mr. Cauldwell))	7
Naval Facilities Engineering Command (NFAC-03)	1
NSRDL, Annapolis (Mr. Greenberg)	1
NSRDC Carderock (Attn: Mr. R. Converse, Mr. P. Granville)	2
NURDC Pasadena (Dodes 2501, 254, 2543) (Attn: Dr. Hoyt, Dr. Donohue)	5
NRL Washington, D. C. (Code 6100-Dr. R. Kagarise, Dr. King)	2
Naval Intelligence Support Center (Code 4324-Mr. B. Valenti)	1
Oceanographer of the Navy	1
Strategic Systems Project Office	1

U.S. Naval Academy (ATTN: Dr. Bruce Johnson)	1
Naval Science and Technical Intelligence Center (Code 234)	1
Air Force Office of Scientific Research 1400 Wilson Blvd Arlington, VA 22090	1
U.S. Army Mobility Equipment R&D Center Fort Belvoir, VA 22060 (Attn: K. L. Treiber)	1
Maritime Administration, Office of R&D 441 G. Street NW Washington, D. C. 20235	2
Library of Congress Science and Technology Division Washington, D. C. 20540	1
National Science Foundation Engineering Division 1800 G. Street NW Washington, D. C. 20550	1
Defense Documentation Center, Alexandria, VA	12
St. Anthony Falls Hydraulic Lab., Univ..of Minn. 3rd Ave. NE Minneapolis, Minn. 55414 (Attn: J. M. Killen, J. Wetzel, J. Ripkin)	3
LTV Research Center P.O. Box 6144 Dallas, Texas 75222 (Attn: C. S. Wells)	1
Columbia Research Corporation P.O. Box 485 Gaithersburg, Md. 20760 (Attn: N.C. Witbeck)	1
University of Rhode Island West Kingston, R. I. (Attn: Prof. V.C. Rose)	1

University of Delaware
Dept. of Chemical Engineering
Newark, Del. 19711
(Attn: Prof. A.B. Metzner) 1

University of Missouri
Dept. Of Chemical Engineering
Rolla, Missouri 65401
(Attn: Prof. G. K. Patterson) 1

Admiralty Underwater Weapons Establishment
Portland, United Kingdom
(Attn: D.R.R. Gawler) 1